

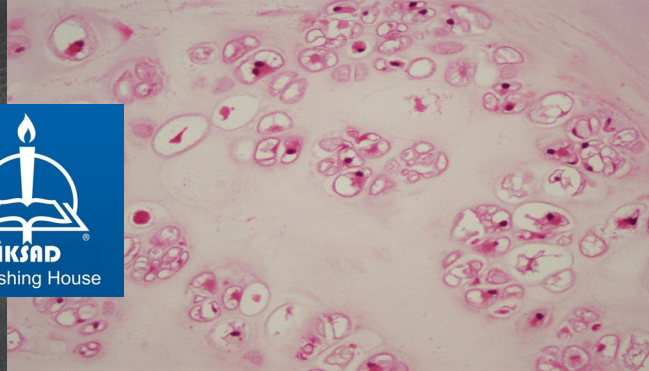
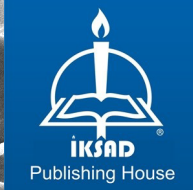
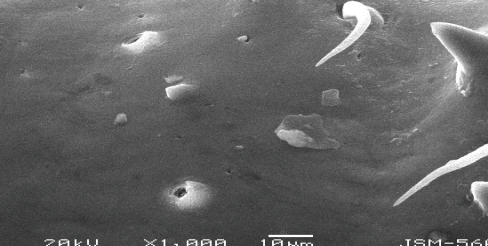
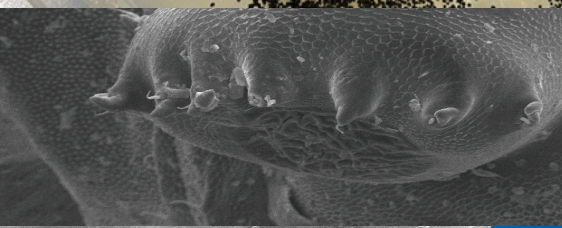
CURRENT APPLICATIONS IN NATURAL SCIENCES II

EDITORS

Prof. Dr. Seçil AKILLI ŞİMŞEK

Assoc. Prof. Dr. Mehmet SEZGİN

Assoc. Prof. Dr. İlkay ÇORAK ÖCAL



20KV X1.000 10µm

JSM-5600

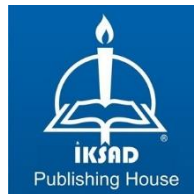
CURRENT APPLICATIONS IN NATURAL SCIENCES II

EDITORS

Prof. Dr. Seçil AKILLI ŞİMŞEK
Assoc. Prof. Dr. Mehmet SEZGİN
Assoc. Prof. Dr. İlkey ÇORAK ÖCAL

AUTHORS

Prof. Dr. Ali KARAIPEKLI
Prof. Dr. Aysel Çağlan GÜNAL
Assoc. Prof. Dr. Ayşenur KAYABAŞ AVŞAR
Assoc. Prof. Dr. Haydar KOÇ
Assoc. Prof. Dr. Melike BİLGİ
Assoc. Prof. Dr. Pınar ARSLAN YÜCE
Assoc. Prof. Dr. Tuba KOÇ
Assoc. Prof. Dr. Oğuz AYDEMİR
Assist. Prof. Dr. Celalettin KAYA
Assist. Prof. Dr. Ebru DERELLİ TÜFEKÇİ
Assist. Prof. Dr. Filiz SARIKAYA PEKACAR
Assist. Prof. Dr. Harun BALDEMİR
Assist. Prof. Dr. Sema GÜLER
Dr. Göktuğ GÜL
Ph.D. Şirin Bahar KARAHASAN
Spec. Ortho. Büşra İlayda BAŞBOĞA
Exp. Bio. Fatma M. A. ISMIEL
Exp. Bio. Sameer Abdulrazzaq ALI
M.Sc. Ayşenur YILMAZ KABACA
M.Sc. Elif KARGALIOĞLU
Fatma Burcu UZUNOĞLU



Copyright © 2024 by iksad publishing house

All rights reserved. No part of this publication may be reproduced, distributed or transmitted in any form or by any means, including photocopying, recording or other electronic or mechanical methods, without the prior written permission of the publisher, except in the case of brief quotations embodied in critical reviews and certain other noncommercial uses permitted by copyright law. Institution of Economic Development and Social Researches Publications®
(The Licence Number of Publicator: 2014/31220)
TÜRKİYE TR: +90 342 606 06 75
USA: +1 631 685 0 853
E mail: iksadyayinevi@gmail.com
www.iksadyayinevi.com

It is responsibility of the author to abide by the publishing ethics rules.
Iksad Publications – 2024©

ISBN: 978-625-367-967-5
Cover Design: İbrahim KAYA
December / 2024
Ankara / Türkiye
Size = 16x24 cm

CONTENTS

PREFACE.....1

CHAPTER 1

THERMAL MANAGEMENT OF LITHIUM-ION BATTERIES USING PHASE CHANGE MATERIALS: RECENT ADVANCES

Fatma Burcu UZUNOĞLU

Prof. Dr. Ali KARAIPEKLİ.....3

CHAPTER 2

EPIGENETIC VARIATIONS IN PLANTS GROWING IN EXTREME HABITATS

Exp. Bio. Fatma M. A. ISMIEL

Assoc. Prof. Dr. Ayşenur KAYABAŞ AVŞAR.....29

CHAPTER 3

IMPORTANCE OF METAGENOMIC ANALYSIS IN DETERMINING MICROBIAL BIODIVERSITY

Assist. Prof. Dr. Ebru DERELLİ TÜFEKÇİ.....55

CHAPTER 4

ASSOCIATION OF TLR2, TLR4 AND TLR9 POLYMORPHISMS WITH URINARY TRACT INFECTIONS

Exp. Bio. Sameer Abdulrazzaq ALI

Assist. Prof. Dr. Filiz SARIKAYA PEKACAR.....77

CHAPTER 5

ENVIRONMENTAL THREATS TO FRESHWATER MUSSELS: THE ROLE OF SODIUM HYDROXIDE

M.Sc. Elif KARGALIOĞLU

Dr. Göktuğ GÜL

Assoc. Prof. Dr. Pınar ARSLAN YÜCE

Prof. Dr. Aysel Çağlan GÜNAL.....115

CHAPTER 6

EXPLORING SIR-TYPE EPIDEMIC MODELS THROUGH NUMERICAL SIMULATIONS IN GNU OCTAVE

Assist. Prof. Dr. Harun BALDEMİR.....135

CHAPTER 7 ORTHOGNATHIC SURGERY Spec. Ortho. Büşra İlayda BAŞBOĞA.....	157
CHAPTER 8 DETAILED PROOFS OF THE CAUCHY-BINET THEOREM, LAPLACE EXPANSION THEOREM, AND THE JACOBI IDENTITY FOR DETERMINANTS Assist. Prof. Dr. Celalettin KAYA.....	177
CHAPTER 9 CAVE-RIPENED CHEESES Assoc. Prof. Dr. Oğuz AYDEMİR.....	191
CHAPTER 10 FIRST CONCEPTS OF GRAPH THEORY Asst. Prof. Dr. Celalettin KAYA.....	221
CHAPTER 11 A REVIEW: SEROTONIN SENSORS BASED ON SCREEN- PRINTED ELECTRODES Assoc. Prof. Dr. Melike BİLGİ Ms. Ayşenur YILMAZ KABACA.....	249
CHAPTER 12 EFFECTS OF PHYSIOLOGICAL CHANGES DURING PREGNANCY ON DRUG PHARMACOKINETICS Assist. Prof. Dr. Sema GÜLER.....	277
CHAPTER 13 TECHNIQUES FOR HANDLING IMBALANCE DATA IN CLASSIFICATION METHODS Assoc. Prof. Dr. Tuba KOÇ Assoc. Prof. Dr. Haydar KOÇ.....	303
CHAPTER 14 IMPACTS OF ROADS ON WILDLIFE Ph.D. Şirin Bahar KARAHASAN.....	323

CHAPTER 15

**DATA VISUALIZATION TOOLS AND TECHNIQUES:
DIABETE DATASET EXAMPLE**

Assoc. Prof. Dr. Haydar KOÇ

Assoc. Prof. Dr. Tuba KOÇ.....361

Dear Readers

The first volume of this book was published in 2023. The second volume has been prepared based on the necessity of emphasizing scientific studies that contribute to issues related to nature and the environment.

Natural sciences are an interpretation of life. Research in natural sciences contributes to human life and shapes the future. This book compiles scientifically rigorous articles from many esteemed experts in the field. We believe it will provide positive contributions to all stakeholders interested in gaining knowledge about nature and environmental topics.

Since the dawn of humanity, the need for knowledge has never ceased, and scientific advancements continue to unfold. Especially in the field of fundamental sciences, research is crucial for uncovering the causes and consequences of many global issues. To address every new problem that arises in the world, science must continually renew itself and develop new methods. Books play an important role in allowing researchers to track studies and share findings with future generations.

We would like to express our gratitude to all the esteemed academics who contributed to the preparation of this book. We hope it will benefit researchers working in this field.

Editors

CHAPTER 1

THERMAL MANAGEMENT OF LITHIUM-ION BATTERIES USING PHASE CHANGE MATERIALS: RECENT ADVANCES

Fatma Burcu UZUNOĞLU¹ & Prof. Dr. Ali KARAIPEKLİ²

DOI: <https://dx.doi.org/10.5281/zenodo.14258591>

¹ Çankırı Karatekin University, Graduate School of Natural and Applied Sciences, Dept. of Chemistry, Çankırı, Türkiye. f.burcu.uzunoglu@gmail.com, Orcid: 0000-0002-4197-785X

² Çankırı Karatekin University, Faculty of Science, Dept. of Chemistry, Çankırı, Türkiye. akaraipekli@karatekin.edu.tr, Orcid ID: 0000-0001-8851-5284

INTRODUCTION

Lithium-ion batteries (LiBs) serve as popular energy storage mediums in various appliances like mobile electronics, electric vehicles, and other energy storage systems (Wu and Ou, 2023). They are known for their high energy-storing capacity, elevated average voltage output, extended operational lifespan, and eco-friendliness (Ning et al., 2022).

In order for LiBs to work efficiently, thermal control plays an important role. Effective thermal control is essential in order to prevent overheating and thermal runaway, which can lead to battery fires or explosions (Chen et al., 1996). During charging and discharging, LiBs generate substantial heat, and without proper temperature control, this could cause safety issues (Wu and Ou, 2023). In addition to these, the operational temperature of LiBs highly affects their effectiveness. To achieve the optimal performance, maintaining the LiB's temperature within a specific range, which is generally between 15-35°C, is crucial (Kumar et al., 2024). Temperature fluctuations may cause reduction in efficiency and loss in capacity (Hannan et al., 2019). Moreover, an effective thermal management (TM) extends the lifespan of LiBs. Nevertheless, extremely high or low temperatures can cause irreversible capacity loss and degrade battery performance over time (Hannan et al., 2019).

Numerous TM strategies, such as active cooling, passive cooling, and smart battery designs, are being researched and implemented in order to handle these challenges and increase the performance properties of LiBs in diverse applications (Jiang et al., 2022).

Being an encouraging solution for thermal control of LiBs, PCMs offer many advantages comparing to other cooling methods. PCMs can absorb and emit substantial amount of latent heat during phase transition so that they help maintain a constant temperature in battery systems (Babu Sanker and Baby, 2023). This ability of PCMs is especially useful for LiBs since they are quite sensitive to temperature changes. For this reason, when operating outside of their optimal temperature range, they can experience reduced performance and safety issues (Hamid et al., 2024).

A number of studies have shown that PCM-based Battery Thermal Management Systems (BTMS) can decrease maximum temperatures and improve the thermal uniformity in LiBs. A study carried out on bio-based PCM integrated LiBs showed that PCM integration reduced the temperature by 6.23%, 10.16%, and 12.44% at 1C, 5C, and 10C discharge rates, respectively (Sinha et al., 2024). Furthermore, storing heat and keeping batteries warm, PCMs may amplify the service life of the LiB up to 76% in cold conditions (Ling, et al., 2016). On the other hand, some PCMs suffer from some issues such as low thermal conductivity, which can result in slow charging and discharging rates. To overcome this problem, researchers have developed several strategies, such as the use of metal foams (Babu Sanker and Baby, 2023), nanoparticles (Karimi et al., 2016), and composite materials (Wang et al., 2024).

LITHIUM-ION BATTERIES

Working Principle of LiBs

LiBs work on the principles of a reversible electrochemical process involving lithium ions during the charging/discharging cycles between anode and cathode, as shown in Figure 1. During discharge, the lithium ions leaving the anode proceed towards the cathode, and electrons travel through an external circuit to generate electrical power. This process is reversed during the charging-cycle: lithium ions return to the electrode (Mekonnen et al., 2016).

The performance of LiBs is highly dependent on electrode and electrolyte properties. Anodes are normally of graphite or carbon-based, while the metal oxides form the cathodes, (Mekonnen et al., 2016; Yuesheng Wang et al., 2018) with organic solutions of lithium salts serving as the electrolyte (Cekic-Laskovic et al., 2016). The predominant selection of these cell materials matters a lot with respect to battery energy density, power output, and cycle life.

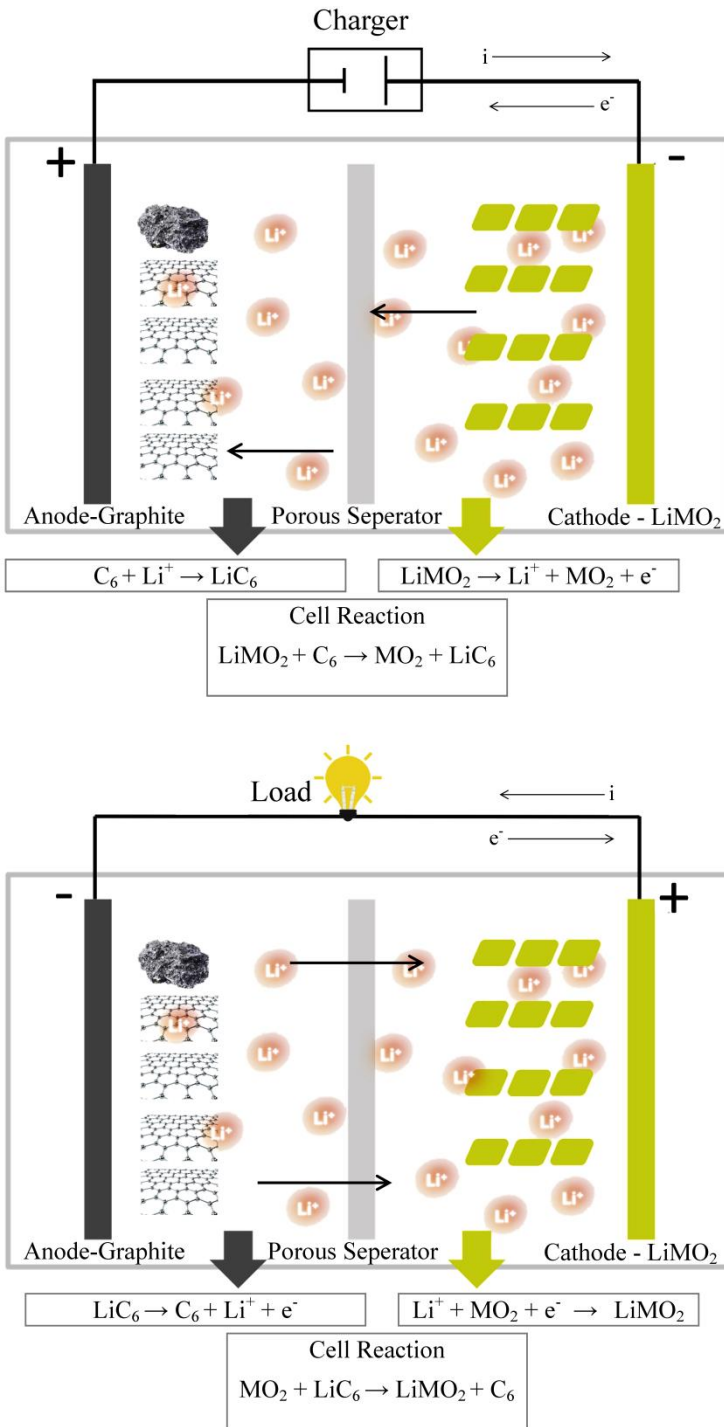


Figure 1. Working principle of LiBs

Types of LiBs

Varieties of LiBs come in many forms and sizes to suit varied applications and devices. The primary kinds LiBs, arranged according to the shape, include: a) coin or button batteries, b) cylindrical batteries, c) prismatic batteries, and d) pouch battery cells, as evident in Figure 2.

- a) Coin or button batteries, which are small, circular batteries commonly used in wristwatches, calculators, and other small electronic appliances.
- b) Cylindrical batteries, which are generally employed in mobile electronic appliances and electric vehicles. They are typically produced in standard sizes and commonly used in laptops, power tools as well as some electric vehicles.
- c) Prismatic batteries, which are rectangular in shape and are usually found in mobile phones, tablets, and thin laptops. They take up much less space and have customizations fit to their specific dimensions.
- d) Pouch battery cells, which are a relatively new type of LiBs with a flexible, flat form. Owing to their high energy storage and tailor-made fit onto very unique form factors, they have popularized in smartphones, wearable devices, and electric vehicles by many endeavored polymer-lithium cell systems.

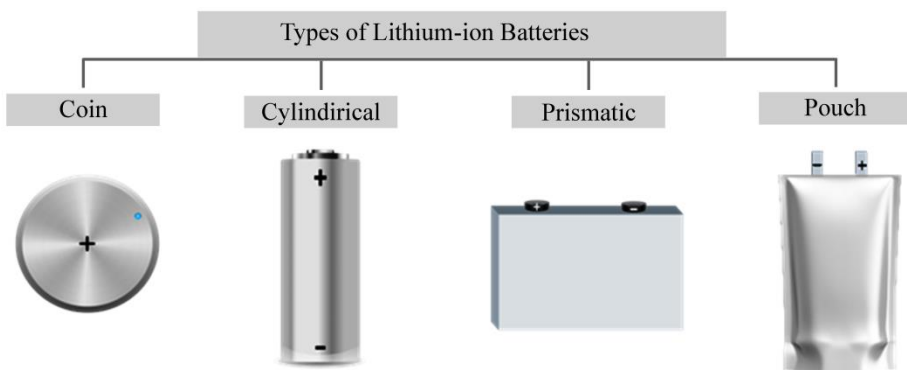


Figure 2. Types of LiBs based on shape

Thermal Issues of LiBs

LiBs are quite sensitive to temperature changes. Generally, these batteries are ideally operated within a temperature ranging from 25°C to 40°C (Saw et al., 2017; Saw et al., 2018). This temperature range is critical for battery performance, safety, and lifespan. Operating outside this temperature range can lead to various issues. At temperatures below 0°C, the battery's internal resistance increases, causing performance failure and, in some cases, lithium plating (Saw et al., 2017). However, the increase in temperature above 40°C may accelerate side reactions, which would reduce lifespan and trigger thermal runaway at temperatures exceeding 90°C (Lyu et al., 2020).

Thermal runaway is one of the main safety issues of LiBs. Because, if the temperature of the LiBs rises uncontrollably, it could result in fire or explosion. This may occur depending on various factors such as high environmental temperatures, overcharging, or internal short circuits. Research findings indicate that during thermal runaway, the peak temperature (T_{max}) can reach nearly 625°C, within the oven temperature of 195°C. During thermal runaway, heat generation mainly stems from the reactions between negative electrode-electrolyte and positive electrode-electrolyte (Liang et al., 2023). The battery may experience an undesirable increase in temperature because of excessive current loading situations, such as rapid charging or sudden accelerations. Moreover, since a LiB is generally placed in a battery module with a series-parallel configuration, the battery cells are closely interconnected. Due to this interconnection, an uneven dynamic load seems to occur (Shahjalal et al., 2021). Consequently, batteries both experience uneven heat generation rates because of their placement in the pack and also encounter temperature fluctuations during charging/discharging periods (Shahjalal et al., 2021). Therefore, temperature control and effective TM strategies are necessary so as to keep the temperature within the optimal and safe range. Several TM systems (TMSs), such as air cooling, mist cooling, PCMs, heat pipes, and liquid cooling systems, have been developed to solve this problem (Chavan et al., 2023; Lei et al., 2020; Saw et al., 2018; Zhang et al., 2014). All these systems aim at maintaining the temperature of the

battery cells within an optimal range whereby consistent performance is ensured during different operating conditions and climates without risking problems related to heat.

Cooling systems have certain essential requirements for adequate performance; the following must, in general, be satisfied (Rao and Wang, 2011).

- i) Maintaining ideal cell temperatures, dissipating heat in warm environments and providing warmth in cold conditions.
- ii) Minimal temperature differences among individual cells, between modules, and across various modules.
- iii) Compactness, lightweight, reliability, and low cost.
- iv) Presence of a ventilation system in case of the emission of hazardous gases from a cell.

Cooling systems could be divided into 3 categories as below, according to the means employed for cooling (Kim et al., 2019).

- i) Maintaining ideal cell temperatures, dissipating heat in warm environments and providing warmth in cold conditions.
- ii) Air cooling
- iii) Liquid cooling
- iv) PCM cooling

PCMs

In terms of thermal energy storage, PCMs are highly favorable materials capable of absorbing and emitting thermal energy in phase transformations. PCMs work by absorbing or storing energy, thereby maintaining a characteristic temperature during phase changes when they are melted; solidification or freeing the latent heat (Mandal, 2024). Phase change behavior of PCMs is shown in Figure 3. Moreover, PCMs have high storage capacity in latent heat, about 5-10 times higher than sensible heat storage of either water or rock, and can reasonably work over a large temperature range varied from -5°C to 190°C (Prajapati and Kandasubramanian, 2019).

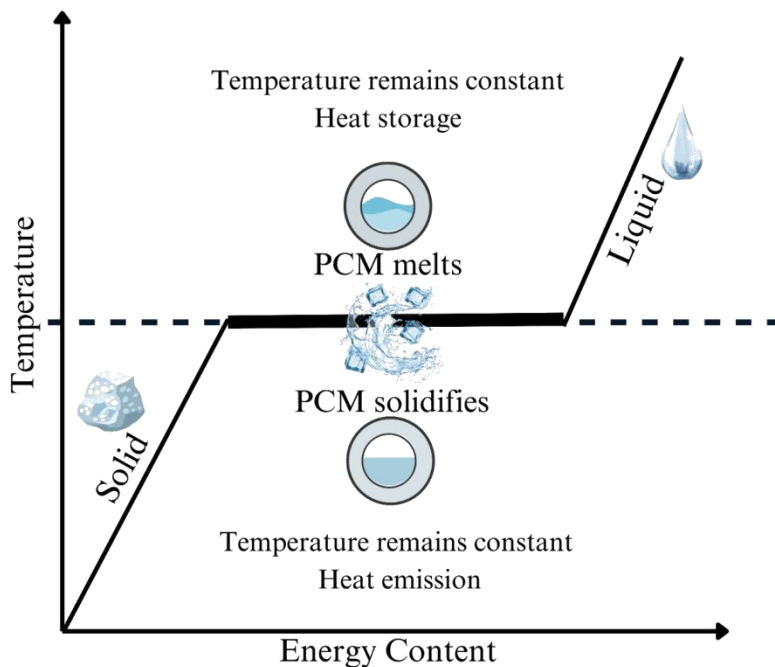


Figure 3. Phase change behavior of PCMs

Types of PCMs

PCMs can generally be divided into three classes, as shown by Figure 4: i) organic, ii) inorganic, iii) eutectic (Mandal, 2024).

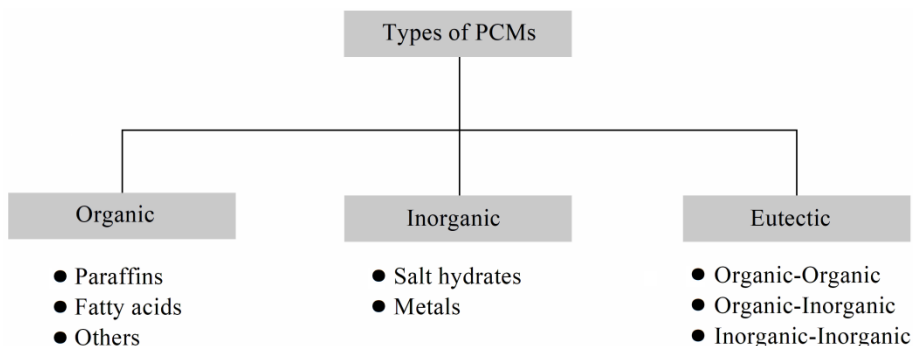


Figure 4. Types of PCMs

- i) Organic PCMs, such as paraffins and fatty acids, generally exhibit high latent heat storage but have low thermal conductivity.
- ii) Inorganic PCMs, such as salt hydrates and metals, provide elevated thermal conductivity but problems arise with supercooling and corrosivity.
- iii) Eutectic PCM is a mixture of various compounds; therefore, their properties vary from one composition to another, thus melting points can be customized with better thermal properties than pure compounds (Mandal, 2024).

Despite their advantageous qualities, PCMs may experience several limitations, such as leakage, incongruent melting, phase separation, and low thermal conductivity (Mitran et al., 2021). To overcome these problems, one of the methods having been developed is the use of shape-stabilized PCMs (ss-PCMs). These materials preserve their solid forms even when the temperature is above the melting point of the active-heat storage compound. This has been achieved through methods such as impregnation into porous matrices, encapsulation, and polymer hybridization (Mandal, 2024; Mitran et al., 2021). Furthermore, studies showed that the inclusion of additives like silver nanoparticles or carbon-based materials can amend the thermal characteristics of PCMs (Muhabie, 2023; Yang et al., 2019).

Selection Criteria of PCMs for LiBs

Various PCMs whose melting temperatures are 30-90 °C are employed for passive cooling in electrical components. For an effective thermal management, they must generally meet the following criteria as well:

- i) Chemical and physical stability.
- ii) Compatibility with electrical components.
- iii) Melting temperature within the required range.
- iv) Large amount of melting/solidification enthalpy.
- v) High thermal conductivity.
- vi) Minimum volume change during phase change.

vii) Non-corrosiveness towards the metallic materials in electrical components.

viii) Non-toxicity.

ix) Non-explosiveness.

THE USE OF PCMs IN LIBs

Being able to help overcome the critical issues resulting from heat generation of the battery systems, PCMs have been considered as a beneficial solution for thermal management in LiBs. Because they can store thermal energy as latent heat during the phase transition at virtually constant temperature, which makes them rather beneficial in terms of passive cooling of LiB designs (Buonomo et al., 2018). On the other hand, although they exhibit high energy density and nearly-constant temperature during phase changes, they may also exhibit low thermal conductivity, which limits their effectiveness. Accordingly, some PCMs may not be able to experience the desired phase transition process. Therefore, it is important to improve their performance by means of various methods. For this purpose, several approaches have been studied and tested, such as the usage of metallic fins increasing the surface area of various PCMs, improving thermal conductivity, and utilization of nano-encapsulated PCMs (Ne-PCMs).

Integration of PCMs in LiBs can notably improve their thermal performance as they can reduce T_{\max} of batter up to 15°C as against air cooling, providing that the PCM preserves its solid state (Alghassab, 2024). Thus, PCMs/LiB systems offer an efficient alternative for overcoming the limitations resulting from excessive heat generation. As research in this field continues to advance, we can expect further improvements in PCM-based thermal management solutions for LiBs, potentially resulting in more efficient and reliable energy storage systems.

When it comes to battery thermal management, choosing an appropriate PCM is crucial and must meet the criteria listed below:

i) Large latent heat and specific heat capacity.

ii) High thermal conductivity.

iii) Low density.

- iv) Chemical inertness towards the electrodes or electrolyte.
- v) Cyclic stability.
- vi) Easily availability.
- vii) Low cost.

In PCM integrated LiB a system, PCM is placed close enough to be in contact with the batteries. With the initiation of charging/discharging operations, the temperature starts to rise. Because of the temperature gradient, the heat flows from the battery towards PCM. The temperature of PCM rises up to its melting point and then remains stable until completely melt down. During this process, PCM absorbs the heat emitted from the LiBs and thus, the LiBs are protected against overheating (Patel and Rathod, 2020).

Integration of PCMs in LiBs

PCM integration into LiBs via various methods can successfully improve their cooling performance and safety. One of the popular methods is to use PCMs together with metal foams or fins, aiming to increase thermal conductivity. Figure 4 shows a diagram of a PCM-cooling system of prismatic LiB via metallic fins.

Another way of improving the thermal conductivity is combining metal foams because of their high porosity and favorable thermophysical features with PCMs (Buonomo et al., 2018). Similarly, metallic fins, especially those composed of thermally-conductive materials such as Cu or Al, can be used with PCMs for better heat transfer. Copper fins with specific dimensions can be used in such systems as they exhibit an acceptable performance in lowering peak temperatures (Alghassab, 2024). The other integration method is the hybrid use of PCMs combined with other methods such as air-cooling, liquid-cooling, and heat-pipe cooling (Khan et al., 2024).

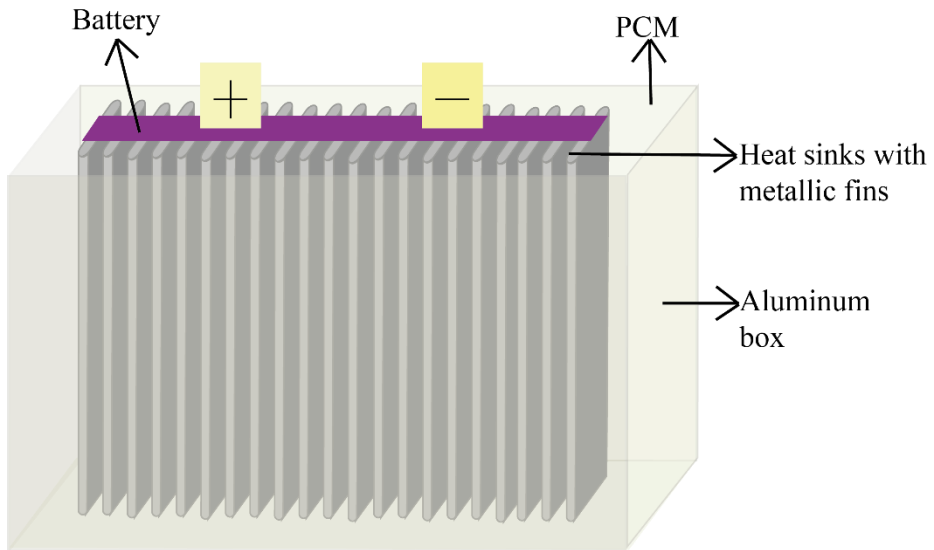


Figure 4. Illustration of PCM/metallic fin cooling method for a prismatic LiB

RECENT STUDIES ON PCM-INTEGRATED LiB SYSTEMS

Table 1. summarizes the outstanding investigation on the use of PCMs with LiBs between 2020 and 2024.

Table1. Summary of the recent studies on PCM cooling for LiBs

PCM	Parrafin wax, GNP, MWCNT, and GSP
Batthey	Cylindrical
Key Results	Tmax < 50 °C in at discharge rates of 1C, 2C, 3C. Uniform temperature distribution in the battery system was achieved.
Ref	(Murali et al., 2021)
PCM	Parrafin wax, GNP, MWCNT, and GSP
Battery	Cylindrical
Key Results	Tmax < 50 °C in at discharge rates of 1C, 2C, 3C. Uniform temperature distribution in the battery system was achieved. ΔT fell by 85.49%, 91.47%, and 84.21%, respectively
Ref	(Masthan Vali and Murali, 2023)
PCM	CA and Hexacosane
Battery	Cylindrical

Key Results	Hexacosane has better cooling performance than CA. Hexacosane can lower T_{max} by 6.54°C.
Ref	(Grimonia et al., 2021)
PCM	Paraffin/EG (of 4mm thickness) + Liquid cooling
Battery	Prismatic
Key Results	Ambient temperature: 37 °C. Discharge rate: 2C T_{max} and ΔT of LiB pack was 48.97 °C and 4.5 °C, respectively.
Ref	(Xin et al., 2023)
PCM	N-eicosane + fins
Battery	Cylindrical
Key Results	Only N-eicosane: T_{max} reduced by nearly 31K. N-Eicosane + fins: T_{max} reduced by 33 K.
Ref	(Narkhede et al., 2024)
PCM	RT44HC/EG (wt.% 88:12)
Battery	Cylindrical
Key Results	T_{max} reduced by 45.25 °C. ΔT reduced by 3.49 °C.
Ref	(Xin et al., 2022)
PCM	Paraffin/EG/nano-copper powder (wt.% 83:15:2) PCM + Micro heat pipe array + Liquid cooling Hybrid system
Battery	Cylindrical
Key Results	ΔT 6.9 °C to 3.9 °C at 2C rate. T_{max} reduced by 13.78% at 2C rate.
Ref	(Xie et al., 2023)
PCM	Paraffin wax
Battery	Cylindrical
Key Results	T_{max} was controlled successfully. At elevated discharge rates, heat absorption was not sufficient.
Ref	(Weng et al., 2020)
PCM	LA/Paraffin/EG
Battery	Prismatic
Key Results	Thermal conductivity: 1.22 W/(m k). (Increment was observed) Melting enthalpy :146.9 J/g. (Increment was observed) Melting temperature: 36.1 °C. T_{max} was 43 °C. ΔT was 1.96 °C.
Ref	(Zhang et al., 2023)
PCM	Paraffin /EG + Metal foam
Battery	Cylindrical

Key Results	T_{\max} and ΔT reduced. Uniformity in temperature was observed.
Ref	(Huang et al., 2020)
PCM	Myristyl alcohol
Battery	Cylindrical
Key Results	T_{\max} decreased by 34.48 % at 3C discharge rate, comparing to natural air cooling. Good thermal management up to 2C discharge rates was achieved. PCM preserved desired conditions for prolonged time of 115.38 % at 3C discharge rate.
Ref	(Goud et al., 2023)
PCM	Paraffin wax/SiC
Battery	Cylindrical
Key Results	Melting enthalpy: 199.4 J/g. Leakage rate: 4.6%. Melting point: 53.6 °C. ΔT was from 300–370 to 303–304 K.
Ref	(Kang et al., 2021)
PCM	Paraffin/CuO and Paraffin/Al ₂ O ₃ and Paraffin/ TiO ₂
Battery	Cylindrical
Key Results	Paraffin wax prolongs battery life by 41%. Paraffin wax + air cooling method decreases ΔT by 4 °C (as against merely paraffin) and by 8 °C (as against merely air cooling.)
Ref	(Vyas et al., 2024)
PCM	Microcapsulated Paraffin@SiO ₂ / GS/ SR Core material: Paraffin core, Shell material: SiO ₂
Battery	Cylindrical
Key Results	SiO ₂ shell improves the thermal conductivity. SiO ₂ /SR double encapsulation restricts the leakage. For the sample with 70 wt%, Pa@SiO ₂ : Latent heat:126.1 J/g. Thermal conductivity:131.25% higher as against pure SR. ΔT :virtually 35 °C at 7.4 C.
Ref	(Kang et al., 2022)
PCM	Paraffin/EG + Fin
Battery	Cylindrical
Key Results	Comparison of thermal management abilities: Paraffin/EG + Fins >Paraffin/EG > Paraffin/Fins. ΔT : nearly 35.5 %. (For Paraffin/EG + Fins)
Ref	(Mei et al., 2022)

PCM	Sodium acetate trihydrate-urea/EG
Battery	Cylindrical
Results	PCM exhibited a high latent heat density within a safe temperature range.
Ref	(Lin et al., 2023)
PCM	$\text{Na}_2\text{SO}_4 \cdot 10\text{H}_2\text{O}$, $\text{KAl}(\text{SO}_4)_2 \cdot 12\text{H}_2\text{O}$ Filler: EG, Support material: Open-cell polyurethane foam
Battery	Pouch
Key Results	For PCMs with 4 wt.% EG: Phase change temperatures: 30.8 °C and 69.8 °C. Latent heat: 226.9 J/g. Thermal conductivity: 1.39 W/(m·K). Achievements: Low subcooling degree, less leakage, super flame retardancy. At 0.5C/1.5C charge/discharge cycles: T_{\max} : 52.47 °C (lowered by 20.4 %) ΔT : 2.20 °C (lowered by 59.7 %)
Ref	(Zhi et al., 2024)
PCM	Palm fatty acid distillate (PFAD)
Battery	Cylindrical
Key Results	Electrical loads: 50W, 100W, and 150W Discharge rates: 0.27C, 0.56C and 0.83C T_{\max} reduced by 9.8 %, 19.5 %, and 12.4 %, respectively.
Ref	(Abdulmunem et al., 2023)
PCM	SA/LA eutectic mixture + fluid cooling
Battery	Cylindrical
Key Results	At discharge rates of 1, 1.5, and 2C, T_{\max} reduced by 46.18%,40.90%, and 22.42%, respectively, compared to the natural cooling. Melting temperature, latent heat and thermal conductivity were 33.29°C, 151.76 J/g and 0.356 W/mK, respectively.
Ref	(Khan et al., 2024)
PCM	$\text{Ca}(\text{NO}_3)_2 \cdot 4\text{H}_2\text{O}/\text{Zn}(\text{NO}_3)_2 \cdot 6\text{H}_2\text{O}$ - Eutectic mixture (55:45)
Battery	Cylindrical
Results	Only $\text{Zn}(\text{NO}_3)_2 \cdot 6\text{H}_2\text{O}$: Temperature dropped by 18.98 °C. (preserving at 42 °C) Only $\text{Ca}(\text{NO}_3)_2 \cdot 4\text{H}_2\text{O}$: Temperature dropped by 14.48 °C. (preserving at 46.50 °C) Eutectic of $\text{Zn}(\text{NO}_3)_2 \cdot 6\text{H}_2\text{O}$ and $\text{Ca}(\text{NO}_3)_2 \cdot 4\text{H}_2\text{O}$:

	Temperature dropped by 21.97 °C. (preserving it at 39.01 °C)
Ref	(Khan et al., 2024)
PCM	LA/SA eutectic mixture + SiC nano particles
Battery	Cylindrical
Results	0.075 vol% SiC particles elevated the thermal conductivity by 75.8 %
Ref	(Pugalenthil et al., 2024)
PCM	LA/SA eutectic mixture, EVA, AlN
Battery	Cylindrical
Results	AlN significantly improves the heat transfer ability. For the sample (SA/EVA/AlN) with 5 wt% AlN: Latent heat : 107.94 J.g ⁻¹ . Thermal conductivity : 0.726 W.(m.K) ⁻¹ . T _{max} dropped below 45 °C (at 4C).
Ref	(Su et al., 2024)
PCM	Na ₂ SO ₄ -10H ₂ O / EG
Battery	Cylindrical
Results	Melting point: 29.05°C. Latent heat: 183.7 J.g ⁻¹ Thermal conductivity: 3.926 W.m ⁻¹ .K ⁻¹ . T _{max} :32°C (15°C ambient temperature, at 3.7C).
Ref	(Zhang et al., 2024)
PCM	Silica encapsulated Na ₂ HPO ₄ ·12H ₂ O
Battery	Cylindrical
Results	The melting temperature and latent heat were 51 °C and 111.69 kJ/kg, respectively. T _{max} reduced by 23.7% (from 86.6 °C to 66.1 °C) at a high discharge rate of 3 °C, and ΔT was within 3 °C.
Ref	(Ping et al., 2023)

*GNP: Graphene nano platelet; MWCNT: Multi walled carbon nanotube; GSP: Graphite synthetic powder; Ne-PCM: Nano-enhanced phase change material; CA: Capric acid; SA: Stearic acid; LA: Lauric acid; EG: Expanded graphite; GS: Graphene sheets; SiC: Silicon carbide; SR: Silicon rubber; CuO: Copper oxide; Al₂O₃: Aluminum oxide; TiO₂: Titanium oxide; SiO₂: Silicone dioxide; EVA: Ethylene-vinyl acetate; AlN: Aluminum nitride

CONCLUSION

Considering the recent studies carried out on the thermal management of LiBs via PCMs, the following inferences, listed in bullet points below, can be drawn:

- Effective thermal management is necessary for LiBs to prevent overheating and thermal runaway.
- In order for LiBs to function effectively and safely, the best temperature range is 15- 35°C.
- PCMs help preserve a constant temperature in LiBs, which makes them ideal mediums for their thermal management.
- Recent studies indicate that PCM integration can reduce the temperature by up to 15°C as against air cooling.
- To improve thermal conductivity of PCMs or minimize their limitations, they can be used with thermally-conductive metal foams or fins.
- Another approach to enhance the thermal performance of LiBs is the utilization of encapsulated PCMs, which can prevent the leakage of PCM.
- Addition of thermally-conductive nanofillers such as MWCNTs, EG and metallic nanoparticles into PCMs can increase the thermal conductivity of PCM and thus contribute to the cooling rate of LiBs.
- Besides organic PCMs such as paraffin, inorganic PCMs and eutectic mixtures also exhibit satisfying results in terms of thermal management of LiBs.

REFERENCES

- Abdulmunem, A.R., Hamed, H.M., Samin, P.M., Mazali, I.I., and Sopian, K. (2023). Thermal management of lithium-ion batteries using palm fatty acid distillate as a sustainable bio-phase change material. *Journal of Energy Storage*, 73, 109187.
- Alghassab, M.A. (2024). Investigating the performance improvement of lithium-ion battery cooling process using copper fins and phase change materials (PCMs). *Case Studies in Thermal Engineering*, 59, 104473.
- Babu Sanker, S., and Baby, R. (2022). A Review on Phase Change Material-metal Foam Combinations for Li-Ion Battery Thermal Management Systems. *Energy Storage Systems: Optimization and Applications*, 115-133.
- Buonomo, B., Ercole, D., Manca, O., and Menale, F. (2018). Thermal cooling behaviors of lithium-ion batteries by metal foam with phase change materials. *Energy Procedia*, 148, 1175-1182.
- Cekic-Laskovic, I., Nowak, S., Schappacher, F., and Winter, M. (2016, June). Electrolytes for Li-Ion Batteries: Limitations, Challenges and Opportunities. In *Electrochemical Society Meeting Abstracts imlb2016* (No. 1, pp. 3-3). The Electrochemical Society, Inc..
- Chavan, U., Prajapati, O., and Hujare, P. (2023). Lithium ion battery thermal management by using coupled heat pipe and liquid cold plate. *Materials Today: Proceedings*, 80, 382-388.
- Chen, Y., Song, L., and Evans, J. W. (1996, August). Modeling studies on battery thermal behaviour, thermal runaway, thermal management, and energy efficiency. In *IECEC 96. Proceedings of the 31st Intersociety Energy Conversion Engineering Conference* (Vol. 2, pp. 1465-1470). IEEE.
- Goud, V.M., Satyanarayana, G., Ramesh, J., Pathanjali, G.A., and Ruben Sudhakar, D. (2023). An experimental investigation and hybrid neural network modelling of thermal management of lithium-ion batteries using a non-paraffinic organic phase change material, Myristyl alcohol. *Journal of Energy Storage*, 72, 108395.
- Grimonia, E., Andhika, M.R.C., Aulady, M.F.N., Rubi, R.V.C., and Hamidah, N.L. (2021). Thermal Management System Using

- Phase Change Material for Lithium-ion Battery. *Journal of Physics: Conference Series*, 2117(1), 012005.
- Hamid, N., Khalifelu, S.S., Joybari, M.M., Rahimi-Ahar, Z., Babapoor, A., Mirzayi, B., and Rahbar, A. (2024). Challenges in thermal management of lithium-ion batteries using phase change nanocomposite materials: A review. *Journal of Energy Storage*, 100, 113731.
- Hannan, M.A., Young, Y.S., Hoque, M.M., Ker, P.J., and Uddin, M.N. (2019, September). Lithium ion battery thermal management system using optimized fuzzy controller. In 2019 IEEE industry applications society annual meeting (pp. 1-9). IEEE.
- He, S., Lei, H., Dong, K., Khan, S. A., and Zhao, J. (2023). A candidate strategy for low-temperature preheating of lithium-ion batteries based on supercooling salt hydrates. *Applied Thermal Engineering*, 230, 120639.
- Huang, R., Li, Z., Hong, W., Wu, Q., and Yu, X. (2020). Experimental and numerical study of PCM thermophysical parameters on lithium-ion battery thermal management. *Energy Reports*, 6, 8-19.
- Jiang, Z.Y., Li, H.B., Qu, Z.G., and Zhang, J.F. (2022). Recent progress in lithium-ion battery thermal management for a wide range of temperature and abuse conditions. *International Journal of Hydrogen Energy*, 47(15), 9428-9459.
- Kang, L., Ren, L., Niu, H., Lv, R., Guo, H., and Bai, S. (2022). Paraffin@SiO₂ microcapsules-based phase change composites with enhanced thermal conductivity for passive battery cooling. *Composites Science and Technology*, 230, 109756.
- Kang, W., Zhao, Y., Jia, X., Hao, L., Dang, L., and Wei, H. (2021). Paraffin/SiC as a Novel Composite Phase-Change Material for a Lithium-Ion Battery Thermal Management System. *Transactions of Tianjin University*, 27(1), 55-63.
- Karimi, G., Azizi, M., and Babapoor, A. (2016). Experimental study of a cylindrical lithium ion battery thermal management using phase change material composites. *Journal of Energy Storage*, 8, 168-174.
- Khan, A., Ali, M., Yaqub, S., Khalid, H.A., Khan, R.R.U., Mushtaq, H Nazir and Said, Z. (2024). Hybrid thermal management of Li-ion

- battery pack: An experimental study with eutectic PCM-embedded heat transfer fluid. *Journal of Energy Storage*, 77, 109929.
- Khan, R. R. U., Iqbal, N., Noor, T., Ali, M., Khan, A., and Nazar, M. W. (2024). Thermal management of Li-ion battery by using eutectic mixture of phase-change materials. *Journal of Energy Storage*, 90, 111858.
- Kim, J., Oh, J., and Lee, H. (2019). Review on battery thermal management system for electric vehicles. *Applied Thermal Engineering*, 149, 192-212.
- Kumar, S., Shukla, O.M., and Shah, J. (2024). Thermal management lithium-ion battery for electric vehicles with using cold plate. *World Journal of Advanced Engineering Technology and Sciences*, 12, 87-94.
- Lei, S., Shi, Y., and Chen, G. (2020). A lithium-ion battery-thermal-management design based on phase-change-material thermal storage and spray cooling. *Applied Thermal Engineering*, 168, 114792.
- Liang, K., Zhu, Q., and Zhou, X. (2023). Simulation and Characteristic Analysis of High-Temperature Thermal Runaway Process in Ternary Lithium-Ion Batteries.
- Lin, S., Ling, Z., Li, S., Cai, C., Zhang, Z., and Fang, X. (2023). Mitigation of lithium-ion battery thermal runaway and inhibition of thermal runaway propagation using inorganic salt hydrate with integrated latent heat and thermochemical storage. *Energy*, 266, 126481.
- Ling, Z., Wen, X., Zhang, Z., Fang, X., and Xu, T. (2016). Warming-Up Effects of Phase Change Materials on Lithium-Ion Batteries Operated at Low Temperatures. *Energy Technology*, 4(9), 1071-1076.
- Lyu, P., Liu, X., Qu, J., Zhao, J., Huo, Y., Qu, Z., and Rao, Z. (2020). Recent advances of thermal safety of lithium ion battery for energy storage. *Energy Storage Materials*, 31, 195-220.
- Mandal, S. (2024). Advancements in Phase Change Materials: Stabilization Techniques and Applications. *Prabha Materials Science Letters*, 3, 254-267.

- Masthan Vali, P.S.N., and Murali, G. (2023). Experimental Study on Thermal Management of Nano Enhanced Phase Change Material Integrated Battery Pack. *ASME Journal of Heat and Mass Transfer*, 146, 1-20.
- Mei, J., Shi, G., Liu, H., Wang, Z., and Chen, M. (2022). Investigation on the optimization strategy of phase change material thermal management system for lithium-ion battery. *Journal of Energy Storage*, 55, 105365.
- Mekonnen, Y., Sundararajan, A., and Sarwat, A.I. (2016). A review of cathode and anode materials for lithium-ion batteries. *SoutheastCon 2016*, 1-6.
- Mitran, R.A., Ioniță, S., Lincu, D., Berger, D., and Matei, C. (2021). A Review of Composite Phase Change Materials Based on Porous Silica Nanomaterials for Latent Heat Storage Applications. *Molecules*, 26(1), 241.
- Muhabie, A. (2023). Healable supramolecular micelle/nano-encapsulated metal composite phase change material for thermal energy storage. *RSC Advances*, 13, 27624-27633.
- Murali, G., Sravya, G.S.N., Srinath, A., and Jaya, J. (2021). An experimental investigation on cooling performance of battery pack by using nano-enhanced phase change material. *Journal of Computational and Theoretical Nanoscience*, 18(4), 1213-1220.
- Narkhede, S., Sur, A., Kothari, G., and Netke, A. (2024). Design and thermal analysis of Fin-PCM-integrated thermal management system for lithium-ion cylindrical battery pack. *Proceedings of the Institution of Mechanical Engineers, Part E: Journal of Process Mechanical Engineering*, 09544089231221668.
- Ning, Y., Tao, R., Luo, J., and Hu, Q. (2022). Application and Research Progress of Heat Pipe in Thermal Management of Lithium-Ion Battery. *Trends in Renewable Energy*, 8, 130-144.
- Patel, J.R., and Rathod, M.K. (2020). Recent developments in the passive and hybrid thermal management techniques of lithium-ion batteries. *Journal of Power Sources*, 480, 228820.
- Ping, P., Dai, X., Kong, D., Zhang, Y., Zhao, H., Gao, X., and Gao, W. (2023). Experimental study on nano-encapsulated inorganic phase change material for lithium-ion battery thermal

- management and thermal runaway suppression. *Chemical Engineering Journal*, 463, 142401.
- Prajapati, D.G., and Kandasubramanian, B. (2019). Biodegradable Polymeric Solid Framework-Based Organic Phase-Change Materials for Thermal Energy Storage. *Industrial and Engineering Chemistry Research*, 58(25), 10652-10677.
- Pugalenthi, S., Chellapandian, M., Dharmaraj, J.J.J., Devaraj, J., Arunachalam, N., and Bright Singh, S. (2024). Enhancing the thermal transport property of eutectic lauric-stearic acid based phase change material with silicon carbide nanoparticles for usage in battery thermal management system. *Journal of Energy Storage*, 84, 110890.
- Rao, Z., and Wang, S. (2011). A review of power battery thermal energy management. *Renewable and Sustainable Energy Reviews*, 15(9), 4554-4571.
- Saw, L.H., King, Y.J., Yew, M.C., Ching Ng, T., Chong, W.T., and Pambudi, N.A. (2017). Feasibility study of mist cooling for lithium-ion battery. *Energy Procedia*, 142, 2592-2597.
- Saw, L.H., Poon, H.M., Thiam, H.S., Cai, Z., Chong, W.T., Pambudi, N.A., and King, Y.J. (2018). Novel thermal management system using mist cooling for lithium-ion battery packs. *Applied Energy*, 223, 146-158.
- Shahjalal, M., Shams, T., Islam, M.E., Alam, W., Modak, M., Hossain, S. B., Ramadesigan, V., Ahmed, M.R., Ahmed, H., and Iqbal, A. (2021). A review of thermal management for Li-ion batteries: Prospects, challenges, and issues. *Journal of Energy Storage*, 39, 102518.
- Sinha, R.K., Kumar, A., Maurya, A., and Kumar, A. (2024). Thermal management of counter terminal lithium-ion battery using Bio-based PCM. *Thermal Science and Engineering Progress*, 54, 102854.
- Su, Y., Shen, J., Chen, X., Xu, X., Shi, S., Wang, X., Zhou, F., and Huang, X. (2024). Bio-based eutectic composite phase change materials with enhanced thermal conductivity and excellent shape stabilization for battery thermal management. *Journal of Energy Storage*, 100, 113712.

- Vyas, D., Bhatt, J., Rajput, A., Hotta, T.K., Rammohan, A., and Raghuraman, D.R.S. (2024). Investigation on Thermal Management of 18650 Lithium-Ion Batteries Using Nano-Enhanced Paraffin Wax: A Combined Numerical and Experimental Study. *Arabian Journal for Science and Engineering*, 49(11), 15565-15582.
- Wang, Y., Feng, Z., Yang, S.-Z., Gagnon, C., Gariépy, V., Laul, D., Zhu, W., Veillette, R., Trudeau, M.L., Guerfi, A. and Zaghlib, K. (2018). Layered oxides-LiNi_{1/3}Co_{1/3}Mn_{1/3}O₂ as anode electrode for symmetric rechargeable lithium-ion batteries. *Journal of Power Sources*, 378, 516-521.
- Wang, Y., Zhao, L., Zhan, W., Chen, Y., and Chen, M. (2024). Flame retardant composite phase change materials with MXene for lithium-ion battery thermal management systems. *Journal of Energy Storage*, 86, 111293.
- Weng, J., Ouyang, D., Yang, X., Chen, M., Zhang, G., and Wang, J. (2020). Optimization of the internal fin in a phase-change-material module for battery thermal management. *Applied Thermal Engineering*, 167, 114698.
- Wu, H., and Ou, H. (2023). Research Progress and Prospect of Thermal Management of Automotive Lithium-ion Batteries. *International Journal of Energy*, 3(1), 40-43.
- Xie, N., Zhang, Y., Liu, X., Luo, R., Liu, Y., and Ma, C. (2023). Thermal performance and structural optimization of a hybrid thermal management system based on MHPA/PCM/liquid cooling for lithium-ion battery. *Applied Thermal Engineering*, 235, 121341.
- Xin, Q., Xiao, J., Yang, T., Zhang, H., and Long, X. (2022). Thermal management of lithium-ion batteries under high ambient temperature and rapid discharging using composite PCM and liquid cooling. *Applied Thermal Engineering*, 210, 118230.
- Xin, Q., Yang, T., Zhang, H., Yang, J., Zeng, J., and Xiao, J. (2023). Experimental and numerical study of lithium-ion battery thermal management system using composite phase change material and liquid cooling. *Journal of Energy Storage*, 71, 108003.

- Yang, G., Yim, Y.J., Lee, J.W., Heo, Y.J., and Park, S.J. (2019). Carbon-Filled Organic Phase-Change Materials for Thermal Energy Storage: A Review. *Molecules*, 24(11), 2055.
- Zhang, G., Sun, Y., Wu, C., Yan, X., Zhao, W., and Peng, C. (2023). Low-cost and highly thermally conductive lauric acid–paraffin–expanded graphite multifunctional composite phase change materials for quenching thermal runaway of lithium-ion battery. *Energy Reports*, 9, 2538-2547.
- Zhang, J., Liu, Q., Yao, X., Sun, C., Zhu, X., Xu, C., and Ju, X. (2024). Passive battery thermal management and thermal safety protection based on hydrated salt composite phase change materials. *Energy Storage and Saving*.
- Zhang, S., Zhao, R., Liu, J., and Gu, J. (2014). Investigation on a hydrogel based passive thermal management system for lithium ion batteries. *Energy*, 68, 854-861.
- Zhi, M., Fan, R., Zheng, L., Yue, S., Pan, Z., Sun, Q., and Liu, Q. (2024). Experimental investigation on hydrated salt phase change material for lithium-ion battery thermal management and thermal runaway mitigation. *Energy*, 307, 132685.

CHAPTER 2

**EPIGENETIC VARIATIONS IN PLANTS GROWING IN
EXTREME HABITATS**

Exp. Bio. Fatma M. A. ISMIEL¹ &
Assoc. Prof. Dr. Ayşenur KAYABAŞ AVŞAR²

DOI: <https://dx.doi.org/10.5281/zenodo.14258625>

¹Çankırı Karatekin University, Institute of Graduate Studies, Biology Department Çankırı, TÜRKİYE. fatma.m.a.k.54@gmail.com, Orcid ID: 0009-0007-8720-4741

²Çankırı Karatekin University, Faculty of Science, Biology Department Çankırı, TÜRKİYE. aysenurkayabas@karatekin.edu.tr, Orcid ID: 0000-0003-3555-4399

INTRODUCTION

Extreme habitat can be defined as a habitat where it has a negative impact on plant growth. Extreme habitats have a range of soil types and substrates, but plant growth is always limited by water. Consequently, the primary cause of reduced productivity in extreme habitats is water stress. This contrasts with the situation in some temperate and tropical ecosystems where light limitation is the primary cause of reduced productivity.

Widespread environmental changes and habitat destruction worldwide make it necessary to understand the potential of epigenetic change as a tool for plant survival and to predict future evolutionary trajectories.

To understand the evolutionary potential of epigenetic differences in natural environments, it is imperative to understand their regional and habitat-specific nature. This is because epigenetic changes may differ in different environments, and to understand the effects of epigenetic change, it is necessary to compare plants growing in contrasting environments. Since this result in epigenetic change often being upregulated as a rapid response to environmental stress, extreme habitats are the most suitable places to study epigenetic variation.

This is linked to the importance of extreme habitats in plant adaptation, as it is hypothesized that plants exposed to severe environmental stress may have undergone genetic and epigenetic changes as a measure to survive and reproduce. This could ultimately lead to an evolutionary change in species and possibly speciation. Epigenetic changes can produce different phenotypes from the same genotype. Many recent studies have pointed out that epigenetic changes produced in plants can cause the same plant to grow differently under different environmental conditions. Since changes in DNA methylation and histone modifications are reversible and can create variation in phenotype, they provide plants with a potential mechanism to adapt to environmental changes (Angers et al., 2020).

Continuous signals from the changing environment can elicit changes in gene expression, and these changes can be stored as epigenetic memory, which can enable a more rapid response to events

that have already occurred. Epigenetic memory is the most important event that can determine the growth of the same plant in different environments. For example, in *Arabidopsis thaliana*, the FLC (Flowering Locus C) gene has two methylation patterns at cytosine residues and histone modification states. In an inductive environment, these modifications cause blocking of FLC and gradual degradation of the protein in an autonomous pathway and activation of the flowering transition, whereas in a non-inductive environment, FLC continuously blocks the flowering transition (Hofmeister et al., 2017).

Annual plants with the same genotype may have to delay flowering due to such epigenetic determination of gene expression. Over 1-2 generations, plants growing in the same environment may result in the selection of some more adapted genotypes from the same gene pool. Due to the proximity of epigenetic changes with gene expression changes, it is quite possible to obtain a newly adapted genotype from the same gene pool.

The importance of studying epigenetic variation in plants lies in the fact that it is a way for the plant to respond to environmental stimuli and can be a mechanism for faster evolution. Epigenetic changes can be reversible or become permanent in DNA and, therefore can have important implications for the adaptation of plants that thrive in extreme conditions (Ashapkin et al., 2020).

Epigenetic variation in plants growing in extreme habitats is a fascinating and complex area of study that is receiving increasing attention from researchers in the field of plant biology. Plants have developed various strategies to adapt and evolve. One of these strategies involves inherited epigenetic changes. The other is the study of changes in gene expression or cellular phenotype caused by mechanisms other than changes in the underlying DNA sequence. In plants, in general, epigenetic mechanisms can play an important role in how they adapt to extreme environmental conditions.

Epigenetic variation allows plants to adapt and thrive in their specific habitats by regulating gene expression in response to environmental cues and allowing plants to adjust their growth and

development to cope with the challenges presented by their environment.

One of the most important advantages of epigenetic changes is that plants can change their gene expression and dynamically adapt to the environment. Thus, offspring can grow in the same environment in which their ancestors lived and produce the same phenotype, unlike genetic mutations that can take generations to accumulate, this flexibility allows plants to rapidly adjust their gene expression patterns to maximize their chances of survival in harsh environments. Furthermore, epigenetic variation in plants growing in extreme habitats can have important implications for conservation efforts and ecosystem restoration.

Plants have evolved sophisticated systems to replicate and adapt to various stimuli. These systems regulate on different time scales, from instantaneous metabolic and physiological reactions to long-term changes in genes and epigenetics. Theories of epigenetic variation generally agree on how to interpret phenotypic patterns and changes in organisms without affecting the sequences of genetic material.

Epigenetics plays a decisive role in plant evolution and ecological adaptation; it increases a plant's resistance to harsh environmental conditions by influencing variance in growth, morphology, and plasticity. While genetic variation involves changes in DNA sequences, epigenetic control regulates gene expression based on environmental cues without altering the actual genetic sequence. Epigenetic agents act as a link between environmental and genetic factors. Studies of epigenetic variation in plants include the ability to adapt to the environment expressed by morphological traits, the effects of heterogeneous environments on gene expression and the effects of extreme habitats on plant communities.

Definition of Epigenetics

Epigenetics is mainly used to describe changes that affect the phenotype but are not encoded in gene DNA. Such non-genetic effects on phenotypic variation can encompass many traits, including morphological, behavioral and biochemical traits. The complexity of

the effects and the diversity of different mechanisms by which gene expression can be affected have led to an increasing number of descriptions of epigenetics, some of which are the study of differences in organisms caused by changes in gene expression rather than changes in the genetic code itself. This contrasts with the molecular definition, which states that epigenetic changes are changes that can be inherited mitotically and/or meiotically. The difference in these definitions reflects the diversity found in epigenetic mechanisms and the history of studies in this field.

Epigenetics is a stably inherited phenotype resulting from changes in a chromosome without a change in the DNA sequence, these changes can persist for the rest of the cell's life through cell division and can persist for several generations. However, there is no change in the organism's underlying DNA sequence; instead, the expression of the gene changes.

Epigenetic variation is the change in gene expression caused by modification in chromosomal genes. Unlike variation caused by DNA sequence mutation and recombination, epigenetic variation is potentially reversible and does not depend on changes in the gene, so it may or may not affect phenotypic traits. Although epigenetic variation is genetically based, it does not involve changes in the genetic code, so the effect of an epigenetic variant on a phenotype may be quite small. Depending on this, it may or may not be expressed.

Epigenetic variation is a growing field in molecular biology as well as ecological and evolutionary research, and is a subset of 'environmental genetics', which studies the somatic effects of the environment on genetic effects over generations. There are several levels of epigenetic variation that increase complexity. These are categorized as those targeting DNA, RNA, or protein.

Changes in DNA can take the form of direct methylation of DNA, the addition of a methyl group to cytosine or, more rarely, adenine nucleotides, or may involve modification of the histone proteins around which DNA is wrapped. Methylation often acts to repress gene expression and is often associated with transposons and pseudogenes, so altered methylation of this species may promote

alternative adaptive traits in a population (Flores et al., 2013; Howie et al., 2019).

Methylation can also regulate repressed genes, which can lead to a positive or negative selectable trait (e.g. seed size) depending on the methylated state of the gene. Histone modification is diverse and can affect gene expression in genes with different functions. Finally, there is evidence for gene conversion and recombination of methylated and unmethylated alleles, suggesting that methylation may aid short-term selection of advantageous traits (Brukhin, 2020).

A more complex example of epigenetic variation at the DNA level occurs in *Luzula nivea*, which has a holocentric chromosomal structure and partial endoreplication. This results in a range of chromosome numbers for a single genotype. In general, increased methylation can help plants conserve water and survive in arid conditions. Similarly, plants grown at high altitudes may show changes in histone modifications that allow them to thrive in low-oxygen environments. These epigenetic changes may help regulate the expression of genes involved in oxygen transport and metabolism, allowing plants to adapt to their harsh environment (Law and Jacobsen, 2010).

Differences in the karyotypic structure of species distributed in habitats at different altitudes are thought to be an adaptive response, possibly through a frequency-dependent selection of different karyotypes. A higher chromosome number significantly affects the ability of the plant, which is predominantly distributed in alpine areas, to compete with bryophytes and other higher habitat flora. This is an interesting and complex situation because chromosomal variation is assumed to occur as a one-time genetic mutation, whereas epigenetic variation allows for potential reversibility and environment-specific expression of the trait.

Some of the theoretical and conceptual ideas to control genetics in plants include gene dosage compensation, nuclear dominance, genomic imprinting, and gene silencing.

Definition of Extreme Habitats

An extreme habitat is usually characterized by a factor that is above or below the normal range for an interior habitat, and therefore, other environmental factors operate within their normal range. Extreme habitats can occur naturally or because of human activity, such as when an area becomes so polluted that it can no longer support normal biological processes. However, areas of heavy metal pollution can be considered extreme habitats, and within this category, there are a range of pollution levels that will support plant life to varying degrees. This allows comparison of plant responses to different levels/types of heavy metal pollution.

Extreme conditions included in extreme habitats for plants:

-Extreme temperatures: Plant growth, development and survival can be profoundly affected in habitats with extremely high or low temperatures, such as deserts, polar regions, or high-altitude areas. Plants in these environments must withstand extreme temperatures that can exceed the optimal range for plant growth. Therefore, both hot and cold temperatures can stress plants in a variety of ways:

-Limited water availability: Plants in arid or semi-arid habitats with low rainfall or high evaporation rates, such as deserts or saline environments, face water scarcity and must adapt to drought conditions. Limited water availability, known as drought stress, is a major challenge for plants because water is essential for various physiological processes. Limited water causes problems in plants such as reduced photosynthesis, wilting and leaf curling, cellular damage, reduced nutrient uptake, stunted growth and yield loss, physiological adaptations, and drought tolerance etc.

-High salinity: This occurs when salt-affected habitats or areas with high soil salt concentrations, such as salt marshes, coastal areas, or alkaline soils, exceed levels that most plants can tolerate. Plants in these environments must tolerate high levels of salt in soil or water that can disrupt normal plant functions. There are some effects on plants, such as osmotic stress, ion toxicity, nutrient imbalance, reduced growth and yield, oxygen deprivation, and physiological adaptations.

-Low nutrient availability: Plants in habitats with low soil fertility or nutrient-deficient habitats, such as nutrient-poor soils or rocky terrain not easily accessible to plant roots, must adapt to thrive with limited access to essential nutrients. These results in several effects on plants, such as stunted growth, yellowing of leaves (chlorosis), reduced photosynthesis, poor flowering and fruit set, increased susceptibility to stress, altered nutrient uptake and transport, and specific symptoms.

-High radiation levels: Plants in habitats with high levels of solar radiation, such as high-altitude areas or polar regions with reduced ozone protection, may face an increased risk of DNA damage and should have protection mechanisms against radiation-induced stress. These include sunburn and photoinhibition, leaf damage and tissue necrosis, reduced photosynthetic efficiency, heat stress, water loss and dehydration, protective mechanisms and acclimation and adaptation.

-Excessive pH levels: Extreme pH levels can significantly affect plant growth and health. Most plants prefer a pH level within a certain range, typically between 6 and 7, slightly acidic to neutral. Plants in these environments must tolerate extreme pH levels that can affect nutrient availability and soil chemistry. However, some plants have adapted to thrive in more acidic or alkaline conditions. Extreme pH levels can have effects on acidic soil (low pH), alkaline soil (high pH), extreme pH tolerance and microorganisms.

Strong winds or extreme weather events: Habitats prone to strong winds or severe weather events, such as coastal areas or mountain slopes, can have significant impacts on plant growth, health and even survival (physical damage, desiccation, soil erosion, stress, and growth reduction).

Plants adapted to extreme habitats often possess specialized traits and mechanisms that enable them to survive and thrive under such harsh conditions. These adaptations can include morphological features such as reduced leaf size, deep root systems and specialized structures for storing water. For example, researchers have found that plants

growing in deserts often exhibit higher levels of DNA methylation in certain genes involved in stress response pathways.

Importance of Studying Epigenetic Variation in Plants

Studying cultivated plants has provided us with a large amount of information about epigenetic diversity and its function in plant adaptation. Analyses of the transposable RNA element in paramutation have revealed evidence that environmentally induced changes in DNA methylation can affect gene expression. Studies have revealed that the relationship between DNA methylation and gene expression can be quite complex, with induced methylation being associated with both transcriptional silencing and activation (Foust et al., 2016).

According to Srikant et al., (2019), recurrent selection in cultivated plants can also result in methylation changes and phenotypic changes that may be caused by epigenetic mechanisms. The maize plant is known to be an important plant species where research on exotic hybrids has shown a wide diversity in both gene expression and DNA methylation. These species demonstrate the potential to artificially select for specific epigenotypes and show that epialleles can be influenced by natural selection and affect the fitness of an organism.

Since epigenetic diversity underpins the capacity of plants to thrive in diverse environments and withstand drastic environmental changes, this adaptive capacity is particularly important for plants under biotic and abiotic stress. The power of these species to adapt to seasonal changes and unpredictable attacks is crucial. Environmental stress can kill cells or organisms if left untreated. Plants, like all living organisms, have genes that determine their characteristics, including their physical appearance, growth patterns and responses to environmental factors.

Like all living organisms, plants have genes that determine their characteristics, including their physical appearance, growth patterns and responses to environmental factors. The genetic background of a plant species is shaped by various factors such as natural selection, genetic mutations, and genetic recombination. Over time, these

processes lead to genetic diversity in plant populations and contribute to the adaptation and evolution of plants.

Heritable diversity is traditionally thought to be the result of changes in the base pair sequence of DNA, and there is evidence that epigenetic mechanisms may play a critical role. Phenotypic traits can be stably inherited across generations in the absence of changes in the DNA sequence. Some of the intergenerational effects are due to DNA methylation and chromatin modifications that respond to changes in the environment.

Such environmentally induced epigenetic change may be particularly important in determining the phenotype of a plant and its suitability for variable or extreme environments. Since epigenetic changes are reversible and often do not involve changes in DNA sequence, they may provide a mechanism for phenotypic flexibility that can be influenced by natural selection. Therefore, understanding epigenetic variation and its role in plant fitness and adaptation is becoming increasingly important.

Epigenetic variation has become a topic of great interest in modern plant biology. It has long been known that various environmental factors can affect gene expression, that these changes can be heritable, and that the mechanisms are mediated through changes in DNA methylation, histone modification, and other chromatin-based mechanisms (Duarte-Aké et al., 2023). However, the extent to which such environmentally induced changes affect genetic diversity, phenotypic plasticity and adaptation is only beginning to be understood. Recent studies suggest that epigenetic variation may be heritable and contribute to heritable phenotypic differences on which natural selection may act. In this case, epigenetic changes may be like genetic changes, in some cases more frequent and therefore a more abundant source of variation for selection.

There is much speculation about the relative importance of genetic and epigenetic changes in evolution, and some researchers propose opposing theories about the role of epigenetic change. The answer can only come from investigating the extent and maintenance of

epigenetic variation in both natural and experimental populations, as well as its phenotypic effects and fitness consequences.

The Importance of Studying Plants in Extreme Habitats

Although much has been learnt about the effects of climate change on plant communities, predictions of future changes in the distribution of species are not well known. This is because the distribution of many species also depends on their interactions with other organisms. Symbiotic associations involving plant roots and soil organisms such as mycorrhizae or nitrogen fixers influence the adaptation of plants to adverse environmental conditions. These associations can be highly specialized for certain soil types or even for certain plant species. Such symbioses can prevent the establishment of exotic plant species in an area and thus prevent range shifts of native species. This can lead to the decline or extinction of native species, which are widely competed by exotic species, and the establishment of weedy communities. Therefore, predicting future changes in the composition and structure of plant communities due to climate change will require a better understanding of such below-ground interactions.

Experiments simulating climate change have shown that changes in the frequency and timing of germination or flowering due to climate change, as well as increased drought conditions in the Mediterranean, in savannas in the southern United States and in African deserts, may push some species to germinate after the favorable period.

Plants are grown in different habitats that embrace different environmental factors such as radiation, temperature, water, and nutrient availability, which can create different selective pressures that have the potential to leave different epigenetic marks on plant genomes. The study of these epigenetic changes can provide a better understanding of the genetic changes at the molecular level that allow the plant to adapt to the environment. Anthropogenic climate change is observed in many biomes today, and the pace of this change is very rapid compared to the rate at which plants adapt or disperse.

Stressful environments can lead to polymorphism and phenotypic variation but not always to DNA mutation. An extreme selective

pressure can cause an abrupt change in the gene frequency of a particular genotype at a given locus, which is termed selective sweep.

According to Qiu et al., (2021), if the environment causes a change in the phenotype of a genotype, modification of DNA or methylation of genes, it is possible that the change is beneficial for the plant, and this epigenetic change can lead to an increase in fitness over time by increasing the phenotypic plasticity of a genotype that is selectable. This change in gene expression and plasticity may have important evolutionary consequences for plant species.

Elucidating the epigenetic mechanisms of environmental adaptation provides a better understanding of the process of natural selection, whereby an environment alters allele frequencies and selects the most favorable phenotype. The epigenotype of a plant represents the sum of heritable and environmentally induced epigenetic variation, and the ability of a plant to translate its genotype into the correct phenotype depends on the match between its environment and the environmentally sensitive component of its epigenotype.

Adaptation of plant populations to habitat conditions is a fundamental process in evolutionary biology. Over time, plants undergo genetic changes that enable them to survive and reproduce more successfully in their environment. This process is driven by natural selection, where individuals with traits that are advantageous in their habitat have a higher chance of passing on their genes to the next generation. This suggests that epigenetic mechanisms can contribute significantly to the adaptive potential of plant individuals in natural populations, and several studies have found evidence of habitat- or environment-specific epigenetic differences among populations (Pagel et al., 2020).

Extreme habitats often represent a strong selection pressure and, therefore, plants growing in such habitats are often well adapted to certain stresses and are unlikely to grow elsewhere. Several specific plant adaptations to extreme environments have been identified, and many of these are likely to involve epigenetic variation. According to Yaish, (2017), epigenetic mechanisms play an important role in plant

adaptation to stressful environments. Several characteristics of extreme habitats influence the epigenome.

Many of the defense components are controlled by stress-sensitive traits by translating and deciphering specific attributes. It has been described in detail that some changes in DNA and chromatin, as well as small RNA-based components, direct the expression of stress-sensitive traits and constitute another line of defense in the battle of plants against stresses. It is known that the means of stress tolerance derived from hereditary cosmetics, as well as the severity and length of stress, differ among plant species. Transformations in DNA groupings cause characteristic contrasts, and it is vital that plants can keep in mind and learn from the situations they encounter, making them highly versatile to their situation.

These changes are made by modifications in chromatin structure, such as DM, histone modifications (HM) and non-coding RNAs. Step by step, they involve changes in the structure of DNA or related proteins that can affect quality action. These adjustments can be constant and can be transferred to subsequent periods.

Empirical evidence has shown that transgenerational epigenetic inheritance can promote or inhibit the rate of adaptation of a population. Epigenetic modifications can sometimes be passed on to the next generation, often retained in such a way as to lead to transgenerational effects on the phenotype. This phenomenon has been observed in plants exposed to stress; offspring of stressed plants may exhibit enhanced stress tolerance due to inherited epigenetic modifications (Bilichak and Kovalchuk, 2016). Overall, epigenetics is a key component of how many plant species can thrive in the most challenging environments on Earth.

In the current era of rapid environmental change, there is a critical need to better understand the evolutionary antecedent of phenotypic versatility and adaptation, as well as the capacity of populations to survive and thrive under the new conditions they are increasingly discovering for themselves. By elucidating the epigenetic mechanisms underlying the adaptation of plants to extreme environments, researchers can potentially identify targets for the

cultivation of more resilient crops or the conservation of endangered plant species facing environmental challenges.

In the plant kingdom, epigenetic inheritance occurs in two ways: The exchange of non-coded data in DNA between periods and the maintenance of epigenetic adjustments within an individual that are reset between periods. Subsequently, epigenetic components are thought to significantly influence how plants connect with abiotic components. Plants have evolved different defense components, counting morphological adjustments, cellular pathways, specific marking particles and innate resistance, to withstand different abiotic stresses at different developmental stages.

Climate change has devastating effects on plant development and productivity. Abiotic stresses are the primary type of stress faced by plants. The most tedious current required to obtain plant reactions under different abiotic conditions is to search for hereditary precursors that are fundamental for these mechanisms. Plants with great natural variability rely on different climatic conditions that restrict in various ways the capacity of plants to adapt effectively. The aim here is to investigate that there are different reasons why a few plants change phenotypes while others do not; there may be several stochasticity, such as the probability of methylation of a given site may be less than 1 given the environmental stimulus, the micro-heterogeneity of the environmental stimulus may be heritable contrasts between humans that affect the accessibility of sites that may undergo methylation at a given site. However, while phenotypic variation is not necessarily multidirectional in the environment, the phenotypic diversity mobilized may provide the opportunity for stability to mobilize.

If the change in methylation is transmitted from generation to generation (intergenerational versatility), modern epimutation can spread through the population and versatile progression can occur in the absence of heritable change.

Factors Affecting Epigenetic Diversity

-Developmental stages: Epigenetic patterns can change at different developmental stages of a plant such as seed germination,

seedling growth, flowering, and senescence. This is thought to be a mechanism that regulates gene expression during plant development.

-Environmental factors: Environmental cues such as temperature, light, nutrient availability, drought, and pathogen exposure can trigger epigenetic changes in plants. These changes can help plants adapt to their environment.

-Transferable elements: Transposable elements (TEs), also known as 'jumping genes', can induce epigenetic changes such as DNA methylation and histone modifications as a defense mechanism to suppress TE activity and maintain genome stability.

-Stress responses: Plants can undergo epigenetic modifications in response to biotic (e.g. pathogens) and abiotic (e.g. drought, salinity) stresses. These epigenetic modifications can help plants adapt and respond to stressful conditions.

-Genetic factors: Genetic variation such as single nucleotide polymorphisms (SNPs) and insertions/deletions (indels) can lead to heritable epigenetic variation by affecting the formation and maintenance of epigenetic marks.

-Chromatin remodeling: Chromatin remodeling complexes can alter the accessibility of DNA to transcription factors and other regulatory proteins, which can lead to epigenetic changes and alterations in gene expression.

-Intergenerational inheritance: Some epigenetic modifications can be transmitted across generations and lead to inherited epigenetic variation. This phenomenon is known as transgenerational epigenetic inheritance.

-Reproductive processes: Epigenetic changes can occur during gametogenesis (the formation of gametes) and embryogenesis, which can contribute to epigenetic variation in offspring.

It is important to note that these factors can interact with each other, leading to complex patterns of epigenetic variation in plants. Understanding the mechanisms underlying epigenetic regulation is an active area of research in plant biology and has implications for crop improvement, environmental adaptation, and evolutionary processes.

Types of Epigenetic Markers

An epigenetic marker refers to a specific chemical modification that can be detected in DNA or chromatin and is associated with changes in gene expression without altering the underlying DNA sequence.

1. DNA Methylation Modification

DNA methylation modification is a system that can study ADN replication and epigenetic phenomena in plants. Flowering plants do not undergo the systematic genome-wide demethylation that occurs in mammals.

Methylation of DNA may be the primary epigenetic mark reliably transmitted. Chromatin changes investigated in epigenetics include DNA methylation, chemical compounds bound to histone proteins, and other RNA-dependent mechanisms that affect chromatin structure without altering the underlying genetic code (Kim and Costello, 2017).

As noted by Richard et al., (2021), DNA methylation is thought to be the most studied mechanism to date, as histones are protein substances that bind DNA and form chromatin nucleosomes in the cells of higher organisms. This is because the second histone modification is linked to the first mechanism. Gene activity: genome architecture, stability and assembly are affected by DNA methylation on cytosine. In addition, genetic silencing has different functions and manifestations that occur during meristematic cell development and for everyone. In extreme environments, DNA methylation patterns can change in response to environmental stressors, leading to changes in gene expression that enhance stress tolerance.

2. Histone Modification

Covalent post-translational modifications of histone proteins, such as acetylation, methylation, phosphorylation, ubiquitination and SUMOylation, occur mostly at methylated cytosine by DNA methylation. Histone proteins help package DNA into chromatin and modifications to histones can lead to changes in gene expression by altering chromatin structure and accessibility. Modifications to histones

are diverse and covalent. Their centrality is called the histone code. The changes take place in the histone tails, the amino inclusions of the protein, showing disdain for the fact that a few of them can occur in the center, i.e. in the carboxylic result, but only to an exceptional degree. Studies on different plant species have revealed that histone modifications play a fundamental role in plant development and plant defense components (Kang et al., 2022).

Examination of different changes in plants and genome-wide histone modifications has revealed that one histone modification may be linked to other histone modifications or DNA methylation. This epigenetic mechanism acts as a defense mechanism in living organisms, helping to protect the genome from damage and the genetic structure of the species during development. As discussed earlier, histone mutations and DNA methylation are two factors that contribute to epigenesis. Heterochromatin is defined as chromatin that is compacted, regardless of whether methylation is present or not. Gene silencing usually occurs when chromatin is compacted, and heterochromatin becomes inactive, but it can also occur after methylation.

3. RNA-Based Control Mechanisms

Small interfering RNAs (siRNAs), microRNAs (miRNAs) and long non-coding RNAs (lncRNAs) can regulate gene expression post-transcriptionally. RNA-based control mechanisms are related to the formation of RNAi molecules that form complexes, spread throughout the cell, and begin to regulate various gene activity activities. These activities may include inhibiting the replication of genes or removing some important proteins and other molecules from the genome. This is complementary to the function of sRNA (Zhang et al., 2018).

Non-coding RNA particles (ncRNA) and their associated proteins are actively involved in epigenetic control. The first event assisted by RNA splicing is the inactivation of the hereditary chromosome (XCI). The jarring effects in this process are the dysregulation of alternative splicing before RNA and during the processing of RNA particles to

alter the spatial chromatin structure by reducing the messages used or providing interpretable mRNA messages.

These particles have unique beginnings. As with microRNA (miRNA) particles, they can have their own claim attributes. These non-coding atoms vary in type, length, and capacity. Non-coding RNA particles and their associated proteins are actively involved in epigenetic control. These mechanisms are interdependent and do not work independently of each other.

Epigenetic variation in plants is likely to play an important role in enhancing resistance in response to changing environments. Environmental changes can cause epigenetic modifications, leading to short-term plasticity and long-term adaptations. Some of these variations are heritable, contributing to stress memory and better responses to repeated challenges.

Stable epigenetic changes create diversity and stability in plant populations. Recent studies using advanced technologies have shed light on how plants respond to various ecological factors, ultimately improving our understanding of plant adaptability in dynamic environments. In this way, researchers can gain valuable insights into how plants adapt to extreme conditions and develop strategies to increase crop resilience of endangered species and restore ecosystems disrupted by climate change.

Epigenetic mechanisms provide an additional layer of phenotypic flexibility beyond genetic variation. They allow plants to adjust their physiology, growth, and defense mechanisms to harsh conditions without the need for permanent genetic mutations (Yaish et al., 2023).

Phenotypic Versatility

Epigenetic variability has been proposed to refer to the range of observable traits or characteristics that can be expressed by an individual or a population of organisms. This variability results from the interaction between an organism's genotype (its genetic makeup) and the environment it experiences (Eichten et al., 2020).

Most theories of epigenetic variation agree on how phenotypic patterns and changes occurring in an organism should be interpreted

without affecting the sequences of genetic material. It is becoming increasingly important in the field of plant research, as it greatly influences variability in plant growth, morphology, and plasticity. The capacity of plants to adapt to changing environments critically depends on epigenetic variation.

Research in plant ecology is currently focusing on the roles epigenetic phenotypic changes play in adaptation and development, as well as whether these changes are beneficial in the environment and whether they are affected by natural selection.

Plants experiencing epigenetic changes can show phenotypic plasticity, which aids their ability to adapt to harsh environments such as salt, drought, and temperature changes. In other words, adaptation is the handling of invariant changes in plant digestive system and phenotype in response to a changing environment and is monitored in a whole plant population.

This adaptation is the handling of change in response to changes in the environment and allows individual plants to maintain health and maintain/complete their formative preparation. Some researchers consider the legacy of this reaction as intergenerational acclimatization, also called phenotypic versatility (Boyko and Kovalchuk, 2008).

Some important points about phenotypic variability:

-Genotypic variation: Differences in the genetic make-up of individuals can lead to variations in their potential to express different phenotypes. These differences are primarily the result of genetic mutations, recombination during sexual reproduction and gene flow between populations. Genotypic variation underpins the diversity observed in plant populations, allowing them to adapt to various environmental conditions and evolving challenges.

-Environmental influences: Environmental influences play a crucial role in shaping the growth, development, and physiology of plants. These influences cover a wide range of factors, including abiotic (non-living) and biotic (living) components of the environment. Environmental factors such as temperature, nutrition, light, and

stressors can influence the way genes are expressed, leading to different phenotypes even among genetically similar organisms.

-Developmental plasticity: Many organisms can alter their development and physiology in response to environmental cues, leading to different phenotypes. This flexibility enables plants to adapt to changing environmental conditions and optimize their chances of survival and reproduction.

-Epigenetic mechanisms: Changes in gene expression that do not involve changes in DNA sequence, such as DNA methylation and histone modifications, can contribute to phenotypic variability.

-Phenotypic plasticity: Some organisms can reversibly change their phenotype in response to changing environmental conditions, allowing them to adapt and thrive in different environments.

Yet, there is no concrete evidence linking the phenotypic plasticity of plants grown in various environments or under various pressures to epigenetic modifications (Gallusci et al., 2017). It has been proposed that phenotypic plasticity results from changes in gene expression regulated by markers. Epigenetics, therefore, the ability of plants to respond to stress factors and adapt to their environment critically depends on epigenetic diversity (Abdulraheem et al., 2024).

CONCLUSION

Epigenetic variations are an important adaptation mechanism that organisms can use to adapt to environmental stresses. It can also be defined as changes outside the DNA sequence that affect gene expression of organisms. Plants tend to use epigenetic changes to rapidly adapt to changing environmental conditions (Law and Jacobsen, 2010; Thiebaut et al., 2019).

Plants growing under extreme conditions may be exposed to various stress factors such as drought, salinity, and high or low temperature. Under these conditions, plants often adapt to survive and reproduce by making changes in gene expression and phenotype. One way to do this is through epigenetic variations. Epigenetic variations can play an important role in this adaptation process because they can

respond quickly to environmental stresses (Zhang et al., 2018; Boquete and Alonso, 2021).

Epigenetic variations are associated with changes in gene expression without changes in DNA sequence. Mechanisms such as DNA methylation, histone modifications and changes in chromatin structure play an important role in the formation of epigenetic variations. Under extreme conditions, changes in the activity of these mechanisms may occur, helping plants to adapt to environmental stresses (Boyko and Kovalchuk, 2011).

Epigenetic variations occurring in plants grown in extreme conditions can influence the adaptation process. For example, changes in DNA methylation can increase or decrease the expression of certain genes, thus enabling plants to cope with stress. Similarly, histone modifications can help plants adapt to environmental changes by regulating gene expression.

Epigenetic variations have many important functions, such as enabling plants to adapt to environmental stresses, regulating developmental processes and facilitating evolutionary changes. For example, under environmental stresses, epigenetic variations can enable plants to adapt by altering the expression of specific genes (Bilichak and Kovalchuk, 2016).

In conclusion, epigenetic variations are an important factor shaping the adaptation of plants growing in extreme conditions. However, it is still unclear whether epigenetic variations are persistent and can be transmitted from generation to generation. Further research in this area will help us understand the mechanisms by which plants adapt to environmental stresses.

REFERENCES

- Abdulraheem, M. I., Xiong, Y., Moshood, A. Y., Cadenas-Pliego, G., Zhang, H., and Hu, J. (2024). Mechanisms of plant epigenetic regulation in response to plant stress: Recent discoveries and implications. *Plants*, 13(2): 163.
- Angers, B., Perez, M., Menicucci, T., and Leung, C. (2020). Sources of epigenetic variation and their applications in natural populations. *Evolutionary Applications*, 13(6): 1262-1278.
- Ashapkin, V. V., Kutueva, L. I., Aleksandrushkina, N. I., and Vanyushin, B. F. 2020. Epigenetic mechanisms of plant adaptation to biotic and abiotic stresses. *International Journal of Molecular Sciences*, 21(20): 7457.
- Bilichak, A., and Kovalchuk, I. (2016). Transgenerational response to stress in plants and its application for breeding. *Journal of Experimental Botany*, 67(7): 2081-2092.
- Boquete, M. T., Muyle, A., and Alonso, C. (2021). Plant epigenetics: phenotypic and functional diversity beyond the DNA sequence. *American Journal of Botany*, 108(4), 553-558.
- Boyko, A., and Kovalchuk, I. (2008). Epigenetic control of plant stress response. *Environmental and Molecular Mutagenesis*, 49(1): 61-72.
- Boyko, A., and Kovalchuk, I. (2011). Genome instability and epigenetic modification—heritable responses to environmental stress?. *Current Opinion in Plant Biology*, 14(3), 260-266.
- Brukhin, V. (2020). Epigenetic control in plants. *Epigenomes*, 4(3): 11.
- Duarte-Aké, F., Us-Camas, R., and De-la-Peña, C. (2023). Epigenetic regulation in heterosis and environmental stress: The challenge of producing hybrid epigenomes to face climate change. *Epigenomes*, 7(3): 14.
- Eichten, S. R., Srivastava, A., Reddiex, A. J., Ganguly, D. R., Heussler, A., Streich, J. C., and Borevitz, J. O. (2020). Extending the genotype in *Brachypodium* by including DNA methylation reveals a joint contribution with genetics on adaptive traits. *G3: Genes, Genomes, Genetics*, 10(5): 1629-1637.

- Flores, K. B., Wolschin, F., and Amdam, G. V. (2013). The role of methylation of DNA in environmental adaptation. *Integrative and Comparative Biology*, 53(2): 359-372.
- Foust, C. M., Preite, V., Schrey, A. W., Alvarez, M., Robertson, M. H., Verhoeven, K. J. F., and Richards, C. L. (2016). Genetic and epigenetic differences associated with environmental gradients in replicate populations of two salt marsh perennials. *Molecular Ecology*, 25(8): 1639-1652.
- Gallusci, P., Dai, Z., Génard, M., Gauffretau, A., Leblanc-Fournier, N., Richard-Molard, C., and Brunel-Muguet, S. (2017). Epigenetics for plant improvement: Current knowledge and modeling avenues. *Trends in Plant Science*, 22(7): 610-623.
- Hofmeister, B. T., Lee, K., Rohr, N. A., Hall, D. W., and Schmitz, R. J. (2017). Stable inheritance of DNA methylation allows creation of epigenotype maps and the study of epiallele inheritance patterns in the absence of genetic variation. *Genome Biology*, 18(1): 1-16.
- Howie, H., Rijal, C. M., and Ressler, K. J. (2019). A review of epigenetic contributions to post-traumatic stress disorder. *Dialogues in Clinical Neuroscience*, 21(4): 417-428.
- Kang, H., Fan, T., Wu, J., Zhu, Y., and Shen, W. H. (2022). Histone modification and chromatin remodeling in plant response to pathogens. *Frontiers in Plant Science*, 13(7): 986940.
- Kim, M., and Costello, J. (2017). DNA methylation: an epigenetic mark of cellular memory. *Experimental and Molecular Medicine*, 49(4), e322-e322.
- Law, J. A., and Jacobsen, S. E. (2010). Establishing, maintaining and modifying DNA methylation patterns in plants and animals. *Nature Reviews Genetics*, 11(3): 204-220.
- Pagel, E., Poschlod, P., and Reisch, C. (2020). Habitat matters—Strong genetic and epigenetic differentiation in *Linum catharticum* from dry and wet grasslands. *Ecology and Evolution*, 10(18): 10271-10280.
- Qiu, T., Liu, Z., Yang, Y., and Liu, B. 2021. Epigenetic variation associated with responses to different habitats in the context of

- genetic divergence in *Phragmites australis*. *Ecology and Evolution*, 11(17): 11874-11889.
- Richard, G., Jaquiéry, J., and Le Trionnaire, G. (2021). Contribution of epigenetic mechanisms in the regulation of environmentally-induced polyphenism in insects. *Insects*, 12(7): 649.
- Srikant, T., Wibowo, A., Schwab, R., and Weigel, D. (2019). Position-dependent effects of cytosine methylation on FWA expression in *Arabidopsis thaliana*. *BioRxiv*, 77(4): 281.
- Thiebaut, F., Hemerly, A. S., and Ferreira, P. C. G. (2019). A role for epigenetic regulation in the adaptation and stress responses of non-model plants. *Frontiers in Plant Science*, 10, 246.
- Yaish, M. W. (2017). Epigenetic modifications associated with abiotic and biotic stresses in plants: an implication for understanding plant evolution. *Frontiers in Plant Science*, 8(2): 325961.
- Yaish, M. W., Sunkar, R., Liu, J., and Varotto, S. (2023). Epigenetic modifications associated with abiotic and biotic stresses in plants: An implication for understanding plant evolution, Vol. II. *Frontiers in Plant Science*, 13(8): 1117063.
- Zhang, H., Lang, Z., and Zhu, J. K. (2018). Dynamics and function of DNA methylation in plants. *Nature Reviews Molecular Cell Biology*, 19(8): 489-506.

CHAPTER 3

IMPORTANCE OF METAGENOMIC ANALYSIS IN DETERMINING MICROBIAL BIODIVERSITY

Assist. Prof. Dr. Ebru DERELLİ TÜFEKÇİ¹

DOI: <https://dx.doi.org/10.5281/zenodo.14258654>

¹Çankırı Karatekin University, Food and Agriculture Vocational School, Department of Field Crops, Çankırı, Türkiye. ebru.derelli@gmail.com, Orcid: 0000-0003-1097-8574

INTRODUCTION

Four billion years of evolution have led to today's prokaryotic world. Because of this long evolutionary history, prokaryotic microorganisms represent the largest reservoir of genetic diversity on Earth. Prokaryotes are much older than the other four kingdoms - protists, metazoans, plants and animals - and cover a much larger part of the biosphere. New species are being described every day, making it difficult for taxonomists to estimate the limits of the magnitude of prokaryotic diversity. Biodiversity refers to the diversity in the species (taxon) composition of organisms, the genetic information carried by these organisms and the ecosystems they form. Prokaryotic diversity is one of the largest knowledge gaps in the biological sciences and remains largely unexplored (Rodríguez-Valera, 2004). Various microbial communities such as bacteria, archaea, algae, fungi and protozoa play an important role in the environment and human health; however, knowledge about most microorganisms in the ocean, atmosphere, soil and our bodies is limited, as it is not possible to culture and study all microorganisms using conventional culture methods. Although we cannot see them in general, microorganisms are everywhere in human life and are essential for life all over the world (Davison et al., 2015). For example, the chemical cycles that convert the basic elements of life (carbon, nitrogen, oxygen and sulfur) into biologically accessible forms depend heavily on microorganisms.

All plants and animals are closely associated with microbial communities that create essential nutrients, metals and vitamins for their hosts. Bioremediation of toxins in the environment, both those produced naturally and by-products of human activities such as petroleum and chemical wastes, is carried out by microorganisms. In addition, human intestinal and oral microbiota play an active role in various diseases as well as in the digestive system. As can be seen, microorganisms are of great importance and diversity in the world. Therefore, in-depth knowledge about microorganisms is important for understanding the development and sustainability of life on Earth. Furthermore, microorganisms are being investigated for genetic diversity and are a source for screening new biomolecules.

Microorganisms have larger populations than other living organisms, and their small size and low weight are the main factors in their distribution over all areas of the globe (Faust et al., 2012). Traditionally, the only way to study a microbial community is to isolate microorganisms from their environment and obtain and study their cultures in the laboratory. The process of obtaining these cultures involves first increasing the number of the target organism in the community through a process called enrichment and then isolating it as a pure culture. In an enriched culture, a medium and incubation conditions are created that are selective for desired organisms and/or inhibitory for unwanted organisms. Effective enrichment cultures should be as compatible as possible with the organism's natural niche and natural ecosystem conditions. Another example of traditional methods is pure culture isolation. The aim of this method is to obtain a single strain of microorganism without enrichment or with different types of enrichment (Swingland, 2001).

Traditionally, the only way to study a microbial community is to isolate microorganisms from their environment and obtain and study their cultures in the laboratory. The process of obtaining these cultures involves first increasing the number of the target organism in the community through a process called enrichment and then isolating it as a pure culture. In an enriched culture, a medium and incubation conditions are created that are selective for desired organisms and/or inhibitory for unwanted organisms. Effective enrichment cultures should be as compatible as possible with the organism's natural niche and natural ecosystem conditions. Another example of traditional methods is pure culture isolation. The aim of this method is to obtain a single strain of microorganism without enrichment or with different types of enrichment (Madigan and Martinko, 2005). For many years, culture-based approaches have been applied for the isolation and identification of microorganisms. However, this approach has many shortcomings. Many cultured microorganisms are selected in the laboratory according to the composition of the medium and also the culture conditions, and often do not represent the dominant members of their natural environment and conditions. Therefore, the physiology

and biochemistry of culturable microorganisms provide very limited information about the entire community content and biochemical processes. On the other hand, the development and application of DNA-based molecular methods have overcome the limitations of culture-dependent methods to reveal microbial diversity and composition. A number of approaches such as FISH targeting the 16S rDNA gene, terminal restriction fragment length polymorphism (T-RFLP) and DGGE have been used for microbial community analysis. While these methods clarify differences in the composition of the microbial community between samples, they are insufficient to examine phylogenetic diversity in detail, and thus clone libraries of 16S rRNA gene amplicons have been constructed (Ding et al., 2020). Ecological microbiology study has been transformed in recent years by the use of next-generation sequencing (NGS) technology to microbial communities. This has made it possible to sequence DNA samples on a massive scale without requiring extensive information or costly culturing and cloning.

Fluorescence In Situ Hybridization (FISH)

Fluorescence in situ hybridization (FISH) is based on in situ phylogenetic identification of microbial cells by hybridization of fluorescently coupled oligonucleotide probes. Fluorescence in situ hybridization involves the preparation of two main components: the DNA probe and the target DNA to which the probe will hybridize. Many applications such as detection of repetitive elements and single genes on chromosomes, integration of physical and genetic maps, detection of chromosomal translocations, clarification of phylogenetic relationships, quantification of mRNA transcripts, diagnosis of hematological cancers can be performed with FISH technique. The FISH method with rRNA-targeted probes enables the phylogenetic identification of microbial communities without culturing by means of epifluorescence and confocal laser scanning microscopy or flow cytometry, as well as the examination of their distribution and abundance (Levsky and Singer, 2003).

Denaturing Gradient Gel Electrophoresis (DGGE)

PCR products amplified from DNA extracted using universal primers of the 16S rRNA gene are run on polyacrylamide gel electrophoresis containing DNA denaturant (formamide and urea). This method is based on the fact that the base pairs that make up DNA are separated according to their denaturation temperature (T_m) and migrate differently across the polyacrylamide gel. Sequence differences in DNA fragments cause variations in denaturation temperatures. These sequence differences cause the migration to terminate at different positions in the denaturing gradient gel and thus the separation of each different DNA fragment can be achieved by denaturing gradient gel electrophoresis (DGGE). This method is used in environmental microbiology to track population changes and investigate the ecology of microbial communities. However, evolutionary information can be gained by cutting and sequencing band DNA fragments; this approach does not provide that information. To determine which microbes in a community are numerically dominant, DGGE can be used in conjunction with hybridization or sequencing that makes use of phylogenetic probes (Vincent et al., 2021).

Terminal Restriction Fragment Length Polymorphism (T-RFLP)

Terminal restriction fragment length polymorphism (T-RFLP) is based on DNA sequence variations in 16S rRNA genes amplified by PCR. PCR is performed with fluorescently labeled primers. The PCR products are then digested with restriction enzyme, the fluorescently labeled terminal fragments are separated and detected by high-performance liquid chromatography (HPLC) or DNA sequencing. Microbial diversity is estimated by analyzing the size, number and peak heights of the resulting fragment structures (Fukuda et al., 2016).

16S rRNA Gene

An essential component of protein synthesis, the ribosome is an organelle present in all living cells that combines RNA and protein components. Prokaryotic cells have the 30S ribosomal subunit, which is

the small subunit of the ribosome, and prokaryotic cells have the 50S ribosomal subunit, which is the big subunit. There are one or more rRNAs in each subunit. The 16S rRNA gene produces 16S rRNA, one of the 30S ribosomal subunits that make up the ribosome and are present in all prokaryotic cells (Fukuda et al., 2016). 16S rRNA gene sequencing is widely used for diversity analysis in polymicrobial populations. 16S rRNA is universally present in all prokaryotes and has multiple hyper variable subregions, such as V1-V9, which can be used for the identification of prokaryotes. 16S rRNA gene sequencing is widely used for diversity analysis in polymicrobial populations. 16S rRNA is universally present in all prokaryotes and has multiple hyper variable subregions such as V1-V9 (Figure 1), which can be used for the identification of prokaryotes. Furthermore, along with the hyper variable region, there are conserved regions present in all prokaryotes that allow the design of universal primers to amplify the 16S rRNA gene (Lan et al., 2016; Kamble et al., 2020).

These properties of the 16S rRNA gene have made it an important marker for taxonomic classification, leading to the development of several databases such as the Ribosomal Database Project, Greengenes and SILVA (Larsen et al., 1993; Quast et al., 2012; DeSantis et al., 2006). Furthermore, it is not necessary to sequence the entire 16S rRNA gene for microbial diversity analysis. Individual or a combination of different variable regions can be used for diversity analysis. Comparative studies have been conducted using different variable regions for 16S rRNA region selection. It has been reported that the V3-V5 regions are more frequently used in microbial diversity analysis than the V1-V2 region. In the identification of archaeal sequences, the V1-V4 regions were found to give the best results for microbial richness at the genus level and the V3-V5 region at the family level. For the analysis of bacterial sequences, the V1-V4 regions were reported to give the best results with the least error rate for species-level identification. Furthermore, the region used for sequencing, e.g. the V3-V4 region of 16S rRNA, has been the variable region of choice more often because it gives better results and has a lower error rate compared to V8-V9 (Kim et al., 2011). Due to its

shorter length, the V3 or V4 region is most favored for small-length read technologies such as HiSeq and MiniSeq Illumina platforms using paired-end reads. Furthermore, the V4 region is widely used by the World Microbiome Project for large-scale environmental microbiota research (Thompson et al., 2017).

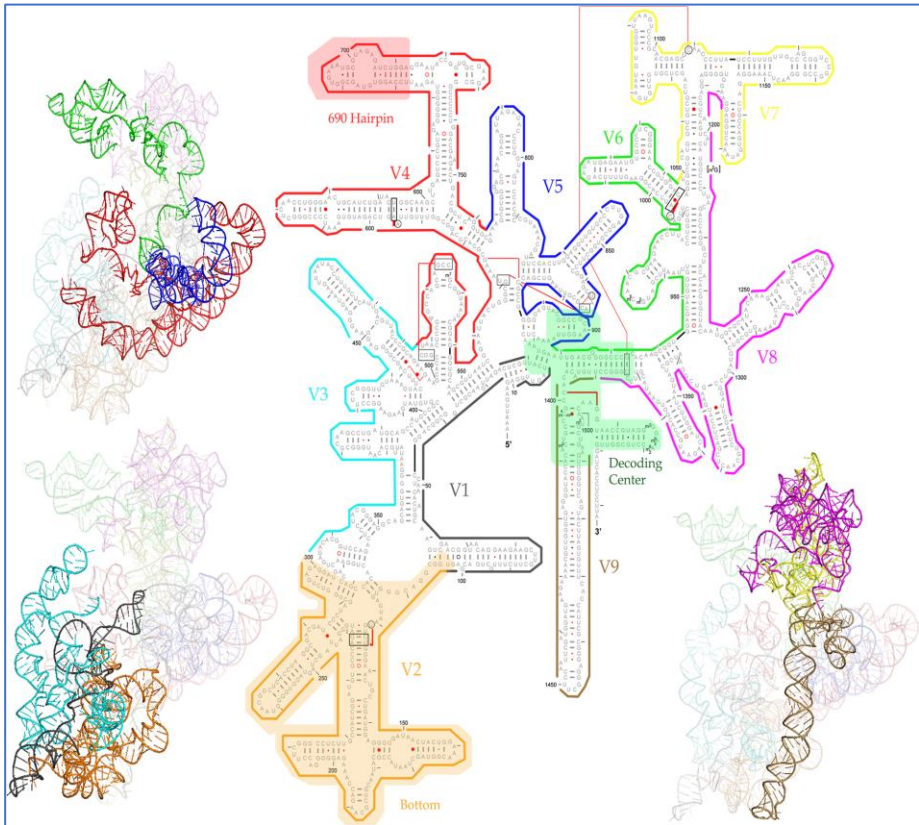


Figure 1. The 16S rRNA gene's 2D and 3D structures. The same hue designates each individual section in the 2D and 3D constructions. A few significant structures are block-colored (Yang et al., 2016)

Genome Sequencing Technologies

One of the biodiversity research methods is whole genome analysis. Whole genome analysis is based on the analysis of a whole genome. Sanger sequencing (Sanger et al., 1977), a method used in this analysis, has been an important method for DNA sequencing technology. The Sanger dideoxy method is based on enzymatic DNA

synthesis and random termination of the synthesized chain with inhibitory nucleotide forms. The DNA strand to be sequenced is the template for the new synthesized strand. The method is based on DNA polymerase using dNTP and ddNTP as substrates. Sanger Sequencing is useful for applications where high throughput is not required. Its most common use is for individual sequencing reactions using a specific DNA primer on a specific template to confirm plasmid constructs or PCR products (Crossley et al., 2020).

Next Generation Sequencing (NGS) is another method of whole genome analysis. Next generation DNA sequencing became widely available in the mid-2000s, moving effectively with advances in computer science and ushering in a revolution in genetic research (Hu et al., 2021). It has made it possible to analyze much larger biological datasets than previously possible. In this method, many sequencing reactions can be run in parallel at the same time, rapidly identifying a large number of sequences in the same time frame.

Many studies used in the determination of microbial biodiversity are now focusing more on using molecular tools and resources (Wensel et al., 2022). For many years, culture-dependent analysis methods have been used to characterize individuals belonging to populations of microbial communities. Although traditional methods are applied to pure cultures to determine the identity of isolates, molecular methods are also frequently applied to these pure cultures. In particular, new methods developed in the last two to three decades have made it possible to directly subject community samples taken from nature to biodiversity (genetic diversity) analysis without any culturing process.

Metagenomics

The term metagenome was first defined in 1998 as “the genomes of the total microbiota found in nature”, the collection of all genomic information of the total microorganisms in a given environment (Handelsman et al., 1998; Simon and Daniel, 2009; Neelakanta and Sultana, 2013). Next-generation sequencing technologies used in metagenomics research enable higher capacity sequencing outputs. The increase in the application of DNA sequencing, which enables more

economical and in-depth sequencing, has made metagenomics a powerful analytical tool. The metagenomics workflow basically consists of 5 steps: experimental workflow, preprocessing, sequencing analysis, post-processing and validation. The most critical step in metagenomic data analysis is the reconstruction of individual genes and genomes of microorganisms in communities using computational programs that assemble small sequence-containing DNA fragments produced by metagenomic approaches and sequencing tools.

The molecular aspect of metagenomic sequencing has triggered the development of computer-based bioinformatics tools available for taxonomic classification, functional identification and visual representation of DNA sequence data (Liu et al., 2021). It is stated that metagenomic analyses can be performed in culture-dependent enrichment studies as well as culture-independent studies and therefore the definition of metagenomics should be kept broad (Figure 2). Designed to provide access to the physiology and genetics of non-culturable organisms, metagenomics, which is the genomic analysis of all or part of a microorganism population or community, is a powerful research method (Handelsman, 2004). Studies of the genomes of individual organisms are limited. First, in order to extract an organism's whole genome, clonal culture is required due to technological limitations. Since only a small portion of naturally occurring microorganisms can be cultivated, the genomic data that are now accessible are extremely inadequate and do not accurately reflect the current condition of microbial species' genomes. Second, species rarely exist in single-species groups and interact with their surroundings, which may include host organisms, as well as with other species. As a result, in terms of organism-to-organism contact, the ensuing population genetic diversity, and biological functions, a clonal culture falls short of accurately representing its natural state (Simon and Daniel, 2009; Wooley et al., 2010).

Metagenomics provides a better understanding of natural community structure and potential functions by eliminating culture-based analysis. Thus, it allows a much more comprehensive investigation of microbial functional genes (Heather and Chain, 2016).

Standard genomic techniques require sequencing of pure cultures, an approach that takes months or even years for culture purification. On the other hand, the metagenomic approach can surpass the laborious techniques of obtaining pure cultures and individual genomes can be successfully extracted from microbial associations. The development of metagenomics shows that microorganisms that have not yet been cultured constitute the vast majority of organisms found in most environments around the world. Metagenomics makes it possible to identify many groups of microorganisms that cannot be cultured. In metagenomic studies, total DNA and/or RNA is isolated and sequenced from a certain microbial community without culture. These metagenome sequences are then compared with previously known sequences to identify known species and discover unknown species (Handelsman, 2004).

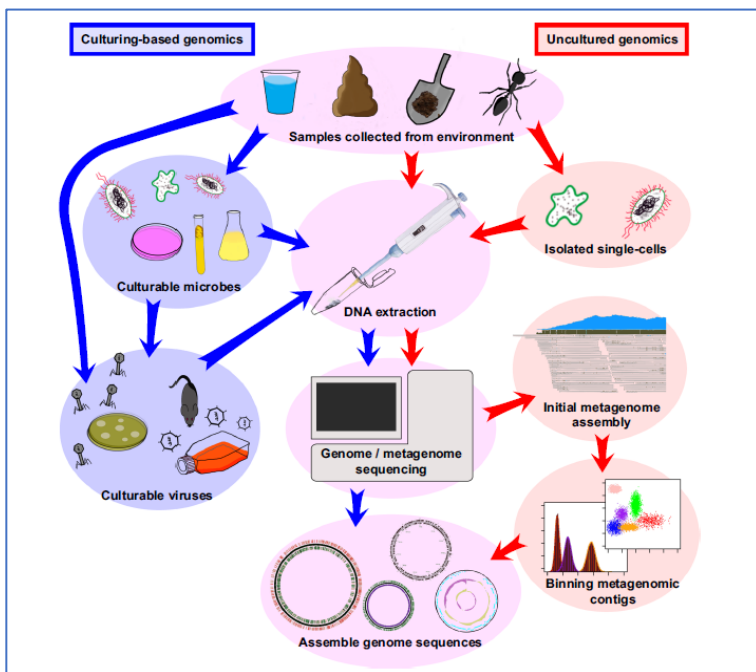


Figure 2. Diagram showing streamlined processes for extracting metagenome sequences from viruses and bacteria, both cultivated and uncultivated. Every protocol has several versions, as do extra procedures (Garza and Dutilh, 2015)

Metagenomics encompasses both sequence-based and function-based approaches. Sequence-based methods investigate the microbial community in a particular habitat or genes encoding new products. The functional metagenomics approach depends on determining the function of the gene product as well as the heterologous expression of the genes responsible for the function (Figure 3). For microbiological analysis using the metagenome, there are two primary strategies that can be used. The examination of the bacterial genome's 16S rRNA gene coding region and the eukaryotic genome's 18S rRNA gene coding region is the most often used technique. Prokaryotic and eukaryotic species have a great deal of similarities in their 16S and 18S rRNA, but they also include nine hyper-variable regions (V1–V9) that can be used to identify different species (Chakravorty et al., 2007).

16S rDNA-based libraries provide a targeted approach to species identification, enabling the detection of naturally occurring low-copy number DNA in purified samples. High-throughput genomic DNA sequencing has enabled rapid and high rate determination of microbial diversity. Thus, metagenomics has become a powerful tool to investigate microbial diversity as well as novel functional genes, microbial pathways, antibiotic resistance genes, and the relationship between microbiota and host (Wang et al., 2015; Sharma et al., 2021).

Bioinformatic analysis of metagenomic data

For metagenomic analysis, sample preparation is a crucial step. After collection, samples need to be frozen or examined right away. Preventing repeated freeze-thawing is particularly crucial since it can change the composition of the microbial population being studied. Microorganisms are lysed either directly in the matrix (in situ) or after isolating microbial cells in order to recover microbial metagenomic DNA from the sample matrix. Various techniques, such as mechanical, chemical, and enzymatic approaches, can be used singly or in combination to lyse the cells. Following the extraction and purification of metagenomic DNA, a metagenomic library is created by inserting different adapters, depending on the sequencing platform to be used, into the end regions of the DNA fragments (Zhang et al., 2019).

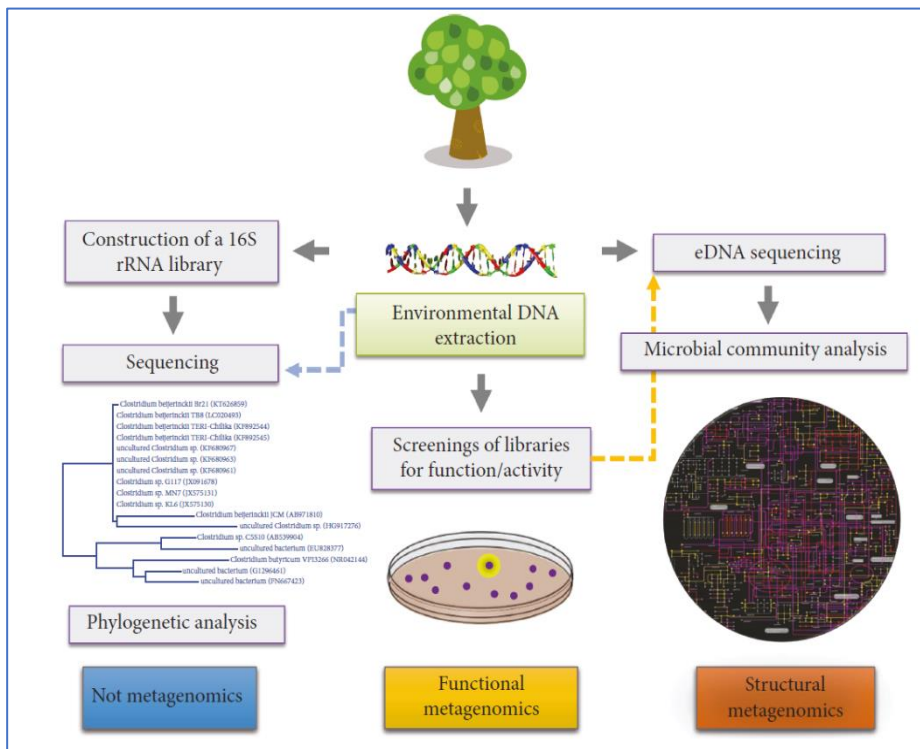


Figure 3. The two primary methodologies within the metagenomics framework. The primary methods for examining important ecological and biotechnological characteristics in environmental samples are structural and functional metagenomic techniques, respectively. Furthermore, 16S rRNA gene surveys and metagenomics can complement each other to enhance our comprehension of microbial ecology (Alves et al., 2018)

When building the library for amplicon sequencing, adaptor-attached primers compatible with the adapters and indexes of the Illumina platform are used. The primer sequences consist of the appropriate Illumina adapter (P5 or P7) that hybridizes with the oligonucleotides on the flow cell, an 8-nt index sequence representing the unique barcode for each sample, a 10-nt pad sequence, a 2-nt linker, and specific primer portions for the selected variable region. With indexing (barcoding), multiplex sequencing can be performed by pooling the sample and correlating each read with the original sample after sequencing. That is, post-sequencing indexing identifies which sample the reads belong to. The Illumina platform has a different

indexing structure that combines adapters and indexes (barcodes) instead of adding indexes to the ends of DNA fragments as in other platforms. The target region is amplified by two rounds of PCR with designed primers. After PCR, the resulting library needs to be purified by selecting DNA fragments of the targeted size and removing free adapters, adapter dimers and other possible contaminants. This step is usually performed with magnetic beads or agarose gel. If adapter dimers are not removed, they can form clusters in the flow cell and cause unnecessary sequencing data to be generated (Pérez-Cobas et al., 2020; Gil et al., 2021).

The term sequencing coverage refers to the fraction of the metagenome represented in the sequencing resultant dataset, which directly affects the sequencing depth. Rarefaction curves are very useful and widely used to determine the required sequencing coverage. In a sequencing study, OTU/ASV diversity increases as coverage increases, and when the full richness of a sample is theoretically reached, the abundance of OTU/ASVs is expected to reach a plateau. The use of rarefaction curves provides information that the sequencing process is accurately capturing the microbial diversity in the sample (Mongad et al., 2021).

The result of primary data analysis consists of the detection and signal analysis of raw data, the generation of readable sequencing and the scoring of basic quality. Typical outputs of this primary analysis are the FASTQ file or BAM file used by Illumina. The PHRED algorithm score is used by most software packages to confirm the quality of the reads obtained after sequencing. The risk that a base was included improperly is indicated by the Phred score. It is customary to employ a Phred value of 25 to 30 to ensure sequence dependability. Base identifications with a Phred score of 10 (Q10) have a 1 in 10 chance of being wrong or 90% accuracy; those with a Q20 score have a 1 in 100 chance of being wrong or 99% accuracy; and those with a Q30 score have a 1 in 1000 chance of being wrong or 99.9% accuracy. A phred score of Q20 or above indicates that the sequences are of sufficient quality for bioinformatic analysis (Gourlé et al., 2019).

The most popular tools for analyzing amplicon sequencing data are QIIME2, MOTHUR and MG-RAST. First, the data needs to be exported to QIIME2 file format and the sequences need to be demultiplexed if there are sequences from different samples in the same file. This can be done with the “q2demux” function if the barcodes are separated from the reads and in a separate file, or with the “cutadapt” plugin if the barcodes are still on the reads. In QIIME2, this can include technical details such as the DNA barcodes used for each sample, or descriptions of the samples such as which subject, environmental parameters, time point or body site each sample came from (Jimenez, 2021). Traditionally, quality control of sequences is performed by trimming and filtering sequences based on their quality score, then clustering them into operational taxonomic units (OTUs) based on a fixed dissimilarity threshold (typically 97%). QIIME2 currently uses denoising via the DADA2 (q2-dada2) and Deblur (q2-deblur) plugins. As a result of both methods, a FeatureTable [Frequency] file is created containing the frequencies of each different sequence in each sample in the dataset. DADA2 involves merging paired end reads throughout the quality control process flow and is therefore easier, whereas in Deblur it is necessary to merge reads independently before denoising using other plugins such as “q2-vsearch's join” (Sankhwar et al., 2024).

Although microbiome data are analyzed without phylogenetic tree construction, there are several commonly used diversity analysis methods, including Faith phylogenetic diversity, weighted and unweighted UniFrac. First, the pipeline uses the mafft (multiple sequence alignment program) to perform multiple sequence alignment of the sequences in FeatureData [Sequence] to create a FeatureData [AlignedSequence] QIIME 2 file. Following this, FastTree is applied to generate a phylogenetic tree from the masked alignment. The FastTree program generates an unrooted tree. There are two main approaches to taxonomic classification, each involving multiple methods. The first is based on aligning reads directly to reference databases: Classify-consensus-blast; BLAST+local alignment and classify-consensus-vsearch; VSEARCH global alignment. The second approach uses a machine learning classifier to assign possible classifications to the

reads and the classifier-sklearn method is applied. Databases such as Silva and Greengenes are used for alignment (Callahan et al., 2016).

Another widely used platform in metagenomics is Mothur, which uses integrated analysis tools. In addition, Mothur is written in C++, which allows a larger number of sequences to be analyzed. A crucial computer tool for taxonomic and functional metagenome study is the MEGAN (Metagenome Analyzer) program. Because the tool operates with read or end sequences, taxonomy analysis has the benefit of not requiring a metagenome assembly.

METAnnotatorX2 enables species-specific reconstruction and gene annotation of microbial genomes from metagenomic data, providing a complete workflow for unmixed and hybrid assemblies of short and long reads. It also hosts customized databases for archaea, bacteria, fungi, protista and viruses, with a range of advanced features (Sun et al., 2020; Douglas et al., 2018).

Results

Metagenomics, one of the most important scientific studies to understand the microbiota, provides new genes, proteins and definitive diagnoses of non-culturable organisms in a short time and with high accuracy compared to other methods, but there are no standard methods or universal tools that can answer all questions about the microbiota in metagenomic studies. Although metagenetic studies have been used for different purposes in recent years, there is still room for improvement.

Significant advancements have been made in the subject of metagenomics throughout the past thirty years, since the initial research employing this concept. A metagenome typically represents a snapshot of a community's DNA at the moment it was collected. To study the entire population dynamics, a well-designed experiment incorporating several techniques such protein studies, culture techniques, DNA and RNA analysis, and, if feasible, metabolic profiling is needed. To address issues pertaining to microbial diversity and ecology in general, microbiology must integrate a number of techniques (such as molecular biology, genetics, bioinformatics, and statistics).

Comparing metagenomics to traditional microbiology or molecular approaches, we can find new genes, proteins, and even entire genomes of non-culturable organisms more quickly and accurately. Nevertheless, metagenomics does not yet have universal instruments or standard procedures that can address any query we have. Metagenomics is actually a case-by-case research because of the lack of standards, which hinders repeatability and comparability between related projects. The experimental design of any metagenome study dictates distinct requirements, thus the computational tools and sequencing equipment chosen must be carefully considered. Despite the serendipity that exists in science, we should not forget that the experimental design is the most important part and must fit each project goal in order to achieve them and answer the biological question behind the project. As datasets become increasingly complex and comprehensive, new bioinformatics tools will be required for analysis, storage and visualization. But scientists' experience in manipulating such tools and interpreting their results will be key to a sensible biological conclusion. These tools will enable the best use of metagenomics as a tool to address fundamental questions about microbial ecology, evolution and diversity, and to derive and test new hypotheses.

REFERENCES

- Alves, L.D.F., Westmann, C.A., Lovate, G.L., de Siqueira, G.M.V., Borelli, T.C., Guazzaroni, M.E. (2018). Metagenomic approaches for understanding new concepts in microbial science. *International Journal of Genomics* 2018(1): 2312987.
- Callahan, B.J., McMurdie, P.J., Rosen, M.J., Han, A.W., Johnson, A.J. A., Holmes, S.P. (2016). DADA2: High-resolution sample inference from Illumina amplicon data. *Nature Methods* 13(7): 581–583.
- Chakravorty, S., Helb, D., Burday, M., Connell, N., Alland, D. (2007). A detailed analysis of 16S ribosomal RNA gene segments for the diagnosis of pathogenic bacteria. *Journal of Microbiological Methods* 69(2): 330-339.
- Crossley, B.M., Bai, J., Glaser, A., Maes, R., Porter, E., Killian, M.L., Clement, T., Toohey-Kurth, K. (2020). Guidelines for Sanger sequencing and molecular assay monitoring. *Journal of Veterinary Diagnostic Investigation* 32(6): 767-775.
- Davison, M., Hall, E., Zare, R., Bhaya, D. (2015). Challenges of Metagenomics and Single-Cell Genomics Approaches For Exploring Cyanobacterial Diversity. *Photosynthesis Research* 126 (1): 135-146.
- DeSantis, T.Z., Hugenholtz, P., Larsen, N., Rojas, M., Brodie, E.L., Keller, K., Hu, P., Andersen, G.L. (2006). Greengenes, a Chimera-Checked 16S rRNA Gene Database and Workbench Compatible with ARB. *Applied and Environmental Microbiology* 72(7): 5069-5072.
- Ding, X., Lan, W., Gu, J.-D. (2020). A Review on Sampling Techniques and Analytical Methods for Microbiota of Cultural Properties and Historical Architecture. *Applied Sciences* 10(22): 8099.
- Douglas, G.M., Beiko, R.G., Langille, M.G. (2018). Predicting the functional potential of the microbiome from marker genes using PICRUSt. *Microbiome analysis: Methods and Protocols*: 169-177.

- Faust, K., Sathirapongsasuti, J.F., Izard, J., Segata, N., Gevers, D., Raes, J., Huttenhower, C. (2012). Microbial Co-Occurrence Relationships in The Human Microbiome. *PLoS Computational Biology* 8(7): e1002606.
- Fukuda, K., Ogawa, M., Taniguchi, H. ve Saito, M. (2016). Molecular Approaches to Studying Microbial Communities: Targeting the 16S Ribosomal RNA Gene. *Journal of UOEH* 38(3): 223-232.
- Gil, P., Dupuy, V., Koual, R., Exbrayat, A., Loire, E., Fall, A.G., ... Gutierrez, S. (2021). A library preparation optimized for metagenomics of RNA viruses. *Molecular Ecology Resources* 21(6): 1788-1807.
- Gourlé, H., Karlsson-Lindsjö, O., Hayer, J., Bongcam-Rudloff, E. (2019). Simulating Illumina metagenomic data with InSilicoSeq. *Bioinformatics* 35(3): 521-522.
- Handelsman, J. (2004). Metagenomics: application of genomics to uncultured microorganisms. *Microbiology and Molecular Biology Reviews* 68(4): 669-685.
- Handelsman, J., Rondon, M.R., Brady, S.F., Clardy, J., Goodman, R.M. (1998). Molecular biological access to the chemistry of unknown soil microbes: a new frontier for natural products. *Chemistry & Biology* 5(10): R245-R249.
- Heather, J.M., Chain, B. (2016). The sequence of sequencers: The history of sequencing DNA. *Genomics* 107(1): 1-8.
- Hu, T., Chitnis, N., Monos, D., Dinh, A. (2021). Next-generation sequencing technologies: An overview. *Human Immunology* 82(11): 801-811.
- Jimenez, R. (2021). Practical metagenomics: microbiome tutorial with QIIME 2. *F1000Research* 10(798): 798.
- Kamble, A., Sawant, S., Singh, H. (2020). 16S Ribosomal RNA Gene-Based Metagenomics: A Review. *Biomedical Research Journal*: 7(1), 5.
- Kim, M., Morrison, M., Yu, Z. (2011). Evaluation of different partial 16S rRNA gene sequence regions for phylogenetic analysis of microbiomes. *Journal of Microbiological Methods* 84(1): 81-87.

- Lan, Y., Rosen, G., Hershberg, R. (2016). Marker Genes That Are Less Conserved in Their Sequences Are Useful for Predicting Genome-Wide Similarity Levels Between Closely Related Prokaryotic Strains. *Microbiome* 4(1): 18.
- Larsen, N., Olsen, G.J., Maidak, B.L., McCaughey, M.J., Overbeek, R., Macke, T.J., Marsh, T.L., Woese, C. R. (1993). The ribosomal database project. *Nucleic Acids Research* 21(13): 3021-3023.
- Levsky, J.M., Singer, R.H. (2003). Fluorescence In Situ Hybridization: Past, Present and Future. *Journal of Cell Science* 116(14): 2833-2838.
- Liu, Y.X., Qin, Y., Chen, T., Lu, M., Qian, X., Guo, X., Bai, Y. (2021). A practical guide to amplicon and metagenomic analysis of microbiome data. *Protein & Cell* 12(5): 315-330.
- Madigan, M.T., Martinko, J. (2005). *Brock Biology of Microorganisms*, 11th Edition: SciELO, Espana.
- Mongad, D.S., Chavan, N.S., Shouche, Y.S. (2021). Computational Techniques Used for Microbial Diversity Analysis. In *Microbiome-Host Interactions*: 21-35, CRC Press.
- Neelakanta, G., Sultana, H. (2013). The use of metagenomic approaches to analyze changes in microbial communities. *Microbiology Insights* 6: MBI-S10819.
- Pérez-Cobas, A.E., Gomez-Valero, L., Buchrieser, C. (2020). Metagenomic approaches in microbial ecology: an update on whole-genome and marker gene sequencing analyses. *Microbial Genomics* 6(8): e000409.
- Quast, C., Pruesse, E., Yilmaz, P., Gerken, J., Schweer, T., Yarza, P., Peplies, J., Glöckner, F.O. (2012). The SILVA ribosomal RNA gene database project: improved data processing and web-based tools. *Nucleic Acids Research* 41(D1): D590-D596.
- Rodríguez-Valera, F. (2004). Environmental genomics, the big picture? *FEMS Microbiology Letters* 231(2): 153-158.
- Sanger, F., Nicklen, S., Coulson, A.R. (1977). DNA sequencing with chain-terminating inhibitors. *Proceedings of The National Academy of Sciences* 74(12): 5463-5467.

- Sankhwar, R., Kumar, A., Kapoor, D.D., Gupta, R.K. (2024). Comparative metagenomic analysis of bacterial diversity in three distantly related soils in India. *Journal of Applied and Natural Science* 16(3): 987-997.
- Sharma, P., Kumar, S., Pandey, A. (2021). Bioremediated techniques for remediation of metal pollutants using metagenomics approaches: a review. *Journal of Environmental Chemical Engineering* 9(4): 105684.
- Simon, C., Daniel, R. (2009). Achievements and new knowledge unraveled by metagenomic approaches. *Applied Microbiology and Biotechnology* 85: 265-276.
- Sun, S., Jones, R.B., Fodor, A.A. (2020). Inference-based accuracy of metagenome prediction tools varies across sample types and functional categories. *Microbiome*: 8, 1-9.
- Swingland, I.R. (2001). Biodiversity, Definition Of. *Encyclopedia of Biodiversity*, 1: 377-391.
- Thompson, L.R., Sanders, J.G., McDonald, D., Amir, A., Ladau, J., Locey, K.J., ... Knight, R. (2017). A communal catalogue reveals Earth's multiscale microbial diversity. *Nature* 551(7681): 457-463.
- Vincent, S.G.T., Jennerjahn, T., Ramasamy, K. (2021). Assessment Of Microbial Structure and Functions in Coastal Sediments. *Microbial Communities in Coastal Sediments* 167-185).
- Wang, W.-L., Xu, S.-Y., Ren, Z.-G., Tao, L., Jiang, J.-W., Zheng, S.-S. (2015). Application of metagenomics in the human gut microbiome. *World Journal of Gastroenterology* 21(3): 803.
- Wensel, C.R., Pluznick, J.L., Salzberg, S.L., Sears, C.L. (2022). Next-generation sequencing: insights to advance clinical investigations of the microbiome. *The Journal of Clinical Investigation* 132(7) :e154944.
- Wooley, J.C., Godzik, A., Friedberg, I. (2010). A primer on metagenomics. *PLoS Comput Biol*, 6: 2,e1000667.
- Yang, B., Wang, Y., Qian, P.E. (2016). Sensitivity and correlation of hypervariable regions in 16S rRNA genes in phylogenetic analysis. *Biomed Central Bioinformatics* 17: (135).

Zhang, L., Loh, K.C., Lim, J.W., Zhang, J. (2019). Bioinformatics analysis of metagenomics data of biogas-producing microbial communities in anaerobic digesters: A review. *Renewable and Sustainable Energy Reviews* 100: 110-126.

CHAPTER 4

ASSOCIATION OF TLR2, TLR4 AND TLR9 POLYMORPHISMS WITH URINARY TRACT INFECTIONS

Exp. Bio. Sameer Abdulrazzaq ALI¹ & Assist. Prof. Dr. Filiz
SARIKAYA PEKACAR²

DOI: <https://dx.doi.org/10.5281/zenodo.14258669>

¹ Çankırı Karatekin University, Graduate School of Natural and Applied Sciences, Biology Department Çankırı, Türkiye, sa4886542@gmail.com,

² Çankırı Karatekin University Science Faculty Dep.of Biology, Çankırı, Türkiye, fspekacar@karatekin.edu.tr, Orcid:0000-0001-9684-9284

INTRODUCTION

A urinary tract infection is a widespread infection that can affect any part of the urinary system, including the urethra, bladder, ureters, and kidneys. It is known that urinary tract infections account for approximately 1% of outpatient treatments (Schappert and Rechtsteiner 2011). Urinary tract infections are generally more common in women. It is known that the prevalence of urinary tract infections is also high among hospitalized patients. According to the study, about 4% of patients with catheters in place for at least 24 hours during their hospitalization experienced a urinary tract infection while urinary tract infection was detected in approximately 1% of patients who were not catheterized (Uçkay et al. 2013).

Symptoms of Urinary Tract Infection

The urinary tract is particularly susceptible to infestation by germs because it opens out. Bacteria are naturally located near the urethral opening and tend to colonize the urethra over time. Among men infected with *Escherichia coli*, the rate of Bacterial colonization of the urethra in urine culture ranges from 1% to 5%, with a higher rate among men who have had sexual intercourse with a woman with a previous urinary tract infection (Foxman et al. 2002). It is known that the rate of urethral colonization is higher among women. In women, Women's periurethral areas tend to be moister, and since the vaginal cavity and rectal opening are nearby, this creates conditions that favor bacterial growth the shorter urethral length in females increases the likelihood of bacterial ascent into the bladder compared to males at the urethral opening. While the incidence of presence of bacteria in urine without symptoms in women is 3.5% (Evans et al. 1978), this rate becomes much higher after sexual intercourse (Evans et al. 1978, Nicolle et al. 1982). Furthermore, the incidence of asymptomatic bacteriuria increases with age in both men and women (Evans et al. 1978, Nicolle et al. 1982, Nicolle 2009). In studies conducted for asymptomatic bacteriuria, symptoms similar to those seen in other urinary tract infections were observed. In other words, positive urine culture and urinalysis findings are the same in all types of infections,

but it is not possible to mention the presence of any signs or symptoms that may cause urinary tract infection (Evans et al. 1978, Nicolle 2009).

Treatment of asymptomatic bacteriuria often leads to the development of symptomatic UTI in healthy individuals and increases the selection of antibiotic-resistant bacteria (Cai et al. 2012). Therefore, screening and treatment of asymptomatic bacteriuria in catheterized patients is not recommended (Hooton et al. 2010). During pregnancy, physiological changes make women with asymptomatic bacteriuria more prone to developing pyelonephritis. (Ramos et al. 2012). The incidence of asymptomatic bacteriuria during pregnancy can vary from 2% to 20%, and if these patients are not treated, pyelonephritis can develop in 20% to 40% of these cases (Kazemier et al. 2012). Pyelonephritis can be life-threatening to both the mother and the newborn (Kazemier et al. 2012). Screening and treatment of asymptomatic bacteriuria during pregnancy can reduce this risk by approximately 80% (Smaill and Vazquez 2007).

Urinary symptoms of a UTI, such as dysuria, can be caused by more than just UTIs, so diagnosing a UTI can be complicated by the high incidence of asymptomatic bacteriuria. Diseases such as vaginitis, chlamydia, and gonorrhea can also cause symptoms similar to those of UTIs. For this reason, it is important that asymptomatic bacteriuria and urinary tract symptoms occur alone. Especially when these conditions are associated with sexual activity, the diagnosis should be made by urine culture and urinalysis. The opposite is also true. For example, women between the ages of 18 and 29 who are sexually active may have negative urine cultures despite being at high risk for UTI with frequency, urgency, and dysuria (Gordon et al. 2013, Bent et al. 2002).

Urinary symptoms in cystitis are limited to the bladder, but upper tract involvement may occur. Dysuria is the most prevalent symptom in premenopausal women, while postmenopausal women, elderly individuals, and children may report issues like weakness, nocturia, incontinence, or urine with an unpleasant odor. Cystitis is quite common. In fact, the prevalence of cystitis among patients presenting to the emergency department with urinary symptoms ranges from 4% to 5% in women and 1.5% to 2% in men (Anger et al. 2008). However,

the prevalence in hospital admissions over one year is 12%-13% in women and 2.5%-3% in men (Laupland et al. 2007). The rate of women experiencing at least one urinary tract infection in their lifetime is between 60% and 65% (Foxman et al. 2000). In pyelonephritis, urinary tracts symptoms may or may not be present, but are often accompanied by fever, chills, back pain, nausea, and vomiting. The incidence of pyelonephritis is lower than that of cystitis, but the age and gender criteria are similar (Ki et al 2004). Women are at higher risk than men however these differences tend to diminish with age (Brown et al. 2005).

In urinary catheterized patients, the risk of developing a UTI increases by 3%-10% for each day of catheterization (Warren et al. 1979). However, catheter-associated bacteriuria cannot be considered a treatable condition in the absence of UTI symptoms and Symptoms like elevated body temperature, chills, or general malaise (Hooton et al. 2010). The use of catheters is the leading contributor to nosocomial urinary tract infections, which account for nearly one-third of all nosocomial infections (Lewis et al. 2013). The risk of catheter-associated UTI does not depend on the type of catheter (Pickard et al. 2012).

Recurrence of Urinary Tract Infection

UTIs tend to recur with varying frequency. Different studies show that the frequency of recurrence within the first year is 19%-22% (Craig et al. 2009, Salo et al. 2012), while the frequency of recurrence within the first six months is 24%-25% (Foxman et al. 2000). However, women with two or more previous UTIs have been found to be 2-5 times more likely to have a recurrence than women with one or no previous UTIs (Hooton et al. 1996). The recurrence rate of UTI is lower in men than in women. In male patients receiving outpatient treatment, the risk of recurrence within the first month is about 4%, while the recurrence rate between one month and one year is about 8% (Drekonja et al. 2013).

It is also important to remember that pyelonephritis often recurs. In fact, the risk of recurrence within the first 12 months is reported to be about 10 per cent in women and 6 per cent in men. The rate of

second recurrence is 20-22 per cent in both men and women, while the rate of fifth recurrence is about 50-55 per cent in both men and women (Ki et al 2004).

Bacteriology

Urine is a very favourable environment for the growth and development of bacteria. For this reason, a large number and variety of bacteria grow in urine. Bacteria that colonize the urinary tract typically do not cause disease. This is because the host has a wide range of effective defences to remove the bacteria from the system. The most important of these are urination and the innate immune response (Mulvey et al 2000). The bacteria that cause urinary tract infections have special characteristics that enable them to survive. These include biofilm formation, invasion of urothelial cells, adhesins, toxins and siderophores. In addition, interventions such as catheterisation that prevent the removal of bacteria from the body are also effective (Mulvey et al 2000, Pitout 2012). In fact, this may explain why the rate of nosocomial infections is higher than the rate of community-acquired infections (Pitout 2012).

Escherichia coli bacteria are responsible for the majority of urinary tract infections, in all age groups, in both sexes and in all settings. In fact, regardless of age group, *E. coli* is the causative bacterium in approximately 75% of outpatient, 70% of nosocomial and 50% of healthcare-associated infections (Laupland et al 2007). *E. coli* causing urinary tract infections vary in the presence of known uropathogenic factors, are highly diverse (Marrs et al. 2005) and represent a large number of different genetic lineages (Wirth et al. 2006). Although the antibiotic resistance of uropathogenic *E. coli* has increased significantly, resistance patterns vary between patient populations and geographical regions (Paulsen et al. 2013). In addition to *E. coli*, a number of other bacterial species can cause UTI with varying degrees of frequency. These include gram-negative *Klebsiella pneumoniae*, *Pseudomonas aeruginosa* and *Proteus mirabilis*, and gram-positive *Streptococcus agalactiae* and *Staphylococcus saprophyticus* (Amna et al. 2013). The risk of developing a UTI caused by pathogens other than *E. coli* is higher in recurrent UTIs, in men, in

cases involving a foreign body or obstruction, and in patients with a urinary catheter (Amna et al. 2013).

Key risk factors

UTI risk factors can be categorized into those that expose the host to potential uropathogens, those that facilitate the colonization of these pathogens, and those that affect the host's response to infections caused by colonization. Uropathogens are found in diverse locations, including the intestines, periurethral region, vaginal cavity, and throughout the urinary tract. They can be transmitted from person to person by direct contact, including sexual activity between individuals, and by the faecal-oral route. Most uropathogens have specialised characteristics that allow them to colonise the urinary tract, as reviewed in the bacteriology section (Terlizzi et al. 2017).

Bacteria within the intestine, periurethral region, and vaginal cavity are perpetually moving toward the urinary system. This movement is increased by manipulation, catheterisation and sexual activity. Women are more at risk for this disease because the urethral opening is closer to the anal opening and vaginal cavity, where potential uropathogens reside. Because women have a shorter distance from the urethral opening to the bladder, bacteria can ascend more readily. Moreover, the periurethral area is generally moister, creating favorable conditions for bacterial growth. It is only when the host's immune response is engaged that symptoms begin to appear. The likelihood of a link to the immune response is increased in patients who are unable to empty their bladder completely, such as those with frequent urination, neurogenic bladder or obstruction, or those who are immunocompromised, have comorbidities and are older (Amna et al 2013, Salvador et al 2012).

The recurrence rate of urinary tract infections is quite high. Patients with a history of UTI are an important risk group (Foxman et al 2000). This may be due to host behaviour, host susceptibility and bacterial factors, or a combination of all three. Sexual activity in both men and women can transport bacteria into the urethra and increase the risk of UTI. Contraceptives also increase the risk of UTIs. In fact, there is a linear relationship between the use of condoms, diaphragms and spermicides and the risk of UTIs (Foxman et al 2000). In addition,

vaginal infections such as bacterial vaginosis are also associated with an increased risk of UTI. Such infections may facilitate the growth and colonisation of *E. coli* (Harmanlı et al. 2000, Scholes et al. 2005). Although the risk factors for pyelonephritis and cystitis, which are symptoms of UTI, are almost the same, anatomical changes that occur during pregnancy make pregnant women more susceptible to pyelonephritis (Scholes et al. 2005, Ramos et al. 2012).

Especially in the case of nosocomial infections, the insertion of a catheter into the patient also poses a risk of infection. The placement of the catheter in the patient facilitates the transfer of bacteria to the bladder. The catheter therefore acts as an additional portal for bacterial invasion. Catheter insertion increases the risk of UTI by up to four times (Uçkay et al. 2010). However, the presence of any medical manipulation and comorbidity increases the risk of UTI. In fact, urinary tract infections are the most common type of infection in people living in places such as nursing homes and care homes (Dwyer et al. 2013). Any surgery, especially surgery involving manipulation of the genitourinary system and insertion of a urinary catheter, greatly increases the risk of UTI (Regenbogen et al. 2011). In addition, the risk of UTI increases in direct proportion to age. The most powerful risk factors in older people are severe cognitive impairment, disability affecting activities of daily living, urinary incontinence and recent UTI (Caljouw et al 2011).

Furthermore, type 2 diabetes has been linked to an elevated risk of urinary tract infections. The incidence of urinary tract infections is approximately four times higher in individuals with diabetes than in those without the disease (Hirji et al., 2012). Nevertheless, evidence indicates that obesity is also a risk factor for UTIs. It has been demonstrated that the risk of developing a UTI is approximately 25% higher in individuals with obesity and a high body mass index. Furthermore, factors associated with metabolic disease, including vitamin D levels, age and daily activity levels, are directly correlated with the risk of UTIs. Furthermore, the disease burden and severity are believed to be the result of an interaction between bacterial virulence genes and the host immune response (Ragnarsdóttir and Svanborg, 2012). In this context, polymorphisms in genes encoding the inflammasome response, such as toll-like receptors (TLRs), interferon

regulatory factors and chemokine receptors, have also been demonstrated to affect disease in individuals with asymptomatic bacteriuria and pyelonephritis (Hawn et al. 2009; Ragnarsdóttir and Svanborg 2012).

The vast majority of urinary tract infections are limited to the bladder. The most common symptoms are haematuria, dysuria, urgency, frequency, nocturia, an offensive odour and abdominal pain. The symptoms persist for approximately four days, result in activity limitation for approximately three days, and cause discomfort for approximately three days. It is uncommon for symptoms to persist for more than three days. The shortest-lasting symptom is haematuria, while the longest-lasting symptom is urinary frequency. However, the total annual cost of urinary tract infections is estimated to reach billions of dollars (Foxman, 2000). The most common cause of urinary tract infection is *E. coli* bacteria. *E. coli* bacteremia is also observed. The risk of bacteremia and death due to bacteremia is significantly elevated in inpatients undergoing urinary catheterization. The risk of death within seven days in patients with catheter-related bacteremia and urinary tract infection is approximately 30% (Melzer and Welch 2013).

Toll-like Receptors

The immune system is responsible for identifying and eliminating pathogenic microorganisms by analysing them and distinguishing between those that belong to it and those that do not. In mammals, the immune system can be divided into two distinct categories: innate immunity and adaptive immunity (Hoffman et al. 1999). Adaptive immunity is capable of detecting non-self through the use of antigen receptors expressed on the surface of B and T cells, which enables the recognition of peptide antigens. To effectively respond to a diverse array of potential antigens, B and T cells undergo a process of rearrangement of immunoglobulin and T cell receptor genes, resulting in the generation of over a thousand different antigen receptor types. The binding of specific antigens to their respective receptors triggers both the clonal expansion of lymphocytes and the creation of antibodies that target the antigen. This complex system, found only in vertebrates, represents a powerful defense mechanism against microbial infections. On the other hand, the innate immune system, recognized around a

century ago, is evolutionarily conserved and can be found in nearly all multicellular organisms (Hoffman et al. 1999).

A Toll family homologue was identified while studying the defense mechanisms of *Drosophila* against fungal infection and was subsequently found in mammals. Afterward a group of proteins with structural similarities to Toll in the fruit fly was identified, and all of them were designated Toll-like receptors (TLRs) (Medzhitov et al., 1997). The Toll-like receptor (TLR) family comprises ten members, from TLR-1 to TLR-10. However, recent developments have revealed that this number may in fact be 13 (Medzhitov et al. 1997, Rock et al. 1998, Takeuchi et al. 1999, Chuang and Ulevitch 2000, Chuang and Ulevitch 2001). Each Toll-like receptor (TLR) gene's location within the chromosome in humans has been defined (Rock et al., 1998; Takeuchi et al., 1999; Chuang and Ulevitch, 2000). TLR1 and TLR6 are situated in close proximity to 4p14 (Rock et al. 1998, Takeuchi et al. 1999), while TLR2 and TLR3 are located on 4q32 and 4q35, respectively. TLR4 and TLR5 are located on TLR7 and TLR8 are located sequentially on Xp22 (Rock et al., 1998), while TLR9 has been mapped on p21.3 (Chuang and Ulevitch, 2000). The TLR family of proteins is distinguished the identification of a leucine-rich repeat (LRR) domain in the extracellular area and a TIR domain in the intracellular area. Comparing the amino acid sequences of human TLR family members bring to light the existence of five subfamilies (Takeuchi et al., 1999).

The TLR9 subfamily comprises three members: TLR7, TLR8 and TLR9. The TLR3, TLR4 and TLR5 families are the only ones that consist of them alone (Takeuchi et al., 1999). The TLR2 subfamily comprises two closely related proteins, TLR1 and TLR6, which indicate 69.3% alignment in their comprehensive amino acid sequence. However, the Both receptors feature TLR domains that are remarkably conserved, with identity levels surpassing 90% (Takeuchi et al., 1999). Given that TLR1 and TLR6 have analogous genomic organizations, comprising a single exon and situated in close proximity on the same chromosome, they may be regarded as the products of evolutionary duplication (Takeuchi et al., 1999). The classification of TLRs into five distinct subfamilies is also founded on their genomic structure. The gene encoding for toll-like receptor 2 (TLR2) comprises two exons.

Typically, Exon 2 contains all coding sequences. Furthermore, the TLR9 subfamily, which includes TLR7, TLR8 and TLR9, is encoded by two exons (Chuang and Ulevitch, 2000; Chuang and Ulevitch, 2001; Du et al., 2000). TLR7 and TLR8 gene sequences have an identity of 42.3% and a similarity of 72.7% in their amino acid compositions. Additionally, they possess analogous genomic structures and are situated in close proximity on the X chromosome (Chuang and Ulevitch 2000, Chuang and Ulevitch 2001, Du et al. 2000).

The TLR4 gene has four exons, and the TLR5 gene has five exons. TLR3 is distinguished from other TLRs by its unique structural characteristics, namely the presence of five exons and the encoding of the protein by exons 2 and 5. This contrasts with the structural and encoding characteristics observed in all other TLRs, which are encoded by a single exon or two exons (Chuang and Ulevitch 2000, Chuang and Ulevitch 2001, Du et al. 2000).

TLR types and molecular mechanisms

It has been demonstrated that the ectopic overexpression of Toll-like receptor 4 (TLR4), the first mammalian Toll-like receptor to be identified, results in the induction of genes encoding various inflammatory cytokines and co-stimulatory factors. It is therefore postulated that TLRs may be participate in immune responses, particularly in the triggering of innate immunity. The function of TLR4 in recognizing lipopolysaccharide (LPS), the principal cell wall component of Gram-negative bacteria, was established in 1998. Subsequently, the concept was proposed that additional members of the TLR family are necessary for the identification of a range of microbial compounds. Hence, the structural similarities of TLRs seem to correspond to their mutual role in the identification of microbial compounds (Medzhitov et al., 1997). It seems appropriate to review the TLR receptors under this heading, grouping them separately in terms of their mutual relationship, structural similarity, and origin. Therefore, the first identified TLR, TLR4, will be examined first, followed by the TLR2, TLR1, and TLR6 receptors that act together, then TLR5 and TLR3 separately, and finally the TLR9 and TLR7 receptor subfamilies, both together.

TLR4

TLR4 is capable of recognizing lipopolysaccharides (LPS). It has long been established that two mice strains, C3H/HeJ and C57BL10/ScCr, exhibit reduced responsiveness to LPS. Two separate studies have identified mutations in the TLR4 gene as the cause of this hypo responsiveness (Poltorak et al. 1998, Qureshi et al. 1999). The C3H/HeJ mouse strain has a point mutation in the intracellular domain of the TLR4 gene, resulting in the alteration of a highly conserved proline by a histidine. This mutation follows in the formation of a dominant negative allele, which in turn leads to defects in TLR4-mediated signaling and the suppression of the response to LPS. The C57BL10/ScCr strain, which is also LPS hyposensitive, has a null mutation in the TLR4 gene (Poltorak et al., 1998; Qureshi et al., 1999). TLR4 knockout mice created through gene targeting have been observed to demonstrate hyposensitivity to LPS, thereby establishing TLR4 as an essential receptor for the recognition of LPS (Hoshino et al., 1999). LPS recognition necessitates the involvement of additional molecules. LPS is bound to LPS-binding protein present in serum, and this LPS-LPS-binding protein complex is then recognized by CD14, a glycosylphosphatidylinositol-associated molecule that is preferentially expressed on monocytes/macrophages and neutrophils. Following LPS stimulation, there is an increase in the physical proximity between CD14 and TLR4, which suggests that CD14 and TLR4 may interact in the process of LPS signaling (Jiang et al. 2000; Da Shilva Correia et al. 2001). MD-2 has been identified as a molecule that associates with the extracellular portion of TLR4, thereby enhancing the LPS response (Shimazu et al. 1999; Akashi et al. 2000). Hyposensitivity to LPS in Chinese hamster ovary cell lines has been linked to mutations in the MD-2 gene (Schromm et al., 2001). MD-2-deficient mice have shown the fundamental importance of MD-2 in responding to LPS. Macrophages, dendritic cells, and B cells from MD-2-deficient mice indicate markedly diminished responses to LPS. Moreover, MD-2-deficient mice exhibit resistance to LPS-induced endotoxin shock, a phenomenon that is analogous to that observed in TLR4-deficient mice (Nagai et al., 2002). MD-2 associates with TLR4 in the endoplasmic reticulum/cis Golgi, and the TLR4/MD-2 complex subsequently relocates to the cell surface, where excess MD-2 is secreted (Visintin et

al. 2001). In cells with a wild-type phenotype, TLR4 is predominantly located on the cell surface, but in MD-2-deficient cells, it is present in the Golgi apparatus. This indicates that MD-2 is essential for the intracellular localization of TLR4 (Nagai et al., 2002). Additionally, another cell surface protein, RP105, has been demonstrated to play a role in LPS recognition. RP105 includes an LRR domain that is structurally related to those found in TLRs' extracellular domains and is largely expressed on the surface of B cells (Miyake et al., 1995).

B cells derived from mice that lack RP105 exhibit a markedly diminished response to LPS. RP105 is involved in the functional recognition of LPS by TLR4. Therefore, it can be inferred that a multitude of components are implicated in the process of LPS recognition, which suggests that a functional LPS receptor forms a complex with a number of other proteins (Ogata et al., 2000). In addition to LPS, TLR4 has been demonstrated to recognize a number of other ligands. Taxol, derived from the Pacific yew tree (*Taxus brevifolia*), has been demonstrated to possess potent antitumor activity in humans. The antimetabolic activity of Taxol is attributable to its capacity to bind and stabilize microtubules, thereby impeding the correct progression of cell division during mitosis. Taxol has been observed to possess immunostimulatory activities that are analogous to those exhibited by LPS in murine models, yet this phenomenon has not been documented in humans. In mice, the LPS-mimetic activity of Taxol is mediated by TLR4 and MD-2 (Byrd-Leifer et al., 2001; Kawasaki et al., 2000; Kawasaki et al., 2001). TLR4 and CD14 have been demonstrated to recognize the fusion protein of respiratory syncytial virus (Kurt-Jones et al. 2000, Haynes et al. 2001). It can therefore be concluded that mice with a mutation in the TLR4 gene, namely the C3H/HeJ and C57BL/10ScNCr strains, exhibit a reduction in immune response and diminished ability to clear respiratory syncytial virus. It has been shown that the activation of B cells by murine retroviruses, like mouse mammary tumor virus, relies on TLR4. The envelope proteins of mouse mammary tumor virus and Moloney murine leukemia virus have been reported to immunoprecipitate with TLR4 (Rassa et al. 2002). Consequently, it can be postulated that TLR4 plays a role in the recognition of a specific group of viruses.

Additionally, TLR4 has been demonstrated to recognize certain endogenous ligands. Heat shock proteins exhibit a high degree of conservation across a broad range of organisms, a plethora of challenging circumstances, including heat shock, ultraviolet radiation, and viral and bacterial infection, have been observed to induce an increase in the compound of heat shock proteins. The principal function of heat shock proteins is to facilitate the folding of proteins that are undergoing development or exhibiting aberrant conformations. Furthermore, heat shock proteins stimulate the secretion of pro-inflammatory cytokines and the expression of costimulatory molecules in macrophages and dendritic cells. As a result, it is proposed that heat shock proteins constitute a kind of endogenous "danger signal," specifically referring to molecules or structures released or produced by cells facing stress or abnormal cell death (necrosis). These signals are recognized by macrophages and dendritic cells, thereby initiating immune responses (Gallucci and Matzinger, 2001). The capacity of heat shock proteins to stimulate immune cells is most clearly exemplified by the heat shock protein HSP60. The immunostimulatory activity of HSP60 is mediated by TLR4 (Ohashi et al., 2000; Vabulas et al., 2001). For example, HSP60 plays a role in the inflammatory processes associated with atherosclerosis, the development of which is linked to chronic infection by *Chlamydia pneumoniae*. HSP60 derived from *Chlamydia pneumoniae* (cHSP60) has been observed to co-localize with macrophages in atheromatous lesions, where it induces an inflammatory response. It is therefore hypothesized that cHSP60 is a contributing factor in the development of atherosclerosis in cases of chronic *Chlamydia* infection. Furthermore, cHSP60 has been observed to activate vascular smooth muscle cells and macrophages via TLR4 (Sasu et al. 2001, Bulut et al. 2002). Mice lacking functional TLR4 exhibit impaired production of inflammatory cytokines in response to HSP60 and HSP70 (Dybdahl et al., 2002; Vabulas et al., 2002; Asea et al., 2002). It can therefore be concluded that TLR4 is responsible for the inflammatory responses elicited by heat shock proteins. However, both TLR2 and TLR4 are necessary for the recognition of HSP70 (Vabulas et al., 2002; Asea et al., 2002). CD91 (α -macroglobulin receptor) has been identified as a receptor for several heat shock proteins, including HSP70 (Basu et al., 2001). Moreover, while HSP60-

induced inflammatory cytokine production was not observed, HSP60 binds to macrophages from TLR4-deficient C57BL/10ScCr mice (Habich et al., 2002). These findings suggest that TLR4 is not directly involved in the recognition of heat shock proteins.

Extracellular matrix components, including fibronectin, hyaluronic acid, and heparin sulfate, are produced in response to tissue injury and play an integral role in tissue remodeling. These components facilitate the containment of the injury agent, facilitate the sealing of the wound, and promote the completion of healing. The type III repeat extra A domain of fibronectin has been demonstrated to elicit immunostimulatory activities comparable to those induced by LPS. This response to the extra A domain of fibronectin is mediated by TLR4 (Okamura et al., 2001). Furthermore, low molecular weight oligosaccharides of hyaluronic acid have been demonstrated to act as potent activators of dendritic cells, with the activation of dendritic cells by hyaluronic acid being mediated by TLR4 (Termeer et al., 2002). Furthermore, polysaccharide fragments of heparin sulfate have been demonstrated to induce the maturation of dendritic cells via TLR4 (Johnson et al., 2002). Extravascular fibrin deposits are regarded as an early and persistent indicator of inflammation that occurs in conjunction with injury, infection, and immune disorders. Fibrin is generated from plasma-derived fibrinogen that is released from the vasculature in response to endothelial cell retraction at sites of inflammation. The capacity of fibrinogen to induce chemokine production by macrophages is mediated by its recognition by toll-like receptor 4 (TLR4) (Smiley et al., 2001). It can therefore be surmised that TLR4 plays a role in the inflammatory response, recognizing endogenous ligands produced during inflammation, even in the absence of infection. It is important to note, however, that all of these endogenous TLR4 ligands only activate immune cells at very high concentrations. This is in stark contrast to the low concentrations required for lipopolysaccharide (LPS). It is therefore possible that these endogenous ligands are contaminated with a genuine TLR4 ligand, such as LPS. This raises the question of whether TLR4 directly recognizes its ligand. A review of the literature on this topic indicates that the recognition of LPS by TLR4 is a direct binding process. Conversely, alternative research indicates that LPS binds to MD-2,

which in turn stimulates TLR4 (Lien et al. 2000, Poltorak et al. 2000, Viriyakosol et al. 2001, Akashi et al. 2001). The species-specific recognition of different ligands provides genetic evidence for a direct interaction. For example, mouse but not human cells recognize Taxol, and this species-specific recognition is mediated by MD-2 (Kawasaki et al., 2001).

In another study, researchers showed that human TLR4 recognizes highly acylated LPS from *Pseudomonas aeruginosa* (Hajjar et al. 2002). TLR4 is considered a key component in the recognition of LPS. However, some studies have also shown that LPS is recognized independently of TLR4 (Hajjar et al. 2002). A study using affinity chromatography, peptide mass fingerprinting, and fluorescence resonance energy transfer identified four molecules that bind LPS on the cell surface (Triantafilou et al. 2001). These are HSP70, HSP90, chemokine receptor 4 (CXCR4), and growth differentiation factor 5 (Triantafilou et al. 2001). After binding to the cell surface, LPS is rapidly transported into the cytoplasm. This intracellular movement appears to be required for certain cellular responses, since agents that block vesicular transport, such as wortmannin or cytochalasin D, block integrin-mediated adhesion of neutrophils in response to LPS (Detmers et al. 1996). This suggests that LPS can be recognized both in the cytoplasm and at the cell surface. Another possible molecule that mediates intracellular recognition of LPS is Nod1. Nod1 was originally described as a molecule structurally related to the apoptosis regulator Apaf-1, containing a caspase recruitment domain and a nucleotide-binding oligomerization domain. Nod1 has an N-terminal caspase-recruitment domain linked to a nucleotide-binding domain and a C-terminal LRR domain. Unlike Apaf-1, Nod1 induces activation of NF- κ B (Inohara et al. 1999). Nod1 mediates activation of NF- κ B in response to LPS and the cell-invasive *Shigella flexneri*, demonstrating that Nod1 is a cytoplasmic receptor for LPS (Inohara et al. 2001, Girardin et al. 2001). These findings suggest that the Nod family of proteins is involved in inflammatory responses, probably through recognition of LPS in the cytoplasm. Nod2, a molecule in the same family as Nod1 and Apaf-1, also mediates LPS-induced NF- κ B activation. Furthermore, frameshift and missense mutations in NOD2 are associated with susceptibility to Crohn's disease. However, the

mutations found in these patients are likely restricted to the LRR domain that recognizes LPS, and the mutant NOD2 protein is defective in LPS-induced NF- κ B activation (Hugot et al. 2001, Ogura et al. 2001).

TLR2

TLR2 recognizes a variety of microbial components, including pathogenic lipoproteins such as gram-negative bacteria, mycoplasma, and spirochetes, peptidoglycan and lipoteichoic acid from gram-positive bacteria, lipoarabinomannan from mycobacteria, glucoinositolphospholipids from *Trypanosoma cruzi*, phenol-soluble module from *Staphylococcus epidermidis*, zymosan from fungi, glycolipids from *Treponema maltophilum*, and porins that form the outer membrane of *Neisseria*. (Aliprantis et al. 2000, Brightbill et al. 1999, Lien et al. 1999, Hirschfeld et al. 1999, , Campos et al. 2001, Underhill et al. 1999, Opitz et al. 2001). Analysis of TLR2-deficient mice reveals that TLR2 is critical for the recognition of peptidoglycan and lipoproteins (Takeuchi et al. 1999, Takeuchi et al. 2000). Accordingly, TLR2-deficient mice show increased susceptibility to infection by the Gram-positive bacterium *S. aureus* than wild-type mice (Takeuchi et al. 2000). Another TLR2-deficient mouse strain shows defective clearance of spirochetes after infection by *Borrelia burgdorferi* and unresponsiveness to *B. burgdorferi* lipoproteins (Wooten et al. 2002). Furthermore, TLR2 recognizes several types of atypical LPS from *Leptospira interrogans* and *Porphyromonas gingivalis*, in contrast to TLR4, which recognizes LPS from enterobacteria such as *Escherichia coli* and *Salmonella spp.* (Hirschfeld et al. 2001, Werts et al. 2001). The atypical LPS recognized by TLR2 is structurally and functionally distinct from the enterobacterial LPS recognized by TLR4. In particular, the two types of LPS differ structurally in the number of acyl chains in the lipid A component. TLR2 and TLR4 may recognize these structural variations in LPS differently. However, as in most of these studies, it is possible that very small amounts of contaminating TLR2 ligand in the LPS preparations may obscure some of these results (Netea et al. 2002). One aspect of TLR2 ligand recognition involves cooperation with other TLR family members, particularly TLR6 and TLR1, which discriminate between

different microbial components. In one study, the role of TLR6 was analyzed by introducing a dominant negative form into the RAW264.7 macrophage cell line. Peptidoglycan and secreted module in from *S. aureus* are TLR2 ligands that induce TNF- α production in RAW264.7 cells, but these responses are suppressed by expression of dominant negative TLR6 (Hajjar et al. 2001, Ozinsky et al. 2000). Coimmunoprecipitation of TLR2 and TLR6 suggests that they physically interact within the cell (Ozinsky et al. 2000). Analysis of TLR6-deficient mice also suggests that TLR6 functionally cooperates with TLR2 to recognize microbial lipopeptides (Takeuchi et al. 2002). For example, bacterial lipopeptides possess a triacylated NH₂-terminal cysteine residue, in contrast to mycoplasmal macrophage-activating lipopeptides 2 (MALP-2), which is solely diacylated. Macrophages derived from mice lacking TLR6 do not exhibit any inflammatory response to MALP-2, whereas these cells do respond normally to bacterial lipopeptides. Macrophages derived from mice lacking TLR2 exhibited an unresponsive phenotype to both lipopeptides. TLR2/TLR6 reconstitution experiments in doubly deficient embryonic fibroblasts indicate that both TLR2 and TLR6 are necessary for the response to MALP-2. Therefore, TLR6 is able to function in conjunction with TLR2, enabling the specific recognition of subtle differences between triacyl and diacyl lipopeptides (Hajjar et al. 2001; Ozinsky et al. 2001).

TLR9

TLR9 is required for the recognition of CPG DNA. Bacterial DNA is a potent activator of immune cells. The critical role of TLR9 in the recognition of bacterial DNA has been demonstrated using TLR9-deficient mice (Hemmi et al. 2000). The immunostimulatory activity of bacterial DNA is attributed to the presence of unmethylated CpG motifs, which are relatively rare in the vertebrate genome and, when they do occur, are typically methylated on cytosine residues and have no immunostimulatory activity. Therefore, CpG DNA is another prototypical molecular model by which the immune system recognizes pathogens. Synthetic ligand-deoxynucleotides containing unmethylated CpG motifs also activate immune cells. Administration of CpG DNA is sufficient to protect against infections caused by intracellular pathogens such as *Leishmania major* and *Listeria monocytogenes* in mice (Elkins

et al. 1999, Krieg et al. 1998, Zimmermann et al. 1998). CpG DNA also activates dendritic cells to produce the Th1-polarizing cytokine IL-12, leading to the development of Th1-like immune responses. Therefore, CpG DNA has promising therapeutic value as an adjuvant and anti-infectious agent (Wagner 1999, Wagner 2001). Human and mouse immune cells are optimally activated by slightly different CpG motifs (Krieg and Wagner 2000). This specificity may be explained by species differences in TLR9s. When mouse or human TLR9 was expressed in the CpG DNA nonresponsive cell line 293, these cells acquired the ability to respond to the optimal mouse or human CpG sequence, respectively (Bauer et al. 2001). These findings also suggest that TLR9 directly recognizes CpG DNA. Therefore, identification of optimal CpG motifs from humans and other animals or other synthetic agonists of TLR9 may lead to the creation of effective adjuvants for each species. Several studies have reported that CpG DNA is recognized in the endosome after nonspecific uptake into cells (Wagner 1999, Wagner 2001). This suggests that recognition of CpG DNA by TLR9 occurs in the endosome. Indeed, CpG DNA-induced activation of signaling cascades such as c-Jun N-terminal kinase (JNK) and NF- κ B is delayed compared with LPS-induced activation in normal macrophages (Hemmi et al. 2000). In studies, a monoclonal antibody against TLR9 was generated, and staining with this antibody revealed the intracellular localization of endogenous TLR9 in a mouse macrophage cell line (Ahmad-Nejad et al. 2002). This is in sharp contrast to TLR1, TLR2 and TLR4, which are expressed on the cell surface (Yang et al. 1999, Visintin et al. 2001). TLR2 is recruited to phagosomes after zymosan stimulation (Underhill et al. 1999, Ozinsky et al. 2000). Therefore, internalization of TLR ligands may be necessary for full activation of immune cells by TLRs, or the signaling pathways through TLR9 may have some different properties from other TLRs.

Molecular Relationship of TLR2, TLR4 AND TLR9 with Type Virulence

Notwithstanding the presence of robust barriers comprising urothelial cells in the human urinary tract, instances have been observed where uropathogenic microorganisms have successfully

gained access to the urinary tract. Upon entry of uropathogenic microorganisms into the urinary tract, innate immune responses are initiated through the expression of relevant Toll-like receptors (TLRs) in the urothelial cells of the bladder (cystitis) and kidneys (nephritis) (Reygaert 2014, Takeuchi and Akira 2010). Consequently, the expression of relevant TLRs results in the initiation of diverse cascade responses, including the release of chemokines, interferons, interleukins, antimicrobial agents and proinflammatory cytokines (Spencer et al., 2014; Bryant et al., 2015; Behzadi et al., 2016).

Urinary tract infection and TLR2

TLR2 typically forms heterodimeric complexes with either TLR1 or TLR6, with each complex exhibiting distinct characteristics and properties. Some studies have demonstrated that TLR2 co-receptors, including TLR1 and TLR6, exhibit a notable degree of amino acid sequence similarity, reaching up to 66%. Nevertheless, the ligand active sites of TLR1 and TLR6 exhibit minimal amino acid sequence similarity, which may result in disparate conformational structures. These diversities permit TLR2 heterodimers to recognise microbial pathogen-associated molecular patterns (PAMPs) and ligands. It is noteworthy that TLR2 homomers do not exhibit any discernible functional characteristics in humans. Accordingly, the literature examines TLR1-TLR2 and TLR2-TLR6 heterodimers in separate subheadings. TLR2 proteins play a crucial role in the recognition of atypical LPS from non-Enterobacteriaceae bacteria, including *Leptospira interrogans*. Among the numerous target ligands, lipoproteins, lipoteichoic acid, peptidoglycans, HSPs (60, 70, 90), and fungal zymosan are of particular importance for the detection and identification of urinary tract infections caused by microbial pathogens (Takeda et al. 2003, Botos et al. 2011, Bryant et al. 2015).

The TLR1-TLR2 heterodimer complex can detect and identify PAMP molecules of triacylated lipoproteins in *Mycoplasma spp*, *Ureaplasma sp*, and Gram-negative bacteria, including *E. coli*, *Klebsiella pneumoniae*, and *Pseudomonas aeruginosa*, which are important bacteria that cause urinary tract infections (LoVullo et al. 2015). Furthermore, other members of Enterobacteriaceae that have triacylated lipoproteins in their outer membrane can be recognized by

TLR1-TLR2 heterodimers. TLR1 contains a hydrophobic channel that binds to one of the lipid molecules of triacylated lipoproteins. This channel promotes the presence of a triacylated lipoprotein as a PAMP to be recognized by TLR1. The TLR2 heterodimer binds to the sol molecules of triacylated lipoproteins. Crystallographic studies show M-shaped structures in TLR1-TLR2 heterodimers. Lipoproteins are proteins combined with lipids. Lipids are normally linked to the NH₂-terminal cysteine of proteins by covalent bonds. Lipoproteins are divided into two main groups: diacylated and triacylated. Therefore, the TLR1-TLR2 heterodimer complex plays a key role in urinary tract infections caused by Gram-negative bacteria, especially members of the Enterobacteriaceae, such as uropathogenic *E. coli* infections (Jahandeh et al. 2015, Kang and Lee 2011, Behzadi and Behzadi 2011). Similar to TLR1-TLR2 heterodimers, the extracellular heterodimers of TLR2-TLR6 share an M-form structure. TLR2-TLR6 heterodimers do not participate in the hydrophobic channel within their structure; therefore, these complexes cannot recognize triacylated lipoproteins. TLR2-TLR6 heterodimers can detect different microbial PAMPs, including diacylated lipoproteins in *Mycoplasma spp.*, zymosan in fungi, especially in yeasts (such as *Saccharomyces cerevisiae* and *C. albicans*), bacterial lipoteichoic acid in *Staphylococcus*, and peptidoglycans and secreted microbial HSPs in gram-positive bacteria. In addition, TLR2-TLR6 heterodimers can detect the 2 kDa mycoplasmal MΦ activating lipoprotein (MALP). However, TLR2 proteins are responsible for distinguishing the type of bacterial lipoproteins. Recognition of the above-mentioned target ligands may lead to the release of proinflammatory cytokines. TLR2-TLR6 heterodimers play a key role in the recognition and detection of important bacteria that cause urinary tract infections, such as *C. albicans*, *Staphylococcus spp.*, *Streptococcus spp.*, *Mycoplasma spp.* and *Ureaplasma spp.* Some studies have reported that bacterial triacylated lipoproteins are target ligands for TLR2-TLR10 heterodimers and diacylated lipoproteins are target ligands for TLR1-TLR10 heterodimers and TLR10-TLR10 homodimers. However, the role of TLR10 in the human innate immune system is unclear (Höfs et al. 2016, Kang and Lee 2011, Regan et al. 2013).

Urinary tract infection and TLR4

The most important target ligands for TLR4 molecules are LPS (such as uropathogenic *E. coli* and other related members of the *Enterobacteriaceae* family that cause urinary tract infections), type I and P fimbriae, and HSP molecules of 60, 70, and 90. TLR4 molecules are expressed in the presence of microbial HSPs secreted by uropathogenic *E. coli*, *C. albicans*, etc. Most uropathogenic *E. coli* strains contain type I fimbriae and the virulence factor FimH. FimH enables uropathogenic *E. coli* to adhere to uroplakin 1a molecules. Uroplakin 1a molecules are found on the surface of urothelial cells lining the inner lining of the bladder in the human urinary tract. Therefore, binding of uropathogenic *E. coli* cells to uroplakin 1 molecules stimulates TLR4 molecules to eliminate foreign pathogens from the bladder. TLR4 molecules are known to be expressed in urothelial cells surrounding the kidneys and bladder in the urinary tract. The severity of urinary tract infection, i.e. the number of uropathogenic *E. coli*, determines the level of expression of TLR4 molecules. For example, the level of TLR4 molecules secretion in patients with reduced asymptomatic bacteriuria infection is significantly lower than in patients with acute and symptomatic urinary tract infection. A healthy immune system is able to clear the urinary tract from microbial pathogens such as uropathogenic *E. coli* within one to several days (Reygaert 2014, Jahandeh et al. 2015, Spencer et al. 2014). LPS molecules found in the outer membrane of Gram-negative bacteria such as members of the *Enterobacteriaceae* family trigger the expression of TLR4 molecules. Active and effective TLR4 molecules include MD-2 (a co-receptor molecule that is serum-soluble and/or bound to the cytoplasmic membrane and/or binds to TLR), LPS-binding proteins (serum-soluble LPSBP), and CD14. (soluble in serum and/or bound to the cytoplasmic membrane and/or binds to TLR). Indeed, the formation of this complex enables TLR4 to effectively eliminate uropathogenic *E. coli* cells from the urinary tract. The MD-2 component facilitates the binding of the hydrophobic portion of LPS to the extracellular domain of TLR4. The number of fatty chains present in the lipid A associated with the LPS molecule is a determining factor in the level of TLR4 expression, which in turn affects the intensity of the inflammatory response. TLR4 molecules are expressed by uropathogenic *E. coli* cells

that invade the urothelial cells of the bladder and kidneys. In the context of TLR4 molecule invasion of urothelial cells, the presence of Type I fimbriae represents an evolutionary adaptation of uropathogenic *E. coli* to evade immunological responses such as those mediated by TLR4. This virulence factor can dominate the TLR4 defence system, thereby promoting the intracellular progression of uropathogenic *E. coli* cells in the urinary tract. Therefore, bacterial components including LPS, FimH adhesin, type I and P fimbriae in UPEC are recognized as TLR4 inducers in the host urinary tract. Most of the invasive uropathogenic *E. coli* cells are resistant to TLR4 molecules, and their presence in the urinary tract results in chronic and/or complicated cystitis and/or pyelonephritis. Therefore, the impairment or dysfunction of innate immune responses facilitates the development and progression of urinary tract infection in humans (West et al. 2006, Takeda et al. 2003, Botos et al. 2011, Spencer et al. 2014, Jin and Lee 2008). In addition to uropathogenic *E. coli* cells, *C. albicans* yeasts trigger the innate immune system through the expression of TLR4 proteins. TLR4 is expressed against *C. albicans* yeasts in types of candidiasis such as urinary tract candidiasis. Expression of TLR4 adaptors is mediated by linear and short chains of O-linked mannan polymers. In contrast to TLR2, expression of TLR4 against *C. albicans* does not lead to the secretion of proinflammatory cytokines but triggers the secretion of type I interferons (IFN). In this context, mannose receptors, which contribute to the fungal phagocytosis process, are blocked for the internalization of zymosan through the expression of TLR4 adaptors. In addition, the recruitment of neutrophils and the secretion of some chemokines are significantly reduced (Höfs et al. 2016, West et al. 2006, Botos et al. 2011, Netea et al. 2006). HSP molecules, including HSP60, HSP70, and 90, are well-known chaperokines that support eukaryotic and prokaryotic cells under normal and stressful conditions. The presence of released microbial HSPs can trigger TLR4 expression in the host urinary tract. These chaperokines are recognized by both uropathogenic *E. coli* and *C. albicans* cells. However, HSPs can link innate immunity to adaptive immunity mechanisms (Medzhitov 2001, Asea 2008).

Urinary tract infection and TLR9

Microbial unmethylated CpG-DNAs represent an appropriate target ligand for TLR9. Consequently, TLR9 molecules are expressed in the presence of unmethylated CpG-DNA motifs belonging to bacteria, fungi, viruses and protozoa. They are capable of distinguishing between nucleic structures that are part of their own structures. TLR9 plays a pivotal role in defending against cytomegaloviruses. Cytomegalovirus infection can be fatal for patients with kidney infection following kidney graft surgery (Bryant et al. 2015, Gluba et al. 2010, Vandewalle 2008).

Results

The relationship between urinary tract infections (UTIs) and Toll-like receptors (TLRs) is of critical importance for the functioning of host defense mechanisms. Toll-like receptors (TLRs) play a pivotal role in the initiation of both innate and adaptive immune responses by recognizing the molecular structures of pathogens. In particular, TLR4 is capable of recognising lipopolysaccharides (LPS) of bacteria such as *Escherichia coli*, which are commonly observed in urinary tract infections, and this results in the triggering of inflammatory responses. However, maintaining equilibrium in the TLR-mediated response is of paramount importance for controlling infection and preventing excessive inflammation. While excessive activation of TLRs can result in tissue damage and chronic inflammation, insufficient activation can facilitate the spread of pathogens and the progression of infection. Therefore, regulating TLRs represents a critical factor for effectively managing UTIs and maintaining optimal host defense.

REFERENCES

- Ahmad-Nejad, P., Häcker, H., Rutz, M., Bauer, S., Vabulas, R. M., and Wagner, H. (2002). Bacterial CpG-DNA and lipopolysaccharides activate Toll-like receptors at distinct cellular compartments. *European journal of immunology*, 32, 1958-1968.
- Akashi, S., Nagai, Y., Ogata, H., Oikawa, M., Fukase, K., Kusumoto, S., and Miyake, K. (2001). Human MD-2 confers on mouse Toll-like receptor 4 species-specific lipopolysaccharide recognition. *International immunology*, 13, 1595-1599.
- Akashi, S., Shimazu, R., Ogata, H., Nagai, Y., Takeda, K., Kimoto, M., and Miyake, K. (2000). Cutting edge: cell surface expression and lipopolysaccharide signaling via the toll-like receptor 4-MD-2 complex on mouse peritoneal macrophages. *The Journal of Immunology*, 164, 3471-3475.
- Aliprantis, A.O., Yang, R.B., Weiss, D.S., Godowski, P. and Zychlinsky, A. (2000). The apoptotic signaling pathway activated by Toll-like receptor. *EMBO J.* 19:3325– 36
- Amna, M.A., Chazan, B., Raz, R., Edelstein, H. and Colodner, R. (2013). Risk factors for non-*Escherichia coli* community-acquired bacteriuria. *Infection*. Apr;41:473-7.
- Anger, J.T., Saigal, C.S., Wang, M. (2008). Urologic disease burden in the United States: veteran users of Department of Veterans Affairs healthcare. *Urology*;72:37–41
- Asea, A., Rehli, M., Kabingu, E., Boch, J.A., Bare. O. (2002). Novel signal transduction pathway utilized by extracellular HSP70: role of TLR2 and TLR4. *J. Biol. Chem.* 277:15028–34
- Asea, A. (2008). Heat shock proteins and toll-like receptors. *Toll-like receptors (TLRs) and innate immunity*: Springer; pp. 111-127.
- Basu, S., Binder, R.J., Ramalingam, T., Srivastava, P.K. (2001). CD91 is a common receptor for heat shock proteins gp96, hsp90, hsp70, and calreticulin. *Immunity* 14:303–13
- Bauer, S., Kirschning, C.J., Hacker, H., Redecke, V., Hausmann, S. (2001). Human TLR9 confers responsiveness to bacterial DNA

- via species-specific CpG motif recognition. *Proc. Natl. Acad. Sci. USA* 98:9237–42
- Behzadi, P. and Behzadi, E. (2008). The microbial agents of urinary tract infections at Central Laboratory of Dr. Shariati Hospital, Tehran, Iran. *Turk Klin Tip Bilim.*; 28: 445-449.
- Bent, S., Nallamotheu, B.K., Simel, D.L. (2002). Does this woman have an acute uncomplicated urinary tract infection? *JAMA*; 287:2701–10.
- Botos, I., Segal, D.M., Davies, D.R. (2011). The structural biology of Toll-like receptors. *Structure*; 19: 447-459.
- Brightbill, H.D., Libraty, D.H., Krutzik, S.R., Yang, R.B., Belisle, J.T. (1999). Host defense mechanisms triggered by microbial lipoproteins through Toll-like receptors. *Science* 285:732–36
- Brown, P., Ki, M., Foxman, B. (2005). Acute pyelonephritis among adults: cost of illness and considerations for the economic evaluation of therapy. *Pharmacoeconomics*; 23:1123–42
- Bryant, C.E., Gay, N.J., Heymans, S., Sacre, S., Schaefer, L., Midwood, K.S. (2015). Advances in Toll-like receptor biology: Modes of activation by diverse stimuli. *Crit Rev Biochem Mol Biol.*; 50: 359-379
- Bulut, Y., Fayure, E., Thomas, L., Karahashi, H., Michelsen, K.S. (2002). Chlamydial heat shock protein 60 activates macrophages and endothelial cells through Toll-like receptor 4 and MD2 in a MyD88-dependent pathway. *J. Immunol.* 168:1435–40
- Byrd-Leifer, C.A., Block, E.F., Takeda, K., Akira, S., Ding, A. (2001). The role of MyD88 and TLR4 in the LPS-mimetic activity of Taxol. *Eur. J. Immunol.* 31:2448–57
- Cai, T., Mazzoli, S., Mondaini, N. (2012). The role of asymptomatic bacteriuria in young women with recurrent urinary tract infections: to treat or not to treat? *Clin Infect Dis*; 55:771–7.
- Caljouw, M.A., den Elzen, W.P., Cools, H.J., Gussekloo, J. (2011). Predictive factors of urinary tract infections among the oldest old in the general population. A population-based prospective follow-up study. *BMC medicine.* Dec;9:1-8.

- Campos, M.A., Almeida, I.C., Takeuchi, O., Akira, S., Valente, E.P.(2001). Activation of Toll-like receptor-2 by glycosylphosphatidylinositol anchors from a protozoan parasite. *J. Immunol.* 167:416–23
- Chuang, T.H., Ulevitch, R.J. (2000). Cloning and characterization of a sub-family of human Toll-like receptors: hTLR7, hTLR8 and hTLR9. *Eur. Cytokine Netw.* 11:372–78
- Chuang, T.H., Ulevitch, R.J. (2001). Identification of hTLR10: a novel human Tolllike receptor preferentially expressed in immune cells. *Biochim. Biophys. Acta* 1518:157–61
- Craig, J.C., Simpson, J.M., Williams, G.J.(2009). Antibiotic prophylaxis and recurrent urinary tract infection in children. *N Engl J Med*; 361:1748–59.
- Da Shilva Correia, J., Soldau, K., Christen, U., Tobias, P.S., Ulevitch, J. (2001). Lipopolysaccharide is in close proximity to each of the protein in its membrane receptor complex. *J. Biol. Chem.* 276:21129–35
- Detmers, P.A., Thieblemont, N., Vasselon, T., Pironkova, R., Miller, D.S. (1996). Potential role of membrane internalization and vesicle fusion in adhesion of neutrophils in response to lipopolysaccharide and TNF. *J. Immunol.* 157:5589–96
- Drekonja, D.M., Rector, T.S., Cutting. A. (2013). Urinary tract infection in male veterans: treatment patterns and outcomes. *JAMA Intern Med*; 173:62–8.
- Du, X., Poltorak, A., Wei, Y., Beutler, B. (2000). Three novel mammalian toll-like receptors: gene structure, expression, and evolution. *Eur. Cytokine Netw.* 11:362–71
- Dybdahl, B., Wahba, A., Lien, E., Flo, T.H., Waage, A. (2002). Inflammatory response after open heart surgery: release of heat-shock protein 70 and signaling through toll-like receptor-4. *Circulation* 105:685–90
- Dwyer, J.P., Dwyer, P.L.(2013). Lactobacillus probiotics may prevent recurrent UTIs in postmenopausal women. *BMJ Evidence-Based Medicine.* Aug 1;18(4):141-2.

- Elkins, K.L., Rhinehart-Jones, T.R., Stibitz, S., Conover, J.S., Klinman, D.M. (1999). Bacterial DNA containing CpG motifs stimulates lymphocyte-dependent protection of mice against lethal infection with intracellular bacteria. *J. Immunol.* 162:2291–98
- Evans, D.A., Williams, D.N., Laughlin, L.W.(1978). Bacteriuria in a population-based cohort of women. *J Infect Dis*;138:768–73.
- Foxman, B., Gillespie, B., Koopman, J.(2000). Risk factors for second urinary tract infection among college women. *Am J Epidemiol*; 151:1194–205.
- Foxman, B., Manning, S.D., Tallman, P. (2002). Uropathogenic *Escherichia coli* are more likely than commensal *E. coli* to be shared between heterosexual sex partners. *Am J Epidemiol*; 156:1133–40.
- Gallucci, S., Matzinger, P. (2001). Danger signals: SOS to the immune system. *Curr. Opin. Immunol.* 13:114–19
- Girardin, S.E., Tournebise, R., Mavris, M., Page, A.L., Li, X. (2001). CARD4/Nod1 mediates NF- κ B and JNK activation by invasive *Shigella flexneri*. *EMBO Rep.* 2: 736–42
- Gluba, A., Banach, M., Hannam, S., Mikhailidis, D.P., Sakowicz, A., Rysz, J.(2010). The role of Tolllike receptors in renal diseases. *Nat Rev Nephrol.*; 6: 224-235.
- Gordon, L.B., Waxman, M.J., Ragsdale, L. (2013). Overtreatment of presumed urinary tract infection in older women presenting to the emergency department. *J Am Geriatr Soc*; 61:788–92
- Harmanli, O.H., Cheng, G.Y., Nyirjesy, P., Chatwani, A., Gaughan, J.P. (2000). Urinary tract infections in women with bacterial vaginosis. *Obstetrics and Gynecology.* May 1;95(5):710-2.
- Habich, C., Baumgart, K., Kolb, H., Burkart, V. (2002). The receptor for heat shock protein 60 on macrophages is saturable, specific, and distinct from receptors for other heat shock proteins. *J. Immunol.* 168:569–76
- Hawn, T. R., Scholes, D., Li, S. S., Wang, H., Yang, Y., Roberts, P. L., Stapleton, A. E., Janer, M., Aderem, A., Stamm, W. E., Zhao, L. P., and Hooton, T. M. (2009). Toll-Like Receptor Polymorphisms and Susceptibility to Urinary Tract Infections in Adult Women.

- PLoS ONE, 4(6), e5990.
<https://doi.org/10.1371/journal.pone.0005990>
- Haynes, L.M., Moore, D.D., Kurt-Jones, E.A., Finberg, R.W., Anderson, L.J. (2001). Involvement of Toll-like receptor 4 in innate immunity to respiratory syncytial virus. *J. Virol.* 75:10730–37
- Hemmi, H., Takeuchi, O., Kawai, T., Kaisho, T., Sato, S. (2000). A Toll-like receptor recognizes bacterial DNA. *Nature* 408:740–45
- Hirji I, Guo Z, Andersson SW, Hammar N, Gomez-Camirero A. (2012). Incidence of urinary tract infection among patients with type 2 diabetes in the UK General Practice Research Database (GPRD). *Journal of Diabetes and its Complications.* Nov 1;26(6):513-6.
- Hirschfeld, M., Kirschning, C.J., Schwandner, R., Wesche, H., Weis, J.H. (1999). Cutting Edge: Inflammatory signaling by *Borrelia burgdorferi* lipoproteins is mediated by Toll-like receptor 2. *J. Immunol.* 163:2382–86
- Hirschfeld, M., Weis, J.J., Toshchakov, V., Salkowski, C.A., Cody, M.J. (2001). Signaling by Toll-like receptor 2 and 4 agonists results in differential gene expression in murine macrophages. *Infect. Immun.* 69:1477–82
- Hoffmann, J.A., Kafatos, F.C., Janeway, C.A., Ezekowitz, R.A.B. (1999). Phylogenetic perspectives in innate immunity. *Science* 284:1313–18
- Hooton, T.M., Bradley, S.F., Cardenas, D.D. (2010). Diagnosis, prevention, and treatment of catheter-associated urinary tract infection in adults: 2009 International Clinical Practice Guidelines from the Infectious Diseases Society of America. *Clin Infect Dis* ; 50:625–63.
- Hooton, T.M., Scholes, D., Hughes, J.P. (1996). A prospective study of risk factors for symptomatic urinary tract infection in young women. *N Engl J Med*;335: 468–74.
- Hoshino, K., Takeuchi, O., Kawai, T., Sanjo, H., Ogawa, T. (1999). Cutting Edge: Toll-like receptor 4 (TLR4)-deficient mice are

- hyporesponsive to lipopolysaccharide: evidence for TLR4 as the Lps hene product. *J. Immunol.* 162:3749–52
- Höfs, S., Mogavero, S., Hube, B. (2016). Interaction of *Candida albicans* with host cells: virulence factors, host defense, escape strategies, and the microbiota. *J Microbiol.*; 54: 149-169
- Hugot, J.P., Chamaillard, M., Zouali, H., Lesage, S., Cezard, J.P. (2001). Association of NOD2 leucine-rich repeat variants with susceptibility to Crohn's disease. *Nature* 411:599–603
- Inohara, N., Koseki, T., del peso, L., Hu, Y., Yee, C. (1999). Nod1, an Apaf-1-like activator of caspase-9 and nuclear factor κ B. *J. Biol. Chem.* 274:14560–67
- Inohara, N., Ogura, Y., Chen, F.F., Muto, A., Nunez, G. (2001). Human Nod1 confers responsiveness to bacterial lipopolysaccharides. *J. Biol. Chem.* 276:2551–54
- Jahandeh, N., Ranjbar, R., Behzadi, P., Behzadi, E. (2015). Uropathogenic *Escherichia coli* virulence genes: invaluable approaches for designing DNA microarray probes. *Cent European J Urol.*; 68: 452-458.
- Jiang, Q., Akashi, S., Miyake, K., Petty, H.R. (2000). Cutting Edge: Lipopolysaccharide induces physical proximity between CD14 and Toll-like receptor 4 (TLR4) prior to nuclear translocation of NF- κ B. *J. Immunol.* 165:3541–44
- Jin, M.S., Lee, J.O. (2008). Structures of the toll-like receptor family and its ligand complexes. *Immunity.*; 29: 182-191.
- Johnson, G.B., Brunn, G.J., Kodaira, Y., Platt, J.L. (2002). Receptor-mediated monitoring of tissue well-being via detection of soluble heparan sulfate by Toll-like receptor 4. *J. Immunol.* 168:5233–39
- Kang, J.Y., Lee, J.O. (2011). Structural biology of the Toll-like receptor family. *Ann Rev Biochem.* 2011; 80: 917-941.
- Kawasaki, K., Akashi, S., Shimazu, R., Yoshida, T., Miyake, K. (2000). Mouse Toll-like receptor 4-MD-2 complex mediates lipopolysaccharide-mimetic signal transduction by Taxol. *J. Biol. Chem.* 275:2251–54

- Kawasaki, K., Gomi, K., Nishijima, M. (2001). Cutting edge: Gln22 of mouse MD-2 is essential for species-specific lipopolysaccharide mimetic action of taxol. *J. Immunol.* 166:11–14
- Kazemier, B.M., Schneeberger, C., De Miranda, E. (2012). Costs and effects of screening and treating low risk women with a singleton pregnancy for asymptomatic bacteriuria, the ASB study. *BMC Pregnancy Childbirth* 2012; 12:52.
- Ki, M., Park, T., Choi, B. (2004). The epidemiology of acute pyelonephritis in South Korea, 1997-1999. *Am J Epidemiol* 2004; 160:985–93.
- Krieg, A.M., Love-Homan, L., Yi, A.K., Harty, J.T. (1998). CpG DNA induces sustained IL12 expression in vivo and resistance to *Listeria monocytogenes* challenge. *J. Immunol.* 161:2428–34
- Krieg, A.M., Wagner, H. (2000). Causing a commotion in the blood: immunotherapy progresses from bacteria to bacterial DNA. *Immunol. Today* 21:521–26
- Kurt-Jones, E.A., Popova, L., Kwinn, L., Haynes, L.M., Jones, L.P. (2000). Pattern recognition receptors TLR4 and CD14 mediate response to respiratory syncytial virus. *Nat. Immunol.* 1:398–401
- Laupland, K.B., Ross, T., Pitout, J.D. (2007). Community-onset urinary tract infections: a population-based assessment. *Infection*; 35:150–3.
- Lewis, S.S., Knelson, L.P., Moehring, R.W. (2013). Comparison of non-intensive care unit (ICU) versus ICU rates of catheter-associated urinary tract infection in community hospitals. *Infect Control Hosp Epidemiol* 2013; 34:744–7.
- Lien, E., Means, T.K., Heine, H., Yoshimura, A., Kusumoto, S. (2000). Toll-like receptor 4 imparts ligand-specific recognition of bacterial lipopolysaccharide. *J. Clin. Invest.* 105:497–504
- LoVullo, E.D., Wright, L.F., Isabella, V., Huntley, J.F., Pavelka, M.S. (2015). Revisiting the Gram-negative lipoprotein paradigm. *J Bacteriol.*; 197: 1705-1715.
- Marrs, C.F., Zhang, L., Foxman, B. (2005). *Escherichia coli* mediated urinary tract infections: are there distinct uropathogenic *E. coli*

- (UPEC) pathotypes?. FEMS microbiology letters. Nov 1;252(2):183-90.
- Medzhitov, R., Preston-Hurlburt, P., Janeway, C.A. (1997). A human homologue of the Drosophila Toll protein signals activation of adaptive immunity. Nature 388:394–97
- Medzhitov, R. (2001). Toll-like receptors and innate immunity. Nat Rev Immunol.; 1: 135-145.
- Melzer, M., Welch, C. (2013). Outcomes in UK patients with hospital-acquired bacteraemia and the risk of catheter-associated urinary tract infections. Postgraduate medical journal. Jun;89(1052):329-34.
- Miyake, K. , Yamashita, Y., Ogata, M., Sudo, T., Kimoto, M. (1995). RP105, a novel B cell surface molecule implicated in B cell activation, is a member of the leucine-rich repeat protein family. J. Exp. Med. 154:3333–40
- Mulvey, M.A., Schilling, J.D., Martinez, J.J. (2000). Bad bugs and beleaguered bladders: interplay between uropathogenic *Escherichia coli* and innate host defenses. Proc Natl Acad Sci U S A; 97:8829–35.
- Nagai, Y., Akashi, S., Nagafuku, M., Ogata, M., Iwakura, Y. (2002). Essential role of MD-2 in LPS responsiveness and TLR4 distribution. Nat. Immunol. 3:667–72
- Netea, M.G., Gow, N.A., Munro, C.A. (2006). Immune sensing of *Candida albicans* requires cooperative recognition of mannans and glucans by lectin and Toll-like receptors. J Clin Invest.; 116: 1642-1650.
- Netea, M.G., Van der Graaf, C.A., Vonk, A.G., Verschueren, I., Van der Meer, J.W., Kullberg, B.J. (2002). The role of toll-like receptor (TLR) 2 and TLR4 in the host defense against disseminated candidiasis. J Infect Dis.; 185: 1483-1489.
- Netea, M.G., van Deuren, M., Kullberg, B.J., Cavaillon, J.M., Van der Maer, W.M. (2002). Does the shape of lipid A determine the interaction of LPS with Toll-like receptors? Trends Immunol. 23:135–39

- Nicolle, L.E., Harding, G.K., Preiksaitis, J. (1982). The association of urinary tract infection with sexual intercourse. *J Infect Dis* ; 146:579–83.
- Nicolle, L.E. (2009). Urinary tract infections in the elderly. *Clin Geriatr Med* 2009;25: 423–36
- Ogata, H., Su, I., Miyake, K., Nagai, Y., Akashi, S. (2000). The Toll-like receptor protein RP105 regulates lipopolysaccharide signaling in B cells. *J. Exp. Med.* 192:23– 29
- Ogura, Y., Bonen, D.K., Inohara, N., Nicolae, D.L., Chen, F.F. (2001). A frameshift mutation in NOD2 associated with susceptibility to Crohn's disease. *Nature* 411:603–6
- Ohashi, K., Burkart, V., Flohe, S., Kolb, H. (2000). Cutting edge: heat shock protein 60 is a putative endogenous ligand of the toll-like receptor-4 complex. *J. Immunol.* 164:558–61
- Okamura, Y., Watari, M., Jerud, E.S., Young, D.W. (2001). The extra domain A of fibronectin activates Toll-like receptor 4. *J. Biol. Chem.* 276:10229–33
- Opitz, B., Schroder, N.W., Spreitzer, I., Michelsen, K.S., Kirschning, C.J. (2001). Toll-like receptor-2 mediates *Treponema* glycolipid and lipoteichoic acid-induced NF- κ B translocation. *J. Biol. Chem.* 276:22041–47
- Ozinsky, A., Underhill, D.M., Fontenot, J.D., Hajjar, A.M., Smith, K.D. (2000). The repertoire for pattern recognition of pathogens by the innate immune system is defined by cooperation between Toll-like receptors. *Proc. Natl. Acad. Sci. USA* 97:13766–71
- Paulsen, M.T., Veloso, A., Prasad, J., Bedi, K., Ljungman, E.A., Tsan, Y.C., Chang, C.W. (2013). Tarrrier B, Washburn JG, Lyons R, Robinson DR. Coordinated regulation of synthesis and stability of RNA during the acute TNF-induced proinflammatory response. *Proceedings of the National Academy of Sciences.* Feb 5;110(6):2240-5.
- Pickard, R., Lam, T., Maclennan, G. (2012). Types of urethral catheter for reducing symptomatic urinary tract infections in hospitalised adults requiring short-term catheterisation: multicentre randomised controlled trial and economic evaluation of

- antimicrobial- and antiseptic-impregnated urethral catheters (the CATHETER trial). *Health Technol Assess*; 16:1–197.
- Pitout, J.D. (2012). Extraintestinal pathogenic *Escherichia coli*: a combination of virulence with antibiotic resistance. *Frontiers in microbiology*. Jan 19;3:9.
- Poltorak, A., He, X., Smirnova, I., Liu, M.Y., Huffel, C.V.(1998). Defective LPS signaling in C3H/HeJ and C57BL/10ScCr mice: mutation in Tlr4 gene. *Science* 282:2085–88
- Qureshi, S.T., Lariviere, L., Leveque, G., Clermont, S., Moore, K.J. (1999). Endotoxintolerant mice have mutations in Toll-like receptor 4 (Tlr4). *J. Exp. Med.* 189:615– 25
- Ragnarsdóttir, B., Jönsson, K., Urbano, A., Grönberg-Hernandez, J., Lutay, N., Tammi, M., Gustafsson, M., Lundstedt, A.-C., Leijonhufvud, I., Karpman, D., Wullt, B., Truedsson, L., Jodal, U., Andersson, B., and Svanborg, C. (2010). Toll-Like Receptor 4 Promoter Polymorphisms: Common TLR4 Variants May Protect against Severe Urinary Tract Infection. *PLoS ONE*, 5(5), e10734. <https://doi.org/10.1371/journal.pone.0010734>
- Ramos, N.L., Sekikubo, M., Dzung, D.T.(2012). Uropathogenic *Escherichia coli* isolates from pregnant women in different countries. *J Clin Microbiol*; 50:3569–74
- Rassa, J.C., Meyers, J.L., Zhang, Y., Kudaravalli, R., Ross, S.R. (2002). Murine retroviruses activate B cells via interaction with Toll-like receptor 4. *Proc. Natl. Acad. Sci. USA* 99:2281–86
- Regan, T., Nally, K., Carmody, R. (2013). Identification of TLR10 as a key mediator of the inflammatory response to *Listeria monocytogenes* in intestinal epithelial cells and macrophages. *J Immunol.*; 191: 6084-6092.
- Regenbogen, S.E., Read, T.E., Roberts, P.L., Marcello, P.W., Schoetz, D.J., Ricciardi, R. (2011). Urinary tract infection after colon and rectal resections: more common than predicted by risk-adjustment models. *Journal of the American College of Surgeons*. Dec 1;213(6):784-92.

- Reygaert, W.C. (2014). Innate Immune Response to Urinary Tract Infections Involving *Escherichia coli*. *J Clin Cell Immunol.*; 5: 280
- Rock, F.L., Hardiman, G., Timans, J.C., Kastelein, R.A., Bazan, J.F. (1998). A family of human receptors structurally related to *Drosophila* Toll. *Proc. Natl. Acad. Sci. USA* 95:588–93
- Salo, J., Uhari, M., Helminen, M. (2012). Cranberry juice for the prevention of recurrences of urinary tract infections in children: a randomized placebo-controlled trial. *Clin Infect Dis* 2012; 54:340–6.
- Salvador, E., Wagenlehner, F., Köhler, C.D., Mellmann, A., Hacker, J., Svanborg, C., Dobrindt, U. (2012). Comparison of asymptomatic bacteriuria *Escherichia coli* isolates from healthy individuals versus those from hospital patients shows that long-term bladder colonization selects for attenuated virulence phenotypes. *Infection and immunity*. 2012 Feb;80(2):668-78.
- Sasu, S., LaVerda, D., Qureshi, N., Golenbock, D.T., Beasley, D. (2001). *Chlamydia pneumoniae* and chlamydial heat shock protein 60 stimulate proliferation of human vascular smooth muscle cells via toll-like receptor 4 and p44/p42 mitogenactivated protein kinase activation. *Circ. Res.* 89:244–50
- Schappert, S.M., Rechtsteiner, E.A. (2011). Ambulatory medical care utilization estimates for 2007. *Vital Health Stat* 13 2011;(169):1–38.
- Scholes, D., Hooton, T.M., Roberts, P.L., Gupta, K., Stapleton, A.E., Stamm, W.E. (2005). Risk factors associated with acute pyelonephritis in healthy women. *Annals of internal medicine*. Jan 4;142(1):20-7.
- Schromm, A.B., Lien, E., Henneke, P., Chow, J.C., Yoshimura, A. (2001). Molecular genetic analysis of an endotoxin nonresponder mutant cell line: a point mutation in a conserved region of MD-2 abolishes endotoxin-induced signaling. *J. Exp. Med.* 194:79–88
- Shimazu, R., Akashi, S., Ogata, H., Nagai, Y., Fukudome, K. (1999). MD-2, a molecule that confers lipopolysaccharide responsiveness on Toll- like receptor 4. *J. Exp. Med.* 189:1777–82

- Smaill, F., Vazquez, J.C. (2007). Antibiotics for asymptomatic bacteriuria in pregnancy. *Cochrane Database Syst Rev*;(2):CD000490.
- Smiley, S.T., King, J.A., Hancock, W.W. (2001). Fibrinogen stimulates macrophage chemokine secretion through Toll-like receptor 4. *J. Immunol.* 167:2887–94
- Spencer, J.D., Schwaderer, A.L., Becknell, B., Watson, J., Hains, D.S. (2014). The innate immune response during urinary tract infection and pyelonephritis. *Pediatr Nephrol.*; 29: 1139-1149.
- Takeda, K., Kaisho, T., Akira, S. (2003). Toll-like receptors. *Annu Rev Immunol.*; 21: 335-376.
- Takeuchi, O., Hoshino, K., Kawai, T., Sanjo, H., Takada, H. (1999). Differential roles of TLR2 and TLR4 in recognition of Gram-negative and Gram-positive cell wall components. *Immunity* 11:443–51
- Takeuchi, O., Kaufmann, A., Grote, K., Kawai, T., Hoshino, K. (2000). Cutting Edge: Preferentially the R-stereoisomer of the Mycoplasmal lipopeptide macrophage-activating lipopeptide-2 activates immune cells through a Toll-like receptor 2- and MyD88-dependent signaling pathway. *J. Immunol.* 164:554–57
- Takeuchi, O., Kawai, T., Muhlradt, P.F., Radolf, J.D., Zychlinsky, A. (2001). Discrimination of bacterial lipopeptides by Toll-like receptor 6. *Int. Immunol.* 13:933–40
- Takeuchi, O., Kawai, T., Sanjo, H., Copeland, N.G., Gilbert, D.J. (1999). TLR6: a novel member of an expanding Toll-like receptor family. *Gene* 231:59–65
- Termeer, C., Benedix, F., Sleeman, J., Fieber, C., Voith, U. (2002). Oligosaccharides of hyaluronan activate dendritic cells via Toll-like receptor 4. *J. Exp. Med.* 195:99–111
- Terlizzi, M.E., Gribaudo, G., Maffei, M.E. (2017). UroPathogenic *Escherichia coli* (UPEC) infections: virulence factors, bladder responses, antibiotic, and non-antibiotic antimicrobial strategies. *Frontiers in microbiology.* Aug 15;8:1566.
- Triantafilou, K., Triantafilou, M., Dedrick, R.L.(2001). A CD14-independent LPS receptor cluster. *Nat. Immunol.* 2:338–45

- Ucka, I., Sax, H., Gayet-Ageron, A. (2013). High proportion of healthcare-associated urinary tract infection in the absence of prior exposure to urinary catheter: a cross-sectional study. *Antimicrob Resist Infect Control*; 2:5.
- Underhill, D.M., Ozinsky, A., Hajjar, A.M., Stevens, A., Wilson, C.B. (1999). The Toll-like receptor 2 is recruited to macrophage phagosomes and discriminates between pathogens. *Nature* 401:811-15
- Underhill, D.M., Ozinsky, A., Smith, K.D., Aderem, A. (1999). Toll-like receptor 2 mediates mycobacteria-induced proinflammatory signaling in macrophages. *Proc. Natl. Acad. Sci. USA* 96:14459–63
- Vabulas, R.M., Ahmad-Nejad, P., da Costa, C., Miethke, T., Kirschning, C.J. (2001). Endocytosed HSP60s use toll-like receptor 2 (TLR2) and TLR4 to activate the toll/interleukin-1 receptor signaling pathway in innate immune cells. *J. Biol. Chem.* 276:31332–39
- Vandewalle, A. (2008). Toll-like receptors and renal bacterial infections. *Chang Gung Med J.* 2008; 31: 525-537.
- Viriyakosol, S., Tobias, P.S., Kitchens, R.L., Kirkland, T.N. (2001). MD-2 binds to bacterial lipopolysaccharide. *J. Biol. Chem.* 276:38044–51
- Visintin, A., Mazzoni, A., Spitzer, J.A., Segal, D.M. (2001). Secreted MD-2 is a large polymeric protein that efficiently confers lipopolysaccharide sensitivity to Toll-like receptor 4. *Proc. Natl. Acad. Sci. USA* 98:12156–61
- Visintin, A., Mazzoni, A., Spitzer, J.H., Wyllie, D.H., Dower, S.K., Segal, D.M. (2001). Regulation of Toll-like receptors in human monocytes and dendritic cells. *J Immunol.* Jan 1;166(1):249-55. doi: 10.4049/jimmunol.166.1.249. PMID: 11123299.
- Wagner, H. (1999). Bacterial CpG DNA activates immune cells to signal infectious danger. *Adv. Immunol.* 73:329–67
- Wagner, H. (2001). Toll meets bacterial CpG-DNA. *Immunity* 14:499–502

- Warren, J.W., Platt, R., Thomas, R.J. (1978). Antibiotic irrigation and catheter-associated urinary-tract infections. *N Engl J Med*; 299:570–3.
- Werts, C., Tapping, R.I., Mathison, J.C., Chuang, T.H., Kravchenko, V. (2001). Leptospiral lipopolysaccharide activates cells through a TLR2-dependent mechanism. *Nat. Immunol.* 2:346–52
- Wirth, T., Falush, D., Lan, R., Colles, F., Mensa, P., Wieler, L.H., Karch, H., Reeves, P.R., Maiden, M.C., Ochman, H., Achtman, M. (2006). Sex and virulence in *Escherichia coli*: an evolutionary perspective. *Molecular microbiology.* Jun;60(5):1136-51.
- Wooten, R.M., Ma, Y., Yoder, R.A., Brown, J.P., Weis, J.H. (2002). Toll-like receptor 2 is required for innate, but not acquired, host defense to *Borrelia burgdorferi*. *J. Immunol.* 168:348–55
- Yang, R.B., Mark, M.R., Gurney, A.L., Godowski, P.J. (1999). Signaling events induced by lipopolysaccharide-activated Toll-like receptor 2. *J. Immunol.* 163:639– 43
- Zimmermann, S., Egeter, O., Hausmann, S., Lipford, G.B., Rocken, M. (1998). CpG oligodeoxynucleotides trigger protective and curative Th1 responses in lethal murine leishmaniasis. *J. Immunol.* 160:3627–30.

CHAPTER 5

ENVIRONMENTAL THREATS TO FRESHWATER MUSSELS: THE ROLE OF SODIUM HYDROXIDE

M.Sc. Elif KARGALIOĞLU¹, Dr. Göktuğ GÜL², Assoc. Prof. Dr.
Pınar ARSLAN YÜCE³, Prof. Dr. Aysel Çağlan GÜNAL⁴

DOI: <https://dx.doi.org/10.5281/zenodo.14258702>

¹ Department of Biology Education, Faculty of Gazi Education, Gazi University, Ankara, Türkiye elif.kargalioglu@gazi.edu.tr, Orcid ID: 0009-0000-2336-0795.

² Department of Medical Services and Techniques, Vocational School of Health Services, Gazi University, Ankara, Türkiye. goktuggul@gazi.edu.tr, Orcid: 0000-0003-1925-0803.

³ Department of Biology, Faculty of Science, Çankırı Karatekin University, Çankırı, Türkiye pinararslan@karatekin.edu.tr Orcid: 0000-0001-5910-2835.

⁴ Department of Biology Education, Faculty of Education, Gazi University, Ankara, Türkiye caglangunal@gazi.edu.tr Orcid: 0000-0002-9072-543X

INTRODUCTION

Sodium hydroxide (NaOH), an inorganic compound commercially called caustic soda, is a white, odorless, alkaline compound easily soluble in water. In case of contact with human tissue, it can cause chemical burns by corrosive effect. NaOH is utilized under laboratory conditions to remove carbon-containing substances, such as CO₂, from the environment (Medina-Martos et al., 2022). Industrially, it has a wide range of applications, including in the production of silk, paper, paint, and detergents, as well as in drain cleaning and neutralization in oil refineries. Due to its domestic and industrial use, NaOH can contaminate aquatic ecosystems through leaks, floods, and other means. Furthermore, its use in chemical control for managing unwanted species in aquatic ecosystems (Calazans et al., 2012; TenEyek, 2009) can lead to increased concentrations in water systems. NaOH can cause sudden and severe changes in pH levels within these systems.

According to the Working Group on Biological Effects of Contaminants (WGBEC), four main methods are required when assessing the effects of pollutants in water. These include residue levels in tissues, subcellular responses, tissue reactions, and the entire organism (Yancheva et al., 2018). Pollutants contaminating aquatic environments threaten all living organisms within these ecosystems (Mason, 2002). When investigating these threats, mortality rates and behavioral effects are evaluated (Maronãs and Damborenea, 2006; Soares et al., 2009).

Aquatic organisms exhibit a wide range of reactions to environmental impacts, which can occur in the form of migration or at the physiological and cellular levels. To study the cellular responses of aquatic organisms to various environmental pollutants, changes in oxidative stress mechanisms such as advanced oxidation protein products (AOPP), glutathione (GSH), and malondialdehyde (MDA) levels can be examined.

AOPP have recently emerged as significant biomarkers indicating oxidative stress's impact on organisms' protein structures (Witko-Sarsat et al., 1996). AOPP, which shares considerable similarities with

advanced glycation end products, is defined as protein products containing dityrosine (e.g., pentosidine). Some researchers have reported that AOPP functions as a cytokine mediator (Büyükgüzel, 2013; Kalousová et al., 2002; Öztürk, 2008).

The glutathione (GSH) mechanism is responsible for detoxifying reactive oxygen species, exhibiting intracellular and extracellular activity (Terpstra et al., 2003; Schmidt & Dringen, 2012; Arslan et al., 2023). In organisms, the glutathione mechanism consists of enzymes such as glutathione synthesis, peroxidase, reductase, and S-transferase. These enzymes are critical in determining the effectiveness of glutathione in detoxification processes. GSH is crucial in adapting organisms to environmental stresses and their survival (Canlı, 2022).

MDA is a highly reactive and colorless compound containing an enol group (Nair et al., 2001). As a product of lipid peroxidation, one of the oxidative stress parameters occurring in organisms in response to environmental stimuli, MDA is associated with cell membrane damage (Charissou et al., 2004; Köprücü et al., 2010).

Among the critical groups of filter-feeding organisms in aquatic ecosystems, freshwater mussels cannot respond to environmental pollutants through migration due to their lack of mobility. Because of the characteristics of mussels, the USEPA developed a mussel monitoring program (Farrington et al., 2016), which has influenced all monitoring studies at an international level (Günel et al., 2018). Freshwater mussels and filter feeders play an essential role in freshwater ecosystems. Their distribution in different aquatic systems and biodiversity depends mainly on their symbiotic relationships with fish species for their reproductive and feeding behaviors. Although the effects of several environmental contaminants on mussels have been investigated in some studies (Bowman & Bailey, 1998; TenEyek, 2009), no research has been found examining the effects of NaOH.

This study examines freshwater mussels' biochemical responses to NaOH, commonly used in domestic and industrial applications. There is no published manuscript on the effects of NaOH on oxidative stress parameters such as AOPP, GSH, and MDA levels in freshwater mussels (*Unio delicatus*). This study is anticipated to contribute to the

literature by providing valuable insights into the impacts of NaOH, frequently used in domestic and industrial sectors, on freshwater ecosystems.

2. MATERIALS VE METHODS

2.1. Procurement of Mussels

Freshwater mussels (*U. delicatus*) were obtained from local fishermen in Bursa, Turkey (n=80, mean weight 32.62 ± 7.5 g) and transported alive to Gazi University, Faculty of Education, Department of Biology, Laboratory-3 (EcoToX-LAB). They were placed in 70 L aquariums filled with dechlorinated tap water that had been aerated with an air pump and underwent a 12-day adaptation and acclimation process (DO: 4.89 ± 0.05 mg/L, pH: 7.92 ± 0.4 , Temperature: 22 ± 1.3 °C, Conductivity: 211.05 ± 0.5 mS/cm). During acclimation, the mussels were fed commercial spirulina at 0.5% of their live weight every two days. No mortalities were observed during the acclimation process. Feeding was stopped 24 h before the experiment began.

2.2. Chemical Procurement

NaOH (Cas No: 1310-73-2) ($98\% \pm 2$ purity) in its commercial form was used for the experiment. The NaOH, supplied in solid form as small round granules, was dissolved in a small beaker of aquarium water before being added to the aquarium.

2.3. Experimental Setup

Preliminary experiments determined the mean lethal concentration (LC₅₀) of NaOH as 88.51 mg/L, based on Finney's Probit analysis method (Finney, 1952). For the acute experiment, sublethal doses of LC₅₀ were used: D1: $\frac{1}{2}$ (44.26 mg/L) and D2: $\frac{1}{4}$ (22.13 mg/L).

At the end of the acclimation period, mussels were randomly selected from the stock aquarium and placed into six tanks containing 10 L of dechlorinated water and aerated by an air pump. Five mussels were placed in each tank. The experiment was conducted in duplicate at 24 and 72-hour intervals. The day-night period was naturally maintained during the experiment, and water quality parameters were

measured daily (DO: 5.32 ± 0.12 mg/L, pH: 7.86 ± 0.7 , Temperature: 22 ± 1.3 °C, Conductivity: 225.33 ± 0.47 mS/cm). No mussel mortality was observed during the experiment.

The acute toxicity experiment concluded after 24 and 72 hours. The digestive glands and gills were dissected under ice anesthesia. The tissues were then immediately frozen using liquid nitrogen to prevent degradation. The tissues preserved in liquid nitrogen were stored in a freezer at -80 °C until the analysis day.

2.4. Biochemical Analyses

In the digestive gland and gill tissues, which were dissected then stored at -80 °C, the levels of AOPP (Witko-Sarsat et al., 1996), GSH (Ellman, 1959), and MDA (Uchiyama & Mihara, 1978) were analyzed.

AOPP analysis is based on a spectrophotometric method to detect oxidized protein products in mussels' gill and digestive gland tissues. The dissected tissues were homogenized in phosphate buffer (20 μ M, pH: 7.4), and the supernatants were collected. Results were expressed as μ M AOPP/mg.

GSH method analyzes the levels of sulfhydryl groups in tissues using aromatic disulfide. The digestive gland and gill tissues dissected from the mussels were homogenized in metaphosphoric acid and centrifuged to collect the supernatants.

The MDA method is based on homogenizing lipoperoxides in tissues with thiobarbituric acid in a 1.15% KCl buffer. Results were expressed in nM/mg.

2.5. Statistical Analyses

The results obtained from the experiments were normalized using the Kolmogorov-Smirnov normality test. One-way ANOVA followed by Tukey's post-hoc test was applied to all data. The significance level of the results was assessed at $p < 0.05$. GraphPad Prism 9 software was used for statistical analysis and graph generation.

3. RESULTS

The results of acute toxicity experiments were evaluated according to 24 and 72-hour NaOH exposures in terms of oxidative stress parameters.

3.1 Effect of NaOH on AOPP Levels

The AOPP values, which are important biomarkers of oxidative stress on protein structures in the digestive gland and gill tissues of *U. delicatus* individuals exposed to NaOH, are shown in Figures 1 and 2 as $\mu\text{M}/\text{mg}$ tissue. In the digestive gland tissues, after 24 hours of exposure, the results of D1 and D2 were similar; nevertheless, both showed a decrease compared to the control group. After 72 hours of exposure, no significant difference was observed between the dose groups and the control group ($p>0.05$). In the gill tissues, no significant difference was observed between the D1 and D2 groups compared to the control group after 24 hours of exposure. However, after 72 hours of exposure, no significant difference was observed in the D1 group compared to the control group ($p>0.05$), while D2 showed an approximately 1.5 times increase ($p<0.05$).

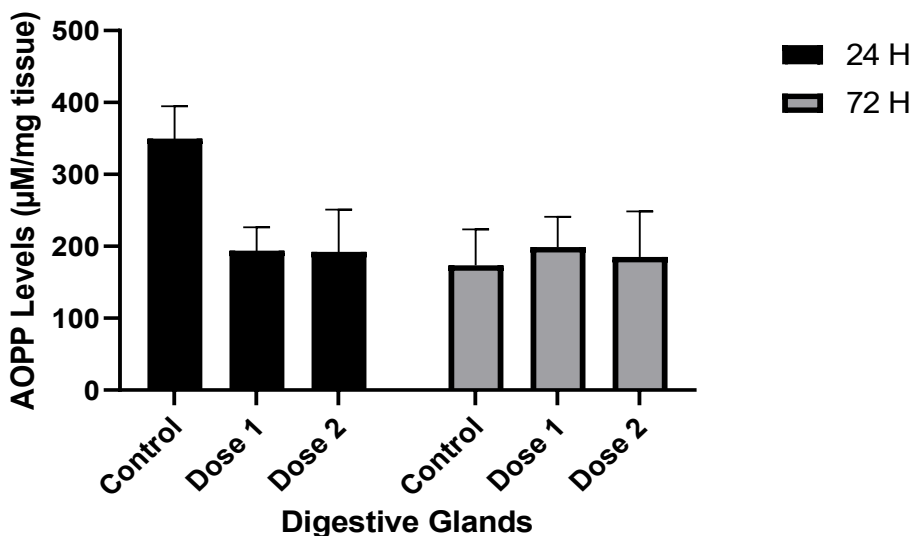


Figure 1. AOPP levels of digestive glands

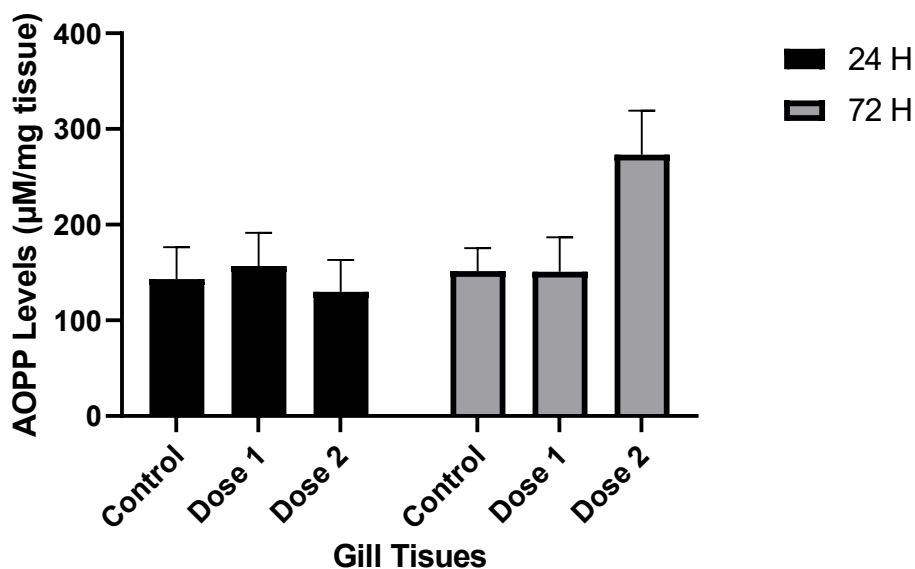


Figure 2. AOPP levels of gill tissues

3.2 Effect of NaOH on GSH Levels

The GSH levels in the digestive tract and gill tissues were determined, as shown in Figures 3 and 4 as µM/mg tissue. In digestive gland tissues, GSH levels increased in D1 after 24 hours of exposure, while in D2, they significantly decreased ($p > 0.05$). After 72 hours of exposure, GSH levels in both D1 and D2 showed a dose-dependent decrease. In gill tissues, GSH levels decreased approximately 4 times in D1 and 2 times in D2 after 24 hours of exposure ($p < 0.05$). Compared to the control groups, GSH levels decreased after 72 hours of exposure but showed an inverse relationship with the dose.

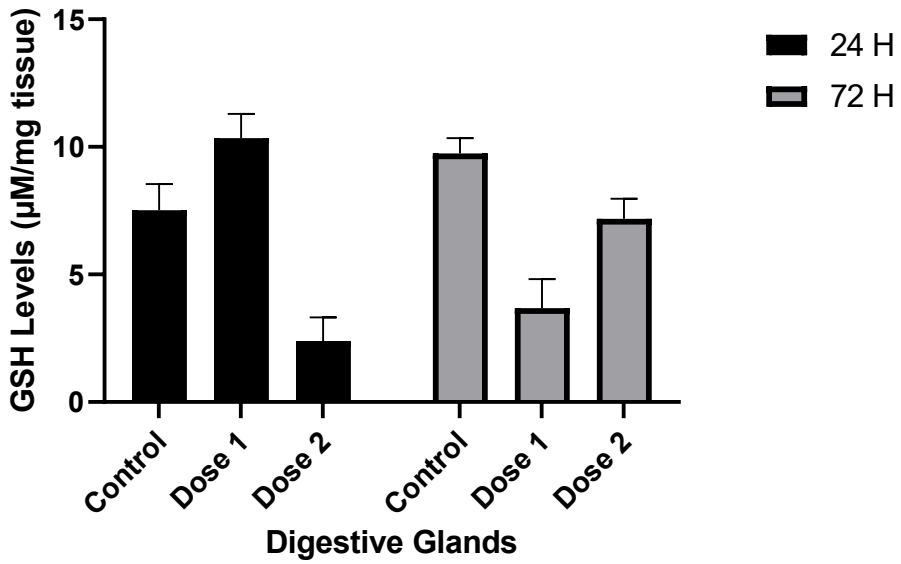


Figure 3. GSH levels of digestive glands

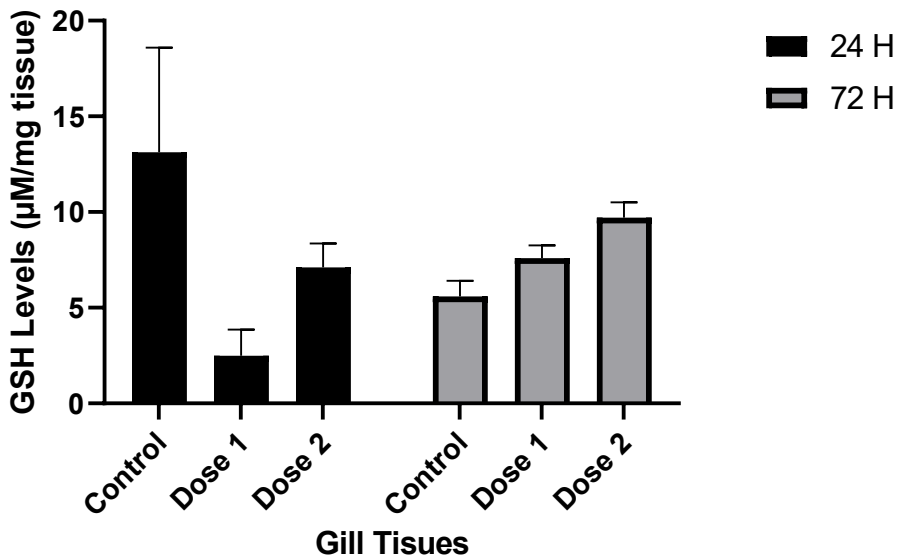


Figure 4. GSH levels of gill tissues

3.3 Effect of NaOH on MDA Levels

The MDA levels, a product of lipid peroxidation, in the digestive glands and gill tissues of mussels in response to NaOH exposure are shown in Figures 5 and 6. In the 24-hour group, MDA levels decreased by approximately 2.5 times in D1 and 4 times in D2 compared to the control group. In the 72-hour group, MDA levels showed no significant difference compared to the control group ($p > 0.05$). In the gill tissues, MDA levels in the 24-hour group were 1.5 times higher in D1 and approximately 2 times higher in D2 compared to the control group. In the 72-hour group, no significant difference was observed between the control and D1 group ($p > 0.05$), while a significant increase was observed in D2 ($p < 0.05$).

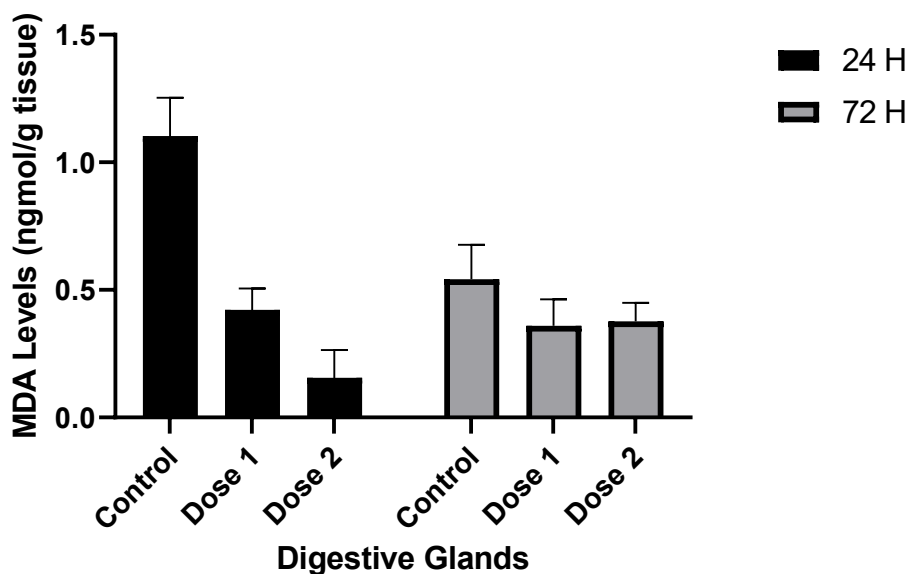


Figure 5. MDA levels of digestive glands

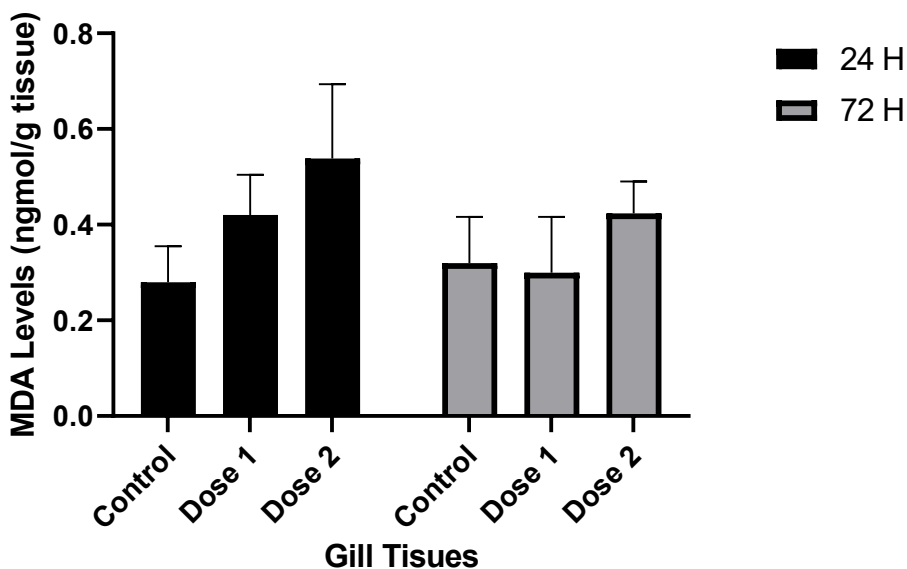


Figure 6. MDA levels of gill tissues

4. DISCUSSION

Various domestic and industrial products are increasingly used due to rapid population growth and industrialization. It is known that some of these products are introduced into the environment through various pathways (floods, leaks, spills). Mussels, as macro-invertebrates, are model organisms used in studies to detect environmental pollution. Mussels have been used in ecotoxicological studies since the 1950s (Van Hassel & Farris, 2007; Paçal et al., 2022).

Environmental pollutants can cause various physiological, biochemical, and genetic effects on aquatic organisms. One of these effects is oxidative stress. Numerous studies in the literature investigate the effects of environmental factors on oxidative stress parameters such as AOPP, GSH, and MDA in mussels (Table 1). When compared to these studies, the current results indicate that environmental factors induce oxidative stress in mussels and that they develop different biochemical responses.

Table 1. Literature studies on oxidative stress in mussels

Species	Tissues	AOPP	GSH	MDA	Notes
<i>Mytilus galloprovincialis</i>	Gills & Digestive Gland	No significant change	Decrease in polluted areas	Increase in polluted areas	Mussels from polluted sites had reduced glutathione and increased oxidative stress in the gills and digestive gland (Moschino et al., 2016)
<i>Unio elongatulus eucirrus</i>	Gills & Digestive Gland		Decrease (dose-dependent)	Increase (dose-dependent)	Exposure to deltamethrin led to increased lipid peroxidation (MDA) and decreased glutathione levels in both gills and digestive gland (Köprücü et al., 2008)
<i>Unio species</i>	Gills & Digestive Gland	Increase	Decrease	Increase	Exposure to phthalates resulted in heightened oxidative stress across multiple biomarkers, indicating significant damage in gill and digestive gland tissues (Kuzukıran et al., 2022)
<i>Perna perna</i>	Gills & Digestive		Increase in gills	Increase in both	Stress response due to air

	Gland			tissues	exposure caused an increase in oxidative damage (Almeida, 2005)
<i>Perna perna</i>	Gills & Digestive Gland	Decrease	Increase		Biomarker responses to environmental pollution (Dos Santos et al., 2022)
<i>Unio elongatulus eucirrus</i>	Gills & Digestive Gland	Decrease	Increase		Effects of cypermethrin exposure on antioxidant status, oxidative stress biomarkers, behavioral changes, and mortality rates (Köprücü et al., 2010)
<i>Unio elongatulus eucirrus</i>	Gills & Digestive Gland	Increase (dose-dependent)	Increase	Decrease	Deltamethrin exposure results in freshwater mussels (Köprücü et al., 2008)
<i>Macra stultorum</i>	Gills	Increase	Decrease	Increase	Acrylamide exposure elevated oxidative damage and protein oxidation (Trabelsi et al., 2020)

<i>Mytilus spp.</i>	Gills & Digestive Gland		Decrease	Increase	Microplastics exposure increased oxidative stress and led to enzyme activities in both tissues (Revel et al., 2019)	
<i>Unio mancus</i>	Gills & Digestive Gland	No significant change	Increase	Increase	The oxidative effects of CuPT exposure of freshwater mussel (Paçal et al., 2022)	
<i>Unio delicatus</i>	Gills & Digestive Gland		Increase	Decrease	Increase	Fipronil exposure resulted in oxidative stress (Arslan and Günal, 2023)
<i>Mytilus galloprovincialis</i>	Gills & Digestive Gland		Increase	Decrease	Increase	Sodium pyrrithione exposure caused oxidative stress biomarkers to increase, reducing antioxidant defenses (Arslan et al., 2023)
<i>Mytilus galloprovincialis</i>	Hemocytes		Decrease	Increase	Contaminated sites caused immune suppression and increased oxidative stress markers	

					(Auffret et al., 2006)
<i>Mytilus galloprovincialis</i>	Gills & Digestive Gland		Decrease	Increase	Protective role of metallothioneins against oxidative stress (Viarengo et al., 2019)
<i>Unio tumidus</i>	Gills & Digestive Gland	Increase	Decrease	Increase	Relationship between MDA and oxidative DNA damage (8-oxodGuo) under pollution exposure (Charissou et al., 2004)
<i>Astacus leptodactylus</i>	Gills & Digestive Gland		Decrease (dose-dependent)	Increase (dose-dependent)	Permethrin exposure induced oxidative stress, increasing MDA and reducing GSH levels (Günel et al., 2021)
<i>Unio delicatus</i>	Gills & Digestive Gland	Decrease in Digestive Glands (exposed time-dependent)	Digestive gland: 24 h D1 Increase D2 Decrease , 72 h D1 and D2 Decrease , Gills 24h D1 and D2	Decrease in Digestive glands and Increase in Gills (time-dependent)	This Study

Decrease,
72h D1
and D2
Increase

This study examined the effects of NaOH on AOPP, GSH, and MDA parameters. When the findings are compared with similar ecotoxicological studies in the literature, both parallels and differences emerge. While the AOPP value decreased in this study, other studies have shown an increase. GSH values showed parallel results with some studies in the literature, while they were opposite in others. The MDA value in the digestive gland tissue differed from the literature, whereas it showed similar results in the gill tissue (Table 1). These results suggest that species may exhibit different responses to stressors. The differences in responses observed compared to the control groups indicate that the mussels developed biochemical responses to environmental factors and that oxidative stress was induced.

5. CONCLUSION

The results obtained from this study show that these mussels must be monitored in response to the presence of a large number of environmental pollutants in order to achieve protection in freshwater ecosystems. No study is in the literature investigating mussels' physiological and biochemical responses to NaOH exposure. As this is the first study to acutely analyze the effects of NaOH, frequently used in domestic and industrial applications, on mussels, it will contribute to the literature.

REFERENCES

- Almeida, E.A., Bainy, A.C.D., Dafre, A.L., Gomes, O.F., Medeiros, M.H., & Di Mascio, P. (2005). Oxidative stress in digestive gland and gill of the brown mussel (*Perna perna*) exposed to air and re-submersed. *Journal of Experimental Marine Biology and Ecology*, 318(1), 21-30.
- Arslan, P., Gül, G., & Günal, A.Ç. (2023). How do biocidals affect the non-target marine organisms: the short-term effects of antifouling agent sodium pyrithione on Mediterranean mussels (*Mytilus galloprovincialis*, Lamarck 1819). *Environmental Science and Pollution Research*, 30(56), 118332-118340.
- Auffret, M., Rousseau, S., Boutet, I., Tanguy, A., Baron, J., Moraga, D. & Duchemin, M., (2006). A multiparametric approach for monitoring immunotoxic responses in mussels from contaminated sites in Western Mediterranean. *Ecotoxicology and Environmental Safety*, 63: 393–405.
- Bowman, M.F., & Bailey, R.C. (1998). Upper pH tolerance limit of the zebra mussel (*Dreissena polymorpha*). *Canadian Journal of Zoology*, 76(11), 2119-2123.
- Büyükgüzel E. (2013). Biochemical and molecular mechanism of protein oxidation. *Karaelmas Science and Engineering Journal*, 3(1), 40- 51.
- Calazans, S.H., Fernandes, L.V., & Fernandes, F.C. (2012). Outros compostos. *Moluscos límnicos invasores no Brasil. Biologia, prevenção, controle, Redes Editora, Porto Alegre*, 311-315.
- Canlı, E. (2022). Investigations on the responses of antioxidant enzymes in freshwater mussels (*Unio tigridis*) Exposed to Copper in Differing Durations. *KSU Tarım ve Doğa Dergisi*, 25(1): 31-41.
- Charissou A.M., Cossu-Leguille, C., Vasseur, P. (2004). Relationship between two oxidative stress biomarkers, malondialdehyde and 8-oxo-7, 8-dihydro-2'-deoxyguanosine, in the freshwater bivalve *Unio tumidus*. *Science of the Total Environment* 322(1-3):109-122.
- Dos Santos, F.S., Neves, R.A., Crapez, M.A.C., Teixeira, V.L., & Krepsky, N. (2022). How does the brown mussel *Perna perna*

- respond to environmental pollution? A review on pollution biomarkers. *Journal of Environmental Sciences*, 111, 412-428.
- Ellman, G.L. (1959). *Tissue sulfhydryl groups*. Archives of biochemistry and biophysics, 82(1), 70-77.
- Farrington, J.W.; Tripp, B.W.; Tanabe, S.; Subramanian, A.; Sericano, J.L.; Wade, T.L.; Knap, A.H.; Edward, D. (2016). Goldberg's proposal of "the Mussel Watch": Reflections after 40 years. *Marine Pollution Bulletin*. 110, 501–510.
- Finney, D.J. (1952). Probit analysis: a statistical treatment of the sigmoid response curve.
- Günel, A.Ç., Katalay, S., Erkmen, B., Ayhan, M.M., Gül, G., & Erkoç, F. (2018). Antifouling bakır pritiyonun midye (*Mytilus galloprovincialis*)'de toplam hemosit sayıları üzerine etkilerinin belirlenmesi. *Ege Journal of Fisheries and Aquatic Sciences*, 35(1), 15-17.
- Günel, A.Ç., Tunca, S.K., Arslan, P., Gül, G., & Dinçel, A.S. (2021). How does sublethal permethrin effect non-target aquatic organisms?. *Environmental Science and Pollution Research*, 28(37): 52405-52417.
- Kalousová K, Krha M, Zima T. (2002). Advanced glycation end-products and advanced oxidation protein products in patients with diabetes mellitus. *Physiological Research* 51:597-60; 2002.
- Köprücü, K., Yonar, S.M., Şeker, E. (2010). Effects of cypermethrin on antioxidant status, oxidative stress biomarkers, behavior, and mortality in the freshwater mussel *Unio elongatulus eucirrus*. *Journal of Fisheries Science* 76(6):1007–1013.
- Köprücü, S.Ş., Yonar, E., & Seker, E. (2008). Effects of deltamethrin on antioxidant status and oxidative stress biomarkers in freshwater mussel, *Unio elongatulus eucirrus*. *Bulletin of environmental contamination and toxicology*, 81, 253-257.
- Kuzukiran, O., Yurdakok-Dikmen, B., Erkmen, B., Günel, A. C., Arslan, P., Pacal, E., Totan, F.E., Filazi, A., & Erkoç, F. (2022). Sublethal responses of the indicator *Unio* species (mussel) to selected phthalate esters. *Biologia*, 77(3), 851-864.
- Maroñas, M. E., Damborenea, M. C., & Darrigran, G. A. (2006). Efecto de biocidas y tolerancia a la exposición al aire. In Darrigran G and Damborenea C (Eds), *Bio-Invasión Del Mejillón Dorado En*

- El Continente Americano, La Plata: Edulp, La Plata, Argentina. Darrigran G and Damborenea C, p. 167-179.
- Mason, C.F. (2002). *Biology of freshwater pollution*. 4th. Edition. 400 pp. Benjamin Cummings Publication, UK.
- Medina-Martos, E., Gálvez-Martos, J. L., Almarza, J., Lirio, C., Iribarren, D., Valente, A., & Dufour, J. (2022). Environmental and economic performance of carbon capture with sodium hydroxide. *Journal of CO2 Utilization*, 60, 101991.
- Moschino, V., Del Negro, P., De Vittor, C., & Da Ros, L. (2016). Biomonitoring of a polluted coastal area (Bay of Muggia, Northern Adriatic Sea): A five-year study using transplanted mussels. *Ecotoxicology and Environmental Safety*, 128, 1-10.
- Nair, V., O'Neil, C.L., Wang, P.G., (2001). Malondialdehyde. *Encyclopedia of Reagents for Organic Synthesis*, 15(3): 2204-2214.
- Öztürk H. (2008). Diabetes mellitus'da Paraoksonaz Aktivitesi ve Aopp Düzeyleri. Tıbbi Biyokimya Uzmanlık Tezi. İstanbul. T.C. Sağlık Bakanlığı Haseki Eğitim ve Araştırma Hastanesi Biyokimya ve Klinik Biyokimya Bölümü.
- Paçal, E., Gümüş, B. A., Günal, A. Ç., Erkmén, B., Arslan, P., Yıldırım, Z., & Erkoç, F. (2022). Oxidative stress response as biomarker of exposure of a freshwater invertebrate model organism (*Unio mancus* Lamarck, 1819) to antifouling copper pyrithione. *Pesticides and Phytomedicine/Pesticidi i fitomedicina*, 37(2), 63-76.
- Revel, M., Lagarde, F., Perrein-Ettajani, H., Bruneau, M., Akcha, F., Sussarellu, R., Rouxel, J., Costil, K., Decottignies, P., Cognie, P., Châtel, A., & Mouneyrac, C. (2019). Tissue-specific biomarker responses in the blue mussel *Mytilus* spp. exposed to a mixture of microplastics at environmentally relevant concentrations. *Frontiers in Environmental Science*, 7, 33.
- Schmidt, M.M. and Dringen, R. (2012) Glutathione (GSH) synthesis and metabolism. In: *Neural metabolism in vivo*. Springer, Boston, MA, pp 1029-1050.
- Soares, S. C., Esteves, F., Lundqvist, D., & Öhman, A. (2009). Some animal specific fears are more specific than others: Evidence

- from attention and emotion measures. *Behaviour research and therapy*, 47(12), 1032-1042.
- TenEyek, M. (2009). *Sodium hydroxide (NaOH). Great ships initiative bench-scale test findings*. Technical Report—Public GSI/BS/5.
- Terpstra M, Henry, P.G., Gruetter, R. (2003) Measurement of reduced glutathione (GSH) in human brain using LC model analysis of difference-edited spectra. *Magn Reson Med* 50(1):19–23.
- Trabelsi, W., Fouzai, C., Chetoui, I., Bejaoui, S., Telahigue, K., Rabeh, I., Cafsi, M.E., & Soudani, N. (2020). Oxidative stress biomarkers in the gills of the bivalve *Macra stultorum* exposed to acrylamide. *Scientia Marina*, 84(2), 143-150.
- Uchiyama, M., & Mihara, M. (1978). Determination of malonaldehyde precursor in tissues by thiobarbituric acid test. *Analytical biochemistry*, 86(1), 271-278.
- Van Hassel, J. H., & Farris, J. L. (2007). *A review of the use of unionid mussels as biological indicators of ecosystem health*. Freshwater bivalve ecotoxicology. CRC Press, Boca Raton, Florida, and SETAC Press, Pensacola, Florida, 19-49.
- Viarengo, A., Burlando, B., Cavaletto, M., Marchi, B., Ponzano, E., & Blasco, J. (1999). Role of metallothionein against oxidative stress in the mussel *Mytilus galloprovincialis*. *American Journal of Physiology-Regulatory, Integrative and Comparative Physiology*, 277(6), R1612-R1619.
- Witko-Sarsat V, Friedlander M, Capeillere-Blandin C, Nguyen-Khoa T, Nguyen AT, Zingraff J, (1996). Advanced oxidation protein products as a novel marker of oxidative stress in uremia. *Kidney Int.*; 49: 1304-13.
- Yancheva, V.S., Stoyanova, S.G., Georgieva, E.S., & Velcheva, I.G. (2018). Mussels in ecotoxicological studies - Are they better indicators for water pollution than fish? *Ecologica Balcanica*, 10(1), 57–84.

CHAPTER 6

EXPLORING SIR-TYPE EPIDEMIC MODELS THROUGH NUMERICAL SIMULATIONS IN GNU OCTAVE

Asst. Prof. Dr. Harun BALDEMİR¹

DOI: <https://dx.doi.org/10.5281/zenodo.14258739>

¹ Çankırı Karatekin University, Faculty of Science, Department of Mathematics
Çankırı, Türkiye. harunbaldemir@karatekin.edu.tr, Orcid ID: 0000-0002-2599-1117

INTRODUCTION

Background to Epidemic Modeling

Epidemic modeling serves as a crucial tool in understanding the dynamics of infectious diseases, allowing researchers and public health officials to predict the spread of diseases and evaluate the effectiveness of intervention strategies. The importance of accurately modeling the dynamics of epidemics has been emphasized in various studies (Baldemir et al., 2020; Yang et al., 2020). Among the various mathematical frameworks employed in this field, the Susceptible-Infected-Recovered (SIR) model stands out due to its simplicity and effectiveness in capturing the essential features of disease transmission dynamics. The SIR model, first developed by Kermack and McKendrick in 1927 (Kermack & McKendrick, 1927), divides the population into three compartments namely *susceptible* (S), *infected* (I) and *recovered* (R) individuals, with transitions between these states governed by specific rates of infection and recovery. This compartmental approach provides a foundational framework for analyzing the spread of various infectious diseases, including recent outbreaks such as COVID-19 (Kartono et al., 2021; Wu, 2023).

The classical SIR model operates under the assumption that individuals can transition from being susceptible to infected through contact with infected individuals and subsequently recover from the infection, thereby gaining immunity. The dynamics of this model are typically described by a set of ordinary differential equations (ODEs) that represent the rates of change of each compartment over time. The basic reproductive number, denoted as R_0 , is a crucial metric for assessing the likelihood of an outbreak, representing the average number of new infections generated by one infected person in a fully susceptible population (Hethcote, 2000; Driessche & Watmough, 2002; Liu et al., 2022).

Advances in computational methods have expanded the applicability of the SIR model, allowing researchers to analyze key parameters like transmission and recovery rates in epidemic dynamics (Magal & Webb, 2018). These approaches have been crucial for studying interventions such as social distancing and vaccination, while

integrating agent-based modeling has provided insights into how network structures and behaviors affect disease spread (Tolles & Luong, 2020). During the COVID-19 pandemic, the SIR model has been widely used to understand transmission and assess intervention strategies (Ansumali et al., 2020; Ying & Xiaoqing, 2021), offering rapid parameter estimation and forecasting (Rahimi et al., 2021). However, its assumption of homogeneous population mixing remains a limitation, leading to extensions that incorporate age structure, spatial dynamics, and stochastic elements to improve accuracy (Vasconcelos et al., 2020; Moein et al., 2021; Pastor-Satorras et al., 2015).

Understanding the Classical SIR Model

The SIR model is a foundational tool in epidemiology, widely used to represent the spread of infectious diseases through a population. It divides individuals into three compartments: *Susceptible* (S), those vulnerable to infection; *Infected* (I), those currently infected and capable of transmitting the disease; and *Recovered* (R), those who have recovered and are no longer susceptible or infectious. This compartmental approach, governed by a set of differential equations, allows the SIR model to provide valuable insights into disease dynamics, intervention strategies, and the long-term behavior of outbreaks, making it essential for both theoretical and practical epidemic modeling.

The dynamics of the disease are governed by the following system of ordinary differential equations (ODEs):

$$\begin{aligned}\frac{dS}{dt} &= -\beta SI \\ \frac{dI}{dt} &= \beta SI - \gamma I \\ \frac{dR}{dt} &= \gamma I\end{aligned}\tag{1}$$

In these equations, S , I and R represent the number of *susceptible*, *infected* and *recovered* individuals at time t , respectively. The parameter β is the transmission rate, indicating how frequently a susceptible individual comes into contact with an infected individual

and becomes infected. The parameter γ is the recovery rate, describing the speed at which infected individuals recover and move into the recovered compartment.

The term βSI describes the spread of infection, with the rate of new infections depending on the interaction between the susceptible and infected populations. The larger the infected population, the greater the likelihood that susceptible individuals will come into contact with the disease. Also, the term γI represents the number of infected individuals recovering at a given time.

One of the key outcomes of the SIR model is the *basic reproduction number* (R_0), which is defined as $R_0 = \beta / \gamma$. This value reflects the typical number of additional infections caused by an infected individual in a population that has no immunity. If $R_0 > 1$, the disease will spread and lead to an epidemic. If $R_0 < 1$, the disease will eventually die out.

Extensions of the SIR Model

One of the strengths of the SIR model is its adaptability. While the basic model assumes a simple division of the population into *susceptible* (S), *infected* (I) and *recovered* (R) individuals, more complex disease dynamics can be captured by extending the model. This is often done by adding new compartments or modifying parameters to better represent specific epidemiological features.

Extensions of the classical SIR model are crucial for accurately capturing the complexities of real-world epidemics. One of the most common extensions is the introduction of additional compartments, such as the *Exposed* (E) class in SEIR models or the *Asymptomatic Infected* (A) class in SAIR models. These new compartments allow the model to account for various stages of infection, such as a latent period during which individuals are infected but not yet infectious or cases where individuals recover without displaying symptoms. For instance, the SEIR model incorporates an exposed compartment that reflects the incubation period of diseases like COVID-19, thus providing a more comprehensive understanding of transmission dynamics. Another significant modification is incorporating temporary immunity into models like SIRS, SEIRS or SAIRS, where recovered individuals eventually return to the susceptible class after a period of immunity, reflecting diseases for which immunity is not lifelong. This aspect is

particularly relevant for diseases such as influenza, where immunity wanes over time, necessitating periodic vaccinations (Liu, 2021).

NUMERICAL SIMULATIONS AND PARAMETER ESTIMATION OF SIR-TYPE MODELS IN OCTAVE

When conducting numerical simulations for epidemic models like the SIR framework, the choice of computational tools plays a crucial role. We selected GNU Octave (Eaton et al., 2021) due to its open-source nature, which allows for widespread accessibility without the financial burden of proprietary software licenses. Octave can be downloaded freely from its official website (<https://www.gnu.org/software/octave/>), ensuring that anyone can access it without any cost. It provides a powerful platform for solving ordinary differential equations (ODEs) and performing parameter estimation, essential components of epidemic modeling. By choosing Octave, we ensure that both researchers and students can replicate these simulations in any environment, regardless of budget constraints.

Moreover, GNU Octave is highly compatible with Matlab® (Matlab, 2024), offering similar syntax and functionality. This compatibility facilitates the straightforward transfer of code between the two environments, which is particularly useful for those familiar with Matlab. While Matlab is a well-established tool in numerical computation, Octave serves as a free alternative that mirrors most of the core functionality of Matlab, making it an excellent option for academic and research settings. The choice of Octave thus enables a broader audience to explore, simulate, and analyze epidemic models while maintaining the flexibility to transition to Matlab if needed.

Step-by-Step Simulation of the SIR Model in GNU Octave

In this section, we will guide you through the process of simulating the SIR model using GNU Octave. The simulation is based on solving a system of ordinary differential equations (ODEs) that describe the dynamics of a population. The goal is to numerically solve these equations to understand how an epidemic progresses over time.

The SIR model is governed by a set of differential equations,

given in *Equation (1)* that describe the rates of change for each compartment. In Octave, we define these equations using a function that takes the current state of the system (i.e., the current values of S , I and R), time, and the parameters β (the transmission rate) and γ (the recovery rate). The function returns the rates of change for each compartment at each time step. The system of equations can be expressed in Octave as shown in *Script 1*.

```

1 %% sir_model.m
2 function dydt = sir_model(t, y, beta, gamma)
3 % Define the variables
4 S = y(1); I = y(2); R = y(3);
5 % Define the ODEs
6 dS = -beta * S * I;
7 dI = beta * S * I - gamma * I;
8 dR = gamma * I;
9 % Output as a column vector
10 dydt = [dS; dI; dR];
11 end

```

Script 1. Definitions the differential equations of the SIR model.

This function is central to the simulation. It calculates how the susceptible population decreases as individuals move into the infected group, how the infected population changes over time, and how recovered individuals accumulate as they leave the infected compartment. Once we have defined the model equations, the next step is to set the initial conditions and parameters for the simulation.

```

1 %% sir_simulation_run.m
2 clear; clc;
3 % Initial conditions
4 S0 = 0.99; I0 = 0.01; R0 = 0; y0 = [S0; I0; R0];
5 % Time span for simulation
6 tspan = 1:100;
7 % Define parameters
8 beta = 0.3; gamma = 0.1;

```

Script 2. Initialization of the SIR Model.

In *Script 2*, the simulation begins with a clean setup, where the commands `clear; clc;` ensure that the workspace and command

window are cleared. This prevents any interference from previously defined variables or commands.

Next, the initial conditions are specified. Here, the proportion of susceptible individuals in the population is set to $s_0=0.99$, meaning 99% of the population is initially susceptible to infection. The proportion of infected individuals is $i_0=0.01$, indicating 1% are already infected, and there are no recovered individuals initially, so $r_0=0$. These values are combined into the vector $y_0 = [s_0; i_0; r_0]$ to define the starting state of the system. The time span for the simulation is defined next as $tspan = 1:100$, representing 100 units of time over which the simulation will run. The parameters of the SIR model β and γ are specified.

```

9 % Solve the system using ode45
10 [t, y] = ode45(@(t, y) sir_model(t, y, beta,
    gamma), tspan, y0);

```

Script 3. Running the simulation with ode45 to solve the SIR model over the defined time span and initial conditions.

With the initial conditions and parameters defined, the code proceeds to simulate the evolution of the SIR model over the specified time span, as demonstrated in *Script 3*. The `ode45` solver is used to numerically solve the system of ordinary differential equations utilizing the adaptive Runge-Kutta method. This method iteratively computes solutions by adjusting the time step based on the estimated local error, allowing for accurate integration of the ODEs that describe the dynamics of the SIR model. The solver takes in the function `sir_model`, which describes the dynamics of the SIR system, the time span `tspan`, and the initial conditions `y0`. The function outputs two arrays: `t`, which contains the time points, and `y`, which contains the corresponding values of the susceptible, infected, and recovered

populations at each time step.

Once the simulation is complete, the next step, as shown in *Script 4*, is to visualize the results. We use the `plot` command to create a visualization of the SIR model simulation results. The proportions of the *susceptible* (S), *infected* (I) and *recovered* (R) populations over time are plotted with different colors: blue for S , red for I , and green for R .

```

11 % Plot the results
12 figure;
13 plot(t, y(:,1), '-b', 'linewidth', 2);
14 hold on;
15 plot(t, y(:,2), '-r', 'linewidth', 2);
16 plot(t, y(:,3), '-g', 'linewidth', 2);
17 xlabel('Time'); ylabel('Population');
18 title('SIR Model Simulation'); legend('S','I',
    'R');
19 grid on; set(gca,'FontSize',24); ylim([0 1]);

```

Script 4. Script 4 Plotting the simulation of the SIR model.

Figure 1 provides a clear visual representation of the dynamics of the SIR model. The blue curve shows the decline of the susceptible population as people become infected, the red curve tracks the rise and fall of the infected population, and the green curve illustrates the accumulation of recovered individuals. Together, these curves provide a snapshot of the epidemic's progression.

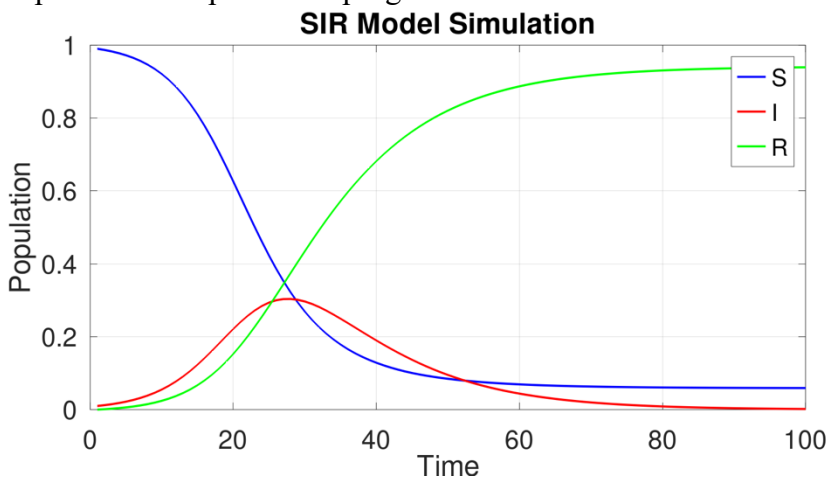


Figure 1. SIR model simulation.

From the simulation, we can observe several key features of epidemic dynamics. Initially, the number of infected individuals rises as the disease spreads through the susceptible population. Over time, as more people recover, the rate of new infections decreases, leading to a peak in the number of infected individuals. Eventually, the infection dies out as the majority of the population either recovers or is no longer susceptible to the disease.

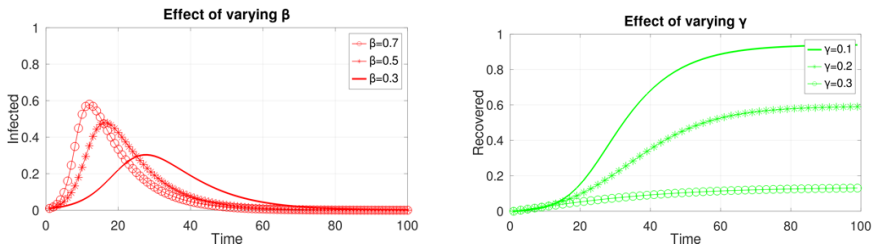


Figure 2. Effect of varying the parameters β and γ .

The specific shape of the curves is determined by the values of β and γ . As seen in *Figure 2*, a higher transmission rate β leads to a faster spread of the disease and a larger peak in the number of infected individuals. In contrast, a higher recovery rate γ causes individuals to recover more quickly, shortening the duration of the epidemic.

Parameter Estimation for the SIR Model Using Octave

After simulating the dynamics of the SIR model, the next step is to calibrate the model to fit real-world data by estimating the key parameters. This process allows us to refine the predictions of the model and improve its accuracy in describing disease spread.

Parameter estimation plays a pivotal role in fitting mathematical models to observed data. For the SIR model, estimating the key parameters is essential for understanding the underlying dynamics of disease progression. This section discusses the estimation of parameters using GNU Octave, utilizing the `optim` package for bounded optimization to ensure that the estimated parameters stay within biologically realistic ranges. This package provides a range of algorithms for solving optimization problems, including those required for constrained optimization in real-world applications, enabling

effective parameter estimation that enhances our understanding of disease dynamics.

The `optim` package can be installed in Octave using the command `pkg install -forge optim`. After installation, you need to load the package to use its functions by typing `pkg load optim`. This package offers several optimization algorithms for parameter estimation, each tailored to specific needs. In unconstrained scenarios, `fminunc` can be utilized, while `lsqcurvefit` is particularly useful for fitting models to data by minimizing the squared differences between observed and predicted values. Additionally, `fminsearch` provides a straightforward method for finding the minimum of a function without requiring gradient information. For bounded parameter estimation, `fmincon` is the function of choice, as it efficiently solves constrained nonlinear multivariable optimization problems, allowing users to specify upper and lower bounds for the parameters to be estimated. This capability is particularly important when estimating β and γ , which are rates (or probabilities) that must lie between 0 and 1.

```

1 %% sir_cost.m
2 function cost = sir_cost(pars, t_data, I_data,
3   y0)
4   % Define the parameters
5   beta = pars(1); gamma = pars(2);
6   % Time span for simulation
7   tspan = t_data;
8   % Solve the system using ode45
9   [t, y] = ode45(@(t, y) sir_model(t, y, beta,
10   gamma), tspan, y0);
11 % Infected data from the simulation
12 I_sim = y(:, 2);
13 % Calculate cost
14 cost = sum((I_sim - I_data').^2);
15 end

```

Script 5. The cost function of the SIR model.

To estimate the parameters β and γ , we need to define a cost function that measures the difference between the observed data (e.g., the number of infected individuals over time) and the values predicted by the SIR model. This cost function quantifies the error between the model and data and serves as the objective that the optimization

algorithm minimizes. This process is outlined in detail in *Script 5*.

The cost function is based on the sum of squared differences (also called the least squares error) between the observed and predicted number of infected individuals. The general form of the cost function can be written as:

$$Cost = \sum_{i=1}^n (I_{obs}(t_i) - I_{sim}(t_i))^2$$

where n is the number of time points for which data is available, $I_{obs}(t_i)$ and $I_{sim}(t_i)$ represent the observed number (or proportion) of infected individuals and the number of infected individuals predicted by the SIR model, respectively, at time t_i . This framework establishes a foundation for the subsequent parameter estimation process.

```

1 %% sir_optimization_run.m
2 clear; clc;
3 % Infected data
4 I_data = [0.01, 0.01, 0.02, 0.03, 0.03, 0.04,
0.05, 0.07, 0.08, 0.10, 0.12, 0.15, 0.18, 0.20,
0.23, 0.25, 0.27, 0.28, 0.29, 0.29, 0.28, 0.26,
0.24, 0.22, 0.20, 0.17, 0.15, 0.13, 0.12, 0.10,
0.09, 0.08, 0.07, 0.06, 0.06, 0.05, 0.05, 0.04,
0.04, 0.03];
5 % Time span for simulation
6 t_data=1:length(I_data);
7 % Initial parameters (guess)
8 init_pars = [0.9, 0.1, 0.1, 0.01];
9 % Initial conditions
10 S0 = 0.99; I0 = 0.01; R0 = 0; y0 = [S0; I0; R0];
11 % Parameter bounds for the optimization
12 lb = [0, 0]; ub = [1, 1];`

```

Script 6. Initialization step of the parameter estimation of the SIR model.

The process of estimating the parameters begins with initialization, where key variables are defined. The command `clear; clc;` is used to clear the workspace and command window, ensuring a clean execution environment. The infected data, represented as a row vector `I_data`, is defined, capturing the proportion of the population infected at various time points.

The time span for the simulation is established with the vector `t_data`, which is generated as a sequence of integers corresponding to the length of `I_data`. Next, initial guesses for the model parameters are set in the vector `init_pars`, which includes values for the transmission rate (β) and the recovery rate (γ).

Initial conditions for the model are also specified, with the proportion of susceptible individuals set to `s0 = 0.99`, infected individuals to `i0 = 0.01`, and recovered individuals to `r0 = 0`. These initial conditions are combined into the vector `y0`, which will be used in subsequent calculations. Finally, bounds for the parameters are defined. These bounds are essential to ensure that the optimized values are biologically plausible, with both parameters constrained between 0 and 1. The initialization step for parameter estimation of the SIR model is demonstrated in *Script 6*.

```

13 % Optimize the parameters using fmincon
14 opt_pars = fmincon(@(pars) sir_cost(pars, t_data,
    I_data, y0), init_pars, [], [], [], [], lb, ub);
15 %% Run the simulation with the optimized
    parameters
16 tspan = t_data;

```

Script 7. Optimization of the SIR model parameters using the fmincon function.

Following the initialization step, the code proceeds to optimize the parameters, as shown in *Script 7*. The `fmincon` function from the `optim` package is employed to minimize a cost function that quantifies the difference between observed data and model predictions. The cost function, denoted as `sir_cost`, measures the error between the observed infection data and the simulated values produced by the SIR model.

The `fmincon` function is invoked with several parameters: the handle to the cost function, the initial parameter guesses, and the defined lower (`lb`) and upper (`ub`) bounds for the parameters. This function performs iterative adjustments to the parameters, seeking to identify the values that minimize the cost function while conforming to the specified constraints. This optimization process is critical, as it yields the optimal parameter estimates that best fit the observed infection data.

Once the parameters have been optimized, the next phase involves running the SIR model simulation with the refined values, as

shown in *Script 8*. The time span for the simulation is defined as `tspan`, which corresponds to the previously established `t_data`. The optimized parameters β and γ are extracted from the results of the optimization process.

```

17 % Define optimized parameters
18 beta = opt_pars(1); gamma = opt_pars(2);
19 % Solve the system using ode45
20 [t, y] = ode45(@(t, y) sir_model(t, y, beta,
    gamma), tspan, y0);

```

Script 8. Simulation of the SIR model using estimated parameters.

The `ode45` solver is then utilized to numerically solve the system of ordinary differential equations that describe the SIR model. This function computes the evolution of the susceptible, infected, and recovered populations over the defined time span, returning a set of time points `t` and corresponding population values `y`, which includes the predicted number of infected individuals.

```

21 % Plot the results
22 figure;
23 plot(t_data, I_data, 'ro', 'linewidth', 2,
    'MarkerSize', 10); % Plot real data
24 hold on;
25 plot(t, y(:, 2), '-r', 'linewidth', 2); % Plot
    model simulation
26 xlabel('Time'); ylabel('Infected');
27 title('SIR Model'); legend('Real data','Model
    simulation');
28 grid on; set(gca,'FontSize',24); ylim([0 0.5]);

```

Script 9. Plotting the real data and simulation of the SIR model.

In *Script 9*, we show the final step that is to visualize the results of the model against the observed data. A new figure is created, and the actual infection data is plotted using red circles, indicating the real data points. The model's simulation results are overlaid on the same plot as a continuous red line, allowing for a direct comparison between the observed and predicted values.

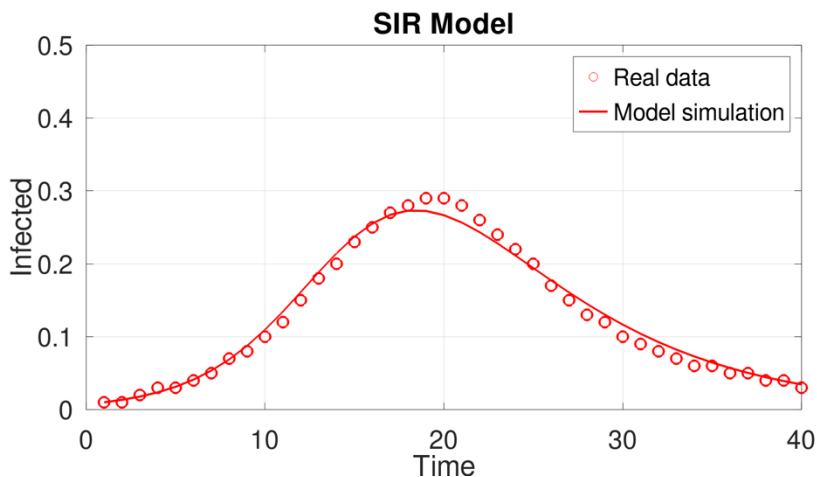


Figure 3. SIR model optimization.

Typically, the fit between the model and the observed data is assessed visually, though additional statistical metrics can also be used to quantify the accuracy. In this example, the close alignment of the predicted and observed infection curves indicates that the estimated values of β and γ successfully capture the dynamics of disease spread (see *Figure 3*). We have provided the complete code for simulation and parameter estimation step by step above, which will assist readers in modifying it for their own analyses or exploring different model scenarios.

Adapting Parameter Estimation for SEIRS

The process of parameter estimation for the SEIRS (Susceptible-Exposed-Infectious-Recovered-Susceptible) model closely follows the approach used for the SIR model, with a few important differences due to the inclusion of the exposed (E) compartment. In the SEIRS model as shown in *Equation (2)*, in addition to estimating the transmission rate β and recovery rate γ , we also estimate the rate of progression from the exposed state to the infectious state, σ , and the waning immunity rate, δ . These parameters add complexity to the model by accounting for the latent period before individuals become infectious and the eventual loss of immunity, leading to reinfection.

The system of equations for the SEIRS model is

$$\begin{aligned}
 \frac{dS}{dt} &= -\beta SI + \delta R \\
 \frac{dE}{dt} &= \beta SI - \sigma E \\
 \frac{dI}{dt} &= \sigma E - \gamma I \\
 \frac{dR}{dt} &= \gamma I - \delta R
 \end{aligned}
 \tag{2}$$

The cost function `seirs_cost.m` provided in the appendix remains similar to that in the SIR model `sir_cost.m`. However, the parameter space is expanded to include σ and δ , and the optimization process must account for these additional dynamics. This extension requires setting initial guesses and bounds for all four parameters; β , σ , γ and δ with the optimization conducted using the same `fmincon` function.

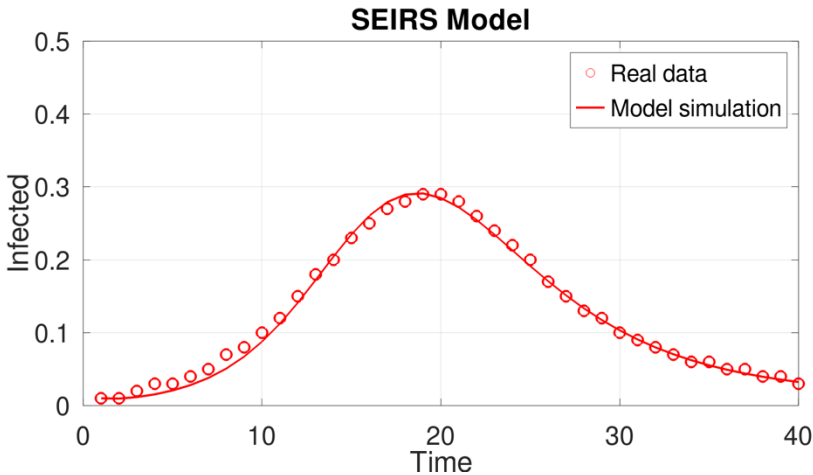


Figure 4. SEIRS model optimization.

As shown in *Figure 4*, the real-world infection data is shown in red circles, while the SEIRS model simulation is represented by the solid red line. The close fit between the two curves suggests that the estimated parameters for the SEIRS model accurately capture the observed dynamics of disease spread.

The SEIRS model scripts provided in the appendix can be a valuable resource for readers. By adjusting the necessary components, these scripts can be adapted to explore other epidemic models, building on the step-by-step SIR model solution shown in the main text.

CONCLUSION

In this chapter, we explored the simulation and parameter estimation of SIR-type epidemic models using GNU Octave. The SIR model, despite its simplicity, provides fundamental insights into epidemic dynamics by dividing the population into *susceptible*, *infected* and *recovered* compartments. Through numerical simulations, we demonstrated the progression of an epidemic over time, highlighting the key roles of the transmission rate (β) and recovery rate (γ) in shaping the epidemic curve.

Additionally, parameter estimation techniques were applied to real-world infection data using the `fmincon` optimization algorithm, ensuring biologically meaningful bounds on the estimated parameters. The optimized parameters allowed for a close fit between the observed data and the model predictions, further illustrating the practical utility of the SIR model.

We also discussed the extension of the SIR model to the SEIRS framework, which incorporates the exposed compartment and includes the possibility of individuals becoming susceptible again after a period of recovery. This extended model provides a more comprehensive view of diseases with latent periods and non-permanent immunity, such as COVID-19 or influenza. Notably, the code implementation of the SEIRS model is similar to that of the SIR model, allowing for straightforward extensions to other SIR-type models.

The use of GNU Octave for numerical simulations and parameter estimation has proven to be a powerful tool for analyzing SIR-type epidemic models. The code provided facilitates these analyses and allows for further extensions to include more complex dynamics. Overall, the numerical simulations and parameter estimation techniques discussed in this chapter highlight the value of mathematical models in understanding and controlling the spread of infectious diseases.

REFERENCES

- Ansumali, S., Kaushal, S., Kumar, A., Prakash, M. K., & Vidyasagar, M. (2020). Modelling the COVID-19 pandemic: Asymptomatic patients, lockdown, and herd immunity. *IFAC-PapersOnline*, 53(5), 823-828.
- Baldemir, H., Akın, A., & Akın, Ö. (2020). Fuzzy modelling of Covid-19 in turkey and some countries in the world. *Turkish Journal of Mathematics and Computer Science*, 12(2), 136-150.
- Eaton, J. W., Bateman, D., Hauberg, S., & Wehbring, R. (2021). *GNU Octave version 6.4.0 manual: A high-level interactive language for numerical computations*. Retrieved from <https://www.gnu.org/software/octave/doc/interpreter>
- Hethcote, H. W. (2000). The mathematics of infectious diseases. *SIAM Review*, 42(4), 599-653.
- Kermack, W. O., & McKendrick, A. G. (1927). A contribution to the mathematical theory of epidemics. *Proceedings of the Royal Society of London. Series A, Containing Papers of a Mathematical and Physical Character*, 115(772), 700-721.
- Kartono, A., Karimah, S. V., Wahyudi, S. T., Setiawan, A. A., & Sofian, I. (2021). Forecasting the long-term trends of coronavirus disease 2019 (COVID-19) epidemic using the susceptible-infectious-recovered (SIR) model. *Infectious Disease Reports*, 13(3), 668-684.
- Liu, P., Hendeby, G., & Gustafsson, F. (2022). Joint estimation of states and parameters in stochastic SIR model.
- Liu, X. (2021). A simple, SIR-like but individual-based epidemic model: Application in comparison of COVID-19 in New York City and Wuhan. *Results in Physics*, 20.
- Magal, P., & Webb, G. F. (2018). The parameter identification problem for SIR epidemic models: Identifying unreported cases. *Journal of Mathematical Biology*, 77(6-7), 1629-1648.
- Matlab. (2024). *Version 9.14.0 (R2024a)*. The MathWorks, Inc. Retrieved from <https://www.mathworks.com>
- Moein, S., Nickaeen, N., Roointan, A., Borhani, N., Heidary, Z., Haghjooy Javanmard, S. H., Gheisari, J., & Gheisari, Y. (2021).

- Inefficiency of SIR models in forecasting COVID-19 epidemic: A case study of Isfahan. *Scientific Reports*, 11(1), 4725.
- Pastor-Satorras, R., Castellano, C., Mieghem, P. J., & Vespignani, A. (2015). Epidemic processes in complex networks. *Reviews of Modern Physics*, 87(3), 925-979.
- Rahimi, I., Gandomi, A., Asteris, P., & Fang, C. (2021). Analysis and prediction of COVID-19 using SIR, SEIQR, and machine learning models: Australia, Italy, and UK cases. *Information*, 12(3), 109.
- Tolles, J., & Luong, T. (2020). Modeling epidemics with compartmental models. *JAMA*, 323(24), 2515.
- Van den Driessche, P., & Watmough, J. (2002). Reproduction numbers and sub-threshold endemic equilibria for compartmental models of disease transmission. *Mathematical Biosciences*, 180(1-2), 29-48.
- Vasconcelos, G. L., Macêdo, A. M., Ospina, R., Almeida, F. A., Duarte-Filho, G. C., Brum, A. A., & Souza, I. C. (2020). Modelling fatality curves of COVID-19 and the effectiveness of intervention strategies. *PeerJ*, 8, e9421.
- Wu, J. (2023). The application of SIR model in COVID-19. *Theoretical and Natural Science*, 9, 38-44.
- Yang, Z., Zeng, Z., Wang, K., Wong, S. S., Liang, W., Zanin, M., ... & He, J. (2020). Modified SEIR and AI prediction of the epidemics trend of COVID-19 in China under public health interventions. *Journal of thoracic disease*, 12(3), 165.
- Ying, L., & Xiaoqing, T. (2021). COVID-19: Is it safe now? Study of asymptomatic infection spread and quantity risk based on SAIR model. *Chaos, Solitons & Fractals: X*, 6, 100060.

APPENDIX**A. SEIRS Model Equations**

```

1 %% seirs_model.m
2 function dydt = seirs_model(t, y, beta, sigma,
   gamma, delta)
3 % Define the variables
4 S = y(1); E = y(2); I = y(3); R = y(4);
5 % Define the ODEs
6 dS = -beta * S * I + delta * R;
7 dE = beta * S * I - sigma * E;
8 dI = sigma * E - gamma * I;
9 dR = gamma * I - delta * R;
10 % Output as a column vector
11 dydt = [dS; dE; dI; dR];
12 end

```

B. SEIRS Model Cost Function

```

1 %% seirs_cost.m
2 function cost = seirs_cost(pars, t_data, I_data,
   y0)
3 % Define the parameters
4 beta = pars(1); sigma = pars(2); gamma = pars(3);
   delta = pars(4);
5 % Time span for simulation
6 tspan = t_data;
7 % Solve the system using ode45
8 [t, y] = ode45(@(t, y) seirs_model(t, y, beta,
   sigma, gamma, delta), tspan, y0);
9 % Infected data from the simulation
10 I_sim = y(:, 3);
11 % Calculate cost
12 cost = sum((I_sim - I_data').^2);
13 end

```

C. SEIRS Model Optimization

```

1 %% seirs_optimization_run.m
2 clear; clc;
3 % Infected data
4 I_data = [0.01, 0.01, 0.02, 0.03, 0.03, 0.04, 0.05,
   0.07, 0.08, 0.10, 0.12, 0.15, 0.18, 0.20, 0.23,
   0.25, 0.27, 0.28, 0.29, 0.29, 0.28, 0.26, 0.24,
   0.22, 0.20, 0.17, 0.15, 0.13, 0.12, 0.10, 0.09,
   0.08, 0.07, 0.06, 0.06, 0.05, 0.05, 0.04, 0.04,
   0.03];

```

```
5 % Time span for simulation
6 t_data=1:length(I_data);
7 % Initial parameters (guess)
8 init_pars = [0.9, 0.1, 0.1, 0.01];
9 % Initial conditions
10 S0 = 0.99; E0 = 0; I0 = 0.01; R0 = 0; y0 = [S0; E0;
    I0; R0];
11 % Parameter bounds for the optimization
12 lb = [0, 0, 0, 0]; ub = [1, 1, 1, 1];
13 % Optimize the parameters using fmincon
14 opt_pars = fmincon(@(pars) seirs_cost(pars, t_data,
    I_data, y0), init_pars, [], [], [], [], lb, ub);
15 %% Run the simulation with the optimized parameters
16 tspan = t_data;
17 % Define optimized parameters
18 beta = opt_pars(1); sigma = opt_pars(2); gamma =
    opt_pars(3); delta = opt_pars(4);
19 % Solve the system using ode45
20 [t, y] = ode45(@(t, y) seirs_model(t, y, beta,
    sigma, gamma, delta), tspan, [S0 E0 I0 R0]);
21 % Plot the results
22 figure;
23 plot(t_data, I_data, 'ro', 'linewidth', 2,
    'MarkerSize', 10); % Plot real data
24 hold on;
25 plot(t, y(:, 3), '-r', 'linewidth', 2); % Plot
    model simulation
26 xlabel('Time'); ylabel('Infected');
27 title('SEIRS Model'); legend('Real data','Model
    simulation');
28 grid on; set(gca,'FontSize',24); ylim([0 0.5]);
```


CHAPTER 7
ORTHOGNATHIC SURGERY

Spec. Ortho. Büşra İlayda BAŞBOĞA¹

DOI: <https://dx.doi.org/10.5281/zenodo.14259098>

¹ Tokat Gaziosmanpaşa University Faculty of Dentistry Department Tokat, Türkiye, busrabasboga95@gmail.com, Orcid ID:0009-0009-8395-9893

INTRODUCTION

If the discrepancy between the jaws is so severe that it cannot be resolved by growth modification or camouflage, orthodontic treatment is preferred in combination with orthognathic surgery to align the jaws and correct the discrepancy. If the condition is very severe, distraction osteogenesis should also be considered as a treatment alternative.

History of Orthognathic Surgery

History of Mandibular Osteotomies

Orthognathic surgery is one of the routine treatments in the field of oral and maxillofacial surgery and can be traced back to Edward Angle and Vilray Blair. In the 20th century, the most important developments in orthognathic surgery include especially Wassmund, Trauner and Obwegeser (Aziz, 2004).

In 1849, Simon P. Hullihen performed the first mandibular osteotomy in history on a patient with mandibular prognathia and anterior open bite. This osteotomy is similar to the anterior subapical method in many respects as shown in Figure 1 (Aziz, 2004, Naini and Gill, 2017).

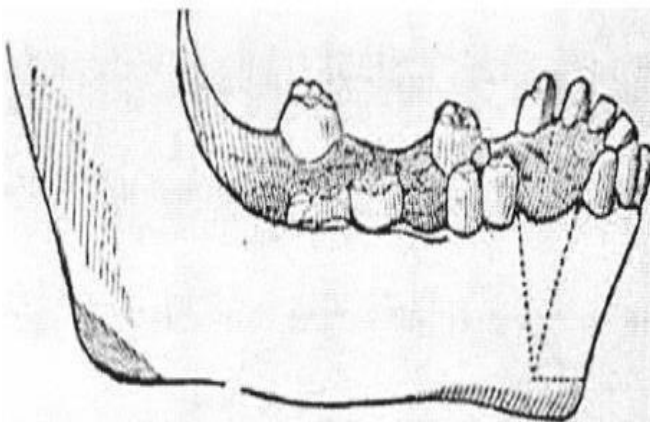


Figure 1. Mandibular osteotomy introduced by Hullihen

"Mandibular body osteotomy" It is one of the most preferred surgeries between 1906-1970. Vilray Papin Blair performed mandibular body osteotomy for the first time. As can be seen in Figure 2, this method has been applied and modified in patients with mandibular prognathia in the past years and is not preferred today (Hausamen, 2001).

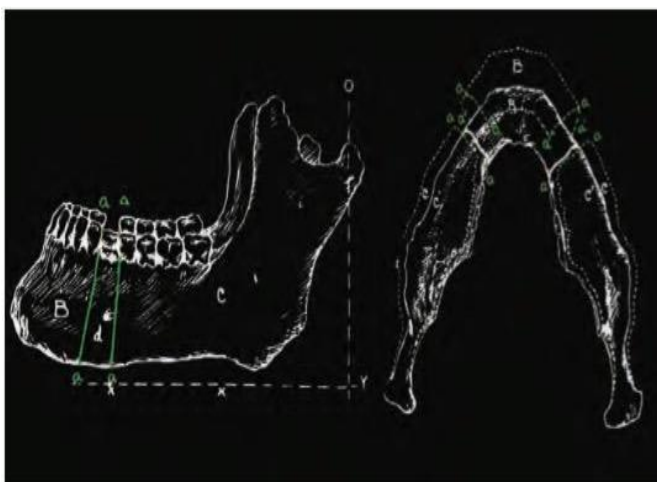


Figure 2. Mandibular osteotomy introduced by Blair

The inverted L osteotomy was described by Wassmund in 1927 and is a modification of the vertical ramus osteotomy as shown in figure 3. Caldwell et al. performed a different modification with a horizontal incision added to the lower edge of the mandible and defined this procedure as "C osteotomy" as seen in Figure 4 (Proffit, White, and Sarver, 2003).



Figure 3. Wassmund inverted L osteotomy

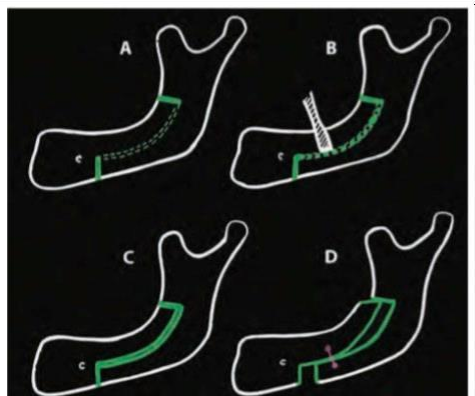


Figure 4. Caldwell C osteotomy

In 1957, intraoral surgical techniques started to come to the agenda. In the treatment of mandibular retrognathia and mandibular prognathia, sagittal split ramus osteotomy was introduced (5). When we look at the advantages of this method, which is shown in Figure 5 and is still frequently preferred today, we can see that it allows movement of the mandible in all directions, changes in the muscles and joints are very small, and there is no need for a graft because of the wide bone contact between the proximal and distal segments (Proffit, White, and Sarver, 2003).

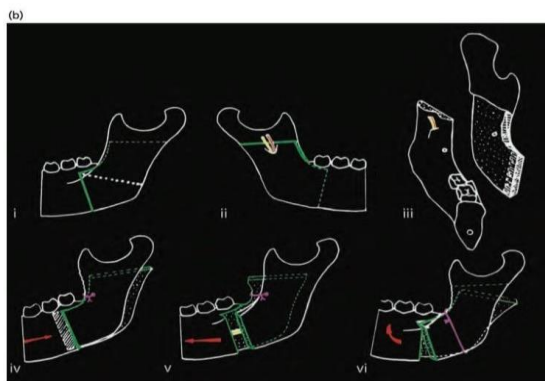


Figure 5. Obwegeser sagittal split osteotomy

History of Maxillary Osteotomies

In 1859, Von Langenback, who performed excision of nasopharyngeal polyps, performed the first Le Fort I surgery. In 1868,

David Williams Cheever reported a right hemimaxillary "down fracture" for the removal of a nasopharyngeal polyp in the treatment of total nasal obstruction due to recurrent epistaxis. In 1901, French surgeon Rene Le Fort performed experiments on cadavers. As a result of his experiments by applying different types of trauma, he reported the Le Fort fractures defined today. While Le Fort I, II and III type osteotomies were defined, they were named according to their similarities to the fracture lines reported by the French surgeon Rene Le Fort (Naini and Gill, 2017).

In 1921, Chon-Stock performed an anterior segmental maxillary osteotomy and used maxillary osteotomies for the first time in history to treat occlusion disorders. In the past years, segmental osteotomies were preferred because it was thought that the supply of the maxilla with palatal arteries would not be sufficient. However, in 1927, Martin Wassmund performed orthognathic surgery by performing Le Fort I osteotomy. Wassmund did not disconnect the connection with the pterygoid plates and did not mobilize the maxilla. The reason for this is to ensure continued feeding of the maxilla. Adjustment of occlusion was performed after surgery with the application of intraoral elastic (Bloomquist and Lee, 2004, Rosen, 2006, Stearns, Fonseca and Saker, 2000).

William H. Bell's revascularization studies are of great importance in the development of orthognathic surgery. Bell's studies on monkeys put the Le Fort I 'down fracture' technique on a scientific basis for the first time. At the end of the studies, it was reported that small necrosis areas were formed with the Le Fort I 'down fracture' technique, but it was histologically reported that nutrition from the palatal and buccal mucosa would continue (Stearns,Fonseca and Saker, 2000). Le Fort 1 incision line is shown in figure 6.

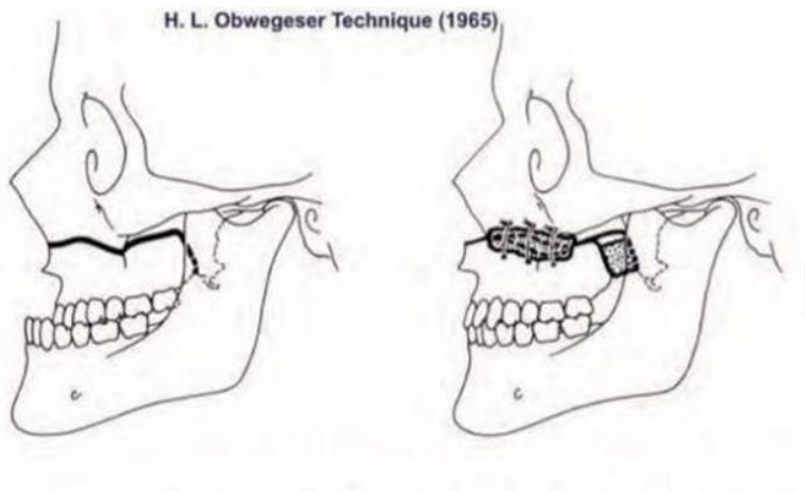


Figure 6. Drawings of Le Fort I osteotomy

Indications for Orthognathic Surgery

- If there is no dental malocclusion but there is skeletal disharmony,
- Dentofacial deformities,
- If a relapse will occur after orthodontic treatment has taken place,
- If rapid treatment is desired in adult individuals
- If aesthetic expectations are high
- If malocclusion cannot be solved with orthodontic treatments (camouflage treatment)

Contraindications to Orthognathic Surgery

- If the amount of movement is too much,
- If the systemic condition is not favorable for the operation,
- Non-compliant patients,
- In patients in whom the malocclusion will improve with orthodontic treatment,
- If growth and development continues (we can consider orthopedic treatment)

Orthognathic Surgery Planning

In orthognathic surgery patients, the cephalometric film should be taken in the natural head position, with the teeth in centric occlusion and the lips at rest.

Extraoral Assessment

When evaluating the face, we divide it vertically into three parts. The upper triad is between trichion and glabella, the middle triad is between glabella and subnasale, and the lower triad is between subnasale and menton. According to the study, the ratio of the upper face should be 0.30, the middle face 0.35 and the lower face 0.35 (Epker, 1986). If there is a deviation in these ratios, the lower triad is intervened with orthognathic surgery.

Gingival visibility should be 2 mm during a smile. It is acceptable for it to be slightly more visible in women. If the amount of gingival visibility is high, the reasons for this may be; the vertical length of the maxilla is high, the lip length is short, and the lip activity during the smile is high. If the aesthetic appearance is too severe to be corrected with mini screws, maxillary impaction is among the treatment preferences.

When evaluated transversally, the face is divided into five parts, the nasal wings should be in the middle fifth. Epker stated in his study that the ideal alar base width is a few mm more than the intercanthal distance (Epker, 1986).

Nasolabial angle is located between the upper lip and columella as seen in Figure 7. Its ideal value is between 85° and 105°. A slightly larger angle is aesthetically acceptable in women. While the angle decreases in patients with class II malocclusion, the opposite is the case in class III patients.

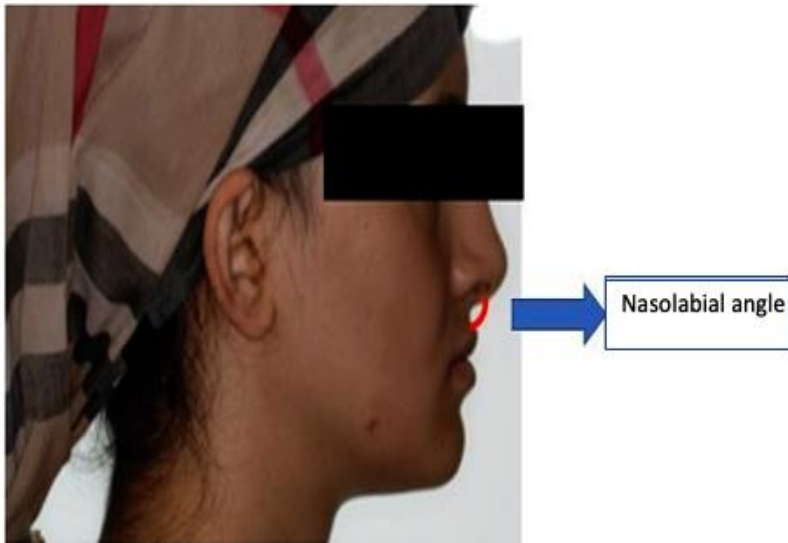


Figure 7. Demonstration of the nasolabial angle

The prominence of the tip of the chin is measured by measuring the distance of the soft tissue pogonion to the line perpendicular to the Frankfurt horizontale and passing through the soft tissue nasion. The soft tissue pogonion should be 0 ± 2 millimeters from this line. When evaluating the chin tip, not only the distance to the planes but also factors such as labiomental depth, lower lip position, macrognathia, micragnathia should be evaluated.

Line E (Ricketts) is drawn from the tip of the nose to the soft tissue pogonion. The upper lip should be 4 millimeters behind this plane and the lower lip 2 millimeters behind it.

The S line is the line at the midpoint of the s-shaped curve between the soft tissue pogonion and the subnasale-pronasale. The upper and lower lips should touch this line.

If we talk about the angles we use most when evaluating hard tissue, the SNA angle is the angle between the SN plane and the nasion A point. Its value should be 82 ± 2 . It gives information about the position of the maxilla relative to the anterior skull base. SNB angle is the angle between the SN plane and the nasion B point. It indicates the position of the mandible relative to the anterior skull base. Its value

should be 80 ± 2 . ANB angle is the angle between the AN plane and the BN plane and gives information about the position of the maxilla and mandible relative to each other. It is ideal to be between 0° and 4° .

Witts is also one of the most frequently used evaluations. It is measured by lowering struts from points A and B to the occlusal plane and looking at the distance between the AO and BO points. It provides information about the relationship between the maxilla and mandible and is not affected by anatomical variations of the cella point. While the AO BO point coincides in women, the BO point is 1 millimeter in front in men.

In the measurement according to McNamara, a perpendicular is lowered from the nasion to the Frankfurt plane and the distance of point A to this perpendicular is measured. The distance must be 0. If point A lies in front of the line, it is positive (McNamara, Brudon and Kokic, 2001).

After the extraoral intraoral and cephalometric evaluations are completed, if the patient is suitable for surgery, the model surgery stage is started.

Orthodontic Treatment Before Surgery

Patients undergo preoperative orthodontic treatment for leveling, correction of crowding and decompensation of compensated incisors. When the case is suitable for orthognathic surgery, preparations are started. The thickest stainless steel archwires are used and this archwire is called the stabilization arch. Stabilization arch should be started 4 weeks before surgery. After surgery, hooks are clamped to the wires to ensure fixation between the jaws. To make surgical splints, upper and lower measurements are taken from the patients and square plaster models are obtained. To determine the occlusion of the patients, facial arch transfer is performed as shown in figure 8.

Model Surgery

For the model surgery to be correct, the occlusion must be in the most posterior position. If the physician does not get the occlusion in

the most posterior position, the face-bow transfer will be incorrect and the surgery will be performed incorrectly.

The location of the Le Fort 1 incision line that will separate the maxilla from the cranium is consulted with the surgical team that will perform the operation. The incision line usually follows the roots of the teeth and is largely parallel to the ground plane. Then, in order to create the same incision line in model surgery, laser marking is made on the models in accordance with the incision line (parallel to the ground plane), as can be seen in Figure 9. According to this marking, the model is trimmed as shown in figure 10 and the plaster models obtained are taken to the articulators through the facial arch. Surgical planning is made by drawing lateral cephalometric films taken from the patient before surgery. The planning is also evaluated on the plaster models and the amount of movement of the jaws is determined by considering the closure relationships.

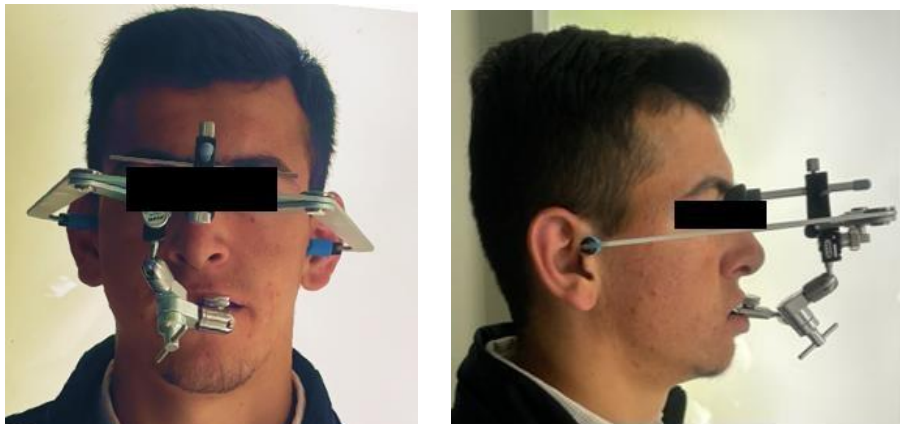


Figure 8. Facial arch application for the preparation of surgical splints

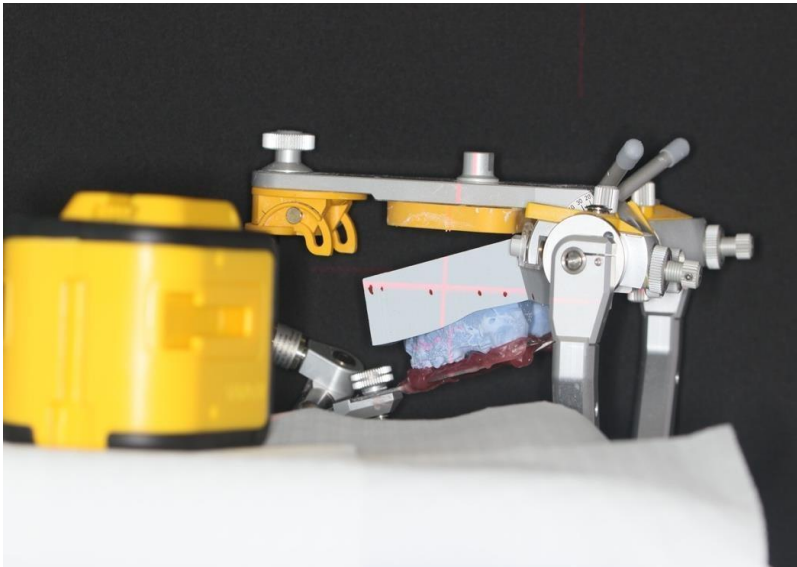


Figure 9. Laser marking on the plaster model to determine the ground plane (incision line)

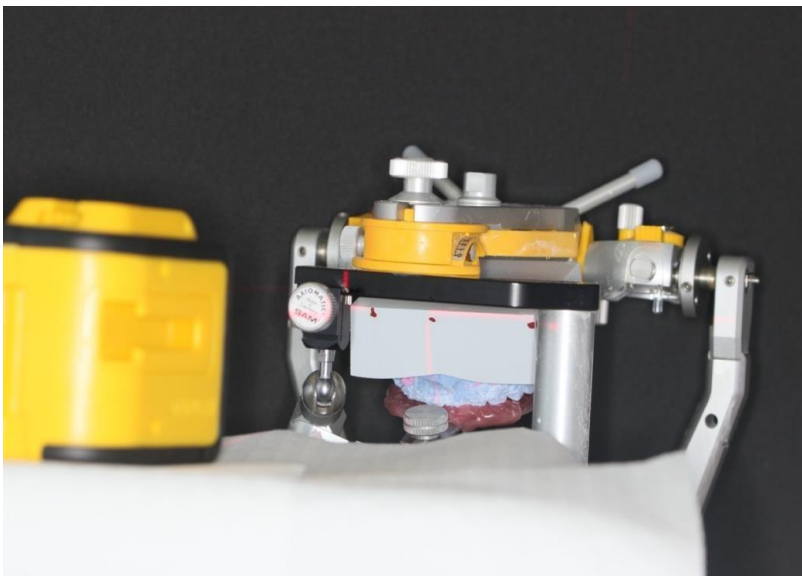


Figure 10. Appropriate model trimming following ground plane determination

Surgeries Applied to the Maxilla

- LeFort I
- LeFort II

- LeFort III
- Wassmund
- Segmental osteotomies

Surgeries Applied to the Mandible

- Bilateral sagittal split osteotomy
- Vertical ramus osteotomy
- Vertical subchondylar osteotomy
- C or L osteotomy for ramus
- Subapical osteotomy
- Genioplasty

Camouflage Treatment? Orthognathic Surgery?

Since camouflage treatment is the opposite of orthognathic surgery, the physician should make the right decision before the treatment begins. After starting camouflage treatment, if surgery is started, the patient will have a reverse orthodontic period to remove the effects of the previous treatment. This will prolong the treatment. Another important issue is tooth extraction. When the tooth is extracted in camouflage treatment, the gaps are used for dental compensation of the incompatibility between the jaws. If camouflage treatment is planned in a Class III patient with maxillary retrognathia, extraction of the lower first premolar should be considered for retraction of the mandibular incisors. Extraction in the maxilla should be avoided.

In a patient with severe class III maxillary insufficiency, tooth extractions are performed differently. Extractions are performed not for dental compensation but to remove existing compensation. In these patients, the mandibular incisors are usually retruded. Extraction from the lower arch is not considered. In the maxilla, the incisors are in a protrusive position. In this case, extraction of the upper first premolars should be considered for ideal anteriorization of the maxilla, correct position of the upper incisors and ideal overjet.

There are some parameters to help physicians decide whether patients should undergo camouflage therapy or surgery.

Situations where camouflage treatment can be successful?

- If there is a slight anteroposterior incompatibility between the jaws
- Has a medium or short face?
- If there is less than 4-6 mm crowding
- Normal soft tissue structure
- No skeletal problem in the transversal direction (no stenosis)

Situations where Camouflage Treatment will not give a successful result

- Moderate or severe anteroposterior incongruence between the jaws
- Has a long vertical face structure?
- If there is more than 4-6 mm of crowding
- In case of exaggerated soft tissue
- In case of skeletal problems in the transversal direction

Mandibular Surgery

Sagittal split ramus osteotomy is currently the most preferred mandibular surgical technique because it has many advantages. The technique allows the mandible to move forward and backward as desired and can change the facial height by allowing rotation. Sagittal split ramus osteotomy is suitable for intraoral rigid fixation.

Other mandibular osteotomies are preferred in cases involving large advances or condyles.

Maxillary Surgery

In the maxilla, the preferred method is LeFort I osteotomy with downfracture. It allows the maxilla to be brought forward and upward in a very stable manner. Total retraction of the maxilla is not possible due to anatomical structures. In case of retraction of the maxilla, consolidation with premolar extraction can be considered or segmental osteotomies with tooth extraction can be preferred.

In adult patients with transversal stenosis in the maxilla, SARME is planned as seen in Figure 11, because in patients who have not

completed their growth and development, orthopedic expansion type sutures provide expansion easily because there is no fusion in the sutures, while in adults, resistance occurs in the sutures. To eliminate the resistance, incisions are made and the procedure is performed with screws to expand the maxilla. Nowadays, surgeons make all the incisions for LeFort I when performing SARME, but do not perform the final step of 'downfracture'. Recent studies have shown that SARME is accompanied by relapse in dental expansion and its long-term stability is similar to segmental osteotomy (Chamberland and Proffit, 2011).



Figure 11. Before and after SARME in a patient with transversal stenosis

Relapse in Orthognathic Surgery

Relapse is influenced by many factors. These include the direction of movement, type of fixation, surgical procedure and neuromuscular balance. Relapse in orthognathic surgery procedures is as follows.

Direction of Movement and Surgical Procedure	Stability Level
Maxilla up	Very Stable
Chin (any direction)	Stable
Maxilla forward	Stable
Maxilla asymmetry correction	Stable
Maxilla and mandible forward together	Moderate Stability
Mandible back	Low Stability
Maxilla down	Problematic
Maxilla widening	Most Problematic

Very Stable: Maxilla upward movements are the most reliable in terms of surgical stability.

Stable: Jaw tip movements and maxillary advancement usually give predictable and stable results.

Moderately Stable: Anteriorization of the maxilla and mandible together may be less stable than anteriorization alone.

Less Stable/Problematic: Retracting the mandible and lowering the maxilla are more risky in terms of stability.

Most Problematic: Maxilla enlargement procedures carry the highest risk of relapse and have the lowest stability.

Distraction Osteogenesis

It is one of the preferred methods for the correction of facial deformities. It is a method based on manipulating the bone for the formation of new bone tissue and soft tissue before calcification begins in the bone in the osteotomy area. Advantages; it provides more movement compared to classical orthognathic surgery methods and can be preferred in younger patients. The biggest disadvantage of this method is that precise movements are not possible, but in these patients, a large amount of movement is required at an early age and dental occlusion is not very important.

Orthognathic Surgery Timing

Orthognathic surgery is a treatment that stops growth and development, so it should be performed when the growth spurt is over. In some special cases of growth failure, surgery can be performed before the growth spurt, but these are very rarely preferred. Early asymmetries are treated with Distraction Osteogenesis.

Result and Discussion

Orognathic surgery is a treatment method used to correct occlusion, dental and facial aesthetics in patients. In order to achieve the ideal results, a good planning is required before surgery (Rustemeyer, 2010).

In a study, it was emphasized that if individuals with Class III malocclusion undergo orthognathic surgery at an early age before completing the growth and development period, it may cause relapse due to the continuation of mandibular growth and this may cause negativity for patients. Even if individuals with Class III malocclusion want to undergo surgery in the early period, physicians have to wait for the appropriate time (Proffit, 2003). Based on the studies in the literature, it is more accurate to perform the surgery in adulthood in order to eliminate the negative effects of the possible growth of the patients in the future.

When we look at the literature, it is seen that female patients have more concerns about their appearance than male patients, so women want orthognathic surgery more than men (Iizuka, 2004, Joss and Thüer, 2008, Mobarak 2001, Storms, 2017). For this reason, female patients are more likely to participate in orthognathic surgery. Planning orthognathic surgery is very difficult for clinicians.

When physicians plan with model surgery, the result is clinically satisfying for the patient and the physician.

Surgical planning on the model can be easily recommended to clinicians because it is easy to implement, practical and gives predictable results.

REFERENCES

- Aziz, S. R. (2004). Simon P. Hullihen and the origin of orthognathic surgery. *Journal of oral and maxillofacial surgery*, 62(10), 1303-1307.
- Bloomquist, D. S., Lee, J. (2004). Principles of mandibular orthognathic surgery. 2, 1135-1178.
- Chamberland, S., & Proffit, W. R. (2011). Short- term and long-term stability of surgically assisted rapid palatal expansion revisited. *American journal of orthodontics and dentofacial orthopedics*, 139(6), 815-822.
- Epker, B. N. (1986). Dentofacial deformities.
- Hausamen, J.E. (2001). The scientific development of maxillofacial surgery in the 20th century and an outlook into the future. *Journal of Cranio-Maxillofacial Surgery*, 29(1), 2-21. Integrated orthodontic and surgical corrections.
- Iizuka, T., Eggensperger, N., Smolka, W., & Thüer, U. (2004). Analysis of soft tissue profile changes after mandibular advancement surgery. *Oral Surgery, Oral Medicine, Oral Pathology, Oral Radiology, and Endodontology*, 98(1), 16–22.
- Joss, C. U., & Thüer, U. W. (2008). Stability of the hard and soft tissue profile after mandibular advancement in sagittal split osteotomies: a longitudinal and long-term follow-up study. *The European Journal of Orthodontics*, 30(1), 16–23.
- McNamara, J. A., Brudon, W. L., Kokich, V. G. (2001). *Orthodontics and Dentofacial Orthopedics*. United States of America: Needham Press.
- Mobarak, K. A., Espeland, L., Krogstad, O., & Lyberg, T. (2001). Soft tissue profile changes following mandibular advancement surgery: predictability and long-term outcome. *American Journal of Orthodontics and Dentofacial Orthopedics*, 119(4), 353–367.
- Naini, F. B., & Gill, D. S. (2017). *Orthognathic surgery: principles, planning and practice*: John Wiley & Sons.
- Proffit, W. R., White, R. P., & Sarver, D. M. (2003). *Contemporary treatment of dentofacial deformity*: Mosby.

- Rosen, H. M. (2006). *Aesthetic orthognathic surgery* (Vol. 2).
- Rustemeyer, J., Eke, Z., &Bremerich, A. (2010). Perception of improvement after orthognathic surgery: the important variable saffecting patient satisfaction. *Oral and maxillofacial surgery*, 14, 155-162.
- Stearns, J., Fonseca, R., &Saker, M. (2000). *Revascularization and Healing of orthognathic surgical procedures*. *Oral and maxillofacial surgery*. Philadelphia, Pa: WBSaunders Co, 151-168.
- Storms, A. S., Vansant, L., Shaheen, E., Coucke, W., de Llano-Pérula, M. C., Jacobs, R., ... &Willems, G. (2017). Three-dimensional aesthetic assessment of class II patients before and after orthognathic surgery and itsassociation with quantitative surgical changes. *International journal of oral and maxillofacial surgery*, 46(12), 1664-1671
- Trauner, R., & Obwegeser, H. (1957). The surgical correction of mandibular prognathism and retrognathia with consideration of genioplasty. Part II. Operating methods formicrogenia and distoclusion. *Oral Surgery, Oral Medicine, Oral Pathology*, 10(8), 787-792.

CHAPTER 8

DETAILED PROOFS OF THE CAUCHY-BINET THEOREM, LAPLACE EXPANSION THEOREM, AND THE JACOBI IDENTITY FOR DETERMINANTS

Asst. Prof. Dr. Celalettin KAYA¹

DOI: <https://dx.doi.org/10.5281/zenodo.14259142>

¹ Çankırı Karatekin University, Science Faculty, Department of Mathematics, Çankırı, Türkiye. ckaya@karatekin.edu.tr, Orcid ID: 0000-0003-4723-1618

INTRODUCTION

In this chapter, we give detailed proofs of the Cauchy-Binet Theorem, Laplace Expansion Theorem, and the Jacobi Identity for Determinants. These three important theorems are used in linear algebra and matrix theory literature frequently and it is not easy to find their proofs in a standard undergraduate textbook or even in many of the related graduate textbooks.

The main sources used in the preparation of this chapter are the textbooks “Matrix Theory: From Generalized Inverses to Jordan Form” by Paziak and Odell (2007) and “Completely Positive Matrices” by Berman and Shaked-Monderer (2003). Essentially, what we do is to study the related parts of the mentioned textbooks to understand and prove the Cauchy-Binet Theorem, Laplace Expansion Theorem, and the Jacobi Identity for Determinants. But of course, no part of the aforementioned books has been quoted exactly, a study has been put forward with our own words and our own sentences. In addition to these two main sources, the sources listed in the references were also consulted.

8.1 Submatrices and Minors

Definition 8.1 Let M be an $m \times n$ matrix over \mathbb{C} (or over \mathbb{R}), i.e., $M \in \mathbb{C}^{m \times n}$ (or $M \in \mathbb{R}^{m \times n}$). A matrix N obtained from M by erasing some of its rows and/or columns is called a “submatrix” of M .

Definition 8.2 Let $M \in \mathbb{C}^{n \times n}$ be a square matrix over \mathbb{C} . A matrix N obtained from M by erasing the rows i_1, i_2, \dots, i_k and the columns i_1, i_2, \dots, i_k is named as a “principal submatrix” of M . If $i_1 = n - (m - 1), i_2 = n - (m - 2), \dots, i_m = m$, then N is named as a “leading principal submatrix” of M ; that is, a $m \times m$ “leading principal submatrix” is a submatrix obtained by taking rows $1, 2, \dots, m$ and columns $1, 2, \dots, m$.

Notation 8.1 Let $M \in \mathbb{C}^{m \times n}$ and let $X \subseteq [m], Y \subseteq [n]$ be non-empty subsets, where $[k] = \{1, 2, \dots, k\}$ for $k \in \mathbb{N}$. Then:

- a) $M[X | Y]$ denotes the submatrix of M comprising of rows and columns with row indices in X and column indices in Y .

b) $M(X | Y)$ denotes the submatrix of M comprising of rows and columns with row indices not in X and column indices not in Y .

Definition 8.3 Let $M \in \mathbb{C}^{m \times n}$ and $k = \min\{m, n\}$. And let $X, Y \subseteq [k]$ be non-empty subsets with $|X| = |Y|$. Then, $\det(M[X | Y])$ is named as a $k \times k$ “minor” of M (or the “ (X, Y) -minor” of M). If $X = Y$, then $\det(M[X | Y])$ is named as a “principal minor” of M ; and if $X = Y = \{1, 2, \dots, l\}$, where $l \leq k$, then $\det(M[X | Y])$ is named as a “leading principal minor” of M .

8.2 A Proof of the Cauchy-Binet Theorem

The Cauchy-Binet theorem is a generalization of the very well-known fact that for any two square matrices M and N , $\det(MN) = \det(M) \det(N)$.

Theorem 8.1 (Cauchy-Binet Theorem) Let $X = [x_{ij}] \in \mathbb{C}^{m \times n}$, $Y = [y_{ij}] \in \mathbb{C}^{n \times p}$, and $Z = XY$. Also, let $r = \min\{m, n, p\}$ and $s \in [r]$. Assume that $M \subseteq [m], P \subseteq [p]$ such that $|M| = |P| = s$. Then:

$$\det(Z[M | P]) = \sum_{N \subseteq [n]} \det(X[M | N]) \det(Y[N | P]),$$

where the summation is taken over all s -subsets of the set $[n]$.

Proof. Let $M = \{1 \leq a_1 < a_2 < \dots < a_s \leq m\} \subseteq [m]$, $P = \{1 \leq b_1 < b_2 < \dots < b_s \leq p\} \subseteq [p]$. Then:

$$\begin{aligned} (XY[M | P])_{ij} &= (XY)_{a_i b_j} = (\text{The } a_i \text{th row of } X) \cdot (\text{The } b_j \text{th column of } Y) \\ &= \sum_{k=1}^n x_{a_i k} y_{k b_j}. \end{aligned}$$

$$\therefore XY[M | P] = \begin{bmatrix} \sum_{k=1}^n x_{a_1 k} y_{k b_1} & \sum_{k=1}^n x_{a_1 k} y_{k b_2} & \dots & \sum_{k=1}^n x_{a_1 k} y_{k b_s} \\ \sum_{k=1}^n x_{a_2 k} y_{k b_1} & \sum_{k=2}^n x_{a_2 k} y_{k b_2} & \dots & \sum_{k=1}^n x_{a_2 k} y_{k b_s} \\ \vdots & \vdots & & \vdots \\ \sum_{k=1}^n x_{a_s k} y_{k b_1} & \sum_{k=1}^n x_{a_s k} y_{k b_2} & \dots & \sum_{k=1}^n x_{a_s k} y_{k b_s} \end{bmatrix}.$$

Then, by the n -linearity of the determinant function, we have:

$$\begin{aligned}
 \det(XY[M|P]) &= \begin{vmatrix} \sum_{k=1}^n x_{a_1 k} y_{k b_1} & \cdots & \sum_{k=1}^n x_{a_1 k} y_{k b_s} \\ \vdots & \ddots & \vdots \\ \sum_{k=1}^n x_{a_s k} y_{k b_1} & \cdots & \sum_{k=1}^n x_{a_s k} y_{k b_s} \end{vmatrix} \\
 &= \begin{vmatrix} x_{a_1 1} y_{1 b_1} & \cdots & x_{a_1 1} y_{1 b_s} \\ \vdots & \ddots & \vdots \\ \sum_{k=1}^n x_{a_s k} y_{k b_1} & \cdots & \sum_{k=1}^n x_{a_s k} y_{k b_s} \end{vmatrix} + \cdots + \\
 &\quad \begin{vmatrix} x_{a_1 n} y_{n b_1} & \cdots & x_{a_1 n} y_{n b_s} \\ \vdots & \ddots & \vdots \\ \sum_{k=1}^n x_{a_s k} y_{k b_1} & \cdots & \sum_{k=1}^n x_{a_s k} y_{k b_s} \end{vmatrix} \\
 &= x_{a_1 1} \begin{vmatrix} y_{1 b_1} & \cdots & y_{1 b_s} \\ \vdots & \ddots & \vdots \\ \sum_{k=1}^n x_{a_s k} y_{k b_1} & \cdots & \sum_{k=1}^n x_{a_s k} y_{k b_s} \end{vmatrix} + \cdots + \\
 &\quad x_{a_1 n} \begin{vmatrix} y_{n b_1} & \cdots & y_{n b_s} \\ \vdots & \ddots & \vdots \\ \sum_{k=1}^n x_{a_s k} y_{k b_1} & \cdots & \sum_{k=1}^n x_{a_s k} y_{k b_s} \end{vmatrix} \\
 &= \sum_{k_1=1}^n x_{a_1 k_1} \begin{vmatrix} y_{k_1 b_1} & y_{k_1 b_2} & \cdots & y_{k_1 b_s} \\ \sum_{k=1}^n x_{a_2 k} y_{k b_1} & \sum_{k=2}^n x_{a_2 k} y_{k b_2} & \cdots & \sum_{k=1}^n x_{a_2 k} y_{k b_s} \\ \vdots & \vdots & \ddots & \vdots \\ \sum_{k=1}^n x_{a_s k} y_{k b_1} & \sum_{k=1}^n x_{a_s k} y_{k b_2} & \cdots & \sum_{k=1}^n x_{a_s k} y_{k b_s} \end{vmatrix} \\
 &= \sum_{k_1=1}^n x_{a_1 k_1} \sum_{k_2=1}^n x_{a_2 k_2} \begin{vmatrix} y_{k_1 b_1} & y_{k_1 b_2} & \cdots & y_{k_1 b_s} \\ y_{k_2 b_1} & y_{k_2 b_2} & \cdots & y_{k_2 b_s} \\ \vdots & \vdots & \ddots & \vdots \\ \sum_{k=1}^n x_{a_s k} y_{k b_1} & \sum_{k=1}^n x_{a_s k} y_{k b_2} & \cdots & \sum_{k=1}^n x_{a_s k} y_{k b_s} \end{vmatrix} \\
 &= \sum_{k_1=1}^n x_{a_1 k_1} \cdots \sum_{k_s=1}^n x_{a_s k_s} \begin{vmatrix} y_{k_1 b_1} & y_{k_1 b_2} & \cdots & y_{k_1 b_s} \\ y_{k_2 b_1} & y_{k_2 b_2} & \cdots & y_{k_2 b_s} \\ \vdots & \vdots & \ddots & \vdots \\ y_{k_s b_1} & y_{k_s b_2} & \cdots & y_{k_s b_s} \end{vmatrix} \\
 &= \sum_{k_1=1}^n \cdots \sum_{k_s=1}^n x_{a_1 k_1} \cdots x_{a_s k_s} \begin{vmatrix} y_{k_1 b_1} & y_{k_1 b_2} & \cdots & y_{k_1 b_s} \\ y_{k_2 b_1} & y_{k_2 b_2} & \cdots & y_{k_2 b_s} \\ \vdots & \vdots & \ddots & \vdots \\ y_{k_s b_1} & y_{k_s b_2} & \cdots & y_{k_s b_s} \end{vmatrix}. \quad (*)
 \end{aligned}$$

Now, if $k_i = k_j$ for $i \neq j$, then the determinant in the summation is zero because i th and j th rows are identical. Therefore, the determinant is $\neq 0$ only if $k_i \neq k_j$ for $i \neq j$; that is, the set $\{k_1, k_2, \dots, k_s\}$ is an s -element subset of $[n]$. Let $\tau: [s] \rightarrow [s]$ be the permutation such that $1 \leq k_{\tau(1)} < k_{\tau(2)} < \dots < k_{\tau(s)} \leq n$, also let $l_i = k_{\tau(i)}$ for each $i = 1, 2, \dots, s$ and $N = \{1 \leq l_1 < l_2 < \dots < l_s \leq n\}$. Then:

$$\det \begin{bmatrix} y_{k_1 b_1} & y_{k_1 b_2} & \dots & y_{k_1 b_s} \\ y_{k_2 b_1} & y_{k_2 b_2} & \dots & y_{k_2 b_s} \\ \vdots & \vdots & \ddots & \vdots \\ y_{k_s b_1} & y_{k_s b_2} & \dots & y_{k_s b_s} \end{bmatrix} = \text{sgn}(\tau) \det(Y[N|P]).$$

Finally, for each $N = \{1 \leq l_1 < l_2 < \dots < l_s \leq n\}$, all the possible permutations of the set N exist in the equation (*).

$$\begin{aligned} \therefore \det(XY[M|P]) &= \\ \sum_{\substack{N \subseteq [n] \\ |N|=s}} \left(\sum_{\tau \in S_s} \text{sgn}(\tau) x_{a_1 l_{\tau(1)}} x_{a_2 l_{\tau(2)}} \dots x_{a_s l_{\tau(s)}} \right) \det(Y[N|P]), \end{aligned}$$

where the outer summation is taken over all the s -element subsets of the set $[n]$; and the inner summation is taken over all the permutations $\tau: [s] \rightarrow [s]$, that is, all the elements of S_s , the symmetric group of over $[s]$.

$$\therefore \det(XY[M|P]) = \sum_{\substack{N \subseteq [n] \\ |N|=s}} \det(X[M|N]) \det(Y[N|P]). \blacksquare$$

8.3 Laplace Expansion Theorem

The Laplace expansion theorem is a generalization of the Laplace cofactor expansion theorem. It expresses the determinant of an $n \times n$ matrix with respect to rows (or columns) and determinants of smaller-order square matrices.

Notation 8.2 Let $A = \{m_1, m_2, \dots, m_l\} \subseteq [n]$. Then: $\text{sum}(A) = m_1 + m_2 + \dots + m_l$.

Theorem 8.2 (Laplace Expansion Theorem) Let X be an $n \times n$ matrix and $Y \subseteq [n]$ (respectively, $Z \subseteq [n]$) with $|Y| = s$ (respectively, $|Z| = s$). Then:

a) (Fix Y)

$$\det(X) = \sum_{\substack{Z \subseteq [n] \\ |Z|=s}} (-1)^{\text{sum}(Y) + \text{sum}(Z)} \det(X[Y|Z]) \det(X(Y|Z)).$$

b) (Fix Z)

$$\det(X) = \sum_{\substack{Y \subseteq [n] \\ |Y|=s}} (-1)^{\text{sum}(Y) + \text{sum}(Z)} \det(X[Y|Z]) \det(X(Y|Z)).$$

Proof.

a) Fix $Y \subseteq [n]$, and let $|Y| = s$. Define

$$D_Y(X) = \sum_{\substack{Z \subseteq [n] \\ |Z|=s}} (-1)^{\text{sum}(Y) + \text{sum}(Z)} \det(X[Y|Z]) \det(X(Y|Z)).$$

First of all, since the determinant is n -linear with respect to columns (and rows) of a matrix and the sum is a linear combination of determinants, D_Y is n -linear with respect to columns (and rows) of X . (Note that a column (or a row) of X belongs to either $X[Y|Z]$ or $X(Y|Z)$.) Therefore, we need to show that D_Y is alternating and $D_Y(I_n) = 1$. Then, by the uniqueness of the determinant, $D_Y = \det$.

i) D_Y is alternating:

Assume that two columns of X are identical, say the u th column of X , denoted by X_u , is equal to the v th column of X , denoted by X_v , where $u < v$. If $u, v \in Z$ (respectively, $u, v \notin Z$), then $\det X[Y|Z] = 0$ (respectively, $\det X(Y|Z) = 0$). Therefore, to compute $D_Y(X)$, we only need to consider the following two cases: $u \in B$ and $v \notin B$ or $u \notin B$ and $v \in B$.

Assume $u \in B$ and $v \notin B$. Define a new set $Z' = (Z - \{u\}) \cup \{v\}$. Then, $[n] \setminus Z' = (([n] \setminus Z) \setminus \{v\}) \cup \{u\}$. Now, $\text{sum}(Z') - \text{sum}(Z) = v - u$: First, we have the equation:

$$(-1)^{\text{sum}(Z)} \det X[Y|Z] \det(X(Y|Z)) + (-1)^{\text{sum}(Z')} \det(X[Y|Z']) \det(X(Y|Z')) = 0:$$

Assume that $Z = \{1 \leq z_1 < z_2 < \dots < z_s \leq n\}$, $[n] \setminus Z = \{1 \leq w_1 < w_2 < \dots < w_{n-s} \leq n\}$, and $u = z_\alpha, v = w_\beta$. Then Z and Z' (also $n - [Z]$ and $n - [Z']$) coincide except for the range from u to v , and there are $v - u + 1$ positive integers between and including u and v . Let $z_{\alpha+\gamma-1} < v < z_{\alpha+\gamma}$. Then, we have: $1 \leq z_1 < z_2 < \dots <$

$z_\alpha = u < z_{\alpha+1} < \dots < z_{\alpha+\gamma-1} < v < z_{\alpha+\gamma} < \dots < z_s \leq n$. And:

$X[Y|Z] = X[Y|Z']$. $P(\sigma^{-1})$, where σ is the γ -cycle $(\alpha + \gamma - 1, \alpha + \gamma - 2, \dots, \alpha - 1, \alpha)$ and $P(\sigma^{-1}) = [\delta_{w, \sigma^{-1}(u)}]$.

$(\delta_{w, \sigma^{-1}(u)} = \begin{cases} 1, & \text{if } w = \sigma^{-1}(u) \\ 0, & \text{if } w \neq \sigma^{-1}(u) \end{cases}$. That is, $P(\sigma^{-1})$ interchanges the columns of I_s with respect to the permutation σ . Therefore, $X[Y|Z']P(\sigma^{-1})$ is the matrix obtained from $X[Y|Z']$ by moving the u th column of $X[Y|Z']$ into the $\sigma(u)$ th column.)

(Note that the u th and the v th (namely, z_α th and w_β th) columns of X are identical. Therefore, since $Z' = (Z \setminus \{u\}) \cup \{v\}$, the column sets of $X[Y|Z]$ and $X[Y|Z']$ are the same; but of course in a different order, and thus, we multiply $X[Y|Z']$ from the right by $P(\sigma^{-1})$ to interchange the columns of it to obtain $X[Y|Z]$.)

On the other hand, let $w_{\beta-\zeta} < u < w_{\beta-\zeta+1}$. Then we have: $1 \leq w_1 < w_2 < \dots < w_{\beta-\zeta} < u < w_{\beta-\zeta+1} < \dots < w_\beta = v < w_{\beta+1} < \dots < w_s \leq n$. And: $X(Y|Z') = X(Y|Z) P(\tau^{-1})$, where τ is the ζ -cycle $(\beta - \zeta + 1, \beta - \zeta + 2, \dots, \beta - 1, \beta)$.

(Note that the length of the cycle is ζ . And, $\zeta = v - u + 1 - \gamma$: The number of positive integers between and including u and v is $v - u + 1$. And, with respect to our notation, $\gamma (= ((\alpha + \gamma - 1) - \alpha) + 1)$ of them is in Z . Therefore, $(v - u + 1) - \gamma$ of them is in the complement of Z in $[n]$, namely, in the set $[n] \setminus Z$.)

$$\therefore (-1)^{\text{sum}(Z')} \det(X[Y|Z']) \det(X(Y|Z'))$$

$$= (-1)^{\text{sum}(Z')} \text{sgn}(\sigma^{-1}) \text{sgn}(\tau^{-1}) \det(X[Y|Z]) \det(X(Y|Z)).$$

\therefore Since $\text{sgn}(\sigma^{-1}) = \text{sgn}(\sigma)$ and $\text{sgn}(\tau^{-1}) = \text{sgn}(\tau)$, and since the sign of an θ -cycle is $(-1)^{\theta-1}$, we have:

$$(-1)^{\text{sum}(Z')} \det(X[Y|Z']) \det(X(Y|Z'))$$

$$= (-1)^{\text{sum}(Z')} (-1)^{\gamma-1} (-1)^{(v-u+1-\gamma)-1} \det(X[Y|Z]) \det(X(Y|Z)).$$

Now, $(\text{sum}(Z') + \gamma - 1 + v - u - \gamma) - \text{sum}(Z) = (\text{sum}(Z') - \text{sum}(Z)) + (v - u) - 1 = (v - u) + (v - u) - 1 = 2(v - u) - 1$ is an odd number.

$\therefore (\text{sum}(Z') + v - u - 1)$ and $\text{sum}(Z)$ have different parities. That is, one of them is odd and the other is even.

$$\begin{aligned} \therefore (-1)^{\text{sum}(Z)} \det(X[Y|Z]) \det(X(Y|Z)) \\ + (-1)^{\text{sum}(Z') + v - u - 1} \det(X[Y|Z]) \det(X(Y|Z)) = 0. \end{aligned}$$

As a result, since the sets Z and Z' occur in pairs in the set $\{Z|Z \subseteq [n] \text{ and } |Z| = s\}$, $D_Y(X) = 0$ if X has two identical columns.

$\therefore D_Y$ is alternating.

ii) $D_Y(I) = 1$:

$$D_Y(I) = \sum_{\substack{Z \subseteq [n] \\ |Z|=s}} (-1)^{\text{sum}(Y) + \text{sum}(Z)} \det(I[Y|Z]) \det(I(Y|Z)), \quad (*)$$

and $I(Y|Z)$ contains a zero row if $Z \neq Y$.

\therefore The sum has only one nonzero term corresponding to $Z = Y$.

$$\therefore D_Y(I) = (-1)^{\text{sum}(Y) + \text{sum}(Y)} \det(I[Y|Y]) \det(I(Y|Y)) = 1 \cdot 1 \cdot 1 = 1.$$

As a result of (i) and (ii), by the uniqueness of the determinant, $D_Y(X) = \det(X)$.

b) Apply part (a) to X^T :

Since for any square matrix M , $\det(M) = \det(M^T)$; by part (a) we have:

$$\begin{aligned} \det(X) &= \det(X^T) \\ &= \sum_{\substack{Z \subseteq [n] \\ |Z|=s}} (-1)^{\text{sum}(Y) + \text{sum}(Z)} \det(X^T[Y|Z]) \det(X^T(Y|Z)) \\ &= \sum_{\substack{Z \subseteq [n] \\ |Z|=s}} (-1)^{\text{sum}(Y) + \text{sum}(Z)} \det((X[Z|Y])^T) \det((X(Z|Y))^T) \\ &= \sum_{\substack{Z \subseteq [n] \\ |Z|=s}} (-1)^{\text{sum}(Z) + \text{sum}(Y)} \det((X[Z|Y])) \det((X(Z|Y))) \\ &= \sum_{\substack{Z \subseteq [n] \\ |Z|=s}} (-1)^{\text{sum}(Y) + \text{sum}(Z)} \det((X[Y|Z])) \det((X(Y|Z))) \end{aligned}$$

(In the last equation, we interchange the symbols Y and Z , namely $Y \leftrightarrow Z$.) ■

The usual Laplace cofactor expansion theorem is a particular case of the previous theorem, we just take $Y = \{i\}$ in part (a) and $Z = \{j\}$ in part (b).

There exists an amazing relation between determinants and inverses as stated in the next theorem.

Definition 8.4 Let M be a square matrix of order n . The “ (s, t) -cofactor” of M is the scalar $(-1)^{s+t} \det(M(s | t))$. The “cofactor matrix” of M , denoted by $\text{cof}(M)$, is the matrix whose (s, t) -entry is the (s, t) -cofactor of M . The “adjoint” of M , denoted by $\text{adj}(M)$, is the matrix whose (s, t) -entry is $(-1)^{t+s} \det(M(t | s))$, that is, $\text{adj}(M) = \text{cof}(M)^T$.

(We take transpose to define an adjoint matrix because the following theorem is true in this case.)

Theorem 8.3 Let M be an $n \times n$ matrix. Then:

- a) $M \text{adj}(M) = \text{adj}(M)M = \det(M)I_n$.
- b) M is regular $\Leftrightarrow \det(M) \neq 0$. And if M is regular, then:

$$M^{-1} = (\det(M))^{-1} \text{adj}(M).$$

8.4 The Jacobi Identity for Determinants

Theorem 8.4 (The Jacobi identity for determinants) Let Z be an $n \times n$ regular matrix, and let $W = Z^{-1}$. Also let X, Y be proper nonempty subsets of $[n]$ with $|X| = |Y| = s$. Then:

$$\det(W(X|Y)) = \frac{\det(Z[Y|X])}{\det(Z)}.$$

Proof. Let $X = \{1 \leq i_1 < i_2 < \dots < i_\theta \leq n\}$ and $Y = \{1 \leq j_1 < j_2 < \dots < j_\theta \leq n\}$. Also, let σ and τ be permutations on $[n]$ such that

$$\sigma(\gamma) = \begin{cases} \alpha, & \text{if } \gamma = i_\alpha \in X; \\ \gamma, & \text{if } \gamma \notin X; \end{cases} \quad \text{and} \quad \tau(\gamma) = \begin{cases} \beta, & \text{if } \gamma = j_\beta \in Y; \\ \gamma, & \text{if } \gamma \notin Y. \end{cases}$$

Moreover, Let $P(\sigma)$ and $P(\tau)$ be the corresponding permutation matrices.

Step 1. The following are elementary facts:

- a) $P(\tau^{-1}) = P(\tau)^{-1} = P(\tau)^T = P(\tau)^*$.
- b) $P(\sigma)M$ is the matrix derived from M by moving the α th row of M into the $\sigma(\alpha)$ th row of M for each $\alpha = 1, 2, \dots, n$.

c) $MP(\tau^{-1})$ is the matrix derived from M by moving the β th column of M into the $\tau(\beta)$ th column of M for each $\beta = 1, 2, \dots, n$.

Step 2. Let Z be a regular matrix. Then:

$$\begin{aligned} ZZ^{-1} = I &\Rightarrow P(\sigma)ZZ^{-1}P(\sigma)^{-1} = I \\ &\Rightarrow P(\sigma)ZP(\tau^{-1})P(\tau)Z^{-1}P(\sigma)^{-1} = I \\ &\Rightarrow (P(\sigma)ZP(\tau^{-1}))(P(\tau)Z^{-1}P(\sigma)^{-1}) = I \\ &\Rightarrow (P(\sigma)ZP(\tau^{-1}))(P(\sigma)ZP(\tau^{-1}))^{-1} = I \end{aligned}$$

\therefore If $W = Z^{-1}$ (i.e., if $W^{-1} = Z$), then $P(\sigma)W^{-1}P(\tau^{-1})$ is the inverse of $(P(\sigma)ZP(\tau^{-1}))^{-1}$ for any permutation matrices $P(\sigma)$ and $P(\tau^{-1})$.

Step 3. Let M be an $m \times n$ matrix and let $X, Y \subseteq [n]$ be as defined at the beginning of the proof. (In fact, for this step, the condition $|X| = |Y|$ does not necessarily hold). Then:

$$M[X|Y] = P(\sigma)MP(\tau^{-1})[[\theta] | [\theta]].$$

is true because, on the left side, we take the submatrix of M with the row indices in X and the column indices in Y ; on the right side, we first carry rows with indices in X to the first θ rows and columns with indices in Y to the first θ columns, then we take the submatrix of the resulting matrix with the row and column indices in $[\theta]$. Similarly, we have:

$$M(X|Y) = P(\sigma)MP(\tau^{-1})[[n] - [\theta] | [[n] - [\theta]]].$$

Step 4. Therefore, since

$$\begin{aligned} \det(P(\sigma)WP(\tau^{-1})[[\theta]||[\theta]]) &= \det(W[X|Y]), \\ \det(P(\sigma)ZP(\tau^{-1})([\theta]||[\theta])) &= \det(Z(Y|X)), \end{aligned}$$

we have:

$$\begin{aligned} \det(W[X|Y]) &= \frac{\det(Z(Y|X))}{\det(Z)} \Leftrightarrow \\ \det(P(\sigma)WP(\tau^{-1})[[\theta]||[\theta]]) &= \frac{\det(P(\sigma)ZP(\tau^{-1})([\theta]||[\theta]))}{\det(Z)}. \end{aligned}$$

\therefore Instead of taking X and Y as arbitrary nonempty proper subsets of $[n]$, we can take $X = Y = [\theta]$, where $1 \leq \theta < n$. This simplifies (the notations in) the proof of the theorem.

Step 5. Without loss of generality, let $X = Y = [\theta]$, where $1 \leq \theta < n$. First of all, since Z is invertible, any square submatrix of Z is invertible, in particular, $Z(Y|X)$ is invertible. Now, let $Z = \begin{bmatrix} M_{\theta \times \theta} & N \\ P & Q \end{bmatrix}$. Then $Z/M = Q - PM^{-1}N$, and:

$$\begin{bmatrix} I & 0 \\ -PM^{-1} & I \end{bmatrix} \begin{bmatrix} M & N \\ P & Q \end{bmatrix} \begin{bmatrix} I & -M^{-1}N \\ 0 & I \end{bmatrix} = \begin{bmatrix} M & 0 \\ 0 & Q - PM^{-1}N \end{bmatrix}.$$

$\therefore \det(Z) = \det(M) \det(Q - PM^{-1}N)$.

And, we have:

$$\begin{aligned} W = Z^{-1} &= \left(\begin{bmatrix} I & 0 \\ -PM^{-1} & I \end{bmatrix}^{-1} \begin{bmatrix} M & 0 \\ 0 & Z/M \end{bmatrix} \begin{bmatrix} I & -M^{-1}N \\ 0 & I \end{bmatrix}^{-1} \right)^{-1} \\ &= \begin{bmatrix} I & -M^{-1}N \\ 0 & I \end{bmatrix} \begin{bmatrix} M^{-1} & 0 \\ 0 & (Z/M)^{-1} \end{bmatrix} \begin{bmatrix} I & 0 \\ -PM^{-1} & I \end{bmatrix} \\ &= \begin{bmatrix} * & * \\ * & (Z/M)^{-1}_{(n-\theta) \times (n-\theta)} \end{bmatrix} \end{aligned}$$

$\therefore W(X|Y) = (Z/M)^{-1}_{(n-\theta) \times (n-\theta)}$.

$$\begin{aligned} \therefore \det(W(X|Y)) &= \det((Z/M)^{-1}) = \det(Z/M)^{-1} = \left(\frac{\det(Z)}{\det(M)} \right)^{-1} \\ &= \frac{\det(M)}{\det(Z)} = \frac{\det(Z|Y|X)}{\det(Z)}. \blacksquare \end{aligned}$$

Note 8.1

$$\begin{aligned} \det(Z^{-1}(X|Y)) &= \frac{\det(Z|Y|X)}{\det(Z)} \quad (Z \leftrightarrow Z^{-1}) \\ &\Leftrightarrow \\ \det(Z(X|Y)) &= \frac{\det(Z^{-1}|Y|X)}{\det(Z^{-1})} \Leftrightarrow \det(Z(X|Y)) = \frac{\det(Z^{-1}|Y|X)}{\det(Z)^{-1}} \\ &\Leftrightarrow \det(Z^{-1} [Y|X]) = \frac{\det(Z(X|Y))}{\det(Z)} \quad X \leftrightarrow Y \\ &\Leftrightarrow \\ \det(Z^{-1} [X|Y]) &= \frac{\det(Z(Y|X))}{\det(Z)}. \end{aligned}$$

$\therefore \det(Z^{-1} [X|Y])$ can be expressed in terms of $\det(Z(Y|X))$ and $\det(Z)$.

8.5 Result and Discussion

This chapter is a review study, it does not contain any original results. As stated at the beginning of the chapter, we benefited greatly from Piziak and Odell (2007) and Berman and Shaked-Monderer (2003) in preparing this study.

The purpose of this chapter is to prove the Cauchy-Binet Theorem, Laplace Expansion Theorem, and the Jacobi Identity for Determinants at a basic level. In other words, we aim to present a tutorial source proving these three theorems without leaving any parts of the proofs to the reader. Therefore, we hope this self-contained chapter will be useful for students and researchers who want to learn proofs of these three very important theorems of linear algebra and matrix theory.

Finally, as it is known, there are lots of good resources about linear algebra and matrix theory. We especially recommend Piziak and Odell (2007), Zhang (2011), or a more detailed graduate textbook Horn and Johnson (2012). In particular, one of the good textbooks about positive definite matrices is Berman and Shaked-Monderer (2003), or its newer version Berman and Shaked-Monderer (2021).

REFERENCES

- Berman, A. and Shaked-Monderer, N. (2003). Completely Positive Matrices. World Scientific, New Jersey.
- Berman, A. and Shaked-Monderer, N. (2021). Copositive and Completely Positive Matrices. World Scientific, New Jersey.
- Horn, R. A. and Johnson, C. R. (2012). Matrix analysis (2nd Ed.). Cambridge University Press, 662, Cambridge.
- Piziak, R. and Odell, P. L. (2007). Matrix theory: From generalized inverses to Jordan form. CRC Press, Boca Rotan.
- Zhang, F. (2011). Matrix theory: Basic results and techniques (2nd Ed.). Springer, New York.

CHAPTER 9

CAVE-RIPENED CHEESES

Assoc. Prof. Dr. Oğuz AYDEMİR¹

DOI: <https://dx.doi.org/10.5281/zenodo.14259161>

¹ Çankırı Karatekin University, Faculty of Engineering, Department of Food Engineering, Çankırı, Türkiye. oaydemir@karatekin.edu.tr, Orcid ID: 0000-0003-0538-2311

INTRODUCTION

The ripening of cheeses in caves is an age-old tradition used in different cultures, which provides favourable conditions for the ripening and preservation of the product. This process results in favourable physicochemical, biochemical and microbiological processes to obtain the desired sensory characteristics of the cheese. Caves have been and still are used worldwide for the ripening of many types of cheese.

In Southern Europe, many cheese varieties are still produced as artisanal following specific traditional methods (without starter culture). The production and ripening methods determine the cheese characteristics and the microbial flora of the cheese. Accordingly, these artisanal cheeses are characterised by their unique characteristics. Many artisanal cheeses have obtained the PDO (Protected Designation of Origin), Protected Geographical Indication (PGI), and Traditional Specialty Guaranteed (TSG) certificates. The PDO certificate can also show differences between producers or regions. According to the PDO definition, there is a relationship between "the region of origin", "traditional cheese making procedures" and the "specific characteristics of the final product" (Randazzo et al., 2009; Varriale and Ciaravino, 2022; Alexa et al., 2024).

Cheese microflora has a crucial effect in the ripening process of cheese with the biochemical reactions it causes. It includes changes such as the activity of starter culture microorganisms, the enzymes subsequently released because of the death and breakdown of these starters, the development of non-starter microflora from milk or contaminated from the environment, and, as in many cheese types, the growth of a secondary microflora. The cheese ripening process generally involves 4 basic biochemical reactions: (1) glycolysis of residual lactose and lactate catabolism, (2) citrate catabolism, (3) lipolysis and catabolism of free fatty acids, and (4) proteolysis and catabolism of amino acids (McSweeney, 2004). Starter and non-starter lactic acid bacteria (LAB) are involved in both primary and secondary biochemical processes, while moulds, e.g. *Penicillium roqueforti* in blue cheeses, *Penicillium camemberti* or *Geotrichum candidum* in soft

cheeses such as Camembert and Brie, metabolise fatty acids and amino acids in secondary biochemical processes (Dupont et al., 2017).

With the pasteurization process and the use of commercial starter cultures in industrial cheese production, the microbial flora naturally present or contaminated in raw milk loses its typical characteristics due to replacement by starter cultures (González-Crespo and Mas 1993). However, recently, due to concerns about food safety in terms of health hazards, it has become legally mandatory to pasteurize milk (Wouters et al. 2002) or to ripen cheeses produced from raw milk for certain periods of time. In cheese production, starter cultures are utilised to improve the sensory quality of cheese. However, the textural, microbiological and sensory properties of cheeses produced using commercial starter cultures and pasteurization process are different from those of conventionally produced cheeses (Aydemir and Dervisoglu, 2010). The flavour and aroma of raw milk cheeses are generally much more intense. Cheeses made from raw milk contain a wide variety and variability of microorganisms from the environment. This high microbial diversity has the capacity to produce many flavour compounds, making the flavour of such cheeses less uniform and atypical (Grappin and Beuvier 1997). The main source of the enzymatic activity that forms the basis of cheese flavour is the cheese microbiota. The main substrates of flavour and aroma formation are carbohydrates, organic acids, lipids and proteins. Among these biomacromolecules, proteins and the catabolism of amino acids resulting from the protein degradation are the most important in flavour and aroma development (Steel et al., 2013).

Studies have shown that the flavour compounds produced by non-starter strains differ from those formed by industrial strains. It is thought that non-starter lactococci improve cheese flavour positively due to the more active amino acid converting enzymes they possess compared to starter strains (Ayad et al., 1999; Morales et al., 2003). Non-starter LAB isolates was found to have very different amino acid converting activities depending on the strain. Among these strains, those that can give cheese a pleasant and rich flavour should be identified and their use in the cheese industry should be investigated

(De Palencia, et al. 2006). Standardization is very important in the production of cheese which is traditionally ripened in caves. For this purpose, it is necessary to identify the microflora of these cheeses and to identify the important strains that enable cheese ripening. When these microorganism strains are included in the cheese production process under controlled conditions, standardised and high-quality products can be obtained (Ozturkoglu-Budak et al., 2016a).

Artisanal cheeses have a highly diverse microflora that determines their quality and safety (Alexa et al., 2024). Cheese rind microflora with low species numbers generally contain many *Penicillium* species. These can be *P. camemberti*, added as a starter culture to produce Camembert or Brie cheeses, “wild” moulds found naturally in caves, as in Cheddar and Tomme-style cheeses, or nuisance microbes, such as the blue spots caused by *P. bifforme* in some bloomy rind cheeses. Depending on the ecological diversity among *Penicillium* species on the cheese surface, there are differences in their ability to direct the growth of bacterial species (Ye et al., 2024). Mould-ripened cheeses have two types. First, cheeses ripened by the growth of the desired moulds inside the cheese. For example, Roquefort, Stilton, Gorgonzola, and Danish Blue fall into this group. Secondly, cheeses those are ripened performing moulds growing on the surface of the cheese. These Blue cheeses are traditionally ripened either in caves (Roquefort, Gorgonzola) or in cellars (Stilton) at low temperature and high humidity. Furthermore, different strains of *Penicillium roqueforti* are used in the production of all these cheeses (Stark, 2007). It is reported that Roquefort blue cheese was discovered by chance when a child left a cheese in a cave and found it mouldy after months. The mould that transformed this cheese into Roquefort was *P. roqueforti* (Fabricant, 1982; Vabre and Bergeron, 2015; Ferroukhi et al. (2024). In the Massif Central region of southern France, the making and ripening of Roquefort cheese was carried out under the control of monasteries in the Cambalou caves, known for sheep breeding and cheese production until the 11th century. The use of sheep's milk, the treatment of the cheese surface with plenty of salt and the cave conditions created favourable conditions for the growth of *P. roqueforti*. Gorgonzola

cheese is believed to have been first made near Milan in 879 AD (Del Piano, Tari and Carmagnola, 2012), while some sources report that Gorgonzola originated in Pasturo in Valsassina, famous for its natural caves (Ferroukhi et al. 2024).

Among artisanal cheeses, there are many types of cheese ripened in caves (or cellars) around the world. These cave-ripened cheeses have attracted attention especially in recent years with their unique flavours and aromas. The problem of perishability of food production from ancient times to the present day, the instability of food supply due to seasonality and climate dependence have been effective in the formation of traditional food production methods and local diets. These problems have stimulated the development of food preservation methods. Sometimes such ways or methods have led to the emergence of new food products that have become important elements of local cultural heritage. Underground spaces have been used for the preservation and transformation of food. For this purpose, both natural and artificial underground spaces have been chosen, sometimes in rural areas close to production sites, sometimes in settlements where food is traded or consumed. Throughout history, these natural spaces have been used to preserve foods that require constant temperature conditions, are affected by sunlight, but are not refrigerated. They have ensured that raw foods and processed foods have gradually become an important part of the normal diet and traditional foods. The use of caves for this purpose has an important effect on both the cheese making treatment and the product itself. Cellars, underground workshops or caves, which are an important part of the production process, not only represent cultural heritage but also closely associate cheese with its local historical and cultural context. Cave cheeses are internationally recognised gourmet products, offered with original marketing strategies linked to both local landscapes and historical monuments. In Valle de Roncal (Spain), for example, cave cheeses are a symbol of rural identity and an important tourist destination. The cave-oriented approach has always been the marketing tactic of choice for French Roquefort cheese producers (Varriale and Ciaravino, 2022).

Dağlı et al. (2020) stated that caves generally have a cool, humid and year-round stable climate. Therefore, they are used for food preservation and ripening. The water in the cheese is gradually released during ripening. This process takes place in caves in the Alps in northern Italy. In these caves, cool environmental conditions of 13 to 20 °C and 50-80% relative humidity are naturally achieved in the summer (Hirata et al. 2018). Cave climate affects the microbiological properties of the environment and especially high humidity supports microbial growth. Microbiological characteristics of the cave environment affect Tulum cheeses. A high and very high positive relationship was found between the microbial properties of the cave environment and Tulum cheeses. The taste and odour of cave ripened Tulum cheeses were more appreciated than fresh cheese produced under similar conditions Dağlı et al. (2020). Non-starter microorganisms of cave environments directly affect the cheese microflora and are effective in cheese ripening (Alexa et al., 2024). The air chemical content, surface and air flora, temperature and humidity of each cave will vary. Thus, cheese flavour and aroma will gain different characteristics according to the cheese varieties and these properties of the cave.

Types of cave-ripened cheeses produced worldwide

Cave-ripened cheeses, which are the product of a centuries-old tradition, are very diverse. As a packaging material, these cheeses are usually ripened in goat or sheep skin-bag, as in Turkish Tulum, but it is seen that most cheeses are generally ripened without packaging. Depending on the hygienic conditions related to animal husbandry, milking, milk processing and cheese making, and the air and surface microflora of the ripening caves, each cheese has a unique microflora. With the primary effect of this microflora, each cheese undergoes a unique ripening process under ambient conditions. Thus, each cheese has its own unique flavour-aroma, structure-texture and appearance-colour characteristics. Although there are different cave-ripened traditional cheeses in various countries of the world that have not been included in the literature and have not been scientifically investigated,

this chapter is based only on the cheeses mentioned in scientific review articles or books and in research articles. As a result of the scientific literature review, the studies on cave-ripened cheeses are presented in Table 1. It was observed that most of these studies were on cheese microbiology.

Table 1. Cave-ripened cheeses produced worldwide

Cheese	Country	Analyses	References
Livanjski	Bosnia and Herzegovina	Review	Dizdarević and Mulaomerović (2023)
Cave	Brasilia	Determination of ochratoxin A and ochratoxigenic fungi	Marcelão et al. (2024)
Blue	France	<i>P. roqueforti</i> genotyping	Dumas et al. (2020)
Bleu des Causses		Review	İNAO (2022)
		Review	Ferrokhi et al. (2024)
Bleu d'Auvergne		Review	Ferrokhi et al. (2024)
Fourme d'Ambert		Review	Ferrokhi et al. (2024)
Fourme de Montbrison		Review	Ferrokhi et al. (2024)
Roquefort		Review	Ferrokhi et al. (2024)
Tsalafouti	Greece	Chemical, microbiological and sensory characteristics	Pappa et al. (2022)
Apulian	Italy	Identification of <i>Penicillium sp.</i>	Anelli et al. (2018)
Castelmagno		Microbial dynamics and identification of LAB	Dolci et al. (2010)
Fontina		Microbial dynamics	Dolci et al. (2013)
		Microbial dynamics	Dolci et al. (2014)
Cave		Fungal mycobiota and mycotoxins	Anelli et al. (2019)
Caciocavallo Podolico Lucano		Metagenomic, microbiological, chemical and sensory profiling	Busetta et al. (2023)
Caciocavallo		Cheese manufacturing variations	Uzun et al. (2020)

Pecorino		Biogenic amines content	Torracca et al. (2015)
		Biogenic amines content and sensory properties	Torracca et al. (2016)
Pecorino Bagnolese		Physicochemical and microbiological characterization	Mazzocca et al. (2024)
Pecorino di Filiano		Microbial dynamics	Bonomo and Salzano (2012)
		Genotypic and technological diversity of <i>Brevibacterium linens</i>	Bonomo et al. (2015)
		Review	Varriale and Ciaravino (2022)
Pecorino Romano		Review	Varriale and Ciaravino (2022)
Pecorino Siciliano		Non-starter lactic acid bacteria	Guarcello et al. (2016)
		Bacterial microbiome, free fatty acid and volatile compounds	Gaglio et al. (2020)
Asiago		Review	Varriale and Ciaravino (2022)
BRA		Review	Varriale and Ciaravino (2022)
FioreSardo		Review	Varriale and Ciaravino (2022)
Castelmagno		Review	Varriale and Ciaravino (2022)
Taleggio		Review	Varriale and Ciaravino (2022)
Fossa di Sogliano		Review	Varriale and Ciaravino (2022)
Caciocavallo irpino di grotta		Review	Varriale and Ciaravino (2022)
Caciocavallo pugliese di grotta		Review	Varriale and Ciaravino (2022)
Canestrato di Moliterno		Review	Varriale and Ciaravino (2022)
Grotta del Caglieron		Review	Varriale and Ciaravino (2022)
Gran Cru di Grotta		Review	Varriale and Ciaravino (2022)
OI Minadùr		Molecular characterization of mycobiota	Anelli et al. (2024)

Pit		Physicochemical and microbiological characterization	Toppino et al. (1992)
Năsal	Romania	<i>Brevibacterium linens</i> and physicochemical characterization	Mihaiu et al. (2008)
Alhama de Granada	Spain	Physicochemical characteristics	Fernández-Salguero and Gómez (1997)
Bejes–Tresviso		Proteolytic activity and mycotoxins in <i>Penicillium roqueforti</i> strains	Fernández-Bodega et al. (2009)
Cabrales		Metabolome, microbiome and resistome	Alexa et al. (2024)
		Determination of cheese mites, (Acari: Acaridae)	Sánchez-Ramos et al. (2007)
		Microflora characterization	Núñez (1978)
		Yeast and mould characterization	Núñez et al. (1981)
		Proteolytic activity and mycotoxins in <i>Penicillium roqueforti</i> strains	Fernández-Bodega et al. (2009)
Gamonedo		Physicochemical and microbiological characterization	De Llano et al. (1992)
Picón Bejes-Tresviso		Physicochemical and biochemical characterization	Prieto et al (1999)
		Biochemical characterization	Prieto et al (2000)
Valdeón-artisan		Proteolytic activity and mycotoxins in <i>Penicillium roqueforti</i> strains	Fernández-Bodega et al. (2009)
Tulum	Türkiye	Microbial dynamics	Dağlı et al. (2020)
		Characteristics of goat skins	Gün and Güzel-Seydim (2022)
Divle Tulum		Determination of Aflatoxin M1	İşleyici et al. (2011)
		Determination of mineral substance and heavy metals	İşleyici et al. (2017)
		Microbial dynamics	Ozturkoglu-Budak

			et al. (2016a)
		Volatile compounds	Ozturkoglu-Budak et al. (2016b)
		Temporal microbiota and biochemical profiles	Ozturkoglu-Budak et al. (2018)
Küflü Tulum		Identification of the filamentous fungi	Kirtil et al. (2024)
		Physicochemical and biochemical characterization	Hayaloglu et al. (2008)
		Mycobiota and diversity of <i>Penicillium roqueforti</i> isolates	Seri and Metin (2021)
Erzincan Tulum		Review	Hastaoğlu et al. (2021)
		Review	Tekinşen ve Akar (2017).
Şavak Tulum		Review	Hastaoğlu et al. (2021)
Çepni Tulum		Review	Hastaoğlu et al. (2021)
Afyon Tulum		Review	Hastaoğlu et al. (2021)
Çimi Tulum		Review	Hastaoğlu et al. (2021)
İzmir Tulum		Review	Hastaoğlu et al. (2021)
Kaşar		Review	Hastaoğlu et al. (2021)
Cheddar	USA	Mites and sensory characteristics	Krishnan et al. (2019)
Rind blue		Metabolomic domestication of wild <i>Penicillium</i>	Bodinaku et al. (2019)
White mold		Crystallization and demineralization phenomena	Tansman et al. (2017)
Minnesota Blue		Surface microflora	Morris et al. (1951)
Blue		Surface microflora	Hartley and Jezeski (1954)

Fungi in cave-ripened cheeses

When the surface microflora of Minnesota blue (in USA), a cave cheese, was examined, it was determined that it initially consisted mostly of yeasts and some moulds, and then cocci and rod bacteria

became dominant on the surface. During ripening, the surface layer (smear) becomes alkaline and the acidity of the cheese decreases. The activity of the surface microflora or more favourable ripening conditions at the surface increase the total volatile acidity, pH and amino nitrogen percentage, thereby improving the cheese body and texture (Morris et al., 1951). The smear on blue cheese (in USA) developed in a regular pattern depending on the environment and the initial flora was found to be predominantly yeasts and some mould (*P. roqueforti*), with an increase in cocci and rod forms at later stages. The predominant species in the smear layer of ripened cheeses was identified as *B. erythrogenes* at 46 and 49 °F. *B. linens* was the predominant rod-shaped species in cheese curing at 55 to 58 °F and was absent in smears developed at 46 to 49 °F (Hartley and Jezeski, 1954). Banks et al. (2023) studied fungi in the air of a man-made cheese cave in the United States. Most of the genera isolated were identified as *Penicillium* and *Scopulariopsis*, taxa associated with cheese. The only other taxon identified was *Cladosporium*, which was isolated from both indoor and outdoor air environments and from cheese. *Penicillium*-Fasciculata isolates found in cheese cave air showed growth characteristics like wild *Penicillium*. Anelli et al. (2018) investigated the mould flora of Apulian cheeses, a cave cheese from Gravina di Puglia (Italy), and identified several *Penicillium* species. They identified a new species, *Penicillium gravinicaesei*, which is closely related to *P. parvulum* and *P. cinnamopurpureum*. They reported that this new species did not synthesise mycotoxins (ochratoxin A, sterigmatocystin, citrinin, patulin, or aflatoxin B1 toxins). Anelli et al. (2019) identified twenty-four fungal species by molecular identification on the outer surface of a traditional Italian cave cheese (semi-hard). The most abundant species were *Aspergillus westerdijkiae* and *P. biforme*, followed by *P. roqueforti* and *P. solitum*. At least one toxigenic species was determined in 86% of the samples. They detected the ochratoxygenic species *A. westerdijkiae* and *A. steynii* in 45% of the cheeses. Furthermore, OTA was found in the rind of 36% of the cheeses. They reported that cave cheese is a potential medium for toxigenic mould growth and OTA formation. They

emphasized the need to develop appropriate scientific tools to meet the sensory expectations of consumers and cheese safety and to avoid consuming cheeses that mould under uncontrolled conditions and are not monitored to avoid mycotoxin risk. *A. westerdijkiae*, whose effect on the sensory properties of Apulian cheese is unknown, could not be isolated from the cheese surface. Some *A. westerdijkiae* strains that have lost the ability to produce OTA have been identified. These strains can be added to cheese to prevent colonisation by OTA-producing strains to ensure food safety (Susca et al., 2021). In another study, a total of 130 samples of Brazilian artisanal cave cheeses with naturally mouldy rinds from different ripening periods were examined. Some samples from three companies and markets showed *Aspergillus* section *Circumdati* between 10^2 and 10^6 cfu/g. Among the *Aspergillus spp.*, *A. westerdijkiae* was the highest (67%), followed by *A. ostianus* (22%) and *A. steynii* (11%). Ochratoxin A (OTA) was determined in 22% of the cheeses at levels ranging from 1.0 to 1000 $\mu\text{g}/\text{kg}$, while five samples had OTA levels above 1000 $\mu\text{g}/\text{kg}$, indicating the necessity of continuous monitoring and quality control (Marcelão et al. 2024). Anelli et al. (2024) stated that identification of fungi growing on cheese ripened in natural and uncontrolled environments is important in terms of providing information about potential mycotoxin risk. Autochthonous mycobiota colonizing Ol Minadùr cheese, produced by five dairies and ripened for 90 to 180 days in the Dossena mines was identified by them. Among the filamentous fungi collected from 58 out of 68 cheeses, *P. biforme* and among the yeasts, *Debaryomyces hansenii* were found to be the most dominant species, and none of them were reported to pose a health risk for human consumption. It was observed that the richness of the mycobiota increased after 180 days of ripening, while significant differences were observed in the mycobiota composition of the cheeses from different dairies. Local, blue-veined cheeses of good quality produced in villages in the Cabrales, Valdeón and Bejes-Tresviso valleys in northern Spain were analysed by Fernández-Bodega et al. (2009). They found strains of *P. roqueforti* in each of these blue cheeses and compared them with the *P. roqueforti* CECT 2905 wild strain and the 'Valdeón-industrial' strain used for

large-scale manufacture of Valdeón cheese, and they identified all strains as *P. roqueforti*. The industrial strain exhibited high aspartyl protease AspA activity, while this was not the case for the isolated wild strain. Lipolytic activity levels were close to each other in strains obtained from local blue cheeses. The authors stated that the strains obtained from local blue cheese varieties synthesised moderate levels of PR toxin, while the Valdeón-industrial strains released high levels of the same toxin. All authentic strains exhibited similar levels of roqforin C. The level of the antitumoural compound andrastin A differed in all cheeses. *P. roqueforti* strain CECT 2905 was found to be able to produce high levels of andrastin A. İşleyici et al. (2011) detected aflatoxin M1 at a level not exceeding the legal limits in 10 of 55 Divle Tulum cheeses they examined. Ozturkoglu-Budak et al. (2016a) studied the microflora of Divle cheese (Türkiye) throughout cave ripening. It was observed that bacilli and Gammaproteobacteria were dominant at the beginning of ripening, while Actinobacteria became dominant in the later stages. When the yeast and mould content was examined, the most identified species were *P. roqueforti*, *P. biforme*, *P. polonicum*, *P. chrysogenum* and *Debaryomyces hansenii*. Microflora showed similar communities between cheeses, while high diversity was observed in the cheese throughout ripening. Kirtil et al. (2024) obtained 43 moulds from Küflü (mould-ripened) cheeses in Türkiye, including cave-ripened ones. As a result, nine different *Penicillium* species (*P. roqueforti*, *P. biforme*, *P. corylophilum*, *P. crustosum*, *P. rubens*, *P. spinulosum*, *P. paneum*, *P. brevicompactum*, and *P. solitum*) were identified by FTIR HTS-XT method. Seri and Metin (2021) identified 53 of 54 filamentous fungi as *Penicillium roqueforti* and 8 yeast isolates as *Candida zeylanoides*, *Pichia membranifaciens*, *Geotrichum candidum* and *Debaryomyces hansenii* from 26 Küflü Tulum cheeses. *P. roqueforti* isolates showed genetically and phenotypically very similar characteristics.

Bacteria in cave-ripened cheeses

Dolci et al. (2010) determined microbiota of Castelmagno (PDO) cheese by both culture-dependent and culture-independent analyses in

milk, curd and cheese samples at different ripening times. Culture-dependent methods showed that a thermophilic streptococcal population, including *Streptococcus thermophilus* and *S. agalactiae* species, was initially dominant. Later, mesophilic lactococci with *Lactococcus lactis* appeared in the first month of ripening. Among lactobacilli, *Lactobacillus plantarum* and *Lb. casei* were dominant throughout ripening. The culture-independent analysis emphasised the crucial role of *L. lactis* in both production and ripening. Culture-independent methods based on PCR-DGGE and RT-PCR-DGGE were trialled to research the bacterial microflora in Italian Fontina (PDO) cheese (Dolci et al 2013). As in other smear ripened cheeses, coryneform bacteria were observed to be actively involved in rind formation. In particular, the presence of *Brevibacterium*, *Corynebacterium* and *Arthrobacter* genera was noted. The RT-PCR-DGGE method was more successful in characterising the biodiversity of the Fontina (PDO) surface and RNA molecules provided more informative data than DNA. Bonomo et al. (2012) studied the microbial properties of Pecorino di Filiano cheese ripened in a cave and in a ripening-room. They found that *Brevibacterium linens* was dominant on the cheese surface. They reported that *Lactobacillus delbrueckii subsp. bulgaricus* and *Lactobacillus paracasei subsp. paracasei* were the most obtained both on the surface and inside the cheese, and *Leuconostoc lactis* and *Leuconostoc mesenteroides subsp. mesenteroides* were dominant among *Leuconostoc* spp. They concluded that the ripening environment is very effective in determining the cheese properties. Bonomo et al. (2015) isolated twenty-two *Brevibacterium linens* strains from Pecorino di Filiano cheese ripened in cave and ripening-room conditions. They reported that there was significant heterogeneity among *B. linens* strains in terms of physiological and technological properties. They reported that the ripening environment determines the typical characteristics of the cheese and is effective in the formation of the surface microflora. In a study on Romanian Năsal cheese, it was reported that *B. linens* was found only in a natural cave in Taga in Cluj region and naturally contaminated the cheese during cheese ripening, contributing to the

cheese's unique characteristics (Mihaiu et al. 2008). During all ripening periods, 50% *B. linens* and 35% *Micrococcus spp.* were found on the cheese surface, while 20% lactic *Streptococcus* was found in the 2nd and 3rd periods. In addition, 50% *B. linens* and 45% *Corynebacterium spp.* were found on the cave walls and 50% *B. linens* and 50% *Pseudomonas spp.* were found on the cave ceiling. Dağlı et al. (2020) examined Turkish Tulum cheeses ripened in the cave in Derbent district of Konya and cave conditions. They reported that *Staphylococcus*, coliforms, yeasts and moulds found in unhygienic conditions were found in the cave environment and contaminated Tulum cheese. *Staphylococcus* and coliform numbers in Tulum cheese were found to be within acceptable limits according to the Turkish Food Codex on Microbiological Criteria. Moulds have a dominant character and dynamic structure, limiting the growth of harmful bacteria such as coliforms and *Staphylococcus* or causing them to disappear. The taste and odour of the cave ripened Tulum cheeses were liked more than other fresh Tulum cheeses. Busetta et al. (2023) analysed cave-ripened Caciocavallo Podolico Lucano (CPL) cheese produced using traditional methods in 4 different establishments. While 18 taxonomic groups were identified in the cheeses, they found that streptococci and lactobacilli were the main groups of wood vat biofilms and lactobacilli constituted almost all the bacterial community in the cheeses. The main microbiological counts and species were found to be quite similar between the dairies, while the physicochemical properties and organoleptic characteristics of the cheeses were quite consistent among the dairies. This study showed that the strict implementation of the traditional CPL cheese manufacturing procedure among dairies is the preferred strategy to harmonise microbial evolution and keep the final properties of CPL cheese almost constant. It was concluded that the differences in microbiological levels and species diversity among dairies were related to the production environment of the final cheeses. Gaglio et al. (2020) produced Pecorino Siciliano cheese (PDO) using lactic acid bacteria (LAB) culture composed of starter and non-starter strains and analysed the bacterial communities. They reported that streptococci and lactobacilli were predominant in cheeses produced

without starter or addition of any bacteria, whereas lactococci, streptococci and lactobacilli were predominant in cheeses obtained with the addition of a multi-strain culture. Shannon index increased in cheeses obtained with the addition of mixed culture.

Mite in cave-ripened cheeses

Two mite species, *Acarus farris* and *Tyrophagus neiswanderi*, were detected in Asturias Cabrales (Spain) cheese ripened in a cave. It was found that the optimum growth temperature for both species was 27-28 C and that the level of development of *A. farris* was higher at the cooler temperatures observed in the cheese caves. It was reported that it may be possible to control mite populations during cheese ripening by temperature manipulation based on modelling predictions (Sánchez-Ramos et al., 2007). Krishan et al. (2019) investigated the effects of using food-grade ingredients as surface coating agent or draining cloth in cave-type Cheddar cheese to prevent *Tyrophagus putrescentiae* (Acaridae) growth. Carrageenan + alginate + Propylene glycol and Xanthan gum + Propylene glycol coatings and the use of draining cloth were found to be effective in reducing the number of *T. putrescentiae*, while ripening at 10 C or lower and 75% relative humidity or lower was determined to be necessary to minimise moulding and maintain the sensory properties of the cheese.

Chemical and biochemical characteristics of cave-ripened cheeses

Hayaloglu et al. (2008) investigated a total of 28 Küflü cheeses, a Turkish variety ripened by mould. They found that the mean titratable acidity, moisture, salt in moisture, fat in dry matter, total protein and pH were 0.96%, 49.97%, 7.49%, 12.18%, 37.84% and 6.29%, respectively. They reported that proteolysis index values and casein degradation rate were high. They reported that the peptide profiles of the cheeses were qualitatively similar. The main volatile compounds of the cheeses were ketones and alcohols, while significant amounts of terpenes and sulphur compounds were detected in most of the cheeses. Ozturkoglu-Budak et al. (2016b), in their study aiming to analyse the volatile compounds in Turkish Divle Cave cheese, identified 110

compounds including acids, alcohols, ketones, esters and terpenes. They identified butanoic, acetic and valeric acids, 2-butanol, 2-butanone, 2-heptanone, ethyl butanoate, α -pinene and toluene as the most common compounds, while esters showed an increasing trend until the end of ripening. Ozturkoglu-Budak et al. (2018) examined Divle cheese during ripening and reported that lipolysis and proteolysis levels increased throughout the ripening. They reported that an intense level of proteolysis and lipolysis detected at 120 days of ripening could be due to natural enzymes present in raw milk as well as secondary microflora entering the cheese from the air or contaminated equipment. Busetta et al. (2023) produced traditional cave-ripened Caciocavallo Podolico Lucano (CPL) cheese in 4 different establishments. Significant differences were observed between cheeses for unsaturated fatty acids and antioxidant capacity. It was emphasised that the use of traditional wooden tools gives the final products a unique character. Gaglio et al. (2020) produced Pecorino Siciliano cheese (PDO) using LAB and analysed the bacterial communities. This treatment prevented the dulling of the flavour detected by both sensory analysis and volatile compound analysis. It is concluded that the use of the selected strains is the right procedure to maintain the identity of local cheeses and to regulate the current manufacture. New studies should focus on strategies to ensure standardised quality production of Pecorino Siciliano cheese in different seasons and to ensure product safety at all stages from milk to cheese. İşleyici et al. (2017) reported that the heavy metal levels of Divle Tulum cheeses were in accordance with the limits of national and international standards. They reported that other mineral substances in its composition significantly increased the nutritional value of cheese.

Domestication of microorganisms in cave-ripened cheese

In recent decades, it has been possible to improve the stability, quality, flavour and texture of fermented foods by domestication of microorganisms. Domestication processes take place through food production processes involving the repeated use of target microorganisms at high food content. In new agri-food niches, the

metabolic requirements of target microorganisms have become regular and predictable. This has led to rapid genomic specialisation by mechanisms such as pseudogenization, genome degradation, interspecies hybridisation, gene duplication and horizontal gene transfer. As a result, domesticated microorganisms with the desired fermentative capacity could be produced (Gibbons and Rinker, 2015). Cheese can be considered as a substrate with rich nutritional content that provides a suitable ecological environment for microorganisms from the natural environment and equipment microflora. Rind cheese enterprises offer more stable environments for microorganisms due to the low level of stress factors encountered in nature. Due to the measures taken to ensure food safety in enterprises, wild moulds from natural populations generally form the surface flora of cheese varieties where rind formation is particularly desired. It has been determined that *Penicillium* species adapt to the cheese environment by losing energy-costly features such as spore, pigment and mycotoxin production in the first few weeks. Most of the starter *P. camemberti* strains are of European origin and offer a limited texture and flavour pattern. It has been shown that new *Penicillium* strains can be produced for cheese production with deliberate and controlled domestication processes (Bodinaku et al. 2019). Historically, many species of fungi have been domesticated for use in the manufacture of different fermented foods. Some species are specific to the cheese environment (e.g. *F. domesticum*, *P. camemberti*, *S. casei*, *S. flava*, *M. lanceolatus*), while others have the potential to be ubiquitous (e.g. *S. candida*, *S. fusca*, *P. roqueforti*). This raises the need to understand if and how these species are adapted to the cheese environment. Microorganisms can exchange genes through non-vertical descent and even between distant species. *Penicillium* fungi show rapid adaptation through frequent horizontal gene transfers (HGTs) occurring under selection within cheeses. *Penicillium* fungi show rapid adaptation through frequent HGTs occurring under selection within cheeses. Microorganisms can exchange genes through non-vertical descent and even between distant species. Recent data show that domestication of cheese fungi alters their reproductive patterns and reduces their fertility. (Dupont et al.

2017). Dumas et al. (2020) found that the Blue cheese mould *P. roqueforti* was domesticated twice at different times. In the 1st domestication, it acquired characteristics such as slow growth in cheese and high spore production on bread, which would be useful to produce pre-industrial Roquefort cheese. In the 2nd domestication, a single clonal lineage was selected. This lineage showed phenotypic characteristics favourable to cheese, such as high lipolytic activity, good retention in cheese cavities and salt tolerance. The phenotypic characteristics of domesticated fungal populations useful for food production are considerably improved compared to wild populations. Ropars et al. (2020) studied domestication, a very important phenomenon as it involves novel adaptation under strong human selection and rapid diversification, on *P. camemberti*, a mould used for ripening soft cheeses like Brie and Camembert. Whole genome-based analyses showed that the grey-green mould *P. biforme* used in cheese manufacturing emerged by differentiation from the blue-green wild fungus *P. fuscoglaucum*. A more recent domestication was also the emergence of the clonal lineage *P. camemberti* as a sister group to *P. biforme*. *P. biforme* showed stronger phenotypic adaptation to manufacturing process than *P. fuscoglaucum* in terms of faster growth, less toxin production and antagonistic effect against other fungi on cheese in the cave. Moreover, the *P. camemberti* lineage provided even stronger evidence of domestication for the same phenotypic traits. The potential important contribution of wild fungi acquiring favourable phenotypic traits through domestication for cheese science and technology is highlighted. Alexa et al. (2024) produced Cabrales blue-veined cheese in three different dairies and ripened it in natural caves. They reported that both the dairy farm and the cave significantly affected the cheese microflora. *Lactococcus* and the former *Lactobacillus* genera dominated the cheeses at the beginning of ripening. As ripening progressed, the cheeses were dominated by *Corynebacterium*, *Tetragenococcus*, *Yaniella*, *Brevibacterium*, and *Staphylococcus* genera. They found that the *Tetragenococcus* genus had a high rate of HGTs with other community of the cheese microflora. Bennetot et al. (2023) genetically analysed 53 *G. candidum*

strains isolated from different cheese from five European countries, Canada and the USA for domestication. Cheese *G. candidum* populations were reported to lack the two beta-lactamase-like genes found in the wild clade, that are involved in the clearance of xenobiotics, and to contain higher amounts of transposable elements, probably due to lose selection. They also observed evidence of domestication in *G. candidum*, which appears to have led to diversification into different varieties with contrasting phenotypes. Some traits acquired by cheese strains have been reported to show affinity with other distantly related fungi used in cheese ripening.

Suggestions for the future of cave-ripened cheeses

The Cabrales mountain in the Picos de Europa National Park in Spain is the site of the manufacture of blue cheese, a product of a thousand years of culture, famous for its flavour. A PDO certificate was obtained for this cheese 40 years ago and thus commercial success was achieved. The introduction of control measures for production with this certificate, together with the increase in demand, led to the closure of insufficient small holdings and the development of livestock management practices. The PDO certificate has contributed to the protection of the rural system. However, the excessive increase in livestock management practices has also caused some problems related to landscape and environmental protection. It is important that local administrations and their stakeholders should work on measures to produce quality products and to protect the environment and landscape together (García-Hernández et al. 2022). In Italian wine tourism, it has become a tradition to organise an ‘Open Cellars’ event every year. Since 1993, the event has attracted more and more interest and nowadays it has attracted more than 21,000 businesses and has led to the creation of more than 170 specialised local networks (Varriale and Ciaravino, 2022). The cheese caves could also be opened for people to visit and tasting and purchasing areas could be created for visitors. In this context, cheese caves can also be a good tourism tool, contributing to the development and economy of countries. According to Dağlı et al. (2020), it is necessary to install a shelf system to stack the cheeses in

the cave in an organized manner and to increase the storage capacity. For this purpose, it is recommended to use stainless steel or plastic materials. The use of wood material is not considered appropriate because it creates a suitable environment for the sheltering of microorganisms. According to Varriale and Ciaravino (2022), as a traditional and regional cultural heritage, cave cheeses have the potential to contribute to the promotion and sustainable development of the region. In this context, it can be proposed to establish a common framework study based on the comparative analysis of case studies, to define common guidelines for classifying cultural heritage elements related to cheese production, and to institutionalise the link between tangible and intangible values in cheese making. It is important that all stakeholders, including public institutions, local authorities, civil society organisations and businesses, support the current research of scientists.

In fact, natural caves are highly influenced by cave air microflora and cave surface microflora, especially for unpackaged ripening cheeses. There is a risk that this microflora may contain pathogenic microorganisms. In addition, insects, animals and mites living in the cave have the potential to pose serious hygiene and safety risks. Due to these hazards, it could suggest working on the design of a ripening room suitable for hygiene and sanitation within the caves. Especially for unpackaged products, it could also be possible to create a more reliable ripening process by providing the humidity and temperature conditions of the natural cave in man-made caves, cellars or rooms with controlled conditions and taking hygienic measures. Further studies on the adaptation and domestication of microflora from natural cave cheeses or caves are necessary. In this way, reliable favourable strains can be used as starter cultures in cheese production.

REFERENCES

- Alexa, E. A., Cobo-Díaz, J. F., Renes, E., O' Callaghan, T. F., Kilcawley, K., Mannion, D., ... & Alvarez-Ordóñez, A. (2024). The detailed analysis of the microbiome and resistome of artisanal Blue-veined cheeses provides evidence on sources and patterns of succession linked with quality and safety traits. *Microbiome*, 12(1), 78.
- Anelli, P., Peterson, S. W., Haidukowski, M., Logrieco, A. F., Moretti, A., Epifani, F., & Susca, A. (2018). *Penicillium gravinicensei*, a new species isolated from cave cheese in Apulia, Italy. *International Journal of Food Microbiology*, 282, 66-70.
- Anelli, P., Haidukowski, M., Epifani, F., Cimmarusti, M. T., Moretti, A., Logrieco, A., & Susca, A. (2019). Fungal mycobiota and mycotoxin risk for traditional artisan Italian cave cheese. *Food Microbiology*, 78, 62-72.
- Anelli, P., Dall'Asta, C., Cozzi, G., Epifani, F., Carella, D., Scarpetta, D., ... & Susca, A. (2024). Analysis of composition and molecular characterization of mycobiota occurring on surface of cheese ripened in Dossena's mine. *Food Microbiology*, 104587.
- Ayad, E. H., Verheul, A., de Jong, C., Wouters, J. T., & Smit, G. (1999). flavour forming abilities and amino acid requirements of *Lactococcus lactis* strains isolated from artisanal and non-dairy origin. *International Dairy Journal*, 9(10), 725-735.
- Aydemir, O., & Dervisoglu, M. (2010). The effect of heat treatment and starter culture on colour intensity and sensory properties of Kulek cheese. *International Journal of Dairy Technology*, 63(4), 569-574.
- Banks, A., Behrmann, E., & Robertson, L. (2023). Identification and characterization of fungi isolated from a cheese cave in the Eastern United States. *Proceedings of the West Virginia Academy of Science*, 95(3).
- Bennetot, B., Vernadet, J. P., Perkins, V., Hautefeuille, S., Rodríguez de La Vega, R. C., O'donnell, S., ... & Ropars, J. (2023).

- Domestication of different varieties in the cheese-making fungus *Geotrichum candidum*. Peer Community Journal, 3.
- Bodinaku, I., Shaffer, J., Connors, A. B., Steenwyk, J. L., Biango-Daniels, M. N., Kastman, E. K., ... & Wolfe, B. E. (2019). Rapid phenotypic and metabolomic domestication of wild *Penicillium* molds on cheese. *MBio*, 10(5), 10-1128.
- Bonomo, M. G., & Salzano, G. (2012). Microbial diversity and dynamics of Pecorino di Filiano PDO, a traditional cheese of Basilicata region (Southern Italy). *International Journal of Dairy Technology*, 65(4), 531-541.
- Bonomo, M. G., Cafaro, C., & Salzano, G. (2015). Genotypic and technological diversity of *Brevibacterium linens* strains for use as adjunct starter cultures in 'Pecorino di Filiano' cheese ripened in two different environments. *Folia Microbiologica*, 60, 61-67.
- Busetta, G., Garofalo, G., Barbera, M., Di Trana, A., Claps, S., Lovallo, C., ... & Settanni, L. (2023). Metagenomic, microbiological, chemical and sensory profiling of Caciocavallo Podolico Lucano cheese. *Food Research International*, 169, 112926.
- Dağlı, A., Sert, D., & Uzun, A. (2020). Mağaraların peynir olgunlaştırılmada kullanımı, bir örnek araştırma: Peynirini Mağarası, Derbent/Konya. *Türk Coğrafya Dergisi*, (75), 131-138.
- De Llano, D. G., Ramos, M., Rodriguez, A., Montilla, A., & Juárez, M. (1992). Microbiological and physicochemical characteristics of Gamonedo blue cheese during ripening. *International Dairy Journal*, 2(2), 121-135.
- De Palencia, P. F., De La Plaza, M., Amárita, F., Requena, T., & Peláez, C. (2006). Diversity of amino acid converting enzymes in wild lactic acid bacteria. *Enzyme and Microbial Technology*, 38(1-2), 88-93.
- Dizdarević, T., & Mulaomerović, J. (2023). Proizvodnja Sira U Livnu I Dizdareva Pećina. Izdavač–Publisher Speleološko društvo “Bosansko-hercegovački krš”, Sarajevo Centar za krš i speleologiju, Sarajevo Branilaca Sarajeva 30, 71000 Sarajevo Redakcija–Editorial board, 26.

- Dolci, P., Alessandria, V., Rantsiou, K., Bertolino, M., & Cocolin, L. U. C. A. (2010). Microbial diversity, dynamics and activity throughout manufacturing and ripening of Castelmagno PDO cheese. *International Journal of Food Microbiology*, 143(1-2), 71-75.
- Dolci, P., Zenato, S., Pramotton, R., Barmaz, A., Alessandria, V., Rantsiou, K., & Cocolin, L. (2013). Cheese surface microbiota complexity: RT-PCR-DGGE, a tool for a detailed picture? *International Journal of Food Microbiology*, 162(1), 8-12.
- Dolci, P., De Filippis, F., La Stora, A., Ercolini, D., & Cocolin, L. (2014). rRNA-based monitoring of the microbiota involved in Fontina PDO cheese production in relation to different stages of cow lactation. *International Journal of Food Microbiology*, 185, 127-135.
- Dupont, J., Dequin, S., Giraud, T., Le Tacon, F., Marsit, S., Ropars, J., ... & Selosse, M. A. (2017). Fungi as a source of food. *Microbiology Spectrum*, 5(3), 10-1128.
- Fabricant, F. (1982). Blue-veined cheeses: The expanding choices. *The New York Times* <https://www.nytimes.com/1982/06/23/garden/blue-veinedcheeses-the-expanding-choices.html>.
- Fernández-Bodega, M. A., Mauriz, E., Gómez, A., & Martín, J. F. (2009). Proteolytic activity, mycotoxins and andrastin A in *Penicillium roqueforti* strains isolated from Cabrales, Valdeón and Bejes–Tresviso local varieties of blue-veined cheeses. *International Journal of Food Microbiology*, 136(1), 18-25.
- Fernández-Salguero, J., Gómez, R., 1997. Estudio de los quesos tradicionales de Andalucía. Publicaciones de la Universidad de Córdoba y Obra Social y Cultural Cajasur, Córdoba, Spain.
- Ferroukhi, I., Chassard, C., & Mardon, J. (2024). A comprehensive overview of blue-veined cheeses. *International Dairy Journal*, 105926.
- Gaglio, R., Franciosi, E., Todaro, A., Guarcello, R., Alfeo, V., Randazzo, C. L., ... & Todaro, M. (2020). Addition of selected

- starter/non-starter lactic acid bacterial inoculums to stabilise PDO Pecorino Siciliano cheese production. *Food Research International*, 136, 109335.
- García-Hernández, C., Ruiz-Fernández, J., & Rodríguez-Gutiérrez, F. (2022). Geographical indications in cheese mountain areas: Opportunity or threat to landscape and environmental conservation? The case of Cabrales (Spain). *Applied Geography*, 146, 102753.
- Gibbons, J. G., & Rinker, D. C. (2015). The genomics of microbial domestication in the fermented food environment. *Current Opinion in Genetics & Development*, 35, 1-8.
- González Crespo, J., & Mas, M. (1993). The use of autochthonous starters in the manufacture of a pressed goat milk cheese from pasteurized milk. *Alimentaria*, 30(243), 51-53.
- Grappin, R., & Beuvier, E. (1997). Possible implications of milk pasteurization on the manufacture and sensory quality of ripened cheese. *International Dairy Journal*, 7(12), 751-761.
- Guarcello, R., Carpino, S., Gaglio, R., Pino, A., Rapisarda, T., Caggia, C., ... & Todaro, M. (2016). A large factory-scale application of selected autochthonous lactic acid bacteria for PDO Pecorino Siciliano cheese production. *Food Microbiology*, 59, 66-75.
- Gün, İ., & Seydim, Z. (2022). The characteristics of goat skins used in the production of Tulum cheese and changes in ripening environments. *Gıda*, 47(5), 729-743.
- Hartley, C. B., & Jezeski, J. J. (1954). The microflora of blue cheese slime. *Journal of Dairy Science*, 37(4), 436-445.
- Hastaoğlu, E., Erdoğan, M., & Işkın, M. (2021). Gastronomi turizmi kapsamında Türkiye peynir çeşitliliği haritası. *Atatürk Üniversitesi Sosyal Bilimler Enstitüsü Dergisi*, 25(3), 1084-1113.
- Hayaloglu, A. A., Brechany, E. Y., Deegan, K. C., & McSweeney, P. L. H. (2008). Characterization of the chemistry, biochemistry and volatile profile of Kufli cheese, a mould-ripened variety. *LWT-Food Science and Technology*, 41(7), 1323-1334.

- Hirata, M., Kimura, J., & Barattin, T. (2018). Characteristics and development of matured hard cheese from the Dolomites mountain region in northern Italy. *Milk Science*, 67(1), 1-14.
- INAO, (2022). Institut national de l'origine et de la qualité. Cahier des charges de l'appellation d'origine "Bleu des Causses" <https://www.inao.gouv.fr/produit/3265>.
- İşleyici, Ö., Sancak, Y. C., & Morul, F. (2011). Divle tulum peynirinde aflatoksin M1 düzeyi üzerine bir araştırma. *Yüzüncü Yıl Üniversitesi Veteriner Fakültesi Dergisi*, 22(2), 105-110.
- İşleyici, Ö., Sancak, Y. C., Tuncay, R. M., & Yücel, U. M. (2017). Determination of mineral substance and heavy metal levels in Divle tulum cheese. *Van Veterinary Journal*, 28(3), 151-156.
- Kirtil, H. E., Cebi, N., Yildirim, R. M., Metin, B., & Arici, M. (2024). A rapid spectroscopic method for the identification of the filamentous fungi isolated from Turkish traditional mold-ripened cheeses. *Journal of Microbiological Methods*, 217, 106884.
- Krishnan, K., Campbell, Y. L., To, K. V., Lima, G., Byron, M. D., Zhang, X., ... & Schilling, M. W. (2019). Effects of temperature, relative humidity, and protective netting on *Tyrophagus putrescentiae* (schrank) (sarcoptiformes: Acaridae) infestation, fungal growth, and product quality of cave-aged Cheddar cheese. *Journal of Stored Products Research*, 83, 44-53.
- Marcelão, C. V., Souza, M. C., Silva, J. J., Couto, F. A., Lacorte, G. A., Pinto, U. M., ... & Taniwaki, M. H. (2024). Unveiling ochratoxin A and ochratoxigenic fungi in Brazilian artisanal Cheeses: Insights from production to consumption. *Food Research International*, 183, 114214.
- Mazzocca, R., Di Paolo, M., Peruzy, M. F., Rippa, A., Santoro, A. M. L., Peretti, V., ... & Murru, N. (2024). Physicochemical and microbiological characterisation of a typical Italian raw ewe's milk cheese: Pecorino Bagnolese. *International Dairy Journal*, 105998.
- McSweeney, P. L. (2004). Biochemistry of cheese ripening: Introduction and overview. In *Cheese: Chemistry, physics and microbiology* (Vol. 1, pp. 347-360). Academic Press.

- Mihaiu, M., Mihaiu, R., Dan, S. D., Chirila, F., Ghidali, M., Mihaiu, L., & Valasutean, G. (2008). The Ripening Of The Traditional Cheese “Năsal”, Quality Aspects And Characteristics. *Buletin USAMV Veterinary Medicine*, 65, 2.
- Morales, P., Fernández-García, E., Gaya, P., & Nuñez, M. (2003). Formation of volatile compounds by wild *Lactococcus lactis* strains isolated from raw ewes' milk cheese. *International Dairy Journal*, 13(2-3), 201-209.
- Morris, H. A., Combs, W. B., & Coulter, S. T. (1951). The relation of surface growth to the ripening of Minnesota Blue Cheese. *Journal of Dairy Science*, 34, 209.
- Nuñez, M. (1978). Microflora of Cabrales cheese: changes during maturation. *Journal of Dairy Research*, 45(3), 501-508.
- Nuñez, M. P. G. M., Medina, M., Pilar, G. A. Y. A., & Carmen, D. A. (1981). Les levures et les moisissures dans le fromage bleu de Cabrales. *Le lait*, 61(601-602), 62-79.
- Ozturkoglu-Budak, S., Figge, M. J., Houbraken, J., & de Vries, R. P. (2016a). The diversity and evolution of microbiota in traditional Turkish Divle Cave cheese during ripening. *International Dairy Journal*, 58, 50-53.
- Ozturkoglu-Budak, S., Gursoy, A., Aykas, D. P., Koçak, C., Dönmez, S., de Vries, R. P., & Bron, P. A. (2016b). Volatile compound profiling of Turkish Divle Cave cheese during production and ripening. *Journal of Dairy Science*, 99(7), 5120-5131.
- Ozturkoglu-Budak, S., Aykas, D. P., Kocak, C., Dönmez, S., Gursoy, A., De Vries, R. P., & Bron, P. A. (2018). Temporal microbiota and biochemical profiles during production and ripening of Divle Cave cheese. *International Journal of Dairy Technology*, 71, 99-106.
- Pappa, E. C., Kondyli, E., Malamou, E., Kakouri, A., Vlachou, A. M., & Samelis, J. (2022). Chemical, microbiological and sensory characteristics of ‘Tsalafouti’ traditional Greek dairy product. *Food Research*, 6, 170-179.
- Prieto, B., Urdiales, R., Franco, I., Tornadijo, M. E., Fresno, J. M., & Carballo, J. (1999). Biochemical changes in Picon Bejes-Tresviso

- cheese, a Spanish blue-veined variety, during ripening. *Food Chemistry*, 67(4), 415-421.
- Prieto, B., Franco, I., Fresno, J. M., Bernardo, A., & Carballo, J. (2000). Picon Bejes-Tresviso blue cheese: an overall biochemical survey throughout the ripening process. *International Dairy Journal*, 10(3), 159-167.
- Randazzo, C. L., Caggia, C., & Neviani, E. (2009). Application of molecular approaches to study lactic acid bacteria in artisanal cheeses. *Journal of Microbiological Methods*, 78(1), 1-9.
- Ropars, J., Didiot, E., de La Vega, R. C. R., Bennetot, B., Coton, M., Poirier, E., ... & Giraud, T. (2020). Domestication of the emblematic white cheese-making fungus *Penicillium camemberti* and its diversification into two varieties. *Current Biology*, 30(22), 4441-4453.
- Sánchez-Ramos, I., Álvarez-Alfageme, F., & Castañera, P. (2007). Development and survival of the cheese mites, *Acarus farris* and *Tyrophagus neiswanderi* (Acari: Acaridae), at constant temperatures and 90% relative humidity. *Journal of Stored Products Research*, 43(1), 64-72.
- Seri, M., & Metin, B. (2021). Mycobiota of Konya mold-ripened (Kufllu) Tulum cheese and the diversity of *Penicillium roqueforti* isolates. *Ankara Universitesi Veteriner Fakultesi Dergisi*, 68, 349-354.
- Stark, J. (2007). Cheese and fermented sausages. In *Food Mycology* (pp. 333-346). CRC Press.
- Steele, J., Broadbent, J., & Kok, J. (2013). Perspectives on the contribution of lactic acid bacteria to cheese flavor development. *Current Opinion in Biotechnology*, 24(2), 135-141.
- Susca, A., Anelli, P., Haidukowski, M., Probyn, C. E., Epifani, F., Logrieco, A. F., ... & Proctor, R. H. (2021). A PCR method to identify ochratoxin A-producing *Aspergillus westerdijkiae* strains on dried and aged foods. *International Journal of Food Microbiology*, 344, 109113.

- Tansman, G. F., Kindstedt, P. S., & Hughes, J. M. (2017). Crystallization and demineralization phenomena in stabilized white mold cheese. *Journal of Dairy Science*, 100(8), 6074-6083.
- Tekinşen, K. K., & Akar, D. (2017). Erzincan tulum peyniri. *Atatürk Üniversitesi Veteriner Bilimleri Dergisi*, 12(2), 218-226.
- Toppino, P. M., Drava, G., Contarini, G., Manfredini, M., & Emandi, G. C. (1992). Typical characteristics of 'Pit cheese'. *Rivista della Società Italiana di Scienza dell'Alimentazione*, 21(4), 389-414.
- Torracca, B., Nuvoloni, R., Ducci, M., Bacci, C., & Pedonese, F. (2015). Biogenic amines content of four types of "Pecorino" cheese manufactured in Tuscany. *International Journal of Food Properties*, 18(5), 999-1005.
- Torracca, B., Pedonese, F., López, M. B., Turchi, B., Fratini, F., & Nuvoloni, R. (2016). Effect of milk pasteurisation and of ripening in a cave on biogenic amine content and sensory properties of a pecorino cheese. *International Dairy Journal*, 61, 189-195.
- Uzun, P., Serrapica, F., Masucci, F., Assunta, B. C. M., Yildiz, H., Grasso, F., & Di Francia, A. (2020). Diversity of traditional Caciocavallo cheeses produced in Italy. *International Journal of Dairy Technology*, 73(1), 234-243.
- Vabre, S., & Bergeron, L. (2015). *Le sacre du roquefort: L emergence d une industrie agroalimentaire (Vol. 1)*. PU Rennes: Presses universitaires de Rennes et de François-Rabelais Tours. <https://pufr-editions.fr/produit/le-sacre-du-roquefort/>.
- Varriale, R., & Ciaravino, R. (2022). Underground Built Heritage and Food Production: From the Theoretical Approach to a Case/Study of Traditional Italian "Cave Cheeses". *Heritage*, 5(3), 1865-1882.
- Wouters, J. T., Ayad, E. H., Hugenholtz, J., & Smit, G. (2002). Microbes from raw milk for fermented dairy products. *International Dairy Journal*, 12(2-3), 91-109.
- Ye, R., Biango-Daniels, M., Steenwyk, J. L., Rokas, A., Louw, N. L., Nardella, R., & Wolfe, B. E. (2024). Genomic, transcriptomic, and ecological diversity of *Penicillium* species in cheese rind microbiomes. *Fungal Genetics and Biology*, 171, 103862.

CHAPTER 10

FIRST CONCEPTS OF GRAPH THEORY

Asst. Prof. Dr. Celalettin KAYA¹

DOI: <https://dx.doi.org/10.5281/zenodo.14259196>

¹ Çankırı Karatekin University, Science Faculty, Department of Mathematics, Çankırı, Türkiye. ckaya@karatekin.edu.tr, Orcid ID: 0000-0003-4723-1618

INTRODUCTION

In this chapter, we briefly review basic notions of graph theory, give fundamental definitions, and present essential techniques and methods of graph theory by proving some important and fundamental theorems of this area. We want to present a self-contained and concise chapter for graphs.

The main source used in the preparation of this chapter is the graduate textbook "Combinatorial Mathematics" by West (2021). Essentially, what we do is to study the related parts of the mentioned textbook to understand and explain the basics of graph theory. But of course, no part of the aforementioned book has been quoted exactly, a study has been put forward with our own words and our own sentences; almost every proof has been written in more detail, and parts of the book that were left to the reader have been explained completely and the subject has been presented more understandably. The proofs of the stated but unproven theorems can be found in West (2021). In addition to West (2021), the sources listed in the references were also consulted.

10.1 Fundamental Definitions

Definition 10.1 Let V and E be sets called a "vertex set" and an "edge set", respectively, such that each element of E (called an "edge") is a 2-element subset of V (each of its elements is called a "vertex"). Then, a "graph" Γ is an ordered pair (V, E) , and write $\Gamma = (V, E) = (V(\Gamma), E(\Gamma))$. If $e = \{x, y\} \in E(\Gamma)$, then x and y are called "end-vertices" of the edge e , and we also denote e simply as xy . $|V(\Gamma)|$ (respectively, $|E(\Gamma)|$) is the "order" (respectively "size") of Γ . An " n -vertex graph" is a graph with order n . If $|V(\Gamma)|$ and $|E(\Gamma)|$ are both finite, then Γ is a "finite" graph. If $|E(\Gamma)| \geq 1$ then Γ is called a "non-trivial graph".

Definition 10.2 If the vertex of Γ can be ordered as x_1, x_2, \dots, x_n such that $E(\Gamma) = \{x_j x_{j+1} \mid 1 \leq j \leq n-1\}$ (respectively, $E(\Gamma) = \{x_j x_{j+1} \mid 1 \leq j \leq n-1\} \cup \{x_n x_1\}$), then Γ is called a "path", denoted by P_n , (respectively, a "cycle", denoted by C_n) on n vertices. In this case, we write $\Gamma = (x_1, x_2, \dots, x_n)$ (respectively, $\Gamma = [x_1, x_2, \dots, x_n]$). The

number of edges of a path or a cycle is called its "length". If the length of a cycle is odd (respectively, even), then it is called an "odd cycle" (respectively, an "even cycle"). C_n is also called a n -cycle. The length of a shortest cycle in Γ is the "girth" of Γ , if there is a cycle in Γ , if not the girth is defined as infinity. Let C be cycle in Γ . An edge $e = \{x, y\} \in E(\Gamma) \setminus E(C)$ with $x, y \in V(C)$, is called a "chord" of C .

Note 10.1 The paths (x_1, x_2, \dots, x_n) and $(x_n, x_{n-1}, \dots, x_1)$ are the same. For cycles, since the starting point (one of n vertices) and the direction (one of 2 directions) are not important, there are $2n$ ways to denote an n -vertex cycle.

Definition 10.3 Let $\Gamma = (V(\Gamma), E(\Gamma))$, $\Omega = (V(\Omega), E(\Omega))$ such that $V(\Omega) \subseteq V(\Gamma)$ and $E(\Omega) \subseteq E(\Gamma)$. Then Ω is called a "subgraph" of Γ . If $V(\Omega) = V(\Gamma)$, then Ω is a "spanning subgraph". Let $W \subseteq V(\Gamma)$. Then, the subgraph $\Lambda = (V(\Lambda) = W, E(\Lambda) = \{xy \in E(\Gamma) \mid x, y \in W\})$ is the "induced subgraph" of Γ , "induced by" W , and we use the notation $\Lambda = \Gamma[W]$.

Definition 10.4 Let $v, w \in V(\Gamma)$. If $vw \in E(\Gamma)$, then v and w are "adjacent" or "neighbors". We write $v \sim w$ (respectively, $v \not\sim w$) if v is (respectively, is not) adjacent to w . $N_\Gamma(v) = N(v) = \{w \in V(\Gamma) \mid vw \in E(\Gamma)\}$ is the "neighborhood" of v in Γ . If $N(v) = \emptyset$, then v is an "isolated vertex".

Definition 10.5 The number of edges with one of its end-vertex $v \in V(\Gamma)$ is the "degree" of v , denoted by $\rho_\Gamma(v)$ or $\rho(v)$. The minimum (respectively, maximum) vertex degree of Γ is denoted by $\delta(\Gamma)$ (respectively, $\Delta(\Gamma)$). If $\delta(\Gamma) = \Delta(\Gamma) = k$, then Γ is called a "regular" or " k -regular" graph. 3-regular graphs are also named as "cubic graphs".

Definition 10.6 If in a graph any two vertices are adjacent, then it is called a "complete graph", a complete graph on n vertices is denoted by K_n . (K_3 is also called a "triangle".) Let $W \subseteq V(\Gamma)$. If $W = K_m$, then $\Gamma[W]$ or W is called an " m -clique" or just a "clique" in Γ . If any two vertices of W are non-adjacent, then W is called an "independent set" or "stable set" in Γ . The "complement" of Γ is the graph denoted by $\bar{\Gamma}$ or Γ^c such that $V(\Gamma^c) = V(\Gamma)$ and $x, y \in E(\Gamma^c)$ if and only if $xy \notin E(\Gamma)$.

Note 10.2 K_n is $(n - 1)$ -regular and C_n is 2-regular. $V(K_n)$ is a clique. For any graph Γ , $|E(\Gamma^c)| = \binom{n}{2} - |E(\Gamma)|$. If Γ is k -regular on n vertices, then Γ^c is $((n - 1) - k)$ -regular.

Definition 10.7 If $V(\Gamma) = U \cup V$, where U and V are independent sets (called "partite sets" or "parts" of Γ), then Γ is called a "bipartite" graph. In this case, (U, W) is a "bipartition" of Γ , and Γ is also called " U, W -bigraph". If each vertex of U is adjacent to each vertex of W , then Γ is a "complete bipartite graph". If $V(\Gamma)$ can be written as the union of k independent sets, then Γ is called a " k -partite graph".

Notation 10.1 The complete bipartite graph with partite sets of orders r and s is denoted by $K_{r,s}$. $K_{1,m}$ is called a "star".

To define a graph Γ , we need to specify $V(\Gamma)$ and $E(\Gamma)$. A primitive way of this is to give these sets by listing their elements. But there are other more convenient ways, such as matrix presentations:

Definition 10.8 First, order the vertices of Γ : x_1, x_2, \dots, x_n . The 0,1,-matrix $A(\Gamma) = [a_{ij}]$ such that " $a_{ij} = 1$ if and only if $x_i \sim x_j$ " is called the "adjutancy matrix" of Γ .

Definition 10.9 Let $x \in V(\Gamma)$ and $e, f \in E(\Gamma)$. If x is one of the end-vertices of e , then we say that " x and e are incident". If e and f have a common end-vertex, then we also say that " e and f are incident". Now, order $V(\Gamma)$ as x_1, x_2, \dots, x_n and $E(\Gamma)$ as e_1, e_2, \dots, e_m . The 0,1,-matrix $M(\Gamma) = [m_{ij}]$ such that " $m_{ij} = 1$ if and only if $x_i \in e_j$ " is called the "incidence matrix" of Γ .

The adjacency (respectively, incidence) matrix depends on the ordering of vertices (respectively, orderings of vertices and edges). But the graph itself does not depend on these orderings or on how it is drawn:

Definition 10.10 Let Γ and Ω be two graphs. A bijective map $\varphi: V(\Gamma) \rightarrow V(\Omega)$ (it can also be denoted by $\varphi: \Gamma \rightarrow \Omega$) such that " $xy \in E(\Gamma)$ if and only if $\varphi(x)\varphi(y) \in E(\Omega)$ " is called an "isomorphism between Γ and Ω , and if " Γ is isomorphic to Ω " then we denote it as $\Gamma \simeq \Omega$, or $\Gamma = \Omega$.

Remark 10.1 Let $\varphi: \Gamma \rightarrow \Omega$ and $\psi: \Omega \rightarrow \Lambda$ be isomorphisms of graphs. Then, $\varphi^{-1}: \Omega \rightarrow \Gamma$ and $\psi \circ \varphi: \Gamma \rightarrow \Lambda$ are both isomorphisms. Also, the identity map $i: \Gamma \rightarrow \Gamma$ is obviously an isomorphism. Therefore, the "isomorphism relation", namely, the set of graph pairs (Γ, Ω) such that $\Gamma \simeq \Omega$, is an equivalence relation on the collection of all graphs. A drawing of a graph is just an element of its isomorphism class; and thus, in a drawing, vertex or edge labelings do not matter. In fact, the expression "unlabeled graph" refers to an isomorphism class.

Note 10.3 By the relation $\Omega \subseteq \Gamma$, we actually mean that Γ has a subgraph Λ which is isomorphic to Ω ; and in fact, Λ is a "copy" of Ω in Γ .

Definition 10.11 An isomorphism $\varphi: \Gamma \rightarrow \Gamma$ is called an "automorphism" of Γ . Γ is "vertex-transitive" (respectively, "edge-transitive") if $\forall x, y \in V(\Gamma)$ (respectively, $\forall e, f \in E(\Gamma)$), there is an automorphism φ of Γ such that $\varphi(x) = y$ (respectively, $\varphi(e) = f$, where of course, edges are considered as 2-element sets of vertices).

Now, let's define some of the binary operations to combine two graphs.

Definition 10.12 The "Cartesian product" of Γ and Ω , denoted by $\Gamma \square \Omega$ or $\Gamma * \Omega$, is the graph with $V(\Gamma \square \Omega) = V(\Gamma) * V(\Omega)$ and $(x, y) \sim (z, w)$ if and only if " $x = z$ and $y \sim_{\Omega} w$ " or " $y = w$ and $x \sim_{\Gamma} z$ ".

Definition 10.13 The "union" of Γ and Ω denoted by $\Gamma \cup \Omega$, is the graph with $V(\Gamma \cup \Omega) = V(\Gamma) \cup V(\Omega)$ and $E(\Gamma \cup \Omega) = E(\Gamma) \cup E(\Omega)$. If $V(\Gamma) \cap V(\Omega) = \emptyset$, then $\Gamma \cup \Omega$ is called the "disjoint union" and denoted by $\Gamma + \Omega$. $m\Gamma$ denotes the disjoint union of m copies of Γ . The "join" of two disjoint graphs (that is, graphs with disjoint vertex sets) Γ and Ω , denoted by $\Gamma \vee \Omega$ or $\Gamma \diamond \Omega$, is the graph with $V(\Gamma \vee \Omega) = V(\Gamma) \cup V(\Omega)$ and $E(\Gamma \vee \Omega) = E(\Gamma + \Omega) \cup \{xy \mid x \in V(\Gamma) \text{ and } y \in V(\Omega)\}$.

10.2 Vertex Degrees

10.2.1 Enumeration

We can enumerate edges with respect to vertex degrees. This gives the "First Theorem of Graph Theory":

Proposition 10.1 (Degree- Sum Formula) Let Γ be a graph. Then:

$$|E(\Gamma)| = \frac{1}{2} \sum_{x \in V(\Gamma)} \rho(x).$$

Proof. Count the number of pairs (x, e) such that $e \in E(\Gamma)$ is incident to $x \in V(\Gamma)$ by two ways:

i) Since each edge has two end vertices, there are $2|E(\Gamma)|$ such pairs.

ii) Since each vertex x has $\rho(x)$ incident edges, there are $\sum_{x \in V(\Gamma)} \rho(x)$ such pairs.

$$\therefore 2|E(\Gamma)| = \sum_{x \in V(\Gamma)} \rho(x).$$

Concisely, summing degrees enumerate each edge twice. ■

Corollary 10.1 Γ has an even number of vertices with odd degrees. That is if Γ has a vertex x with $\rho(x)$ -odd, then it has another odd-degree vertex. (Therefore, for k odd, there is no k -regular graph Ω with $|V(\Omega)|$ -odd.) ■

Definition 10.14 Let $V(\Gamma) = \{x_1, x_2, \dots, x_n\}$, and assume that $\rho(x_1) \geq \rho(x_2) \geq \dots \geq \rho(x_n)$. Then, the non-increasing sequence $(\rho(x_1), \rho(x_2), \dots, \rho(x_n))$ is called the "degree sequence" or "degree list" of Γ . A finite non-increasing sequence, say ρ , of nonnegative integers, is called "graphic" if there is a graph Ω "realizing" ρ , that is, if there is Ω whose degree list is ρ . The graph obtained from a graph Λ by deleting a vertex x and all the edges with one end-vertex x is denoted by $\Lambda - x$ or $\Lambda \setminus x$, and this procedure is called a "vertex deletion".

Which finite sequences of non-negative integers are graphic?

Theorem 10.1 (Havel-Hakimi Theorem (Havel 1955, Hakimi 1962)) Let $n > 1$ be an integer and ρ be a sequence of nonnegative

integers of length n . And let $\tilde{\rho}$ be the sequence of length $n - 1$ obtained from ρ by deleting the largest element (that is, the first element) of ρ , say m , and decreasing each of m next largest ρ elements 1. Then, we have:

ρ is graphic if and only if $\tilde{\rho}$ is graphic. ■

The operation used in the proof of the previous theorem is important, and it has other applications. Thus, it deserves a name:

Definition 10.15 Let $uv, zw \in E(\Gamma)$ and $uw, vz \in E(\Gamma^c)$. The operation of interchanging $\{uv, zw\}$ with $\{uw, vz\}$ in Γ is called a "2-switch".

Theorem 10.2 (Fulkerson-Hoffman-McAndrew (1965), Berge (1970)) Let $V(\Gamma) = V(\Omega) = V$. Then, Γ can be obtained from Ω by 2-switches if and only if $\rho_\Gamma(x) = \rho_\Omega(x) \quad \forall x \in V$. ■

10.2.2 Extremality

To choose an extremal object having some property is an important technique in combinatorics because this gives additional power to prove a related result. We state two results about extremality and, as an example, we prove one of them.

Theorem 10.3 Let Γ be a graph. Then, Γ does have a bipartite subgraph Ω with $|E(\Omega)| \geq \frac{|E(\Gamma)|}{2}$.

Proof. Let \mathcal{C} be the collection of all bipartite subgraphs of Γ , and let $\Omega \in \mathcal{C}$ be a member having the largest number of edges. Without loss of generality, assume that (U, W) be a bipartition of Ω such that $U \cup W = V(\Omega)$. (If $V(\Omega) \subsetneq V(\Gamma)$, then add the vertices in $V(\Gamma) \setminus V(\Omega)$ to U or W as isolated vertices.) Also, since $|E(\Omega)|$ is largest, if $e = \{x, y\} \in E(\Gamma)$ such that $x \in U$ (respectively, $x \in W$) and $y \in W$ (respectively, $y \in U$), then $e \in E(\Omega)$.

Now, let $v \in U$ (respectively, $v \in W$). Then, $|N_{\Gamma[U]}(v)| \leq \left\lceil \frac{|N_\Gamma(v)|}{2} \right\rceil - 1$ (respectively, $|N_{\Gamma[W]}(v)| \leq \left\lceil \frac{|N_\Gamma(v)|}{2} \right\rceil - 1$): Suppose not. Then, $|N_{\Gamma[U]}(v)| > \left\lceil \frac{|N_\Gamma(v)|}{2} \right\rceil - 1$. That is, $|N_{\Gamma[U]}(v)| \geq \left\lceil \frac{|N_\Gamma(v)|}{2} \right\rceil$. Now, Let $U' = U - \{v\}$ and $W' = W \cup \{v\}$, and consider the U', W' - biograph

Ω' . $|E(\Omega')| \geq |E(\Omega)| + \left\lfloor \frac{N_{\Gamma}(v)}{2} \right\rfloor - \left(\left\lfloor \frac{N_{\Gamma}(v)}{2} \right\rfloor - 1 \right) = |E(\Omega)| + 1$, which contradicts with the maximality of Ω .

\therefore If $v \in U$ (respectively, $v \in W$), then $|N_{\Gamma[W]}(v)| \geq \left\lfloor \frac{|N_{\Gamma}(v)|}{2} \right\rfloor + 1$ (respectively, $|N_{\Gamma[U]}(v)| \geq \left\lfloor \frac{|N_{\Gamma}(v)|}{2} \right\rfloor + 1$).

As a result, since $\Omega \subseteq \Gamma$ is bipartite with the maximum number of edges, $\rho_{\Omega}(v) \geq \frac{\rho_{\Gamma}(v)}{2}$ for every vertex v in Γ .

$\therefore \sum_{v \in V(\Gamma)} \rho_{\Omega}(v) \geq \sum_{v \in V(\Gamma)} \frac{\rho_{\Gamma}(v)}{2}$.

$\therefore 2|E(\Omega)| \geq \frac{1}{2} 2|E(\Gamma)| = |E(\Gamma)|$.

$\therefore |E(\Omega)| \geq \frac{1}{2}|E(\Gamma)|$. ■

Before the next result, we need a definition.

Definition 10.16 Γ is "triangle-free" if $K_3 \not\subseteq \Gamma$. Γ is " Ω -free" if Γ does not have an induced subgraph $\Lambda \simeq \Omega$. The complete r -partite graph on n vertices with partite sets W_1, W_2, \dots, W_r such that $|W_i| - |W_j| \leq 1$ for all $i \neq j \in \{1, 2, \dots, r\}$ is called the "Turan graph", and it is denoted by $T_{n,r}$.

Theorem 10.4 (Turan's Theorem (Turan 1941)) Let Γ be an n vertex K_{r+1} -free graph with the maximum number of edges. Then, $\Gamma = T_{n,r}$. If $r = 2$, that is, if Γ is triangle-free, $|E(\Gamma)| = |E(T_{n,2})| = \left\lfloor \frac{n^2}{4} \right\rfloor$. ■

10.2.3 Directed graphs

With respect to the definition of a graph, an edge $e = \{x, y\}$ is a set of two distinct vertices, and thus the order of the vertices does not matter. Therefore, a graph can model symmetric, but irreflexive (because $\{x, x\} = \{x\}$ is not an edge by definition) binary relation. On the other hand, a binary relation R on a set S is a subset of $S \times S$. Therefore, to model a relation, an edge should be on an ordered pair of vertices.

Definition 10.17 Let V and E be sets called a "vertex set" and an "edge set", respectively, such that each element of E (called an "edge") is an ordered pair of one or two elements of V (each element of V is

called a "vertex"), that is, $E \subseteq V \times V$. Then, a "directed graph" or "digraph" Γ_D is an ordered pair (V, E) , and we write $\Gamma_D = (V, E) = (V(\Gamma_D), E(\Gamma_D))$. An edge $e = (x, y)$ "starts" or "exists" from x (called the "tail" of e) and "ends at" or "enters" y (called the "head" of e). An edge $e = (x, y) \in E(\Gamma_D)$ can also be denoted by xy or $x \rightarrow y$. An edge $e = (x, x)$ is called a "loop" at x .

The analogue of vertex degree in digraphs should consider starting and ending edges independently.

Definition 10.18 Let $v \in V(\Gamma_D)$. Then, " $\rho_{\Gamma_D}^-(v)$ or $\rho^-(v)$ " (respectively, " $\rho_{\Gamma_D}^+(v)$ or $\rho^+(v)$ ") is the number of edges ending (respectively, starting) at v . The "in-neighborhood" $N_{\Gamma_D}^-(v)$ or $N^-(v)$ (respectively, the "out-neighborhood" $N_{\Gamma_D}^+(v)$ or $N^+(v)$) is a vertex set defined by $N^-(v) = \{u \in V(\Gamma) \mid u \rightarrow v\}$ (respectively, $N^+(v) = \{w \in V(\Gamma_D) \mid v \rightarrow w\}$). If $\rho^-(v) = 0$ (respectively, $\rho^+(v) = 0$), then v is called a "source" (respectively, "sink").

Definition 10.19 Let $V(\Gamma_D)$ and $E(\Gamma_D)$ both are ordered as x_1, x_2, \dots, x_n and e_1, e_2, \dots, e_m , respectively. Then, the 0,1-matrix $A(\Gamma_D) = A[a_{ij}]$ (respectively, the (-1),0,1-matrix $M(\Gamma_D) = M[m_{ij}]$) defined by " $a_{ij} = 1$ if and only if $x_i \rightarrow x_j \in E(\Gamma_D)$ " (respectively, " $m_{ij} = 1$ if x_i is the starting vertex of e_j , $m_{ij} = -1$ if x_i is the ending vertex of e_j , and $m_{ij} = 0$ otherwise") is called the "adjacency matrix" (respectively "incidence matrix") of Γ . (Note that incidence matrix is defined only for digraphs without a loop, because if $e = (x, x)$ is a loop, then x is both the starting and the ending vertex of e .)

In fact, a graph can be considered as a particular digraph:

Definition 10.20 Let $V(\Gamma_D) = \{x_1, x_2, \dots, x_n\}$. If $A(\Gamma_D)$ is symmetric, that is if " $a_{ij} = 1$ (\Leftrightarrow there is an edge $x_i \rightarrow x_j$) if and only if $a_{ji} = 1$ (\Leftrightarrow there is an edge $x_j \rightarrow x_i$)" does hold, then Γ_D is called a "symmetric digraph". If at most one of $u \rightarrow v$ or $v \rightarrow u$ is an edge of Γ_D , then Γ_D is called an "antisymmetric digraph". If the edges of an antisymmetric digraph Γ_D are taken as unordered pairs, then we obtain the "underlying graph" Γ of Γ_D . If an antisymmetric digraph Γ_D has the

underlying graph Γ , then Γ_D is called an "orientation" of Γ or an "oriented graph" without referring to Γ .

Fundamental properties of digraphs and graphs are similar (for example, the definitions of "subdigraphs" and "isomorphism" are almost the same in both cases); and thus, essentially, it is enough to study graphs. However, there are still interesting problems with digraphs, especially, if the orientations of graphs are considered:

Definition 10.21 An orientation of a K is called a "tournament" and is denoted by Γ_{T_n} . Let Ω_D be a digraph. If $V(\Omega_D)$ can be ordered as x_1, x_2, \dots, x_n such that " $x_k \rightarrow x_l$ if and only if $l = k + 1$ ", then Ω_D is called a "(directed) path", and denoted by (x_1, x_2, \dots, x_n) . If we add the edge $x_n \rightarrow x_1$ to a directed path (x_1, x_2, \dots, x_n) , then we obtain a "(directed) cycle". (Note that in a digraph Γ_D , an orientation of a path or a cycle is a "consistent" orientation of the underlying path or cycle, respectively.)

Definition 10.22 Let $v, x, y, z \in V(\Gamma_D)$. If starting from v , we can reach each vertex of $V(\Gamma_D)$ by a path containing at most 2 edges, then v is called a "king". If $yz \in E(\Gamma_D)$ (respectively, $xy \in E(\Gamma_D)$), z (respectively, x) is called a "successor" (respectively, "predecessor") of y .

Proposition 10.2 (Landau (1953)) There is a king of each tournament Γ_{T_n} .

Proof. Let $u \in V(\Gamma_{T_n})$ be such that $\rho^+(u) = \Delta^+(\Gamma_{T_n})$. Then u is a king of Γ_{T_n} : Suppose not. Then, there is a $w \in V(\Gamma_{T_n})$ such that starting from u , we can not reach w by a path containing at most 2 edges. Therefore, if $u \rightarrow v \in E(\Gamma_{T_n})$, then $v \rightarrow w \notin E(\Gamma_{T_n})$. And thus, if $u \rightarrow v \in E(\Gamma_{T_n})$, then $w \rightarrow v \in E(\Gamma_{T_n})$ by definition of a tournament. As a result, $\rho^+(w) \geq \rho^+(u) + 1$, where $+1$ corresponds to $w \rightarrow u \in E(\Gamma_{T_n})$. That is, $\rho^+(w) > \rho^+(u)$, which contradicts with the maximality of u with respect to its out-degree. ■

10.3 Connection and Decomposition

Paths and cycles are defined in the previous section. Now, by using these notions, we can consider connectedness. In this section, we also define decomposition and multigraphs.

10.3.1 Components and walks

Definition 10.23 Let $x, y \in V(\Gamma)$. A path in Γ , starting from x and ending at y is called an " x, y -path", and it is said that " x is connected to y "; x and y are "end-vertices" and the others are "internal vertices". If for all $x, y \in V(\Gamma)$, there is an x, y -path, then Γ is called "connected". A maximal connected subgraph Ω is called a "component" of Γ . Let $W \subseteq V(\Gamma)$. If $\Gamma[W]$ is connected, then, W is called a "connected set". (Note that if Γ has only one component, then it is connected).

For digraphs, the corresponding notion is stronger:

Definition 10.24 If for each ordered pair (x, y) , $x, y \in V(\Gamma_D)$, there is an x, y -path (of course, in the directed sense, that is, such an x, y -path is a subdigraph of Γ_D), then Γ_D is called "strongly connected". A maximal strongly connected subdigraph Ω_D is called a "strong component" of Γ_D . (Note that if Γ has only one strong component, then it is strongly connected.)

Definition 10.25 Let $x, y \in V(\Gamma_D)$. if there are both x, y -path and y, x -path, then it is said that x and y are "strongly connected".

The notion of a path can easily be generalized such that the definitions and results are valid in both (directed and undirected) cases:

Definition 10.26 A finite vertex sequence (x_0, x_1, \dots, x_m) such that " $x_k x_{k+1} \in E(\Gamma)$ for each $k = 0, 1, \dots, m - 1$ " is called a "walk". The number of edges in a walk is its "length". If the length of a walk is odd (respectively, even), then it is an "odd" (respectively, "even") walk. Let $x, y \in V(\Gamma_D)$. A walk starting from x and ending at y is a " x, y -walk", and x and y are "end-vertices" of this walk. If the end-vertices of a walk are the same, then it is a "closed walk".

Lemma 10.1 Let G be a graph or a digraph, $x, y \in V(G)$ and $x \neq y$. And let W be a x, y -walk. Then there is a x, y -path P such that $V(P)$ is a subsequence of $V(W)$.

Proof. First of all, the relation " $V(P)$ is a subsequence of $V(W)$ " need not be a subgraph relation, because the vertices of P may not be consecutive in the sequence of the vertices of W .

Now, if W does not contain a repeated vertex, then it is a x, y -path. If W contains a repeated vertex, say z , then delete all the vertices from the first appearance of z (but not z) to the next appearance of z (inducing z). Then, we detain a shorter x, y -walk, say \tilde{W} , such that \tilde{W} is in W . Therefore, if P is a shortest x, y -walk in W , then P does not have any repeated vertex, and thus, P is an x, y -path. ■

Corollary 10.2 If W_1 is an x, y -path and W_2 is an y, z -path, then the concatenation $W_1 \cup W_2$ has an x, z -path. (Therefore, being connected is a transitive relation.)

Proof. $W_1 \cup W_2$ is an x, z -walk. Therefore, by the previous lemma, it has an x, z -path. ■

Remark 10.2 The previous corollary implies that for an undirected graph Γ , Γ is connected if and only if $\exists x \in V(\Gamma)$ such that there is an x, y -path $\forall y \in V(\Gamma)$.

Remark 10.3 Let Γ (respectively, Γ_D) be a graph (respectively, digraph). Then, by the previous corollary, the connection relation (respectively, the strong connection relation) on $V(\Gamma)$ (respectively, on $V(\Gamma_D)$) is an equivalence relation, and the equivalence classes are the vertex sets of components (respectively, strong components), they are the maximal (respectively, strongly maximal) connected (respectively, strongly connected) sets. (Note that generally, the connection relation for digraphs is not symmetric; for example, just consider a path.)

The previous lemma does have an analogue for closed walks. (By the way, a walk W consisting of a single vertex is a closed walk with length 0, but W is not a cycle.)

Lemma 10.2 Let W be a closed walk in a graph or in a digraph. If the length of W is odd, then there is an odd cycle C such that $V(C)$ is a subsequence of $V(W)$.

Proof. First of all, we consider W cyclically, without fixing a vertex of it as a starting vertex. Let C be a closed walk such that $V(C)$ is a subsequence of $V(W)$ and the length of C is minimal. Then, C is an odd cycle: Suppose not. Then, $\exists x \in V(C)$ such that x repeats in C . But then, split C into two closed walks, say \tilde{W}_1 and \tilde{W}_2 , at the vertex x . Since the length of C , denote it by $\ell(C)$, is odd either $\ell(\tilde{W}_1)$ or $\ell(\tilde{W}_2)$ is odd (and the other other is even), say $\ell(\tilde{W}_1)$ is odd. Therefore, $\ell(\tilde{W}_1) < \ell(C)$, and $\ell(\tilde{W}_1)$ is odd, which contradicts with the minimality of C . As a result, no vertex repeats in C , that is, C is an odd cycle satisfying the requirement of the lemma. ■

By using the previous lemma, we can characterize bipartite graphs:

Theorem 10.5 (König's Theorem (König 1936)) Let Γ be a graph. Γ is bipartite if and only if Γ does not contain any odd cycle.

Proof.

(\Rightarrow) A walk in Γ alternates between the partite sets of Γ . Therefore, the length of a closed walk (in particular, a closed cycle) is even.

(\Leftarrow) Without loss of generality, we can assume that Γ is connected; because a graph is bipartite if and only if each of its components is bipartite. Select an $x \in V(\Gamma)$. Then, for each $y \in V(\Gamma)$, there is either an odd x, y -walk or an even x, y -walk: Suppose not. Then $\exists z \in V(\Gamma)$ such that there exists both an even x, z -walk, say W_1 and an odd x, z -walk, say W_2 . But then $W = W_1 \cup W_2$ is a closed walk of odd length. Therefore, by the previous lemma, it has an odd cycle, which contradicts with the hypothesis that Γ does not contain any odd cycle.

Not, let $V_1 = \{y \in V(\Gamma) \mid \text{the length of an } x, y\text{-walk is odd}\}$ and $V_2 = \{y \in V(\Gamma) \mid \text{the length of an } x, z\text{-walk is even}\}$. Then Γ is an V_1, V_2 -digraph: If $yz \in E(\Gamma)$, then an x, y -walk and an x, z -walk (for example, an x, y -walk + the edge yz) have different parities; and thus, y and z cannot be both in V_1 or in V_2 . Therefore (V_1, V_2) is a bipartition of Γ . ■

10.3.2 Cycles and cut-edges

Like a vertex deletion, an edge deletion does also exist.

Definition 10.27 Let $e \in E(\Gamma)$. If e is deleted, then the resulting subgraph of Γ is denoted by $\Gamma - e$ or $\Gamma \setminus \{e\}$.

Definition 10.28 Let $x \in V(\Gamma)$ and $e \in E(\Gamma)$. If $\Gamma - x$ (respectively, $\Gamma - e$) has more components than Γ , then x (respectively, y) is called a "cut-vertex" (respectively, "cut edge" or "bridge").

We can characterize cut-edges by using cycles.

Proposition 10.2 $e \in E(\Gamma)$ is a bridge if and only if there is no cycle containing e . Also let $x, y \in V(\Gamma)$ and $f = \{x, y\} \notin E(\Gamma)$. Then, the number of components, denote by nc , of $\Gamma + f$, that is, $nc(\Gamma + f)$, is equal to $nc(\Gamma)$ or $nc(\Gamma) - 1$.

Proof. Let $e = xy \in E(\Gamma)$. If x and y belong to the same component of $\Gamma - e$, then the number of components of Γ and $\Gamma - e$ are the same. Therefore, we have:

$e = xy$ is a bridge of Γ if and only if x and y belong to the different components of $\Gamma - e$ if and only if $\Gamma - e$ does not have an x, y -path if and only if e does not belong to any cycle of Γ .

For the second part of the proposition, let $e = uv \in E(\Gamma)$. Then:

$$nc(\Gamma - e) = nc(\Gamma) \text{ or } nc(\Gamma - e) = nc(\Gamma) + 1.$$

$\therefore nc(\Gamma + f) = nc(\Gamma)$ or $nc(\Gamma + f) = nc(\Gamma) - 1$, because if $\Omega = \Gamma + f$, then $\Gamma = \Omega - f$. More precisely: $nc(\Omega - f) = nc(\Omega) + 1 \Rightarrow nc(\Omega = \Gamma + f) = nc(\Gamma = \Omega - f) - 1$. ■

Corollary 10.3 If $|V(\Gamma)| = n$ and $|E(\Gamma)| = k$, then $nc(\Gamma) \geq n - k$. Therefore, if Γ is connected, $E(\Gamma) \geq n - 1$ (and, equality does hold for paths).

Proof. First of all, if $|V(\Gamma)| = n$ and $|E(\Gamma)| = 0$, then $nc(\Gamma) = n$. Therefore, since the addition of an edge decreases nc at most 1, the addition of k edges decreases nc at most k . As a result, if $|E(\Gamma)| = k$ then $nc(\Gamma) \geq n - k$. ■

Obviously, if Γ is a finite graph, then Γ contains with respect to the number of edges) a maximal path. Therefore, we have:

Proposition 10.3 Let Γ be a non-trivial graph. Then, there are at least two vertices of Γ , say x and y , such that x and y are not cut vertices.

Proof. Let $P \subseteq \Gamma$ be a maximal path with end-vertices x and y . Then, both $P - x$ and $P - y$ are connected, and $N(x) \subseteq V(P)$ and $N(y) \subseteq V(P)$, because P is maximal with respect to the number of edges of it.

$\therefore N(x)$ and $N(y)$ are subsets of the same component of $\Gamma - x$ and $\Gamma - y$, respectively. ($N(x) \subseteq V(P) - x \subseteq \Gamma - x$ and $V(P) - x$ is connected. $\therefore N(x)$ is a subset of the same component of $\Gamma - x$, similarly for $N(y)$.)

\therefore Both x and y are not cut vertices. ■

Lemma 10.3 Let $\delta(\Gamma) \geq 2$. Then Γ contains a cycle.

Proof. Let $P \subseteq \Gamma$ be a maximal path, and let $x \in V(\Gamma)$ be one of the end-vertices of P . Also, let $u \in V(P)$ be such that $ux \in E(\Gamma)$. Now, since $\rho(x) \geq \delta(\Gamma) \geq 2$, $\exists w \in V(\Gamma)$ such that $xw \in E(\Gamma)$. But since P is maximal with respect to the number of edges, $w \in V(P)$. Therefore, the portion of P between x and w , and the edge xw give a cycle in Γ . ■

Now, we apply the previous lemma to the next theorem. But first, we need a definition.

Definition 10.29 A set of subgraphs of Γ partitioning $E(\Gamma)$ is called a "decomposition" of Γ . If $\rho(x)$ is even for $\forall x \in V(\Gamma)$, then Γ is called an "even graph".

Theorem 10.6 Let Γ be an even graph. Then, there is a decomposition of Γ into cycles.

Proof. The proof is by induction on $|E(\Gamma)| = m$.

$m = 0$: A trivial graph (that is, a graph not containing any edges) is decomposed into 0 cycles.

$m > 0$: Γ does have a nontrivial component Ω , and $\delta(\Omega) \geq 2$ (because $\Omega \subseteq \Gamma$ is an even graph).

\therefore By the previous lemma, Ω does have a cycle C . Let $\Lambda = \Gamma - E(C)$. Then, Λ is again an even graph, because $\rho_C(x) = 2, \forall x \in V(C)$.

\therefore By the induction assumption, Λ does have a decomposition into cycles.

\therefore With the cycle C , Γ does have a decomposition into cycles. ■

More generally, let \mathcal{F} be a family of graphs, and let Γ be a given graph. Does Γ decompose into graphs in \mathcal{F} ? As an example, let \mathcal{F} be the family of stars, and Γ be a given graph. Under what conditions, does Γ decompose into stars? (Let $K_{1,n}$ be a star with $n \geq 2$. Then the vertex of $K_{1,n}$ with the maximum degree is called the "center" of $K_{1,n}$).

Proposition 10.4 Let Γ be an m -regular graph. Then, Γ does have a decomposition into copies of $K_{1,m}$ if and only if Γ is bipartite.

Proof.

(\Leftarrow) Let (U, W) be a bipartition of Γ . And let \mathcal{F} be the family of stars with centers at the vertices of U . Then, since Γ is m -regular, each of the stars in \mathcal{F} is $K_{1,m}$. Also, since each $e \in E(\Gamma)$ does have one and only one end-vertex is U , \mathcal{F} is a decomposition of Γ .

(\Rightarrow) If $m = 1$, then Γ does have a decomposition into copies of the star $K_{1,1}$, that is, $E(\Gamma)$ consists of non-incident edges, and thus Γ is bipartite: Γ does not contain any cycle, and so, it does not contain any odd cycle.

\therefore Suppose that $m \geq 2$.

Let \mathcal{F} be a decomposition of Γ into copies of the stars $K_{1,m}$. And let $u = \{x \in V(\Gamma) \mid x \text{ is the center of a } K_{1,m} \in \mathcal{F}\}$. Now, since Γ is m -regular and since $\rho_{K_{1,m}}(x) = m$ for each center x , there is no edge between two centers in U . Therefore, U is an independent set. On the other hand, since \mathcal{F} is a decomposition of Γ , the union of the edges of the stars in \mathcal{F} gives $E(\Gamma)$. Thus, there is no edge with both end-vertices outside U . Therefore, $W = V(\Gamma) \setminus U$ is also an independent set. As a result, Γ is U, W -bigraph. ■

10.3.3 Eulerian circuits

To model the origin of graph theory, namely, the "Königsberg Bridge problem", we need a more general graph definition:

Definition 10.30 Let V be a set and E be a "multiset" (the only difference between a set and a multiset is the following: In a multiset, repetition of elements is allowed, but still the order of elements does not matter) called a "vertex set" and an "edge set" such that each

element of E ("called an "edge") is a 1-element or 2-element subset of V (each of its elements is called a "vertex"). Then, a multi-graph Γ_m is an ordered pair (V, E) , and we write $\Gamma_m = (V, E) = (V(\Gamma_m), E(\Gamma_m))$. If $e \in E(\Gamma_m)$ consists of one vertex, i.e., it is a 1-element subset of V , then e is called a "loop". If $e \in E(\Gamma_m)$ is repeated (in $E(\Gamma_m)$), i.e., if there are at least two copies of e such that each copy has the same end-vertices, then e is called "multi-edge". The number of copies of an edge e in $E(\Gamma_m)$ is called the "multiplicity" of e , and denoted by $m(e)$. The "degree" of a vertex $x \in V(\Gamma_m)$, again be noted by $\rho_r(x)$ or $\rho(x)$, is defined by $\rho(x) = \sum_{x \in e} m(e) + 2$. (the number of loops at x).

Note 10.4 In a multi-graph, a loop and a pair of multi-edges are considered as cycles with lengths 1 and 2, respectively.

Definition 10.31 Let Γ_m be a multi-graph. A graph Γ such that $V(\Gamma) = V(\Gamma_m)$, and as sets $E(\Gamma) = E(\Gamma_m)$, that is, each $e \in E(\Gamma)$ does have multiplicity 1, is called the "underlying graph" of Γ_m .

Remark 10.4 Almost all definitions and theorems (and their proofs) related to graphs are also valid for multi-graphs with a slight modification if needed. Let Γ_m be a multi-graph, and $V(\Gamma_m) = \{x_1, x_2, \dots, x_n\}$. Then:

- a) $A(\Gamma_m) = [a_{ij}]$ such that a_{ij} is the number of edges with end vertices x_i and x_j .
- b) If Γ_m does not have any loops, then it can be considered as a graph, say Γ , such that there is a weight function, namely, the multiplicity function $mf: E(\Gamma) \rightarrow \mathbb{Z}^+ \cup \{0\}$, assigning each edge $e \in E(\Gamma)$ its multiplicity $m(e)$ in Γ_m .
- c) An isomorphism of multi-graphs Γ_{m_1} and Γ_{m_2} is bisection $\varphi: V(\Gamma_{m_1}) \rightarrow V(\Gamma_{m_2})$ such that edge multiplications are preserved, that is, " $e = \{x, y\} \in E(\Gamma_{m_1})$ with $m(e) = m$ if and only if $\varphi(e) = \{\varphi(x), \varphi(y)\} \in E(\Gamma_{m_2})$ with $m(\varphi(e)) = m$."
- d) Since there may exist more than one edge between two vertices of a multigraph Γ_m , a walk in Γ_m should be defined as an alternating sequence of vertices and edges such as:

$x_0, e_1, x_1, \dots, x_{k-1}, e_k, x_k$, (If there are no multi-edges, then of course it is sufficient to list vertices.)

e) Since graphs do not have loops or multi-edges, a graph can also be called a "simple graph".

Definition 10.32 Let T be a walk in a multi-graph Γ_m . If T passes through each $e \in E(\Gamma_m)$ at most once, then T is called a "trial". A closed trail is called a "circuit". (For a circuit, there is no starting vertex, the vertices (and edges) are considered cyclically.) A trail passing through each edge of Γ_m is called an "Eulerian trail", and a closed Eulerian trail is called an "Eulerian circuit".

Theorem 10.7 Let Γ_m be a multigraph. Γ_m does have an Eulerian circuit C_E if and only if Γ_m does have at most one non-trivial component and $\rho_{\Gamma_m}(x)$ is even $\forall x \in V(\Gamma_m)$.

Proof.

(\Rightarrow) Each passing of C_E through a vertex $x \in V(\Gamma_m)$ uses two edges incident at x , one for entrance and the other for exit. Therefore, each passing of C_E through vertex $x \in V(\Gamma_m)$ contributes 2 to $\rho(x)$. As result, $\rho(x)$ is even $\forall x \in V(\Gamma_m)$.

Also, since an Eulerian circuit passes through all edges of Γ_m , Γ_m has at most one non-trivial component.

(\Leftarrow) First of all, since Γ_m is even, it can be decomposed into cycles, say \mathcal{D} , by the last theorem of the previous subsection. And each cycle gives a closed trail by traversing its edges. Therefore, such a decomposition \mathcal{D} partitions $E(\Gamma_m)$ into edge-disjoint circuits.

Now, choose a smallest (with respect to the number of circuits, i.e., with respect to the number of elements in it) such \mathcal{D} , say \mathcal{D}_s . Then \mathcal{D}_s composes a unique Eulerian circuit: Suppose not. First, \mathcal{D}_s contains two distinct circuits; because if there is only one circuit in \mathcal{D}_s , then it is an Eulerian circuit. Second, there are two circuits in \mathcal{D}_s having a common vertex: Suppose not. Then, the set of edges of each circuit belongs to a distinct non-trivial component of Γ_m , but this contradicts with the assumption that Γ_m does have at most one non-trivial component. As a result, \mathcal{D}_s does have two distant circuits having a common vertex, say $x \in V(\Gamma_m)$. But then, by starting from the vertex

x , we can first pass through all the edges of one of these circuits and end at x , then by starting from x again, we can pass through all the edges of the other one and end at x again.

Therefore, we form a single circuit from these two circuits, and thus partitions $E(\Gamma_m)$ into fewer number of circuits than \mathcal{D}_S , which contradicts with the minimality of \mathcal{D}_S . As a result, \mathcal{D}_S has only one circuit traversing each edge of Γ_m , and thus, Γ_m does have an Eulerian circuit. ■

Corollary 10.4 Let Γ_m be connected, and let the number of odd degrees $x \in V(\Gamma_m)$ be $2m$ where $m > 0$. Then, there is a decomposition \mathcal{D} of Γ_m into trails with $|\mathcal{D}| = m$, and there is no such decomposition containing $< m$ trails.

Proof. First, for such a \mathcal{D} , $|\mathcal{D}| \geq m$: Let T be a trial in Γ_m with end-vertices $x, y \in V(\Gamma_m)$. Then, $\rho_T(x)$ and $\rho_T(y)$ are odd, and $\rho_T(z)$ is even $\forall z \in T$. Therefore, a decomposition into trails must contain a trail T_x for each odd-degree vertex $x \in V(\Gamma_m)$ such that one of the end-vertices of T_x is x . Therefore, since each trial has two end-vertices and since there are $2m$ odd-degree vertices, the number of elements of such \mathcal{D} is $\geq m$.

Second, there is such a \mathcal{D} with $|\mathcal{D}| = m$: Add m edges between each of two pairs of vertices having odd degrees. Then, the obtained multigraph, say $\tilde{\Gamma}_m$, is even, and thus does have an Eulerian circuit C_E by the previous theorem. Now delete these added m edges from C_E . Then, since any two such deletions of added edges give two edge-disjoint trails, deletions of m added edges from C_E (in $\tilde{\Gamma}_m$) give m edge-disjoint trails (in Γ_m) such that the union (in fact, the disjoint union) of their edges is $E(\Gamma_m)$. ■

10.4 Trees and Distances

Definition 10.33 If Γ does not contain any cycles, then Γ is called an "acyclic graph". An acyclic graph is called a "forest". A connected forest is called a "tree". If $T \subseteq \Gamma$ is both a spanning subgraph and a tree, then T is called a "spanning tree".

10.4.1 Properties of trees

Definition 10.34 A vertex $x \in V(T)$, where T is a tree, $\rho(x) = 1$ is called a "leaf".

Proposition 10.5 Let T be a non-trivial tree, i.e. $|E(T)| \geq 1$. Then, there are at least two leaves of T . And, if $x \in V(T)$ is a leaf, then $\tilde{T} = T - x$ is also a tree.

Proof. First of all, since T is a non-trivial tree, $T \neq K_1$. Therefore, T has no isolated vertex, because a tree is connected by definition.

Now, Let $P \subseteq T$ be a maximal path with end-vertices x and y . Then, x and y are both leaves: Suppose not. Then, $\rho_T(x) \geq 2$ or $\rho_T(y) \geq 2$. Without loss of generality, assume that $\rho_T(x) \geq 2$. On the other hand, since P is maximal, $N_T(x) \subseteq P$. Therefore, since $\rho_T(x) \geq 2$, there are at least two vertices, say $a, b \in N_T(x)$ such that $bx \notin E(P)$, but $ax \in E(P)$. But then, the portion of P between the vertices b and x plus the edge bx gives a cycle in T , which is a contradiction, because T is a tree. As a result, $\rho_T(x) = 1$ and $\rho_T(y) = 1$, i.e., the end-vertices x and y of a maximal path P are both leaves of T .

Finally, let $x \in V(T)$ be a leaf. Then, $\tilde{T} = T - x$ is a tree: First, $T - x$ does not have a cycle, because $T - x \subseteq T$ and T is acyclic. (A cycle in a subgraph of a graph is of course a cycle in the graph itself). Second, since $\rho_T(x) = 1$, x does have a unique neighbor in only one component of $T - x$. Therefore, x is not a cut-vertex, because a cut-vertex z in a graph Γ must have neighbors in different components of $\Gamma - z$. Therefore, $nc(T - x) = nc(T) = 1$, that is, $T - x$ is connected. As a result, since $T - x$ is acyclic and connected, it is a tree. ■

Note 10.5 The previous proposition indicates that a tree T with $|V(T)| = n$ is obtained from a tree \tilde{T} with $|V(\tilde{T})| = n - 1$ by making adjacent a new vertex to one of the vertices of \tilde{T} .

The well-known and basic property of a tree T is the equality $|E(T)| = V(T) - 1$:

Proposition 10.6 Let Γ be a graph with $|V(\Gamma)| = n$. Then any two of the statements:

- a) Γ is acyclic.

b) Γ is connected.

c) $|E(\Gamma)| = n - 1$.

implies the third.

Proof. First of all, let $e = \{x, y\} \notin E(\Gamma)$ where $x, y \in V(\Gamma)$. Then, $nc(\Gamma + e) = nc(\Gamma) - 1$ if and only if x and y are in distinct components of Γ if and only if $\Gamma + e$ does not have a cycle containing e : The first if and only if is obviously true. For the second if and only if, the only if part, that is, the implication (\Rightarrow) is obvious; the if part, that is, the implication (\Leftarrow) is true, because if x and y are in the same component of Γ , then there is an x, y -path $P \subseteq \Gamma$, but then $P + e$ gives a cycle in $\Gamma + e$ containing the edge e .

\therefore If $|E(\Gamma)| = k$, then $nc(\Gamma) = n - k$ if and only if Γ does not have any cycle: Starting from the trivial graph on n vertices (of course, the trivial graph on n vertices has n compartments), each added edge decreases the number of components by 1 if and only if the addition of this new edge does not create any cycle. By continuing in this way, the result is concluded: With the addition of k edges, the number of components decreases by k if and only if none of these edges does create any cycles if and only if Γ does not have any cycles.

Now, we can prove the proposition easily:

i) Let Γ be an acyclic graph. Then, Γ has one component if and only if Γ does have $n - 1$ edges. ($\therefore (a) + (b) \Rightarrow (c)$ and $(a) + (c) \Rightarrow (b)$.)

ii) Let $|E(\Gamma)| = n - 1$. Then, $nc(\Gamma) = n - (n - 1) = 1$, that is, Γ is connected if and only if Γ is acyclic. ($((c) + (b) \Rightarrow (a)$ and $(c) + (a) \Rightarrow (b)$.) ■

There are other characterizations of trees:

Proposition 10.7 Let Γ be a graph. Then, TFAE:

a) Γ is a tree.

b) Γ is connected and $\forall x \in E(\Gamma)$ is cut-edge.

c) Γ does have precisely one x, y - path $\forall x, y \in V(\Gamma), x \neq y$.

d) Γ does not have any cycle but for each $e = \{x, y\} \notin E(\Gamma)$, where $x, y \in V(\Gamma)$, $\Gamma + e$ does have exactly one cycle.

Proof.

(a) \Rightarrow (b): First, by definition of a tree, Γ is connected. Second, by the first proposition of the second subsection of the previous section an $e \in E(\Gamma)$ is a cut-edge if and only if there is no cycle containing e . Therefore, since Γ is a cyclic, $\forall e \in E(\Gamma)$ is a cut-edge.

(b) \Rightarrow (c): Let $x, y \in V(\Gamma)$. First, since Γ is connected there exists an x, y -path. And, this x, y -path is unique: Suppose not. Then, there exists more than one x, y -path. Therefore, $\exists vw \in E(\Gamma)$ such that vw is an edge of one of these x, y -paths, but not an edge of all of these x, y -paths. This implies that there is a v, w -path in $\Gamma - vw$: There is a v, x -path an x, y -path (because vw does not belong to every x, y -path by our choice), an y, w -path. Therefore, there is a v, w -path by the first corollary of the previous section.

Now, since there is a v, w -path in $\Gamma - vw$, vw is not a cut-edge and this contradicts with the hypothesis.

(c) \Rightarrow (d): First, Γ does not have any cycle: Suppose not. Then, there is a cycle C in Γ . Let $x, y \in V(C)$. Then, there are two x, y -paths along C , which contradicts with the uniqueness of x, y -path.

Second, let $x, y \in V(\Gamma)$, and $e = \{x, y\} \notin E(\Gamma)$. Then, $\Gamma + e$ does have exactly one cycle, because Γ does have exactly one x, y -path.

(d) \Rightarrow (a): First, Γ is a cyclic by the hypothesis.

Second, Γ is connected: Let $x, y \in V(\Gamma)$, and $e = \{x, y\} \notin E(\Gamma)$. Then, $\Gamma + e$ does have exactly one cycle by the hypothesis. Therefore, Γ has an x, y -path. As a result, Γ is connected.

\therefore Since Γ is acyclic and connected, it is a tree by definition. ■

Proposition 10.8 Let Γ be a connected graph. Then, Γ does have a spanning tree.

Proof. If an edge e is deleted from a cycle C in Γ , then $\Gamma - e$ is still connected. Therefore, if we start by deleting an edge from a cycle, and proceed iteratively by deleting an edge from one of the remaining cycles; then at the end, we obtain an acyclic and connected subgraph of Γ . Since only edges are deleted, that is, since none of the vertices are deleted, the obtained graph is also a spanning subgraph of Γ .

\therefore Γ does have a spanning tree. ■

10.4.2 Distance and diameter

Definition 10.35 Let G be a graph or a digraph and let $v, w \in V(G)$. If there is a v, w -path in G , then the "distance" from v to w , denoted by $\rho_G(v, w)$ or $\rho(v, w)$, is the minimum of the lengths of v, w -paths, that is, it is the number of edges of a shortest v, w -path. If there is no v, w -path in G , then $\rho(v, w)$ is defined as ∞ .

Note 10.6 Let Γ (respectively, Γ_D) be a graph (respectively, digraph). Then:

a) $\rho_\Gamma: V(\Gamma) \times V(\Gamma) \rightarrow \mathbb{R}$ is a metric on $V(\Gamma)$:

i) Obviously, ρ_Γ is nonnegative by definition, that is, $\rho_\Gamma(v, w) \geq 0 \forall v, w \in V(\Gamma)$.

ii) $\rho_\Gamma(v, w) > 0$ for $v \neq w$: $\rho_\Gamma(v, w) = 0 \Leftrightarrow v = w$. $\therefore \rho_\Gamma(v, w) > 0 \Leftrightarrow v \neq w$.

iii) $\rho_\Gamma(v, w) = \rho_\Gamma(w, v) \forall v, w \in V(\Gamma)$, that is, ρ_Γ is symmetric.

iv) The triangle inequality holds, that is, $\rho_\Gamma(u, v) + \rho_\Gamma(v, w) \geq \rho_\Gamma(u, w)$:

Let $P_{u,v}, P_{v,w}, P_{u,w}$ be a shortest u, v -path, v, w -path, u, w -path respectively. Then, the concatenation $P_{u,v} + P_{v,w}$ contains a u, w -path by the first corollary of the previous section. Let $\ell(W)$ denote the length of the walk W . Then:

$$\ell(P_{u,w}) = \rho_\Gamma(u, w) \leq \ell(P_{u,v} + P_{v,w}) = \ell(P_{u,v}) + \ell(P_{v,w}) = \rho_\Gamma(u, v) + \rho_\Gamma(v, w).$$

b) ρ_{Γ_D} satisfies (i), (ii), (iv) of part (a), but it is symmetric only if Γ_D is symmetric.

Definition 10.36 Let Γ be a graph. Then, the number:

$$\text{diam}(\Gamma) = \max_{x, y \in V(\Gamma)} \rho(x, y)$$

is called the "diameter" of Γ . Let $x \in V(\Gamma)$. Then, the number:

$$\varepsilon(x) = \max_{y \in V(\Gamma)} \rho(x, y)$$

is called the "eccentricity" of the vertex x . And, the number:

$$\text{rad}(\Gamma) = \min_{x \in V(\Gamma)} \varepsilon(x)$$

is called the "radius" of Γ . Then, the set:

$$C(\Gamma) = \{x \in V(\Gamma) \mid \varepsilon(x) = \text{rad}(\Gamma)\}$$

Is called the "center" of Γ .

Note 10.7

a) If Γ is disconnected, then $diam(\Gamma) = rad(\Gamma) = \infty$ and $\varepsilon(x) = \infty \forall x \in V(\Gamma)$.

b)
$$diam(\Gamma) = \max_{x,y \in V(\Gamma)} \rho(x,y) = \max_{x \in V(\Gamma)} \max_{y \in V(\Gamma)} \rho(x,y) = \max_{x \in V(\Gamma)} \varepsilon(x).$$

$\therefore diam(\Gamma)$ is the maximum of the eccentricities of vertices.

c) $diam(K_n) = 1$ and $diam(K_{1,n}) = 2$.

d) Computing distances is very easy for trees, because each path is unique in Γ , and thus, it is a shortest path between its end-vertices.

\therefore The diameter of a tree is just the number of edges of a longest path.

As an example of results related to the topics of this subsection, let's state a well-known result of Jordan proved in 1869:

Theorem 10.8 (Jordan (1869)) Let T be a tree. Then, $C(T) = \{x\}$ or $C(T) = \{x, y \mid xy \in E(T)\}$, that is, the center of T comprises just one vertex or two adjacent vertices. ■

10.5 Result and Discussion

This chapter is a review study, it does not contain any original results. As stated at the beginning of the chapter, we mainly used West (2021) to prepare this study.

The purpose of this chapter is to introduce this rich and active research area at a basic level. In other words, we aim to present an introduction source about graph theory for non-experts in this area. Therefore, we hope this self-contained chapter will be useful for students and researchers who want to learn the basics of this immensely enjoyable, fascinating, and influential area of mathematics.

Finally, as it is known, there are lots of good resources about graph theory. We especially recommend West (2002), which is one of the best textbooks written in graph theory, West (2021), which is a more comprehensive graduate combinatorial mathematics textbook,

and Diestel (2024), which is an excellent graduate textbook on graph theory.

REFERENCES

- Berge C., (1970). Une propriete des graphes k -stables-critiques. In *Combinatorial Structures and Their Applications*: 7–11.
- Diestel, R. (2024). *Graph theory* (6th Ed.). Springer, Berlin.
- Fulkerson, D. R., Hoffman, A.J., and McAndrew, M.H. (1965). Some properties of graphs with multiple edges. *Canad. J. Math.*, 17: 166–177.
- Hakimi, S. L. (1962). On the realizability of a set of integers as degrees of the vertices of a graph. *SIAM J. Appl. Math.*, 10: 496–506.
- Havel, V. (1955). A remark on the existence of finite graphs (Czech). *Casopis Pest. Mat.*, 80: 477–480.
- Jordan, C. (1869). Sur les assemblages de lignes. *J. Reine Angew. Math.*, 70: 185–190.
- König, D. (1936). *Theorie der endlichen und unendlichen graphen*. Akademische verlagsgesellschaft m. b. h., Leipzig.
- Landau, H.G. (1953). On dominance relations and the structure of animal societies, III: The condition for score structure. *Bull. Math. Biophys.*, 15: 143–148.
- Turan, P. (1941). Eine Extremalaufgabe aus der Graphentheorie. *Mat. Fiz Lapook*, 48: 436–452.
- West, D. B. (2002). *Introduction to graph theory* (2nd Ed.). Prentice-Hall, New Jersey.
- West, D. B. (2021). *Combinatorial mathematics*. Cambridge University Press, Cambridge.

CHAPTER 11

A REVIEW: SEROTONIN SENSORS BASED ON SCREEN-PRINTED ELECTRODES

Assoc. Prof. Dr. Melike BİLGİ¹ & Ms. Ayşenur YILMAZ KABACA²

DOI: <https://dx.doi.org/10.5281/zenodo.14259245>

¹ Çankırı Karatekin University, Faculty of Science, Chemistry Department Çankırı, Türkiye. melikesahin@karatekin.edu.tr, Orcid ID: 0000-0002-3381-7522

² Çankırı Karatekin University, Şabanözü Vocational School, Department of Medical Laboratory Techniques, Çankırı, Türkiye. aysenuryk@karatekin.edu.tr, Orcid: 0000-0002-1189-405X

INTRODUCTION

This review aims to summarize and contextualize studies conducted between 2020 and 2024 with various screen-printed electrodes (SPE) for the determination of serotonin (SER), one of the most common feedback mechanisms between the brain and the digestive system. The different classes of electroactive substances used as mediators, as well as the surface strategies used in these sensors – such as nanoparticles (NPs) or carbon-based materials – are also discussed. Such sensors are mostly applied in the field of neuroscience to study the release of SER around cells. Scanning is restricted due to their slow response and poor selectivity; therefore, long-term monitoring in the presence of the cells is often performed with these kinds of sensors.

Neurotransmitters

Comprehending the intricate operations of the brain is a significant barrier in scientific research. Developing *in vivo* biosensors to monitor the activity of neurotransmitters and signaling pathways in the brain is an attractive option. To activate receptors on postsynaptic cells, chemical messengers known as neurotransmitters flow across synapses and allow cells in the central nervous system to connect with one another. Neurotransmitters include biogenic amines such as SER, dopamine (DA), epinephrine, and norepinephrine, and amino acids such as glutamate and γ -aminobutyric acid (Si and Song 2018, Kerage et al. 2019).

Neurotransmitters synthesized by some glands (the pituitary, pineal, and adrenal glands, etc.) are sequestered in clustered vesicles within neuron terminals. An action potential at a synapse triggers the release of neurotransmitters, which are then reabsorbed to traverse the synaptic cleft and bind to the receptor site of another neuron or cell. An action potential is generated at the axon terminal, prompting the subsequent cell to release a corresponding neurotransmitter that conveys information to an adjacent neuron. Consequently, neurons provoke a physiologic reaction (Moon et al. 2018). Neurotransmitters are present in multiple bodily fluids (serum, plasma, platelets,

cerebrospinal fluid (CSF), urine, saliva, etc.) Alterations in neurotransmitter activity, crucial for human mental and physical well-being, can lead to significant diseases and psychological problems. Consequently, the surveillance of these neurotransmitters is essential for medical intervention and clinical evaluation (Si and Song 2018).

Serotonin (SER)

SER is a monoamine neurotransmitter identified by Vittorio Erspamer and generated in the brain, intestines, and spinal cord of the body. SER plays a crucial role in regulating numerous physiological systems, particularly human emotions (Moon et al. 2018). It is located in smooth muscles, platelets, and the gastrointestinal, central, and peripheral nervous systems (Cernat et al. 2020). SER is synthesized in the body through two phases. In the initial phase, tryptophan is transformed into 5-hydroxytryptophan by tryptophan hydroxylase, and in the subsequent phase, 5-hydroxytryptophan undergoes decarboxylation to yield 5-hydroxytryptamine (SER) (Kerage et al. 2019). SER can be released into the bloodstream as it is absorbed by circulating platelets and retained in elevated amounts. Platelet release significantly elevates plasma SER concentrations. SER demonstrates autocrine and paracrine effects in the gastrointestinal tract, central nervous system, and various other organs. SER is synthesized in the brain by the raphe nuclei. Consequently, alterations in mood and cognition are noted (Kerage et al. 2019).

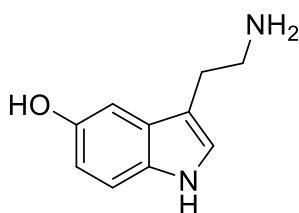


Figure 1. Chemical structure of SER

SER (3-(2-aminoethyl)-1H-indol-5-ol) possesses a molecular structure characterized by an indole ring including two functional

groups: an acidic hydroxyl group at position 5 and an ethylamine side chain (Figure 1). The two functional groups are ionizable and possess pKa values of approximately 9 to 10. SER can exist in both positively and negatively charged states. The pKa value is 10.2. At pH < 10.2, both groups are protonated, resulting in SER being primarily positively charged. At pH exceeding 10.2, both groups undergo deprotonation, resulting in the hydroxyl group acquiring a negative charge. The cationic form predominates at physiological pH. Besides the ionic forms, the adaptability of both groups enables SER to adopt many low-energy conformations referred to as conformational isomers. The ethylamine side chain may either extend away from the hydroxyl group or fold toward it.

Importance of SER Detection

SER levels are intricately linked to conditions like hypertension, neuropsychiatric disorders, neurodegenerative illnesses, vascular problems related to metabolic disorders, and diabetes. In individuals with depressive disorders, serum levels of SER are approximately 300 nM in whole blood and 3 nM in CSF. Lower SER levels of approximately 5-10 nM are observed in Type 2 Diabetes, while patients with carcinoid tumors exhibit levels around 280 $\mu\text{M}/24$ h in urine samples. Normal SER levels range from 270 nM to 1490 nM in serum, approximately 300-1650 nM in urine, and are less than 0.0568 nM in CSF (Khoshnevisan et al. 2020). It is essential for regulating numerous behavioral and physiological activities, including mood, sleep, vomiting, sexuality, and appetite (Young and Leyton 2002). Reduced SER levels are related to numerous diseases and disorders (Alzheimer's disease, infantile autism, intellectual disability, sleep disorders, etc.), mental health conditions such as depression and anxiety, migraines, nonregular hemostasis, blood coagulation issues, and sudden infant death syndrome (SIDS) (Jones and Blackburn 2002; Maximino 2012, Lin et al. 2014; Moon et al. 2018).

Conversely, elevated SER levels can result in considerable toxicity, leading to severe consequences known as the syndrome of carcinoid and SER (Birmes et al. 2003; Buckley et al. 2014). Moreover,

other biological and psychopathological processes, such as eating disorders, autism, alcoholism, anxiety and obsessive-compulsive disorder, and psychosis, have been linked to SER (Hasanzadeh et al. 2017; Moon et al. 2018). Consequently, the determination of SER is crucial for comprehending the role of SER in certain neurological illnesses and for diagnosing various diseases. Given that diminished SER levels in the brain may indicate depression, assessing SER concentrations in blood, serum, plasma, and platelets is crucial for diagnosing the condition. The concentration range of SER in healthy human serum is reported to be 0.6-1.6 μM (Hasanzadeh et al. 2017).

SER DETECTION TECHNIQUES

Various analytical techniques have been used to detect SER. These include fluorimetry, high-performance liquid chromatography-electrochemical determination (He et al., 2019), capillary electrophoresis (Roychoudhury et al. 2020), enzyme immunoassay, chemiluminescence (Ma et al. 2020), enzyme-linked immunosorbent assay and mass spectrometry (Darwish and Refaat 2006; Danaceau et al. 2003; Song et al. 2019). These traditional procedures are arduous, time-intensive, and typically necessitate sample pretreatment. These methods render the swift and practical assessment of SER unsuitable. The practical, sensitive, inexpensive, and quick determination of SER is essential.

Electrochemical methods effectively quantify SER owing to its electroactive characteristics. These methods for the quantification of SER provide great sensitivity and stability, an extensive linear range, and exceptional repeatability. Moreover, these methods are more cost-effective than conventional analytical procedures. Electrochemical sensors and biosensors hold significant importance in the determination of SER due to their selectivity, cost-effectiveness, and rapid response compared to sophisticated approaches. Electrochemical biosensors have the benefits of miniaturizing intricate systems, exhibiting high specificity and sensitivity, and enabling direct measurement of analytes in tiny volume and low-concentration samples (Hou et al. 2016; Su et al. 2017). Normal SER concentrations in bodily fluids are in the

nanomolar range in blood, urine, and CSF samples. These values have been attained through the utilization of sensors derived from NPs and nanocomposites. The capacity to quantify SER in bodily fluids is essential and significant for medical diagnosis. Electrochemical sensor analyses are effective for screening and monitoring SER in point-of-care testing (POCT) (Dăscălescu and Apetrei 2021).

Electrochemical detection of SER

Electrochemical determination of SER with electrochemical sensors provides numerous benefits, such as the ability to directly measure analytes that have excellent specificity and sensitivity, even within samples characterized by tiny volumes and low concentrations. Additionally, they present opportunities for the miniaturization of complex devices (Hou et al. 2016; Su et al. 2017). Nonetheless, the highly sensitive and accurate electrochemical detection of SER on bare electrodes presents significant challenges due to the low concentrations of SER present in bodily fluids (Samie and Arvand 2019). The presence of various compounds that interfere, particularly ascorbic acid (AA) and DA, in bodily fluids poses a considerable challenge to the electrochemical determination of SER. At proximate potentials, both AA and DA can undergo oxidation, leading to an overlap in the voltammetric response. A widely adopted approach to address these challenges involves the use of a modified electrode designed to improve the sensitivity of the SER sensor and mitigate the effect of AA and DA in SER determination. Consequently, alternative electrochemical techniques employing modified electrodes have been proposed for the measurement of the SER (Kundys-Siedlecka et al., 2019; Abad-Gil et al., 2021). The electrochemical determination of SER presents challenges due to the complexity of its electrooxidation process. The products generated in the electrooxidation reaction are promptly electropolymerized into oligomers (Manasa et al., 2017; Wang et al., 2021). They are primarily adsorbed onto the surface of the electrode via π - π stacking interactions, leading to electrode fouling. The fouling impact significantly diminishes the current answer and sensitivity, even when performing short-term experiments, thereby

compromising the sensitivity of the sensor in amperometric detections (Wang et al., 2021; Hosu et al., 2021). The disposable electrodes inherently eliminate the fouling effect. The use of disposable SPE-based sensors minimizes the possibility of contamination between analysis experiments (Samie and Arvand 2019).

Screen-printed electrodes (SPE): An overview

The screen-printing technology, derived by the microelectronics sector, is utilized, amongst other applications, for the production of SPEs. The primary features needed to acquire electrochemical measurement systems for on-site analysis can be found in these electrodes. The utilization of SPEs as transducers in diverse electrochemical sensors and biosensors has consistently increased. Screen printing is a popular and established method for creating electroanalytical devices these days.

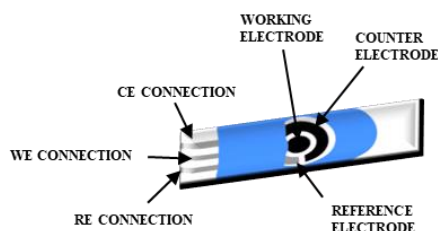


Figure 2. Structure of SPEs

Three electrodes—one for working (WE), one for reference (RE), and one for counter (CE)—are printed on a solid substrate to form an electrochemical cell, which is a common component of SPEs (Figure 2). The electrodes can be printed using a variety of inks (carbon and metallic inks are the most popular) and substrates (usually ceramic or plastic) (Moru et al., 2023; Ahamed et al., 2021). A lot of tiny, inexpensive, and throwaway electrodes can be mass-produced using the SPEs because of how quickly they can be fabricated. Consequently, there is no need to clean and/or polish them, saving a great deal of time by avoiding laborious preparatory procedures. On the other hand, traditional electrodes (such as glassy carbon or gold disk) have superior electrochemical properties and durability compared to printed

electrodes. SPEs exhibit sufficient electroanalytical characteristics for sensing applications, and their affordability and user-friendliness, which eliminate the necessity for highly skilled analysts, render them distinctly favorable as transducers for on-site, disposable measurements. Furthermore, SPEs do not require large quantities of reagents or samples due to their compact design, which enables them to be transported for on-site measurements and real-time analysis (Satyanarayana et al., 2015; Satyanarayana et al., 2019). Consequently, SPEs have been extensively utilized in the fabrication of enzymatic biosensors (Bilgi and Ayrancı, 2018; Bilgi et al., 2018), immunosensors (Yılmaz and Bilgi, 2024; Vurro et al., 2024; Bilgi Kamaç et al., 2023a and 2023b), and DNA biosensors (Yuhana Ariffin et al., 2020; García-Mendiola et al., 2020; Hassan et al., 2019).

When it comes to POCT in biomedical settings, SPEs are an excellent choice for deployment. POCTs are crucial because they enable users to conduct analyses in a quick and inexpensive manner, without the need for specialist training, and regardless of the location or time (Gubala et al., 2012; Bilgi Kamaç et al., 2023a; 2023b). The combination of POCT devices and biosensors makes it possible to conduct analysis that is uncomplicated, quick, and economical. This is especially useful in the fields of healthcare (Bilgi Kamaç et al., 2023a; 2023b; Fahem et al., 2019), food safety control (Kampeera et al., 2019; Yousefi et al. 2018), and environmental monitoring (Jeromiyas et al., 2019; Schwarz et al., 2016).

SER SENSORS BASED ON SPEs

In a SER sensor, SER is detected through electrochemical methods using an electrode capable of performing of SER oxidation. To perform selective and sensitive SER detection in the existence of other oxidizable species (DA, AA, etc.), electrodes are modified with metal (Salova et al., 2024) and/or carbon-based NPs (Misia et al., 2024) or conductive polymers (Coyle et al., 2024) to both reduce the effect of interfering species and provide a rapid response of the sensor. The utilization of SPE-based disposable electrodes to mitigate the fouling effect caused by the electrooxidation of SER, an organic molecule, facilitates rapid reaction and enhanced sensitivity in SER detection

(Atici et al., 2023; Yılmaz Kabaca et al., 2023). Table 1 shows SPE-based sensors developed for the electrochemical determination of SER between 2020 and 2024. Table 1 also includes SPE-based sensors that simultaneously determine other analytes along with the SER analyte.

Table 1. SPE-based sensors developed for electrochemical determination of SER and simultaneous determination of SER in the presence of other analytes between 2020 and 2024

Electrode	Method	Analyte	LR	LOD	Real sample	Ref
SPE/ZCNT 0.1	SWV	SER	7.5-300 μM	0.66 μM		Mullani et al., 2020
SPE-PPy-Fe ₃ O ₄ NPSL	SWV	SER	0.007-0.1 μM	0.021 μM	Banana	Uwaya et al. 2020
SPE-PPy-Fe ₃ O ₄ NPSf	SWV	SER	0.007-0.1 μM	0.20 μM	Banana	
SPE-MWCNT-AONP	SWV	SER	0.016-0.166 μM	24.6 nM	Tomatoes	Moisasathebe et al., 2021
FeC-AuNPs-MWCNT/SPCE	SWV	SER	0.05-20 μM	17 nM	Urine sample	Wu et al., 2022
OMC-SPE/Lac	SWV	SER	0-1.2 μM	316 nM	Food supplements	Dascalescu et al., 2022
SPE-AuNPs-MPA-(PDDA- <i>o</i> sWCNTs-5-HT aptamer)2-PDDA- <i>o</i> SWCNTs-Tyr	DPV	SER	0.05-0.5 μM 1-20 μM	2 nM	HC sample, IGD sample	Li et al. 2022
DGNW/SPGE	DPV	SER	1-500 μM	0.28 μM	Urine sample	Boonkaew et al., 2022
SPE/ZnONR/PMB _{DES} /AuNP	DPV	SER	0.1-25 μM	1.91	Human blood serum	Atici et al., 2023
NH-HNP-Chit/SPCE	DPV	SER	0.1-30 μM	60 nM	Urine sample, Saliva sample	Moru et al 2023
SPE/MWCNT-S-Au/MIP	DPV	SER	1-12 $\mu\text{mol L}^{-1}$	1.0 $\mu\text{mol L}^{-1}$		Misia et al., 2024
FVMX@SPCE	DPV	SER	25-750 μM	3.0 μM	Human blood serum	Ilanchezhian 2025
SPE/ITO ₂ NP/AuNP/PNBDES	DPV	DA SER	0.3 - 20 μM 0.3 - 20 μM	1.39 μM 2.47 μM	Human blood serum	Kabaca et al., 2023
AgNPs-rGO/SPCE	DPV	DA	10-100 μM	7.0 μM	Urine samples	Moslah et al., 2024
Aptamer/Au	DPV	SER	10-100 μM	7.41 μM		
	DPV	DA	0.1-4 μM	0.06 μM	Serum sampe	Cuhadar et al., 2024
	SER	SER	0.1-4 μM	0.12 μM		
Cu(L ^{NO₂}) ₂ /rGO/SPCE	LSV	SER	2-42 $\mu\text{mol L}^{-1}$ 2-42 $\mu\text{mol L}^{-1}$	42 $\mu\text{mol L}^{-1}$ 53 $\mu\text{mol L}^{-1}$	Human serum/Urine	Nunez et al., 2024
CNT-NiO-CB/Nafion/SPCE	SER	17 β -estradiol	0.06-7.50 μM	11 nM	Human serum	Mool-am-kha et al., 2020
	DA	DA	0.08-6 μM	11nM		

AONP: antimony oxide nanoparticles
Au: gold
AuNP: gold nanoparticle
CB: carbon black
Chit: chitosan
CNT: carbon nanotubes
Cu(L^{NO₂})₂: Cu(ID) triazole complex
DES: deep eutectic solvent
DGNW: diamond graphene nanowalls
Fe₃O₄: ferrocene
Fe₃O₄NPSf: Iron (III) oxide nanoparticles obtained from Callistemon viminalis leaves
Fe₃O₄NPSL: Iron (III) oxide nanoparticles obtained from Callistemon viminalis flowers
FVMX: vanadat nano flakes-Ti₃C₂ MXene hybrid nanocomposites
Lac: lactase
LSV: linear sweep voltammetry
MIP: molecularly imprinted polymer
MPA: ethanolic mercaptopropionic acid
MWCNT: multiwall carbon nanotubes
NiO: nickel oxide
OMC-SPE: organized mesoporous carbon-modified carbon screen-printed electrode
PDDA-*o*SWCNTs: poly(diallyldimethylammonium)-wrapped oxidized single-walled carbon nanotubes
PNB: polymethylene blue
PPy: polypyrrole
rGO: reduced graphene oxide
S: Sulfur
SPGE: screen-printed graphene electrode
ZCNT: zinc oxide-MWCNT nanocomposite

The fouling of the electrode due to the electrooxidation products of SER is an important problem in the electrochemical determination of SER, as it slows down the electron transfer and reduces the current response. To prevent or reduce this, studies have been conducted using molecularly imprinted polymers (MIP) and boron-doped electrodes. For instance, Boonkaew et al., (2022) created a sensor for the electrochemical analysis of SER in synthetic urine by modifying boron and nitrogen-doped diamond-graphene nanowall particles (DGNW) onto a screen-printed graphene electrode (SPGE). This DGNW structure facilitated the electrooxidation of SER molecules by providing an extensive surface area, high conductivity, and superior electrochemical activity on the electrode surface. Boron doping was used to prevent SPGE fouling and increase electrical conductivity, while nitrogen doping was used to improve the active sites of the SPGE surface and strengthen the interaction with SER molecules. These synergistic effects increased the sensitivity and selectivity of the SER sensor. Misia et al., (2024) designed a sensor for the electrochemical analysis of SER in fetal bovine serum. To effectively catalyze the electrooxidation of SER, multi-walled carbon nanotubes (MWCNTs) were decorated with gold NPs (AuNPs) obtained by ligand-free metal vapor synthesis (MSV) to increase their electrocatalytic properties. Moreover, an aryl dibenzoate salt containing sulfur (S) (4,4'-dithiodibenzene diazonium tetrafluoroborate, DTDBBF₄) was used to stabilize MSV-derived AuNPs onto MWCNTs in a stable and controlled manner. In the last step, the MWCNT-S-Au composite was modified onto screen-printed carbon electrodes (SPCE) and then covered with a MIP layer. This study used MWCNTs to improve the sensor's performance owing to their attributes, including strong electrical conductivity, extensive surface area, and chemical stability. A thin layer of MIP was added to the sensor to provide selectivity and anti-fouling properties. It was stated that thanks to the surface modification of MWCNTs, the sensor interacted more strongly with SER molecules and thus achieved high sensitivity and low detection limit.

Metal or carbon-based nanostructures are used to increase the sensitivity and selectivity of the sensor in the electrochemical detection of SER. For instance, Mullani et al., (2020) improved a sensor for electrochemical SER detection by modifying one-dimensional (1D) zinc oxide nanorods (ZnONRs) $_{1-x}$ (CNs) $_x$ nanocomposites (NCs) to SPCEs with the help of chitosan. The hybrid structure (ZnONRs) $_{1-x}$ (CNs) $_x$ materials combined the enhanced surface area and excellent electrochemical activity of ZnO with the conductivity and mechanical strength of different carbon nanostructures (CNs= MWCNT and reduced graphene oxide). This hybrid structure provided sensitive and accurate signal detection by establishing strong interactions with SER molecules upon the electrode surface. Furthermore, the contribution of CNs increased the electrical conductivity of the sensor, allowing a stronger voltammetric response to be obtained in SER oxidation. The use of chitosan was used to disperse and stabilize the NCs homogeneously. The proposed sensor exhibited a linear response throughout an extensive concentration range and achieved a low detection limit. In another study, Motsaathebe et al., (2021) constructed a novel sensor using SPCEs modified with MWCNT and antimony oxide NPs (AONPs) for the detection of SER in tomatoes. In the developed sensor, the combination of MWCNT and AONPs provided high electrical conductivity and large surface area, allowing SER molecules to interact more strongly with the electrode surface. While MWCNTs formed a good conductive network structure on the electrode, AONPs expanded the electrode surface area and offered additional sites for SER detection. These modifications increased the sensitivity and selectivity of the sensor. The developed sensor showed high selectivity. Wu et al., (2022) proposed a sensitive and selective sensor for the electrochemical analysis of SER in urine using flexible SPCEs modified with ferrocene (FeC)-AuNP-decorated MWCNT. MWCNTs were used to increase both the electrical conductivity and the large surface area. FeC enhanced the voltammetric response of the sensor due to its redox properties, while AuNP provided high sensitivity in SER detection by increasing the surface area. The designed sensor exhibited a linear response and a low

detection limit to different SER concentrations. In conclusion, this study demonstrated that the Fc-AuNp-MWCNT-based electrochemical sensor provides an effective and reliable platform for SER analysis. In a different study, Atici et al., (2023) suggested a novel sensor for the electrochemical detection of SER in human serum using zinc oxide nanorods (ZnONRs), polymethylene blue (PMB)_{DES} prepared in deep eutectic solvent (DES), and AuNPs modified SPCEs. ZnONRs were used because they have a high surface area and are biocompatible materials. PMB_{DES} increased the conductivity on the electrode surface and strengthened the interaction of SER molecules with the electrode. AuNPs facilitated the electrooxidation of SER owing to their superior electrical conductivity and catalytic properties. It was observed that the developed sensor had a broad detection range in SER determination and reached a low detection limit. In addition, it was stated that the sensor reliably detected SER in complex biological samples, such as human serum, and exhibited high selectivity against parasitic signals that may originate from other biomolecules. In a new study, Ilanchezhyan et al., (2025) reported that two-dimensional (2D) iron vanadate nanoflakes (FeVO₄NFs) supported on Ti₃C₂ MXene hybrid nanocomposite were modified upon SPCE and used for the analysis of SER in human serum. In this study, the high electrochemical activity of 2D FeVO₄ nanoflakes, increased conductivity, and extensive surface area of Ti₃C₂ MXene were used to provide ultrasensitive and selective detection of SER molecules. The SER sensor developed using FeVO₄@Ti₃C₂ MXene/SPCE electrode has a low detection limit, broad linear range, and elevated stability, indicating that it is a promising candidate for SER detection.

In the preparation of metal NPs-based SER sensors, various polymers have been used to ensure a homogeneous distribution of NPs on the surface. For instance, Uwaya et al., (2020) constructed a sensor for electrochemical SER analysis in banana samples using SPCEs modified with polypyrrole (PPy) and iron oxide NPs (Fe₃O₄NPs) obtained by green synthesis. PPy synthesized by the green method was also used to ensure a homogeneous distribution of NPs on the electrode surface, in addition to its high conductivity. As a result, the increased

conductivity and extensive surface area of the PPy/Fe₃O₄NP nanocomposite strengthened the electrochemical interactions of SER molecules with the electrode. The suggested sensor demonstrated a broad linear range, low detection limit, and high selectivity. In a different study, Moru et al., (2023) proposed a sensor for the electrochemical analysis of SER using SPCE modified with hexagonal Ni(OH)₂ nanoplates embedded in chitosan layers. In the study, it was stated that high sensitivity was achieved in SER detection due to the extensive surface area and high electrochemical activity of Ni(OH)₂ nanoplates (NPLs). The chitosan layer was used to increase the stability and reproducibility by facilitating the homogeneous distribution of NPLs on the electrode surface and the recognition of biological analytes. The performance of the improved sensor was evaluated by voltammetric measurements performed with different SER concentrations and demonstrated an extensive linear range, low detection limit, and high selectivity.

SER biosensors have been developed using biological materials such as DNA aptamers and enzymes, as well as non-enzymatic sensors for the electrochemical determination of SER. The integration of carbon-based NPs with biological materials, especially DNA aptamers, and enzymes, in the analysis of SER in complex environments such as food supplements, significantly increases the efficiency of electrochemical biosensors. In this context, these biomolecules used together with organized mesoporous carbon (OMC) and carbon nanocomposites offer innovative solutions by offering high sensitivity and selectivity in the detection of analytes. For example, Dascalescu et al., (2022) modified organized mesoporous carbon-based screen-printed electrodes (OMC-SPE) with laccase enzyme for the detection of SER in food supplements. The large surface area, high conductivity, and regular pore structure of OMC enabled effective immobilization of laccase enzyme on the electrode surface and allowed better interaction with SER molecules. Laccase catalyzed the oxidation of SER molecules and provided electrochemical signals. The developed SER sensor exhibited an extensive linear range, low detection limit, and high sensitivity. Furthermore, the reliability and selectivity of the sensor for

the analysis of SER in food supplements were evaluated. The sensor also gave successful results in complex food matrices and effectively distinguished interference signals that may originate from other components. In another study, Li et al., (2022) suggested a novel biosensor for the electrochemical analysis of SER using positively charged poly(diallyldimethylammonium)-wrapped oxidized single-walled carbon nanotubes (PDDA-oSWCNTs) and DNA aptamer-modified SPCEs. Carbon nanocomposites fulfilled a significant function in the interaction of SER with the electrode owing to their increased electrical conductivity and extensive surface area. DNA aptamers provided a selective sensing mechanism against SER molecules with their specific and high-affinity binding properties. The presence of aptamers on the surface formed strong interactions with SER, thereby increasing the detection sensitivity. demonstrated that Electrochemical analyses indicated that the developed biosensor demonstrated a broad linear range for SER, achieved low detection limits, and exhibited high selectivity.

There are also studies in the literature on the simultaneous determination of SER with other neurotransmitters. For example, Mool-am-kha et al., (2020) improved a novel sensor using SPCE modified with carbon nanotubes/nickel oxide/carbon black/Nafion (CNT-NiO-CB/Nafion) composites for the simultaneous electrochemical analysis of SER and DA. Nafion was used to obtain a suitable stable complex by combining CNT and NiO composite. The suggested sensor demonstrated a broad detection range and low detection limit for both analytes. Kabaca et al., (2023) developed a new sensor with titanium dioxide NPs (TiO_2NPs), AuNPs, and poly Nile blue (PNB_{DES})-modified SPCEs prepared in DES for the simultaneous electrochemical analysis of SER and DA. TiO_2NPs facilitate electrochemical reactions as a good semiconductor material, while AuNPs increase the oxidation of analytes due to their high conductivity and catalytic properties. PNB_{DES} was used as a substance to increase the conductivity of the electrode surface and facilitate the interaction of SER and DA with the modified electrode. The developed sensor demonstrated an extensive linear range and a low detection limit for

both SER and DA. Moslah et al., (2024) modified the silver NPs (AgNPs) based reduced graphene oxide (RGO) composite (AgNPs-RGO), produced using an environmentally friendly green synthesis method, onto the surface of SPCEs and used it for the simultaneous detection of SER and DA. The designed sensor increased the oxidation efficiency of DA and SER, while two distinct peaks were obtained in voltammetric measurements without requiring any additional processing before each measurement. It was stated that the distinct separation in the oxidation peaks of DA and SER was due to the synergistic effects of the surface area of RGO and the superior electrochemical conductivity of AgNPs. A broad detection range and low detection limit were acquired for both DA and SER with the improved sensor. Cuhadar et al., (2024) modified screen-printed gold electrodes (Au-SPE) with thiol-modified DA and SER aptamers and used them for the simultaneous detection of SER and DA. The utilization of aptamers, synthetic oligonucleotides capable of selectively binding to target molecules, offers enhanced specificity and sensitivity. The developed biosensor demonstrated a broad detection range and low detection limit for DA and SER. Núñez et al., (2024) modified screen-printed reduced graphene oxide electrodes (RGO-SPE) with Cu (II) triazole complex ($\text{Cu}(\text{L}^{\text{NO}_2})_2$) and used them for the simultaneous determination of SER and 17β -Estradiol. It showed very good electrochemical properties due to the synergistic impact between the triazole ring and the phenyl ring of the ($\text{Cu}(\text{L}^{\text{NO}_2})_2$) complex. The interaction between the ($\text{Cu}(\text{L}^{\text{NO}_2})_2$) complex and RGO made the electrochemical oxidation of analytes more efficient. The proposed sensor showed high sensitivity and a wide linear range for both analytes.

CONCLUSIONS AND FUTURE TRENDS

In this review, we have discussed different SPE-based SER sensors. Different strategies used to increase the selectivity and sensitivity of the proposed SER sensors have shown very promising results. However, there are still areas for improvement. Metallic NPs

have been used due to their biocompatibility and ability to enhance electron transfer between molecules. One of the major limitations of such systems is the reduction of particle aggregation during immobilization on transducer surfaces. A method to increase the stabilization of particles involves the use of conductive polymers that can coat the electrode surface and support stable connections with the NPs. This could be a potential improvement for some sensors; the addition of conductive polymers to the SPE surface can increase stability by supporting the interaction between the NPs and the modified SPE. Using carbon materials as a platform seems essential for the enhancement of mass transport and hence electrochemical signals. In fact, several reports on the use of SPE for electrochemical analysis have shown promising results using nanomaterials such as graphene, carbon nanotubes, or even multi-walled carbon nanotubes. The advantages of using such materials include better charge transfer across the electrode/electrolyte interface, a larger electrochemical field, and high mechanical strength. Modification of SPEs is another simple and cost-effective way to modify the electrode surface and increase the electron transfer with the analyte.

Furthermore, the need to detect SER at physiological levels, it is also important to implement SER detection methods that can be used in *in vivo* applications and can be suitably adapted to monitor the dynamic range of the neurotransmitter. The utilization of SPEs as a basis for the improvement of electrochemical sensors stands out due to their advantages such as easy portability and miniaturization, low cost, possibility of mass production, and good electrochemical performance. Although several SPE-based sensors for SER determination are discussed in this review, there are not many commercial options on the market, especially for sensors based on SPEs. For example, the flexibility of SPEs prepared using polyester material may make them ideal for the development and commercialization of wearable sensors. Improvement of SPEs electrodes by chemical or thermal treatments, addition of a third layer, or even using a hybrid preparation method of the electrodes may lead to improved SER sensors based on SPEs. We hope to stimulate the development of this field by revealing the

important features discussed to achieve more cost-effective, efficient, and user-friendly electrochemical sensors for the quantification of this important neurotransmitter which is SER.

REFERENCES

- Abad-Gil, L., Procopio, J. R., Brett, C. M. (2021). Binary and ternary deep eutectic solvent mixtures: Influence on methylene blue electropolymerisation. *Electrochemistry Communications*, 124, 106967.
- Ahamed, A., Ge, L., Zhao, K., Veksha, A., Bobacka, J. and Lisak, G. (2021). Environmental footprint of voltammetric sensors based on screen-printed electrodes: An assessment towards “green” sensor manufacturing. *Chemosphere*, 278, 130462.
- Atici, T., Kamaç, M. B., Yılmaz, M. and Kabaca, A. Y. (2023). Zinc oxide nanorod/polymethylene blue (deep eutectic solvent)/gold nanoparticles modified electrode for electrochemical determination of serotonin (5-HT). *Electrochimica Acta*, 458, 142484.
- Bilgi Kamaç, M., Altun, M., Yılmaz, M. and Sezgintürk, M. K. (2023a). A label-free dual immunosensor for the simultaneous electrochemical determination of CA125 and HE4 biomarkers for the early diagnosis of ovarian cancer. *Analytical and Bioanalytical Chemistry*, 415(9), 1709-1718.
- Bilgi Kamaç, M., Altun, M., Yılmaz, M., Yılmaz Aktan, A., Aktan, S. and Sezgintürk, M. K. (2023b). Point-of-care testing: a disposable label-free electrochemical CA125 and HE4 immunosensors for early detection of ovarian cancer. *Biomedical Microdevices*, 25(2), 18.
- Bilgi, M. and Ayranci, E. (2018). Development of amperometric biosensors using screen-printed carbon electrodes modified with conducting polymer and nanomaterials for the analysis of ethanol, methanol and their mixtures. *Journal of Electroanalytical Chemistry*, 823, 588-592.
- Bilgi, M., Sahin, E. M. and Ayranci, E. (2018). Sensor and biosensor application of a new redox mediator: Rosmarinic acid modified screen-printed carbon electrode for electrochemical determination of NADH and ethanol. *Journal of Electroanalytical Chemistry*, 813, 67-74.

- Birmes, P., Coppin, D., Schmitt, L., Lauque, D. (2003). Serotonin syndrome: a brief review. *Canadian Medical Association Journal*, 168(11): 1439-1442.
- Boonkaew, S., Dettlaff, A., Sobaszek, M., Bogdanowicz, R., Jönsson-Niedziółka, M. (2022). Electrochemical determination of neurotransmitter serotonin using boron/nitrogen co-doped diamond-graphene nanowall-structured particles. *Journal of Electroanalytical Chemistry*, 926, 116938.
- Buckley, N. A., Dawson, A. H., Isbister, G. K. (2014). Serotonin syndrome. *British Medical Journal*, 348.
- Cernat, A., Ștefan, G., Tertis, M., Cristea, C., Simon, I. (2020). An overview of the detection of serotonin and dopamine with graphene-based sensors. *Bioelectrochemistry*, 136: 107620.
- Coyle, V. E., Brothers, M. C., McDonald, S. and Kim, S. S. (2024). Superlative and Selective Sensing of Serotonin in Undiluted Human Serum Using Novel Polystyrene Sulfonate Conductive Polymer. *ACS omega*, 9(14), 16800-16809.
- Cuhadar, S. N., Durmaz, H., Yildirim-Tirgil, N. (2024). Multi-detection of serotonin and dopamine based on an electrochemical aptasensor. *Chemical Papers*, 78(12), 7175-7185.
- Danaceau, J. P., Anderson, G. M., McMahon, W. M., Crouch, D. J. (2003). A liquid chromatographic-tandem mass spectrometric method for the analysis of serotonin and related indoles in human whole blood. *Journal of analytical toxicology*, 27(7): 440-444.
- Darwish, I. A., Refaat, I. H. (2006). Spectrophotometric analysis of selective serotonin reuptake inhibitors based on formation of charge-transfer complexes with tetracyanoquinodimethane and chloranilic acid. *Journal of AOAC International*, 89(2): 326-333.
- Dăscălescu, D., Apetrei, C. (2022). Development of a novel electrochemical biosensor based on organized mesoporous carbon and laccase for the detection of serotonin in food supplements. *Chemosensors*, 10(9), 365.
- Fahem, D. K., El Houssini, O. M., Abd El-Rahman, M. K. and Zaazaa, H. E. (2019). A point of care screen printed potentiometric sensor for therapeutic monitoring of vecuronium. *Microchemical Journal*, 147, 532-537.

- García-Mendiola, T., Requena-Sanz, S., Martínez-Periñán, E., Bravo, I., Pariente, F. and Lorenzo, E. (2020). Influence of carbon nanodots on DNA-Thionine interaction. Application to breast cancer diagnosis. *Electrochimica Acta*, 353, 136522.
- Gubala, V., Harris, L. F., Ricco, A. J., Tan, M. X., Williams, D. E. (2012). Point of care diagnostics: status and future. *Analytical chemistry*, 84(2), 487-515.
- Hasanzadeh, M., Shadjou, N., de la Guardia, M. (2017). Current advancement in electrochemical analysis of neurotransmitters in biological fluids. *TrAC Trends in Analytical Chemistry*, 86: 107-121.
- Hassan, R. A., Heng, L. Y. and Tan, L. L. (2019). Novel DNA biosensor for direct determination of carrageenan. *Scientific reports*, 9(1), 6379.
- He, Q., Li, M., Wang, X., Xia, Z., Du, Y., Li, Y., Shang, J. (2019). A simple, efficient and rapid HPLC–UV method for the detection of 5-HT in RIN-14B cell extract and cell culture medium. *BMC chemistry*, 13(1): 1-9.
- Hosu, O., Barsan, M. M., Săndulescu, R., Cristea, C., Brett, C. M. (2021). Hybrid nanocomposite platform, based on carbon nanotubes and poly (methylene blue) redox polymer synthesized in ethaline deep eutectic solvent for electrochemical determination of 5-aminosalicylic acid. *Sensors*, 21(4), 1161.
- Hou, S., Zhang, A., Su, M. (2016). Nanomaterials for biosensing applications. *Nanomaterials*, 6(4): 58.
- Ilanchezhiyan, P., Manikandan, R., Sekar, S., Lee, D. J., Jeon, H. C., Lee, S., Kim, D. Y. (2024). Two dimensional FeVO₄ nanoflakes decorated on Ti₃C₂ MXene hybrid nanocomposites as a novel effective electrochemical biosensor for ultrasensitive and selective detection of serotonin (5-HT). *Applied Surface Science*, 161411.
- Jeromiyas, N., Elaiyappillai, E., Kumar, A. S., Huang, S. T. and Mani, V. (2019). Bismuth nanoparticles decorated graphenated carbon nanotubes modified screen-printed electrode for mercury detection. *Journal of the Taiwan Institute of Chemical Engineers*, 95, 466-474.

- Jones, B. J., Blackburn, T. P. (2002). The medical benefit of 5-HT research. *Pharmacology Biochemistry and Behavior*, 71(4): 555-568.
- Kabaca, A. Y., Kamaç, M. B., Yılmaz, M. and Atıcı, T. (2023). Ultra-sensitive electrochemical sensors for simultaneous determination of dopamine and serotonin based on titanium oxide-gold nanoparticles-poly Nile blue (in deep eutectic solvent). *Electrochimica Acta*, 467, 143046.
- Kampeera, J., Pasakon, P., Karuwan, C., Arunrut, N., Sappat, A., Sirithammajak, S., Dechokiattawan, N., Sumranwanich, T., Chaivisuthangkur, P., Ounjai, P., Chankhamhaengdech, S., Wisitsoraat, A., Tuantranont, A. and Kiatpathomchai, W. (2019). Point-of-care rapid detection of *Vibrio parahaemolyticus* in seafood using loop-mediated isothermal amplification and graphene-based screen-printed electrochemical sensor. *Biosensors and Bioelectronics*, 132, 271-278.
- Kerage, D., Sloan, E. K., Mattarollo, S. R., McCombe, P. A. (2019). Interaction of neurotransmitters and neurochemicals with lymphocytes. *Journal of neuroimmunology*, 332: 99-111.
- Khoshnevisan, K., Honarvarfard, E., Torabi, F., Maleki, H., Baharifar, H., Faridbod, F., Khorramizadeh, M. R. (2020). Electrochemical detection of serotonin: a new approach. *Clinica Chimica Acta*, 501: 112-119.
- Kundys-Siedlecka, M., Bącznyńska, E., Jönsson-Niedziółka, M. (2019). Electrochemical detection of dopamine and serotonin in the presence of interferences in a rotating droplet system. *Analytical chemistry*, 91(16), 10908-10913.
- Li, J., Si, Y., Park, Y. E., Choi, J. S., Jung, S. M., Lee, J. E., Lee, H. J. (2021). A serotonin voltammetric biosensor composed of carbon nanocomposites and DNA aptamer. *Microchimica Acta*, 188, 1-8.
- Lin, S. H., Lee, L. T., Yang, Y. K. (2014). Serotonin and mental disorders: a concise review on molecular neuroimaging evidence. *Clinical Psychopharmacology and Neuroscience*, 12(3): 196.
- Ma, L., Zhao, T., Zhang, P., Liu, M., Shi, H., Kang, W. (2020). Determination of monoamine neurotransmitters and metabolites by high-performance liquid chromatography based on Ag (III)

- complex chemiluminescence detection. *Analytical biochemistry*, 593: 113594.
- Manasa, G., Mascarenhas, R. J., Satpati, A. K., D'Souza, O. J., Dhason, A. (2017). Facile preparation of poly (methylene blue) modified carbon paste electrode for the detection and quantification of catechin. *Materials Science and Engineering: C*, 73, 552-561.
- Maximino, C. (2012). *Serotonin and anxiety: Neuroanatomical, pharmacological, and functional aspects*. Springer Science Business Media.
- Misia, G., Evangelisti, C., Merino, J. P., Pitzalis, E., Abelairas, A. M., Mosquera, J., Criado, A., Prato, M. and Silvestri, A. (2024). Design and optimization of an electrochemical sensor based on carbon nanotubes for the reliable voltammetric detection of serotonin in complex biological fluids. *Carbon*, 229, 119550.
- Mool-Am-Kha, P., Themsirimongkon, S., Saipanya, S., Saianand, G., Tuantranont, A., Karuwan, C., Jakmune, J. (2020). Hybrid electrocatalytic nanocomposites based on carbon nanotubes/nickel oxide/nafion toward an individual and simultaneous determination of serotonin and dopamine in human serum. *Bulletin of the Chemical Society of Japan*, 93(11), 1393-1400.
- Moon, J. M., Thapliyal, N., Hussain, K. K., Goyal, R. N., Shim, Y. B. (2018). Conducting polymer-based electrochemical biosensors for neurotransmitters: A review. *Biosensors and Bioelectronics*, 102: 540-552.
- Moru, S., Sunil Kumar, V., Kummari, S. and Yugender Goud, K. (2023). A disposable screen printed electrodes with hexagonal Ni (OH) ₂ nanoplates embedded chitosan layer for the detection of depression biomarker. *Micromachines*, 14(1), 146.
- Moslah, M., Dridi, C. (2024). Development of An Eco-Friendly and cost-effective electrochemical sensor for the simultaneous detection of dopamine and serotonin. *Journal of The Electrochemical Society*.
- Motsaathebe, P. C., Fayemi, O. E. (2021). Serotonin electrochemical detection in tomatoes at MWCNT-AONP nanocomposite modified electrode. *Materials Research Express*, 8(11), 115004.

- Mullani, S. B., Dhodamani, A. G., Shellikeri, A., Mullani, N. B., Tawade, A. K., Tayade, S. N., Delekar, S. D. (2020). Structural refinement and electrochemical properties of one dimensional (ZnO NRs) $1-x$ (CNs) x functional hybrids for serotonin sensing studies. *Scientific reports*, 10(1), 15955.
- Núñez, C., Nelson, R., Tabilo, G., Pefaur, P., Castillo, R., Mestra, A. (2024). Simultaneous detection of serotonin and 17β -Estradiol using rGO/SPCE modified with Cu (II) complex: A novel approach for PMDD diagnosis. *Chemosensors*, 12(8), 164.
- Roychoudhury, A., Francis, K. A., Patel, J., Jha, S. K., Basu, S. (2020). A decoupler-free simple paper microchip capillary electrophoresis device for simultaneous detection of dopamine, epinephrine and serotonin. *RSC advances*, 10(43): 25487-25495.
- Salova, A., Mahmud, S. F., Almasoudie, N. K. A., Mohammed, N., Albeer, A. A. and Amer, R. F. (2024). CuO-Cu₂O nanostructures as a sensitive sensing platform for electrochemical sensing of dopamine, serotonin, acetaminophen, and caffeine substances. *Inorganic Chemistry Communications*, 161, 112065.
- Samie, H.A., Arvand, M. (2019) RuO₂ nanowires on electrospun CeO₂-Au nanofibers/functionalized carbon nanotubes/graphite oxide nanocomposite modified screen-printed carbon electrode for simultaneous determination of serotonin, dopamine and ascorbic acid. *Journal of Alloys and Compounds*, 782, 824-836.
- Satyanarayana, M., Goud, K. Y., Reddy, K. K. and Gobi, K. V. (2015). Biopolymer stabilized nanogold particles on carbon nanotube support as sensing platform for electrochemical detection of 5-fluorouracil in-vitro. *Electrochimica Acta*, 178, 608-616.
- Satyanarayana, M., Goud, K. Y., Reddy, K. K., Kumar, V. S. and Gobi, K. V. (2019). Silver nanoparticles impregnated chitosan layered carbon nanotube as sensor interface for electrochemical detection of clopidogrel in-vitro. *Materials Science and Engineering: C*, 101, 103-110.
- Schwarz, J., Trommer, K. and Mertig, M. (2016). Novel Screen-printed all-solid-state copper (II)-selective electrode for mobile environmental analysis. *American Journal of Analytical Chemistry*, 7(07), 525.

- Si, B., Song, E. (2018). Recent advances in the detection of neurotransmitters. *Chemosensors*, 6(1): 1.
- Song, J., Wang, L., Qi, H., Qi, H., Zhang, C. 2019. Highly selective electrochemical method for the detection of serotonin at carbon fiber microelectrode modified with gold nanoflowers and overoxidized polypyrrole. *Chinese Chemical Letters*, 30(9): 1643-1646.
- Su, H., Li, S., Jin, Y., Xian, Z., Yang, D., Zhou, W., Kerman, K. (2017). Nanomaterial-based biosensors for biological detections. *Advanced Health Care Technologies*, 3: 19-29.
- Uwaya, G. E., Fayemi, O. E. (2020). Electrochemical detection of serotonin in banana at green mediated PPy/Fe₃O₄NPs nanocomposites modified electrodes. *Sensing and Bio-Sensing Research*, 28, 100338.
- Vurro, D., Pasquardini, L., Borriello, M., Foresti, R., Barra, M., Sidoli, M., Pontiroli, D., Fornasini, L., Aversa, L., Verucchi, R., D'Angelo, P and Tarabella, G. (2024). Inflammatory biomarker detection in saliva samples by printed graphene immunosensors. *Sensors and Actuators Reports*, 100211.
- Wang, C., Wang, T., Li, Z., Xu, X., Zhang, X., Li, D. (2021). An electrochemical enzyme biosensor for ammonium detection in aquaculture using screen-printed electrode modified by gold nanoparticle/polymethylene blue. *Biosensors*, 11(9), 335.
- Wu, B., Yeasmin, S., Liu, Y., Cheng, L. J. (2022). Sensitive and selective electrochemical sensor for serotonin detection based on ferrocene-gold nanoparticles decorated multiwall carbon nanotubes. *Sensors and Actuators B: Chemical*, 354, 131216.
- Yilmaz, M., and Bilgi, M. (2024). A disposable impedimetric immunosensor for the analysis of CA125 in human serum samples. *Biomedical Microdevices*, 26(1), 8.
- Young, S. N., Leyton, M. (2002). The role of serotonin in human mood and social interaction: insight from altered tryptophan levels. *Pharmacology Biochemistry and Behavior*, 71(4): 857-865.
- Yousefi, A., Babaei, A. and Delavar, M. (2018). Application of modified screen-printed carbon electrode with MWCNTs-Pt-doped CdS nanocomposite as a sensitive sensor for determination

of natamycin in yoghurt drink and cheese. *Journal of Electroanalytical Chemistry*, 822, 1-9.

Yuhana Ariffin, E., Heng, L. Y., Tan, L. L., Abd Karim, N. H. and Hasbullah, S. A. (2020). A highly sensitive impedimetric DNA biosensor based on hollow silica microspheres for label-free determination of *E. coli*. *Sensors*, 20(5), 1279.

CHAPTER 12

EFFECTS OF PHYSIOLOGICAL CHANGES DURING PREGNANCY ON DRUG PHARMACOKINETICS

Assist. Prof. Dr. Sema GÜLER¹

DOI: <https://dx.doi.org/10.5281/zenodo.14259280>

¹ Ankara Medipol University, Faculty of Medicine, Department of Internal Medical Sciences, Ankara, Türkiye. sema.guler@ankaramedipol.edu.tr, Orcid ID: 0000-0003-4975-3831

PHYSIOLOGICAL CHANGES DURING PREGNANCY

Pregnancy induces significant anatomical and physiological changes across nearly all body systems, profoundly affecting the pharmacokinetics and pharmacodynamics of therapeutic agents. Understanding these changes is crucial for effective medical management during pregnancy" (Feghali et al., 2015; Costantine, 2014; Abduljalil et al., 2012).

Cardiovascular Changes

In the cardiovascular system, pregnancy leads to a 30-50% increase in cardiac output (CO), driven by elevated heart rate and stroke volume. Early in pregnancy, the CO rise is mainly due to increased stroke volume, while later it results from a higher heart rate. Alongside increased CO, systemic and pulmonary vascular resistances decrease significantly. Systemic vascular resistance reaches its lowest between 14 and 24 weeks, then gradually returns to pre-pregnancy levels. Blood pressure typically falls by the end of the first trimester and rises back in the third trimester. These changes can cause physiological hypotension and influence drug distribution by increasing the volume of distribution for hydrophilic substances and raising free levels of highly protein-bound drugs due to decreased albumin" (Capeless and Clapp, 1989; Duvekot and Peeters, 1994).

Respiratory System Changes

Respiratory adaptations include increased estrogen levels causing hypervascularity and edema in the upper respiratory mucosa, leading to higher incidences of rhinitis and epistaxis. Progesterone enhances respiratory center sensitivity to carbon dioxide, resulting in a 30-50% increase in minute ventilation due to elevated tidal volume. This increases arterial oxygen partial pressure and decreases PaCO₂, facilitating efficient carbon dioxide transfer from the fetus to the mother. Maternal respiratory rate and vital capacity remain unchanged. These changes may theoretically enhance drug absorption in the respiratory tract, but no increased toxicity has been observed" (Chapman et al., 2021; Nelson-Piercy, 2001)

Renal Physiological Changes

Renal physiology undergoes significant changes, with a 50% increase in renal blood flow leading to a similar rise in glomerular filtration rate (GFR). This results in increased creatinine clearance and decreased serum creatinine and urea levels. Progesterone promotes natriuresis, while estrogen supports sodium retention. Despite increased GFR causing more sodium loss, high aldosterone levels reabsorb sodium in the distal nephron, leading to net water and sodium retention. This causes significant increases in total body water and slight decreases in serum sodium concentration and osmolality. These changes can shorten the half-lives of renally cleared drugs and increase the volume of distribution for hydrophilic agents" (Beers and Patel, 2020; Brunskill, 2019).

Gastrointestinal Changes

The gastrointestinal system is affected by progesterone-induced inhibition of smooth muscle activity, leading to delayed gastric emptying and prolonged small intestinal transit time. Increased intra-abdominal pressure contributes to gastroesophageal reflux. Elevated serum gastrin levels may increase gastric acidity. Constipation is common due to slower intestinal transit, mechanical obstruction from the growing uterus, decreased maternal activity, reduced motilin levels, increased colonic water and sodium absorption, and routine iron supplementation. Liver function tests generally remain unchanged, but serum alkaline phosphatase levels rise due to placental production. Elevated levels of serum cholesterol, fibrinogen, certain coagulation factors, and binding globulins are observed, likely mediated by estrogen. Decreased gallbladder motility increases the risk of gallstones. These gastrointestinal changes can delay drug absorption and prolong the onset of action for orally administered medications" (Alqudah et al., 2022; Al-Shboul et al., 2018

Hematological Changes

Hematological changes include increased white blood cell counts, primarily neutrophils, while lymphocyte counts decrease in the first

two trimesters before normalizing. Monocyte counts and the monocyte-lymphocyte ratio increase. Red blood cell mass rises by 30%, driven by increased erythropoietin production, coinciding with a larger plasma volume increase, leading to 'physiological anemia of pregnancy.' This anemia peaks at 30-32 weeks and is advantageous as it reduces blood viscosity, improving uterine perfusion, and minimizes blood loss during delivery. Pregnancy induces a hypercoagulable state, with increased levels of fibrinogen, certain coagulation factors, and von Willebrand factor, while factor XI decreases. Protein S levels drop, enhancing thromboembolism risk but reducing postpartum hemorrhage" (Cerneca et al., 1997; Tanaka et al., 2019).

Endocrine Changes

Endocrine changes are profound, with pregnancy considered a diabetogenic state due to increased insulin resistance from elevated hormones like human placental lactogen, progesterone, estrogen, and cortisol. Gestational diabetes reflects carbohydrate intolerance during pregnancy. Pancreatic beta cells undergo hyperplasia, increasing insulin production, leading to fasting hypoglycemia and postprandial hyperglycemia, ensuring a steady glucose supply to the fetus. Maternal serum leptin levels rise, peaking in the second trimester, with leptin also produced by the placenta" (Szlapski et al., 2020; Moyce and Dolinsky, 2018).

Thyroid function adapts to increased demands; thyroid-binding globulin levels rise due to elevated estrogen, necessitating higher thyroid hormone production. The slight thyrotropic effect of hCG, increased maternal metabolic rate, and greater transplacental transfer of thyroid hormones contribute to these changes. TSH levels decrease in the first half of pregnancy due to negative feedback, with the upper normal limit being 2.5 mIU/L. Free cortisol levels increase by 30%. Serum parathyroid hormone and 1,25-dihydroxy vitamin D levels rise to support fetal calcium accumulation, facilitated by a placental calcium pump. The anterior pituitary enlarges 2-3 times, increasing the risk of pituitary infarction in cases of postpartum hypotension, such as Sheehan's syndrome. In summary, pregnancy induces extensive

physiological changes across various systems, significantly impacting drug pharmacokinetics and dynamics. These adaptations ensure fetal support and development but necessitate careful consideration in the pharmacological management of pregnant patients" (Pangkahila and Tangkas, 2023; Hershman, 2004).

THE EFFECT OF PREGNANCY ON DRUG PHARMACOKINETICS

Physiological changes during pregnancy can significantly alter the pharmacokinetics of certain drugs. Whether these changes are clinically significant depends on various factors, notably the drug's therapeutic range. Drugs with a narrow therapeutic range—such as cyclosporine, tacrolimus, lithium, warfarin, carbamazepine, valproic acid, phenytoin, digoxin, vancomycin, and aminoglycosides—are particularly sensitive because therapeutic and toxic concentrations are close. Small fluctuations in drug levels can render these medications ineffective if concentrations drop or cause toxicity if they rise. A 25% respiratory change in concentration is considered clinically significant for these drugs" (Coppola et al., 2023; Jogiraju et al., 2017).

For drugs with a wide therapeutic range, minor pharmacokinetic changes usually have minimal clinical impact. However, during pregnancy, some drugs may experience 2- to 6-fold changes in exposure, potentially affecting even those with a broader safety margin. Such alterations may necessitate dosage adjustments to maintain therapeutic efficacy. In some instances, the pharmacokinetic changes are so substantial that switching medications is advisable" (Moreira et al., 2022; Coppola et al., 2022).

An example is metoprolol, whose oral concentrations can decrease by 2 to 4 times during pregnancy. Due to this variability, alternative beta-blockers like atenolol, which is eliminated via the kidneys, might be preferred for heart rate control in pregnant patients. Atenolol tends to provide more consistent and reliable drug levels despite renal changes during pregnancy. While beta-blockers carry fetal risks like intrauterine growth restriction, if their use is essential, selecting an agent that consistently achieves the desired therapeutic

effect is crucial. This underscores the importance of considering pharmacokinetic changes when choosing medications during pregnancy" (Tanaka et al., 2016; Duan et al., 2018).

Pharmacokinetic Parameters: Extraction Ratio, AUC, and Bioavailability

During pregnancy, physiological changes can significantly alter the pharmacokinetics of drugs, making it essential to understand key pharmacokinetic parameters and their implications. One such parameter is the Extraction Ratio (ER), which measures the proportion of a drug metabolized and eliminated as it passes through an organ like the liver. The ER helps predict how intrinsic clearance, protein binding, and blood flow affect a drug's pharmacokinetics. For drugs with a high ER, variations in blood flow greatly impact drug clearance, whereas intrinsic clearance and protein binding are more influential for drugs with a low ER. Understanding the ER is crucial for optimizing drug dosing to maintain therapeutic effectiveness and safety during pregnancy" (Wilkinson and Shand, 1975; Li and Jusko, 2023).

Another vital parameter is the Area Under the Concentration-Time Curve (AUC), representing the total systemic exposure to a drug. Since direct measurement at the site of action is often impractical, blood, plasma, or serum concentrations are used to calculate the AUC. The AUC depends on the drug's dose, clearance, and bioavailability. For certain drugs, the AUC is the primary determinant of efficacy and safety; for others, peak or trough concentrations may better correlate with clinical outcomes. In low ER drugs, increased enzyme activity or decreased plasma protein binding lowers the total AUC without being affected by blood flow changes. In high hepatic ER drugs administered intravenously, decreased blood flow increases the total AUC, while enzyme activity and protein binding have no effect. For orally administered high ER drugs, reductions in clearance due to decreased blood flow are offset by corresponding decreases in bioavailability, resulting in no net effect on the oral AUC. However, increased enzyme activity or decreased plasma protein binding can reduce the total AUC by affecting oral bioavailability" (Anderson, 2006; Tzimas et al., 1997).

Bioavailability itself—the fraction of an administered dose that reaches systemic circulation unchanged—is influenced by pregnancy-related physiological changes. For orally administered drugs, bioavailability hinges on the amount absorbed from the intestine and the extent of first-pass metabolism in the intestine and liver. In drugs with a low hepatic ER, bioavailability remains unaffected by changes in enzyme activity, hepatic blood flow, or protein binding. Conversely, in high ER drugs, bioavailability decreases with increased enzyme activity, reduced hepatic blood flow, or decreased plasma protein binding. Pregnancy can further affect bioavailability through changes in gastric acidity, prolonged gastrointestinal transit time, and duodenal villus hypertrophy, all of which can alter drug absorption" (Yan, 2017; Anderson, 2006).

In summary, pregnancy can modify pharmacokinetic parameters such as ER, AUC, and bioavailability through alterations in enzyme activity, protein binding, blood flow, and gastrointestinal physiology. These changes impact drug absorption, metabolism, and overall exposure, underscoring the importance of adjusting dosing strategies and monitoring drug levels to ensure therapeutic efficacy and safety in pregnant patients" (Abduljalil et al., 2012; Anderson, 2006).

Clearance is a crucial pharmacokinetic parameter describing how effectively the body metabolizes and eliminates drugs, impacting total drug exposure and steady-state concentrations, and informing maintenance dosing. Hepatic clearance depends on hepatic blood flow, protein binding, and the intrinsic activity of liver enzymes. For drugs with a high hepatic extraction ratio (ER), clearance is significantly influenced by hepatic blood flow because the rate-limiting step is drug delivery to the liver; increased blood flow enhances clearance. Visualizing the liver as an elimination organ where faster delivery leads to quicker clearance can be helpful" (Mehvar, 2016; Groszmann, 2007). In contrast, for drugs with a low ER, clearance is not affected by blood flow but is determined by enzyme activity and protein binding. An increase in enzyme activity or a decrease in protein binding can raise total drug clearance. Physiological, pathological, and drug-induced changes can modify these parameters, altering systemic clearance and

oral bioavailability, which affects patient responses to medications. For drugs with an intermediate ER, clearance is dependent on a combination of changes in enzyme activity, protein binding, and organ blood flow" (Rowland, 1984; Shen et al., 1997).

Protein Binding and Its Effects During Pregnancy

Protein binding is a critical factor influencing drug pharmacokinetics, and pregnancy induces physiological changes that can significantly affect this binding. During normal pregnancy, plasma protein levels, particularly albumin and alpha-1-acid glycoprotein, decrease. Albumin concentrations drop by approximately 1% at 8 weeks, 10% at 20 weeks, and 13% at 32 weeks of gestation. In pregnant patients with pathological conditions, albumin levels may be even lower. These reductions impact the binding of drugs like phenytoin, valproic acid, and carbamazepine, which are highly albumin-bound" (Coppola et al., 2023; Bardy et al., 1990).

Alpha-1-acid glycoprotein levels are reported to be 52% lower in late pregnancy compared to the postpartum period. This protein binds to drugs such as betamethasone, bupivacaine, lopinavir, and lidocaine, affecting their pharmacokinetics. Some drugs, like cyclosporine and tacrolimus, concentrate in red blood cells. Anemia during pregnancy can alter their binding due to decreased hematocrit levels, which drop by about 2% at 8 weeks and 4% between 20-32 weeks" (Honda et al., 1990; Wood and Wood, 1981).

Disease states during pregnancy can exacerbate anemia, further influencing drug binding. Conversely, certain plasma proteins increase during pregnancy. Corticosteroid-binding globulin (CBG) binds glucocorticoids like cortisol and progesterone and can increase by 2-3 times during pregnancy. This elevation affects the binding of drugs such as prednisone and prednisolone" (Nenke et al., 2017; Hodyl et al., 2020).

Understanding drug binding is essential for two primary reasons:

1. **Active Drug Fraction:** The unbound (free) drug is in equilibrium with the site of action and is considered the active form

capable of crossing membranes like the placenta. Changes in protein binding can lead to increased unbound drug levels, potentially causing toxicity. For example, phenytoin, which is highly albumin-bound, can have increased unbound fractions due to decreased albumin levels in pregnancy. Yerby and colleagues reported significant increases in the percentage of unbound phenytoin during the second and third trimesters and at delivery compared to pre-pregnancy levels. Given phenytoin's narrow therapeutic range, this increase in unbound drug is clinically significant" (Musteata, 2012; Sallustio and Morris, 1992).

2. Interpreting Total Drug Concentrations: Protein binding affects the interpretation of total drug concentrations measured in plasma. For drugs like phenytoin, it's crucial to know if protein binding has changed when evaluating total concentrations. Changes in protein binding necessitate either measuring unbound drug concentrations or adjusting the interpretation of total concentrations to account for altered binding (Coppola et al., 2023; Schalkwijk et al., 2017).

An illustrative example involves two scenarios where the unbound drug concentration remains the same, but the total concentration differs due to changes in protein binding. In one case, the total concentration is 10 with an unbound concentration of 1; in the other, the total concentration is 5 with the unbound concentration still at 1. Despite the total concentration halving, no dose adjustment is needed because the active unbound drug level is unchanged. This situation can occur when protein binding decreases without changes in enzyme activity, affecting total clearance but not unbound clearance (Celestin and Musteata, 2021; Wu et al., 2012).

For drugs like prednisone and prednisolone, which bind extensively to albumin and CBG, increased CBG levels during pregnancy enhance their protein binding. Although total prednisolone clearance is lower during pregnancy, unbound clearance remains unchanged, indicating that dose adjustments may not be necessary based solely on pharmacokinetic data. However, this doesn't account for immunological changes during pregnancy. Additionally, prednisone and prednisolone binding is a saturable process, leading to increased

variability and higher unbound fractions at elevated concentrations (Ionita et al., 2014; Ko et al., 1995).

Another scenario is when total drug concentrations remain unchanged, but decreased protein binding leads to increased unbound drug levels, potentially causing toxicity. For highly bound drugs with narrow therapeutic ranges, such as phenytoin, it's important to measure unbound concentrations or adjust total concentrations mathematically to account for binding changes, especially in pregnant patients with low albumin levels (Coppola et al., 2023; Knott et al., 1986).

Tacrolimus binds to red blood cells, albumin, and alpha-1-acid glycoprotein—all reduced during pregnancy. Studies report a 39% higher mean oral clearance of tacrolimus during mid to late pregnancy compared to the postpartum period. While this might suggest the need for increased dosing, the unbound oral clearance of tacrolimus doesn't change, and the percentage of unbound drug nearly doubles during pregnancy. Measuring only total concentrations without considering binding changes could lead to inappropriate dose increases and potential toxicity (Zheng et al., 2012; Hebert et al., 2013).

Physiological changes in pregnancy can alter multiple pharmacokinetic parameters, affecting drug concentration interpretations. Both protein binding and unbound clearance can change, as seen with phenytoin, requiring clinicians to consider both factors when evaluating drug levels. It's also important to note that not all highly protein-bound drugs exhibit increased unbound fractions during pregnancy. Some, like midazolam and glyburide, show minimal changes in protein binding but significant alterations in clearance (Coppola et al., 2023; Gaohua et al., 2012).

In conclusion, pregnancy-induced changes in protein binding and other pharmacokinetic parameters necessitate careful monitoring and interpretation of drug concentrations to ensure therapeutic efficacy and avoid toxicity. This is particularly critical for drugs with narrow therapeutic ranges and high protein binding. Clinicians must account for these physiological changes to make informed dosing decisions during pregnancy (Coppola et al., 2023; Wang et al., 2017).

Changes in Organ Blood Flow and Impact on Drugs

Changes in organ blood flow during pregnancy, especially in the liver and kidneys, can significantly impact drug clearance, notably for drugs with a high extraction ratio (ER). Cardiac output increases markedly during pregnancy—by about 35% in the second trimester and 40% in the third trimester compared to postpartum levels. While some studies suggest that hepatic blood flow increases during the third trimester, findings are inconsistent, and it remains unclear whether liver blood flow increases or stays the same during pregnancy. Limitations in study designs, such as small sample sizes and lack of control groups, contribute to this uncertainty (Robson et al., 1990; Mehvar, 2016).

In contrast, renal blood flow and glomerular filtration rate are known to increase substantially during pregnancy, by approximately 50–85% and 50% respectively. This leads to enhanced renal filtration, increased creatinine clearance, and greater renal clearance of drugs. For medications like metformin, which have a moderately high tubular ER, the increased renal plasma flow can partly explain the observed changes in renal and secretory clearance during pregnancy (Din and Al Amir, 2019; Milliez et al., 1982).

Intrinsic clearance refers to the liver's inherent ability to metabolize drugs through enzyme activity, independent of protein binding and hepatic blood flow. Understanding intrinsic clearance is crucial for predicting how drugs are metabolized during pregnancy, as enzyme activity can alter drug efficacy and safety without being influenced by changes in blood flow or protein binding (Sawada et al., 2020; Kratochwil et al., 2017).

Metabolic Changes: Phase I and Phase II Enzymes

Drug metabolism involves transforming chemical structures through enzymatic processes, significantly impacting a drug's pharmacokinetics, efficacy, and toxicity. Phase I metabolism modifies drugs via oxidation, reduction, and hydrolysis, altering their chemical structures. Key Phase I enzymes include CYP450 enzymes like CYP2D6, CYP1A1, and CYP3A4, as well as esterases and alcohol dehydrogenase.

Phase II metabolism follows by conjugating these modified metabolites with molecules like glucuronic acid, sulfate, or glutathione, enhancing their water solubility for easier elimination. Important Phase II enzymes are UGTs, sulfotransferases, methyltransferases, and glutathione S-transferases.

Individual differences, genetic variations, and environmental factors can affect metabolism, influencing how individuals respond to certain drugs—an aspect particularly crucial during pregnancy. While Phase I typically precedes Phase II metabolism, exceptions exist, and some metabolites can revert to the parent compound. Additionally, prodrugs require metabolic activation to become pharmacologically active (Shin et al., 2009; Gandhi and Ghose, 2012).

Pregnancy induces significant physiological changes that can affect drug metabolism by altering the activity of various enzymes. Understanding these changes is essential for optimizing pharmacotherapy in pregnant women to ensure both maternal health and fetal safety (Costantine, 2014; Abduljalil et al., 2020).

Uridine Diphosphate Glucuronyltransferase (UGT)

UGTs are phase II enzymes that convert drugs into glucuronide conjugates, enhancing water solubility for excretion. Two main subfamilies, UGT1A and UGT2B, are active in the liver.

- UGT1A4 Activity: Increases during pregnancy, starting in the first trimester and returning to pre-pregnancy levels postpartum. This affects drugs like lamotrigine, used for epilepsy (Chen et al., 2009; Khatri et al., 2021).
 - o Lamotrigine clearance increases by 65%, leading to decreased serum concentrations and potential loss of seizure control.
 - o The decline correlates with elevated estradiol levels, which induce UGT1A4.
 - o Clinical implications include the need for dose adjustments to maintain efficacy.

- UGT1A1 and UGT2B7 Activity: Metabolize labetalol, a beta-blocker for hypertension(Chen et al., 2009; Khatri et al., 2021).
- Progesterone induces UGT1A1 via the pregnane X receptor, increasing labetalol clearance.
- Since protein binding and absorption remain constant, enzyme induction is the primary cause.
- May require dosage increases to maintain therapeutic levels.

Acetaminophen Metabolism

- Metabolized by UGT1A1 and CYP2E1.
- Pregnant women eliminate acetaminophen faster, with a 20% shorter half-life in the first trimester.
- Awareness of increased clearance is important for dosing to achieve pain relief (Miners et al., 1986; Anderson, 2005).

UGT2B7 Activity

- Conflicting data exist regarding its activity during pregnancy.
- Metabolizes drugs like zidovudine and morphine.
- Zidovudine pharmacokinetics remain unchanged.
- Morphine clearance increases by 70%, possibly necessitating higher doses for pain control (Kilford et al., 2009; Emoto et al., 2018).

Alcohol Dehydrogenase (ADH)

ADH metabolizes ethanol and other alcohols (Di et al., 2021; Seitz and Oneta, 2009).

- Activity During Pregnancy: Studies in rats show increased alcohol clearance due to heightened gastric ADH activity, while liver ADH remains unchanged(Badger et al., 2005).
- Abacavir Metabolism:
 - Used in HIV/AIDS treatment during pregnancy.
 - Metabolized by ADH and UGT.
 - Pharmacokinetics are stable during pregnancy; no dose adjustments needed (Best et al., 2006; Schalkwijk et al., 2016).

Carbonyl Reductase 1 (CBR1)

CBR1 metabolizes drugs like doxorubicin and bupropion (González-Covarrubias et al., 2009; Bains et al., 2009).

- Activity During Pregnancy: Decreases, likely due to elevated 17β -estradiol levels.
- Effects on Drug Clearance:
 - Doxorubicin clearance decreases by 30–39%, increasing risk of toxicity (Iwata et al., 1990; Li et al., 2020).
 - Dosage reductions may be necessary to prevent adverse effects (Anderson, 2005; Hodge and Tracy, 2007).

Clinical Implications

- Monitoring: Regular drug level monitoring is crucial, especially for drugs with narrow therapeutic windows.
- Dosage Adjustments: May be needed to maintain efficacy or prevent toxicity.
- Individualized Therapy: Enzyme activity changes vary among individuals; personalized treatment plans are essential (Hodge and Tracy, 2007; Moreira et al., 2022).

Monitoring and Dosage Adjustments During Pregnancy

During pregnancy, significant physiological changes impact drug pharmacokinetics and pharmacodynamics, necessitating careful consideration in medication management for pregnant women. Approximately one-third of the top 100 drugs in the U.S. are primarily eliminated via the kidneys. Normal pregnancy sees a 45% increase in creatinine clearance by the 9th week, reaching 150–160% of non-pregnant values by mid-second trimester. However, this elevated clearance may decline in the last six weeks and return to baseline in the final three weeks of pregnancy (Clark et al., 2022; Anderson, 2005).

These renal function changes significantly affect drug metabolism and elimination, especially for drugs primarily cleared renally. For instance, digoxin's renal clearance increases by 61% during pregnancy compared to postpartum levels, often requiring dose adjustments to maintain therapeutic efficacy. A strong correlation ($r = 0.8$) exists between creatinine clearance and digoxin renal clearance, making creatinine clearance a valuable predictor for necessary dosing changes (Luxford and Kellaway, 2004; Gonser et al., 1995).

Variability in drug efficacy and safety during pregnancy is multifactorial, involving both pharmacokinetic and pharmacodynamic alterations. Physiological changes can significantly modify the pharmacokinetics of certain drugs. The clinical significance of these changes depends on factors like the drug's therapeutic range. Drugs with a narrow therapeutic range—such as cyclosporine, tacrolimus, lithium, warfarin, carbamazepine, valproic acid, phenytoin, digoxin, vancomycin, and aminoglycosides—are particularly sensitive because therapeutic concentrations are close to toxic levels. Small fluctuations can render these medications ineffective if concentrations decrease or cause toxicity if they increase. Even a 25% change in concentrations can be clinically significant for these drugs (Slaughter, 2012; Lin, 2007).

Conversely, drugs with a wide therapeutic range are less affected by minor pharmacokinetic changes. However, during pregnancy, some pharmacokinetic changes can be substantial—drug exposure might alter by 2 to 6 times—potentially impacting even those with broader safety margins. This underscores the importance of monitoring drug levels and adjusting dosages as necessary during pregnancy to maintain efficacy and safety (Moreira et al., 2022; Matsui, 2012).

CONCLUSION

In conclusion, the physiological alterations during pregnancy profoundly affect drug pharmacokinetics, particularly renal clearance and therapeutic drug levels. Healthcare providers must remain vigilant in adjusting medication regimens for pregnant patients, especially for drugs with narrow therapeutic windows, to ensure optimal therapeutic outcomes while minimizing risks to both the mother and the fetus.

REFERENCES

- Abduljalil, K., Furness, P., Johnson, T., Rostami-Hodjegan, A., and Soltani, H. (2012). Anatomical, physiological and metabolic changes with gestational age during normal pregnancy. *Clinical Pharmacokinetics*, 51, 365-396.
- Abduljalil, K., Pansari, A., and Jamei, M. (2020). Prediction of maternal pharmacokinetics using physiologically based pharmacokinetic models assessing the impact of the longitudinal changes in the activity of CYP1A2, CYP2D6 and CYP3A4 enzymes during pregnancy. *Journal of Pharmacokinetics and Pharmacodynamics*, 47, 361–383.
- Alqudah, M., Al-Shboul, O., Al Dwairi, A., Al-Udat, D. G., and Alqudah, A. (2022). Progesterone inhibitory role on gastrointestinal motility. *Physiological Research*.
- Al-Shboul, O., Mustafa, A., Omar, A. A., Al-Dwairi, A., Alqudah, M., Nazzal, M. S., Alfaqih, M., and Al-Hader, R. (2018). Effect of progesterone on nitric oxide/cyclic guanosine monophosphate signaling and contraction in gastric smooth muscle cells. *Biomedical Reports*, 9(6), 511-516.
- Anderson, G. (2005). Pregnancy-induced changes in pharmacokinetics. *Clinical Pharmacokinetics*, 44, 989-1008.
- Anderson, G. (2006). Using pharmacokinetics to predict the effects of pregnancy and maternal–infant transfer of drugs during lactation. *Expert Opinion on Drug Metabolism and Toxicology*, 2(6), 947-960.
- Badger, T., Hidestrand, M., Shankar, K., McGuinn, W. D., and Ronis, M. (2005). The effects of pregnancy on ethanol clearance. *Life Sciences*, 77(17), 2111-2126.
- Bains, O. S., Karkling, M. J., Grigliatti, T., Reid, R., and Riggs, K. (2009). Two Nonsynonymous Single Nucleotide Polymorphisms of Human Carbonyl Reductase 1 Demonstrate Reduced in Vitro Metabolism of Daunorubicin and Doxorubicin. *Drug Metabolism and Disposition*, 37, 1107–1114.

- Bardy, A., Hiilesmaa, V., Teramo, K., and Neuvonen, P. (1990). Protein binding of antiepileptic drugs during pregnancy, labor, and puerperium. *Therapeutic Drug Monitoring*, 12, 40–46.
- Beers, K., and Patel, N. (2020). Kidney physiology in pregnancy. *Advances in Chronic Kidney Disease*, 27(6), 449-454.
- Best, B., Mirochnick, M., Capparelli, E., Stek, A., Burchett, S., Holland, D., Read, J., Smith, E., Hu, C., Spector, S., and Connor, J. (2006). Impact of pregnancy on abacavir pharmacokinetics. *AIDS*, 20, 553–560.
- Brunskill, N. (2019). Renal disease in pregnancy. *Obstetrics, Gynaecology and Reproductive Medicine*, 29(6), 180-186.:
- Capeless, E. L., and Clapp, J. F. (1989). Cardiovascular changes in early phase of pregnancy. *American Journal of Obstetrics and Gynecology*, 161(6), 1449-1453.
- Celestin, M. N., and Musteata, F. M. (2021). Impact of changes in free concentrations and drug-protein binding on drug dosing regimens in special populations and disease states. *Journal of Pharmaceutical Sciences*.
- Cerneca, F., Ricci, G., Simeone, R., Malisano, M., Alberico, S., and Guaschino, S. (1997). Coagulation and fibrinolysis changes in normal pregnancy. *European Journal of Obstetrics, Gynecology, and Reproductive Biology*, 73(1), 31-36.
- Chapman, S., Robinson, G., Stradling, J., West, S., and Wrightson, J. (2021). Pregnancy and breathlessness. *Oxford Handbook of Respiratory Medicine*.
- Chen, H., Yang, K., Choi, S., Fischer, J., and Jeong, H. (2009). Up-Regulation of UDP-Glucuronosyltransferase (UGT) 1A4 by 17 β -Estradiol A Potential Mechanism of Increased Lamotrigine Elimination in Pregnancy. *Drug Metabolism and Disposition*, 37, 1841–1847.
- Clark, C., Newmark, R., Wisner, K., Stika, C., and Avram, M. (2022). Lithium Pharmacokinetics in the Perinatal Patient With Bipolar Disorder. *Journal of Clinical Pharmacology*, 62, 1385–1392.
- Coppola, P., Butler, A., Cole, S., and Kerwash, E. (2023). Total and Free Blood and Plasma Concentration Changes in Pregnancy for

- Medicines Highly Bound to Plasma Proteins Application of Physiologically Based Pharmacokinetic Modelling to Understand the Impact on Efficacy. *Pharmaceutics*, 15.
- Coppola, P., Kerwash, E., Nooney, J., Omran, A., and Cole, S. (2022). Pharmacokinetic data in pregnancy: A review of available literature data and important considerations in collecting clinical data. *Frontiers in Medicine*, 9.
- Costantine, M. (2014). Physiologic and pharmacokinetic changes in pregnancy. *Frontiers in Pharmacology*, 5, Article 65.:
- Di, L., Balesano, A., Jordan, S., and Shi, S. M. (2021). The Role of Alcohol Dehydrogenase in Drug Metabolism: Beyond Ethanol Oxidation. *The AAPS Journal*, 23, 1-21.
- Din, A., and Al Amir, H. M. (2019). Pregnancy in patients with chronic kidney disease. *Southern Medical Journal*, 23, 145-153.
- Duan, L., Ng, A. T., Chen, W., Spencer, H., and Lee, M. S. (2018). Beta-blocker subtypes and risk of low birth weight in newborns. *The Journal of Clinical Hypertension*, 20, 1603-1609.
- Duvekot, J., and Peeters, L. (1994). Maternal cardiovascular hemodynamic adaptation to pregnancy. *Obstetrical and Gynecological Survey*, 49(Suppl. 1), S1-S6.
- Emoto, C., Johnson, T., Neuhoff, S., Hahn, D., Vinks, A., and Fukuda, T. (2018). PBPK Model of Morphine Incorporating Developmental Changes in Hepatic OCT1 and UGT2B7 Proteins to Explain the Variability in Clearances in Neonates and Small Infants. *CPT Pharmacometrics and Systems Pharmacology*, 7, 464-473.
- Feghali, M., Venkataramanan, R., and Caritis, S. (2015). Pharmacokinetics of drugs in pregnancy. *Seminars in Perinatology*, 39(7), 512-519.
- Gandhi, A., and Ghose, R. (2012). Altered Drug Metabolism and Transport in Pathophysiological Conditions. InTech.
- Gaohua, L., Abduljalil, K., Jamei, M., Johnson, T., and Rostami-Hodjegan, A. (2012). A pregnancy physiologically based pharmacokinetic (p-PBPK) model for disposition of drugs

- metabolized by CYP1A2, CYP2D6 and CYP3A4. *British Journal of Clinical Pharmacology*, 74(5), 873-885.
- Gonser, M., Stoll, P., and Kahle, P. (1995). Clearance prediction and drug dosage in pregnancy. *Clinical Drug Investigation*, 9, 197-205.
- González-Covarrubias, V., Zhang, J., Kalabus, J., Relling, M., and Blanco, J. (2009). Pharmacogenetics of Human Carbonyl Reductase 1 (CBR1) in Livers from Black and White Donors. *Drug Metabolism and Disposition*, 37, 400-407.
- Groszmann, R. (2007). The Measurement of Liver Blood Flow Using Clearance Techniques. *Hepatology*, 3, 420-424.
- Hebert, M. F., Zheng, S., Hays, K., Shen, D. D., Davis, C. L., Umans, J. G., Miodovnik, M., and Thummel, K. E. (2013). Interpreting tacrolimus concentrations during pregnancy and postpartum. *Transplantation Journal*, 95, 908-915.
- Hershman, J. (2004). Physiological and pathological aspects of the effect of human chorionic gonadotropin on the thyroid. *Best Practice and Research Clinical Endocrinology and Metabolism*, 18(2), 249-265.
- Hodge, L., and Tracy, T. (2007). Alterations in drug disposition during pregnancy implications for drug therapy. *Expert Opinion on Drug Metabolism and Toxicology*, 3(4), 557-571.
- Hodyl, N., Stark, M., Meyer, E., Lewis, J., Torpy, D., and Nenke, M. (2020). High binding site occupancy of corticosteroid-binding globulin by progesterone increases fetal free cortisol concentrations. *European Journal of Obstetrics, Gynecology, and Reproductive Biology*, 251, 129-135.
- Honda, M., Omori, Y., Minei, S., Oshiyama, T., Shimizu, M., Sanaka, M., Kohama, T., Nakabayashi, M., and Hirata, Y. (1990). Quantitative analysis of serum α 1-acid glycoprotein levels in normal and diabetic pregnancy. *Diabetes Research and Clinical Practice*, 10(2), 147-152.
- Ionita, I., Ogasawara, K., Gohh, R., and Akhlaghi, F. (2014). Pharmacokinetics of total and unbound prednisone and

- prednisolone in stable kidney transplant recipients with diabetes mellitus. *Therapeutic Drug Monitoring*, 36, 448–455.
- Iwata, N., Inazu, N., and Satoh, T. (1990). Changes in adrenal carbonyl reductase activity in pregnant rats. *Research Communications in Molecular Pathology and Pharmacology*, 88(2), 225-231.
- Jogiraju, V. K., Avvari, S., Gollen, R., and Taft, D. (2017). Application of physiologically based pharmacokinetic modeling to predict drug disposition in pregnant populations. *Biopharmaceutics and Drug Disposition*, 38, 426–438.
- Khatri, R., Fallon, J. K., Sykes, C., Kulick, N., Rementer, R. J. B., Miner, T., Schauer, A., Kashuba, A., Boggess, K., Brouwer, K., Smith, P. C., and Lee, C. R. (2021). Pregnancy-Related Hormones Increase UGT1A1-Mediated Labetalol Metabolism in Human Hepatocytes. *Frontiers in Pharmacology*, 12.
- Kilford, P., Stringer, R., Sohal, B., Houston, J., and Galetin, A. (2009). Prediction of Drug Clearance by Glucuronidation from in Vitro Data: Use of Combined Cytochrome P450 and UDP-Glucuronosyltransferase Cofactors in Alamethicin-Activated Human Liver Microsomes. *Drug Metabolism and Disposition*, 37, 82–89.
- Knott, C., Williams, C. P., and Reynolds, F. (1986). Phenytoin kinetics during pregnancy and the puerperium. *BJOG: An International Journal of Obstetrics and Gynaecology*, 93.
- Ko, H., Almon, R., and Jusko, W. (1995). Effect of corticosteroid binding globulin on the pharmacokinetics of prednisolone in rats. *Pharmaceutical Research*, 12, 902-904.
- Kratochwil, N., Meille, C., Fowler, S., Klammers, F., Ekiciler, A., Molitor, B., Simon, S., Walter, I., McGinnis, C., Walther, J., Leonard, B., Triyatni, M., Javanbakht, H., Funk, C., Schuler, F., Lavé, T., and Parrott, N. (2017). Metabolic profiling of human long-term liver models and hepatic clearance predictions from in vitro data using nonlinear mixed-effects modeling. *The AAPS Journal*, 19, 534-550.
- Li, Q., Zhang, S., Mao, W., Fu, C., Shen, Y., Wang, Y., and Cao, J. (2020). 17 β -estradiol regulates prostaglandin E2 and F2 α

- synthesis and function in endometrial explants of cattle. *Animal Reproduction Science*, 216, 106466.
- Li, X., and Jusko, W. (2023). Utility of minimal physiologically based pharmacokinetic models for assessing fractional distribution, oral absorption, and series-compartment models of hepatic clearance. *Drug Metabolism and Disposition*, 51, 1403-1418.
- Lin, J. (2007). Pharmacokinetic and pharmacodynamic variability: a daunting challenge in drug therapy. *Current Drug Metabolism*, 8(2), 109-136.
- Loebstein, R., Lalkin, A., and Koren, G. (1997). Pharmacokinetic changes during pregnancy and their clinical relevance. *Clinical Pharmacokinetics*, 33(5), 328-343.
- Luxford, A., and Kellaway, G. (2004). Pharmacokinetics of digoxin in pregnancy. *European Journal of Clinical Pharmacology*, 25, 117-121.
- Matsui, D. (2012). Therapeutic drug monitoring in pregnancy. *Therapeutic Drug Monitoring*, 34(5), 507-511.
- Mehvar, R. (2016). Application of Organ Clearance to Estimation of the In Vivo Hepatic Extraction Ratio. *Current Clinical Pharmacology*, 11(1), 47-52.
- Mehvar, R. (2016). Application of Organ Clearance to Estimation of the In Vivo Hepatic Extraction Ratio. *Current Clinical Pharmacology*, 11(1), 47-52.
- Milliez, J., Belghiti, D., Plouin, P., Cattaneo, A., and Sobel, A. (1982). Kidneys, hypertension and pregnancy. I. Renal function in normal pregnancy. *La Nouvelle presse medicale*, 11(20), 1559-1563.
- Miners, J., Robson, R., and Birkett, D. (1986). Paracetamol metabolism in pregnancy. *British Journal of Clinical Pharmacology*, 22(3), 359-362.
- Moreira, F. de L., Benzi, J. R. de L., Pinto, L., Thomaz, M. de L., Duarte, G., and Lanchote, V. (2022). Optimizing therapeutic drug monitoring in pregnant women: A critical literature review. *Therapeutic Drug Monitoring*.

- Moyce, B. L., and Dolinsky, V. (2018). Maternal β -cell adaptations in pregnancy and placental signalling: Implications for gestational diabetes. *International Journal of Molecular Sciences*, 19.
- Musteata, F. M. (2012). Calculation of normalized drug concentrations in the presence of altered plasma protein binding. *Clinical Pharmacokinetics*, 51, 55-68.
- Nelson-Piercy, C. (2001). Asthma in pregnancy. *Thorax*, 56(4), 325-328.
- Nenke, M., Zeng, A., Meyer, E., Lewis, J., Rankin, W., Johnston, J., Kireta, S., Jesudason, S., and Torpy, D. (2017). Differential effects of estrogen on corticosteroid-binding globulin forms suggest reduced cleavage in pregnancy. *Journal of the Endocrine Society*, 1(3), 202-210.
- Pangkahila, E. S., and Tangkas, L. P. W. S. (2023). Thyroid dysfunction in pregnancy: A literature review. *European Journal of Medical and Health Sciences*.
- Robson, S., Mutch, E., Boys, R., and Woodhouse, K. (1990). Apparent liver blood flow during pregnancy: a serial study using indocyanine green clearance. *BJOG*
- Rowland, M. (1984). Protein Binding and Drug Clearance. *Clinical Pharmacokinetics*, 9, 10-17.
- Sallustio, B. C., and Morris, R. (1992). Unbound plasma phenytoin concentrations measured using enzyme immunoassay technique on the Cobas MIRA analyser—In vivo effect of valproic acid. *Therapeutic Drug Monitoring*, 14, 9–13.
- Sawada, T., Yamaura, Y., Higuchi, S., Imawaka, H., and Yamazaki, H. (2020). Predicting successful/unsuccessful extrapolation for in vivo total clearance of model compounds with a variety of hepatic intrinsic metabolism and protein bindings in humans from pharmacokinetic data using chimeric mice with humanised liver. *Xenobiotica*, 50, 526-535.
- Schalkwijk, S., Colbers, A., Konopnicki, D., Weizsäcker, K., Moltó, J., Tenorio, C. H., Hawkins, D., Taylor, G., Wood, C., van der Ende, M. E., and Burger, D. (2016). The pharmacokinetics of abacavir

- 600 mg once daily in HIV-1-positive pregnant women. *AIDS*, 30, 1239–1244.
- Schalkwijk, S., Greupink, R., and Burger, D. (2017). Free drug concentrations in pregnancy: Bound to measure unbound? *British Journal of Clinical Pharmacology*, 83, 2595-2598.
- Seitz, H., and Oneta, C. (2009). Gastrointestinal alcohol dehydrogenase. *Nutrition Reviews*, 56(2 Pt 1), 52-60.
- Shen, D. D., Kunze, K. L., and Thummel, K. E. (1997). Enzyme-catalyzed processes of first-pass hepatic and intestinal drug extraction. *Advanced Drug Delivery Reviews*, 27(2-3), 99-127.
- Shin, H.-C., Kim, H.-R., Cho, H.-J., Yi, H., Cho, S.-M., Lee, D.-G., Abd el-aty, A. M., Kim, J.-S., Sun, D., and Amidon, G. L. (2009). Comparative gene expression of intestinal metabolizing enzymes. *Biopharmaceutics and Drug Disposition*, 30.
- Slaughter, R. (2012). Outliers: The Case for Individualized Therapy. *Advances in Pharmacoepidemiology and Drug Safety*, 1(S1), E001.
- Szlapinski, S. K., and Hill, D. (2020). Metabolic adaptations to pregnancy in healthy and gestational diabetic pregnancies: The pancreas - placenta axis. *Current Vascular Pharmacology*.
- Tanaka, K., Bharadwaj, S., Hasan, S., Judd, M., Abuelkasem, E., Henderson, R., Chow, J., Williams, B., Mazzeffi, M., Crimmins, S., and Malinow, A. (2019). Elevated fibrinogen, von Willebrand factor, and Factor VIII confer resistance to dilutional coagulopathy and activated protein C in normal pregnant women. *British Journal of Anaesthesia*, 122(6), 751-759.
- Tanaka, K., Tanaka, H., Kamiya, C., Katsuragi, S., Sawada, M., Tsuritani, M., Yoshida, M., Iwanaga, N., Yoshimatsu, J., and Ikeda, T. (2016). Beta-Blockers and Fetal Growth Restriction in Pregnant Women With Cardiovascular Disease. *Circulation Journal*, 80(10), 2221-2226.
- Tzimas, G., Thiel, R., Chahoud, I., and Nau, H. (1997). The area under the concentration-time curve of all-trans-retinoic acid is the most suitable pharmacokinetic correlate to the embryotoxicity of this

- retinoid in the rat. *Toxicology and Applied Pharmacology*, 143(2), 436-444.
- Wang, X., Li, C., Du, C., Gao, J., Zhao, K., and Shi, R. (2017). Plasma protein binding monitoring of therapeutic drugs in patients using a single set of hollow fiber centrifugal ultrafiltration. *Bioanalysis*, 9(7), 579-592.
- Wilkinson, G., and Shand, D. (1975). Commentary: A physiological approach to hepatic drug clearance. *Clinical Pharmacology and Therapeutics*, 18(4), 377-390.
- Wood, M., and Wood, A. (1981). Changes in plasma drug binding and alpha 1-acid glycoprotein in mother and newborn infant. *Clinical Pharmacology and Therapeutics*, 29(4), 522-526.
- Wu, J., LoRusso, P., Matherly, L., and Li, J. (2012). Implications of plasma protein binding for pharmacokinetics and pharmacodynamics of the γ -secretase inhibitor RO4929097. *Clinical Cancer Research*, 18(7), 2066–2079.
- Yan, J.-H. (2017). Food effect on oral bioavailability: Old and new questions. *Clinical Pharmacology in Drug Development*, 6, 659-674.
- Zheng, S., Easterling, T., Umans, J., Miodovnik, M., Calamia, J., Thummel, K., Shen, D., Davis, C., and Hebert, M. (2012). Pharmacokinetics of tacrolimus during pregnancy. *Therapeutic Drug Monitoring*, 34, 660–670.

CHAPTER 13

TECHNIQUES FOR HANDLING IMBALANCE DATA IN CLASSIFICATION METHODS

Assoc. Prof. Dr. Tuba KOÇ¹ and Assoc. Prof. Dr. Haydar KOÇ¹

DOI: <https://dx.doi.org/10.5281/zenodo.14259298>

¹ Çankırı Karatekin University, Faculty of Science, Department of Statistics, Çankırı, Türkiye. tubakoc@karatekin.edu.tr, Orcid ID: 0000-0001-5204-0846
haydarkoc@karatekin.edu.tr, Orcid ID: 0000-0002-8568-4717

INTRODUCTION

An imbalanced dataset is a dataset in which there are significant numerical differences between samples belonging to different classes. This situation occurs when some classes contain many more instances than others. Such imbalances in the data set lead to classes with fewer instances being referred to as 'minority classes' and classes with more instances being referred to as 'majority classes'. It is rare for real-world data to have equal numbers of these classes, leading to the problem of imbalanced data, which is an important issue to consider in data science research. Imbalanced datasets can occur in a variety of domains and may require special methods for accurate modelling. Some of the areas where imbalanced datasets are common are medicine and healthcare, cyber security, fraud detection, quality control and manufacturing, natural disaster and emergency management, natural language processing and text analysis, and finance and economics.

For example, in medicine and health care, in a disease diagnosis scenario, it is much more serious to classify a sick person as not sick than to diagnose a non-sick person as sick. However, the problem becomes even more complex when the data set is imbalanced, and misclassification of the minority class has more serious consequences than the majority class. Because standard classifiers generally focus on maximizing overall accuracy, they learn the majority class better, leading to low error rates for the majority class and high error rates for the minority class. As a result, classifiers tend to classify all data as belonging to the majority class, while they may miss minority classes (Pir, 2022).

There are many factors that affect classification performance, but the most important criteria are the dataset, or the features used in the data sets, the classification algorithms used, and the distribution of the classes. Most classification algorithms assume that the training sets are well balanced. Classification problems can arise when there is an imbalanced data set. If the model focuses on learning the majority class, it may not learn the features of the minority classes well enough. This reduces the ability of the model to generalize to imbalanced data sets in the real world and negatively affects the performance of the

model. Resampling methods are among the most used techniques to eliminate class imbalance. Among these methods, under sampling, oversampling and synthetic minority oversampling (SMOTE) methods stand out to reduce the negative effects of imbalanced data. Each method has its own advantages and disadvantages (Turhan et al., 2020). There are some studies on imbalanced datasets and different methods proposed in the literature. Fernandez-Navarro et al. (2011) included radial basis functions in a memetic algorithm that reduces neural networks in a dynamic oversampling method study to highlight imbalanced data classification with two methods. In this method, the training data is resampled in two stages to solve the class imbalance problem. The first step is to increase the minority class using an oversampling technique. The memetic algorithm oversamples the data at different stages and provides new models of the minimum sensitivity class. Rao et al. (2012) studied with a subsampling approach using one of the clustering techniques for visualization to solve the class imbalance problem. Yu et al. (2013) proposed a heuristic subsampling method based on the idea of ant colony optimization to solve the class imbalance problem. In the study proposed by Krawczyk et al. (2019), a high-speed sampling study was conducted using the multi-class radial basis method, which is a new data sampling algorithm dedicated to multi-class problems. Akin and Terzi (2020) presented the comparative results of Cox regression and random forest methods on survival data with imbalanced datasets. Liang et al. (2020) proposed the LR-SMOTE algorithm, based on the traditional oversampling SMOTE algorithm, to bring the newly created samples close to the sample center and avoid creating outlier samples or changing the distribution of the data sets. Wang et al. (2021) conducted research on the extension and classification of imbalanced data based on the SMOTE algorithm. Akin and Terzi (2021) gave a comparative study of different kernel functions for imbalanced data. The results showed that the resampling method of the random over-sampling examples for linear and sigmoid kernel functions improved the results of the performance metrics compared to the original data. They showed that the performance of the SMOTE method increased for the radial kernel. Pir (2022) proposed a solution

to the classification problem in imbalanced data with a hybrid method. In imbalanced data, it avoided the overfitting problem caused by oversampling and the loss of valuable data caused by sample reduction. Wongvorachan et al. (2023) compared the subsampling, oversampling and SMOTE methods to deal with imbalanced classification in educational data mining. Feng et al. (2023) presented a new hybrid algorithm, Negative binary general, to improve the performance of imbalanced classifications by combining oversampling and a feature selection algorithm. Piyadasa and Gunawardana (2023) investigated oversampling techniques to solve the problem of data imbalance in classification. Zhou and Sun (2024) proposed an adaptive k-means clustering subsampling algorithm that calculates an appropriate k for each dataset.

IMBALANCED DATA SETS

An imbalanced dataset occurs when there is a significant imbalance between classes in a classification problem. That is, one class has a much larger number of instances than the other class. In this case, the minority class becomes difficult to classify correctly because the model focuses more on detecting instances from the majority class and may ignore the minority class.

Imbalanced datasets are common in the real world, especially in healthcare where minority classes are important, such as rare diseases or cancer. Such imbalances can negatively affect research results by making it difficult to correctly identify the minority class.

If the number of samples in the majority class in a model is large, the influence of that class is greater and some observations belonging to the minority class may be misclassified. This reduces the accuracy of the model. Various metrics such as accuracy rate, sensitivity, selectivity, area under the ROC curve and F1 score are used to measure model performance. However, if the imbalance in the data set is too high, some performance measures may be low. The direct use of imbalanced data sets often has a negative impact on classification performance.

SOME METHODS USED TO DEAL WITH IMBALANCED DATA

Data preprocessing techniques, the method of adding class weights, the use of some specialized algorithms and ensemble methods can be used to deal with imbalanced data sets. In this study we will explain data preprocessing techniques under sampling, oversampling and SMOTE.

Under sampling

Sample reduction is done by removing the oversamples in the majority class or by applying sub-sampling techniques. This method aims to reduce the negative effects of imbalance and improve classification performance by ensuring that classes with fewer samples are better represented by the model. Random sub-sampling, one of the most widely used sample reduction techniques, simplifies the data set by removing random samples from the majority class. This method plays an effective role in improving classification performance and generalization ability by reducing the complexity of the model (Liu et al., 2008). The random sub-sampling method is an effective approach that aims to solve the class imbalance problem by removing the excess samples in the majority class. Since it does not lead to the loss of samples in the minority class and is easy to implement, it is widely used, especially in large datasets. The random subsampling method improves the prediction performance of this class by balancing the minority class, while maintaining the representativeness of the dataset if a correct subsampling rate is chosen and minimizing the impact on the generalization ability of the model (Ferguson et al., 2020). However, this method also has some disadvantages. Since random sample extraction is performed, important information may be lost from the dataset, and this may negatively affect the overall performance and generalization ability of the model. Moreover, in asymmetric data distributions, extracting samples only from the majority class does not always fully correct the imbalance and may reduce the representativeness of the data set and reduce the classification success.

Therefore, it is important to carefully determine the sampling rate and maintain the holistic structure of the data set (Demirsöz, 2024).

Oversampling

The sample augmentation method is applied by increasing the number of samples of classes with a small number of samples or by generating synthetic new samples. The aim of this method is to ensure that the minority class is better represented by the model. In this way, the model improves its classification performance by undergoing a more balanced training process in imbalanced data sets. There are many different techniques among sample augmentation methods (Douzas et al., 2018). Random oversampling is one of the simple and effective methods to balance the minority class in imbalanced datasets. In this method, copies are randomly selected from the minority class samples and added to the minority class. This reduces the imbalance between the two classes and makes the data set more balanced. This method can cause the minority class to be over-represented in the data set and the model to over-fit the minority class. It aims to improve the performance of the model by increasing the samples in the minority class, but it negatively affects the performance of the model in case of excessive augmentation or incorrect synthetic data generation (Zheng et al. 2015).

Synthetic Minority Oversampling (SMOTE)

SMOTE is an effective approach for balancing imbalanced datasets. Instead of directly copying minority class data, it generates synthetic data for a given sample based on its nearest neighbors (Fernández et al., 2018). The SMOTE method allows the model to better learn rare cases in imbalanced datasets by strengthening the minority class and provides fast and effective results using a simple algorithm. Although SMOTE is easy to apply to large datasets, it also has some drawbacks. If the data set is small, or if the samples in the minority class are very similar to each other, SMOTE can lead to overfitting of the model and a decrease in the ability to generalize. In addition, synthetic samples generated at class boundaries can blur the

distinction between classes, negatively affecting the performance of the model (Chawla, 2010).

APPLICATION

In this section, firstly, a logistic regression model is developed to simulate the data with a high majority class ratio. Then, the obtained data were balanced by using under sampling, oversampling and SMOTE methods to eliminate the imbalance. After this balancing process, various machine learning techniques were applied to evaluate which method performed better. This process is critical for effective processing of imbalanced datasets and improving classification success.

Data description

Logistic regression is a statistical technique used to model the relationship between independent variables and the dependent variable when the dependent variable is binary. Consequently, imbalanced simulation data suitable for logistic regression were generated. The general logistic regression model, as outlined by Akın (2023), is given by:

$$P\{Y = 1 \setminus X\} = \frac{1}{1 + \exp(-X\beta)} \quad (1)$$

The X represents the predictors, while β represents the weights or coefficients for predictors. Four X_1, X_2, X_3, X_4 predictors were randomly selected, after which the model was established.

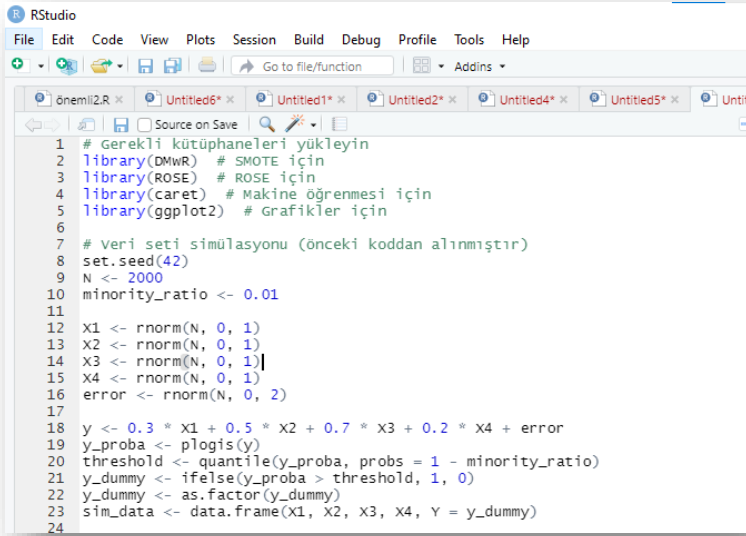
$$X\beta = 0.3X_1 + 0.5X_2 + 0.7X_3 + 0.2X_4 \quad (2)$$

The data were generated with a sample size of 2000. To evaluate the effectiveness of the proposed model, the minority class ratio was set at 0.01%. Further details about the majority and minority classes can be found in Table 1.

Table 1. An overview of the datasets

Minority Class	Yes	0.01%	20
Majority Class	No	0.99 %	1980

Figure 1 shows the R code for generating simulation data using logistic regression.



```

1 # Gerekli kütüphaneleri yükleyin
2 library(DMwR) # SMOTE için
3 library(ROSE) # ROSE için
4 library(caret) # Makine öğrenmesi için
5 library(ggplot2) # Grafikler için
6
7 # veri seti simülasyonu (önceki koddan alınmıştır)
8 set.seed(42)
9 N <- 2000
10 minority_ratio <- 0.01
11
12 X1 <- rnorm(N, 0, 1)
13 X2 <- rnorm(N, 0, 1)
14 X3 <- rnorm(N, 0, 1)
15 X4 <- rnorm(N, 0, 1)
16 error <- rnorm(N, 0, 2)
17
18 y <- 0.3 * X1 + 0.5 * X2 + 0.7 * X3 + 0.2 * X4 + error
19 y_proba <- plogis(y)
20 threshold <- quantile(y_proba, probs = 1 - minority_ratio)
21 y_dummy <- ifelse(y_proba > threshold, 1, 0)
22 y_dummy <- as.factor(y_dummy)
23 sim_data <- data.frame(X1, X2, X3, X4, Y = y_dummy)
24

```

Figure 1. The R code for generating simulation data with logistic regression

Table 2 shows the first 20 observations of the simulation data.

Table 2. First 20 observations of data

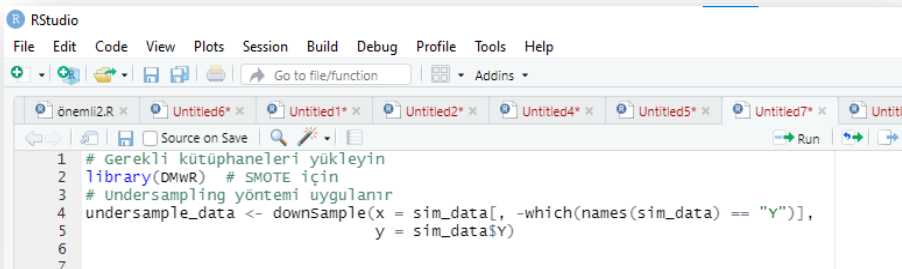
X1	X2	X3	X4	Y
1.397	-2.098	-2.445	1.724	0
0.019	0.457	-0.947	-0.387	0
0.550	0.373	0.405	0.409	1
1.484	-0.542	0.083	0.181	0
0.771	1.991	0.707	0.366	0
-1.077	1.691	0.310	-0.162	0
1.239	-0.804	0.541	0.786	0
-0.599	0.141	-1.101	0.997	0
-0.663	-1.506	0.676	-0.035	0
2.335	1.480	-0.488	-1.921	0
-0.406	-0.870	-0.203	-1.041	0
1.265	-0.020	0.349	0.710	0
1.215	0.844	0.309	-0.623	0
-1.329	0.777	0.488	0.333	0
-1.166	-1.670	-1.181	-1.141	0

-1.781	0.131	-0.592	-0.378	0
-0.285	-0.612	-1.878	-0.233	0
0.790	-1.867	0.264	-0.495	0
-0.080	0.410	-0.080	0.963	0
-1.376	-0.239	1.306	0.737	0

Our data set shows that the target variable (y) has an imbalanced distribution. When the first 20 samples are analyzed, all observations have a value of "0", while no sample has a value of "1". Such imbalances can cause severe problems in sampling methods because the sample is biased towards the majority class, and it is impossible to represent a minority. The results of imbalanced data sets can often be because the model underrepresents the minority group and adversely affects its performance. To overcome this problem, we use data balancing techniques such as under sampling, oversampling and SMOTE. These methods can improve overall performance and class prediction accuracy by making the model closer to the two classes in a balanced way.

Under sampling algorithms for imbalanced classification

The first method to address the large imbalance in our dataset is the under-sampling technique. The code in Figure 2 shows the under-sampling algorithm implemented to improve the overall performance on imbalanced data.



```

1 # Gerekli kütüphaneleri yükleyin
2 library(DMWR) # SMOTE için
3 # Undersampling yöntemi uygulanır
4 undersample_data <- downSample(x = sim_data[, -which(names(sim_data) == "Y")],
5                               y = sim_data$Y)
6
7

```

Figure 2. The R codes for the under-sampling algorithms

Initially, a subgroup of Y variables (1) was largely missing from the dataset, which could also make it difficult for the model to adjust for observation; to solve this problem, a statistical procedure was adapted to the corrected by statically converting over random samples excluded from the population (i.e., class 0). Table 3 shows the first 20 observations on this dataset.

Table 3. First 20 observations of data with under sampling algorithms

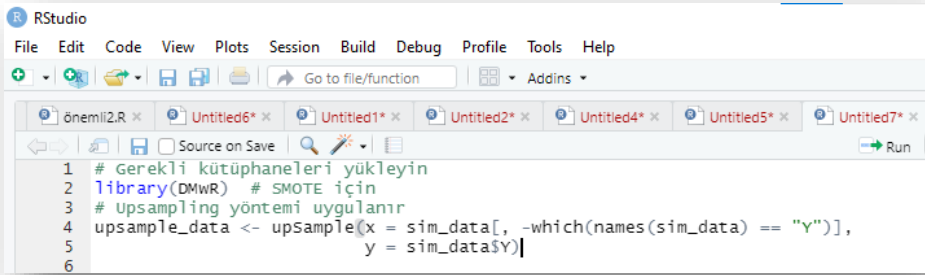
X1	X2	X3	X4	Class
-0.654	-0.279	1.331	-1.026	0
1.502	0.399	0.231	-1.171	1
-1.661	-0.765	-1.605	1.901	0
-0.533	0.977	-0.450	-1.158	0
-0.485	-0.161	0.524	0.301	1
0.605	2.002	1.024	-0.629	1
-2.071	0.004	1.574	1.176	1
0.970	3.471	2.137	0.887	1
1.446	0.626	1.477	0.112	1
1.728	1.776	1.936	0.314	0
-0.091	2.861	0.448	1.082	0
-1.966	-0.972	1.072	0.593	1
0.076	1.504	1.131	-0.584	0
0.084	1.544	-0.742	1.324	0
-0.097	1.597	0.610	1.543	0
0.892	0.545	-1.473	-0.099	0
-1.781	-0.068	1.529	1.453	1
0.129	-0.185	1.747	0.508	1
0.931	0.594	0.887	-0.646	0
0.049	-0.231	-0.095	-0.361	0

After using the under-sampling set of rules while reading the primary 20 objects, eight "1" findings were observed. Because of the utility of this system, the range of sophistication zero samples decreased, and a more balanced distribution was acquired among the two instructions. This enhancement improved the model's sensitivity to the minority magnificence, contributing to forecasting performance's overall stability and accuracy. However, this balancing manner should

result in missing statistics by omitting a few pieces of information from the majority class. While this could enhance the model's overall performance, it can affect the size and representativeness of the statistics set.

Oversampling algorithms for imbalanced classification

A second technique, oversampling, was used to address magnificent imbalances in our information set. The code in Figure 4 indicates the implementation of the oversampling algorithm set of rules, which is a step to improve the model's overall performance on imbalanced facts sets.



```

1 # Gerekli kütüphaneleri yükleyin
2 library(DMwR) # SMOTE için
3 # Upsampling yöntemi uygulanır
4 upsample_data <- upsample(x = sim_data[, -which(names(sim_data) == "Y")],
5                           y = sim_data$Y)
6

```

Figure 3. The R codes for the oversampling algorithms

Using the oversampling method, samples from class 1 were added to address imbalances in the dataset. By increasing the number of samples of the minority class, this method ensures that both classes are represented in the data set in a balanced way. The application was implemented using the upSample library in the R language. This process was carried out according to specific guidelines to ensure that the dataset and the samples from the subgroup were balanced. The first 20 observations on this list are shown in Table 4.

Table 4. First 20 observations of data with oversampling algorithms

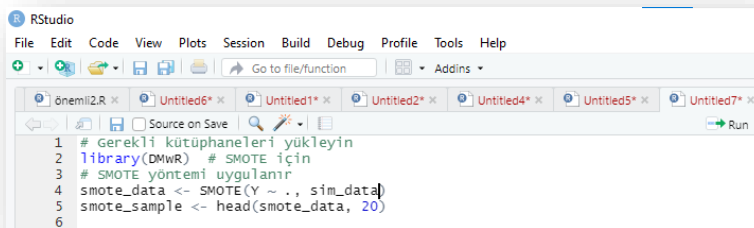
X1	X2	X3	X4	Class
0.550	0.373	0.405	0.409	1
1.446	0.626	1.477	0.112	1
0.747	-0.008	1.259	-1.395	0

1.354	0.347	-0.673	-0.582	0
0.468	3.175	0.659	0.668	1
0.426	0.228	2.115	0.812	1
-0.185	-1.352	-0.923	1.167	0
-1.376	0.292	-1.083	-1.472	0
-2.172	-0.084	0.468	-1.348	0
0.550	0.373	0.405	0.409	1
0.755	1.572	0.240	0.191	1
1.446	0.626	1.477	0.112	1
-1.663	0.538	2.519	0.304	1
0.592	0.565	-0.177	-0.140	0
-1.663	0.538	2.519	0.304	1
0.556	0.899	0.666	-0.370	1
1.446	0.626	1.477	0.112	1
0.949	0.186	0.591	-0.728	0
0.556	0.899	0.666	-0.370	1
0.605	2.002	1.024	-0.629	1

When the first 20 studies were reviewed, 13 "1"s were identified after applying the up-sampling algorithm. The up-sampling procedure aims to correct the imbalance in the data set by increasing the number of samples from the minority class and randomly copying the old minority class observations into the dataset.

SMOTE for imbalanced classification

Finally, let's balance the dataset by generating new synthetic samples from the minority class using the SMOTE technique. Figure 4 illustrates the implementation of the SMOTE algorithm.



```

1 # Gerekli kütüphaneleri yükleyin
2 library(DMwR) # SMOTE için
3 # SMOTE yöntemi uygulanır
4 smote_data <- SMOTE(Y ~ ., sim_data)
5 smote_sample <- head(smote_data, 20)
6

```

Figure 4. The R codes for the SMOTE algorithms

This set of rules balances the statistics by means of growing the wide variety of minority class samples in imbalanced facts units. The code in Figure 4 implements the SMOTE approach using the DMwR library. Y is selected as the goal variable, and the SMOTE approach is applied to the dataset. This includes a newly updated version for the minority class, and the primary 20 observations on this list are offered in Table 5.

Table 5. First 20 observations of data with SMOTE algorithms

X1	X2	X3	X4	Y
1.382	-1.807	1.421	1.395	0
0.531	0.529	0.297	0.203	1
-2.063	-0.071	1.535	1.131	1
-0.279	-0.282	0.865	-1.852	1
0.515	0.263	2.059	0.751	1
-0.026	0.077	0.471	0.349	1
-0.440	-0.187	0.599	-0.172	1
1.188	-1.810	-0.924	0.378	0
0.295	-0.545	1.676	1.999	0
0.704	2.251	-0.341	-1.250	0
0.545	2.745	0.547	0.540	1
0.426	0.228	2.115	0.812	1
0.556	0.899	0.666	-0.370	1
-0.611	-1.508	-0.171	0.201	0
1.371	0.251	-0.142	0.173	0
0.558	1.516	0.109	0.699	0
0.536	0.030	0.575	-1.540	1
-0.093	0.390	1.639	0.528	1
-1.686	0.507	2.465	0.355	1
0.551	0.461	0.449	0.279	1

When the primary 20 features were examined, 13 features identified as '1' were found after applying the SMOTE algorithm. Thanks to the SMOTE method, the initial number of samples became more balanced, resulting in a fair distribution between the two classes. These improvements enabled the model to perform better, leading to more balanced and accurate predictions.

Comparison of imbalance handling methods

Figure 5 shows the original state of the imbalanced dataset, and the balanced versions achieved using three different methods.

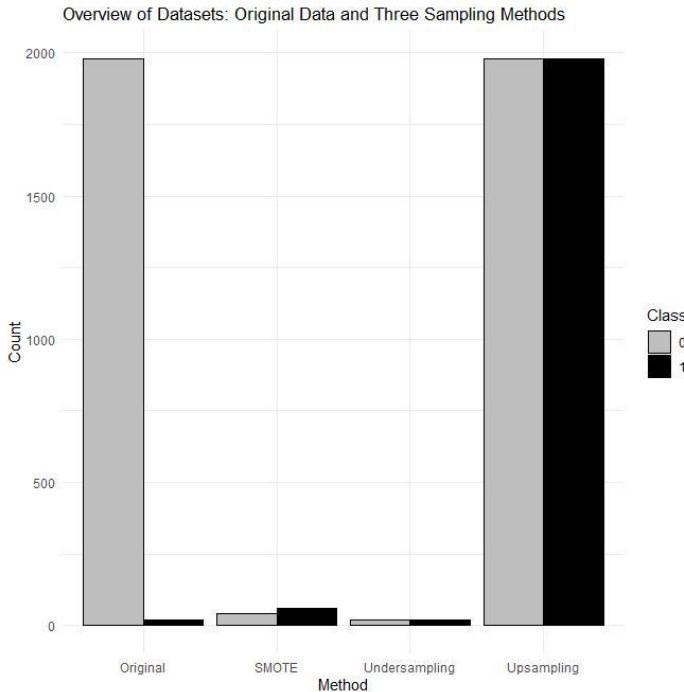


Figure 5. The overview of datasets: original data and three sampling methods

In the original data set, the "0" class contains most of the samples (1980 samples), while the "1" class contains only a few (20 samples). The SMOTE method increases the number of samples in class "1" by generating synthetic data (class 0: 40, class 1: 60), while under sampling decreases the number of instances in class "0" and the balance between classes (20) instances of both classes). Oversampling increases the number of "1" class samples up to 1980, bringing the classes to a total balance. These methods aim to eliminate class imbalances and increase the prediction accuracy of the models. Table 6 evaluates the performance of imbalanced class methods in different models.

Table 6. Effects of different balancing methods on machine learning model performance metrics

Method	Model	Accuracy	Precision	Sensitivity	F_measure	G_mean
Original	SVM	0.990	NaN	0.000	NaN	0.000
	CART	0.991	1.000	0.125	0.222	0.125
	RF	0.991	1.000	0.125	0.222	0.125
	NaiveBayes	0.875	0.852	0.958	0.902	0.958
SMOTE	SVM	0.800	0.750	1.000	0.857	1.000
	CART	0.875	0.880	0.917	0.898	0.917
	RF	0.800	0.864	0.792	0.826	0.792
	NaiveBayes	0.875	0.800	1.000	0.889	1.000
Under sampling	SVM	0.813	0.727	1.000	0.842	1.000
	CART	0.875	0.800	1.000	0.889	1.000
	RF	0.688	0.667	0.750	0.706	0.750
	NaiveBayes	0.934	0.884	1.000	0.938	1.000
Oversampling	SVM	0.819	0.760	0.933	0.837	0.933
	CART	0.997	0.994	1.000	0.997	1.000
	RF	0.895	0.826	1.000	0.905	1.000
	NaiveBayes	0.990	NaN	0.000	NaN	0.000

The effects of SMOTE, under sampling and oversampling methods affect model performance in different ways. Precision can be misleading if subgroups are not correctly identified, as high predictive accuracy for most classes may indicate that the sample does not adequately represent minorities, so the G-mean is used to accurately assess model performance on imbalanced datasets. The table shows the effect of imbalanced representation strategies on the four models. On the original data, the Support Vector Machine (SVM) performs poorly with small class sizes and all metrics are unavailable, while the Classification and Regression Tree (CART) and Random Forest (RF) models provide high accuracy values (99.1%) but low accuracy (12.5%) with small class sizes. Using the SMOTE method, the accuracy of the SVM decreased to 80.0%, while the sensitivity increased to 100.0%. The CART model achieved an accuracy of 87.5% and a G-mean of 91.7%. The accuracy of the SVM using the under-

sampling method was 81.3% and the sensitivity was 100.0%. The naive Bayes model achieved an accuracy of 93.4% and a g-mean of 100.0%. The oversampling method gave the best performance, especially for the CART and random forest models, with good results like 99.7% accuracy and 100.0% G-mean.

These results show that oversampling is the most effective method to handle class imbalances, and SMOTE and under sampling methods also improve performance but are not as extensive as oversampling.

CONCLUSION AND DISCUSSION

Enhancing the effectiveness of machine learning models depends critically on avoiding data imbalance. Class imbalances can negatively affect the overall performance of the model, especially when minority groups are underrepresented. Therefore, data preprocessing techniques to deal with imbalanced datasets have become a great need.

Methods such as oversampling, under sampling and SMOTE significantly improve the overall sample accuracy through their ability to represent smaller populations. The selection and application of these techniques play a critical role in achieving successful, accurate and balanced forecasts. In particular, the effective integration of these techniques improves the learning process of the model while ensuring that minority classes are accurately represented.

Therefore, the careful selection of appropriate modelling techniques to deal with imbalances in the dataset is a fundamental step to improve model performance and obtain reliable and valid results. By focusing on the further integration and optimization of these techniques, future work can contribute to achieving more balanced and accurate results in machine learning applications. In this context, addressing data imbalances will not only improve the success of the model, but also allow for more fair and effective results in real-world applications.

REFERENCES

- Akın, P., and Terzi, Y. (2020). Dengesiz veri setli sağkalım verilerinde cox regresyon ve rastgele orman yöntemlerin karşılaştırılması. *Veri Bilimi*, 3(1), 21-25.
- Akın, P., and Terzi, Y. (2021). Comparison of unbalanced data methods for support vector machines. *Türkiye Klinikleri Biyoistatistik*, 13(2), 138-146.
- Akın, P. (2023). A new hybrid approach based on genetic algorithm and support vector machine methods for hyperparameter optimization in synthetic minority over-sampling technique (SMOTE). *AIMS Mathematics*, 8(4), 9400-9415.
- Chawla, N.V. (2010). Data mining for imbalanced datasets: An overview. *Data mining and knowledge discovery handbook*, 875-886.
- Demirsöz, S. (2024). Dengesiz veri setlerinde sınıflandırma performansını etkileyen yaklaşımların incelenmesi (Yüksek Lisans Tezi, Selçuk Üniversitesi).
- Douzas, G., Bacao, F., and Last, F. (2018). Improving imbalanced learning through a heuristic oversampling method based on k-means and SMOTE. *Information sciences*, 465, 1-20.
- Feng, F., Li, K. C., Yang, E., Zhou, Q., Han, L., Hussain, A., and Cai, M. (2023). A novel oversampling and feature selection hybrid algorithm for imbalanced data classification. *Multimedia Tools and Applications*, 82(3), 3231-3267.
- Ferguson, A. J., Hernandez, J. G., Junghans, D., Lalejini, A., Dolson, E., and Ofria, C. (2020). Characterizing the effects of random subsampling on lexibase selection. *Genetic programming theory and practice XVII*, 1-23.
- Fernández, A., García, S., Galar, M., Prati, R.C., Krawczyk, B., and Herrera, F., (2018). *Learning from imbalanced data sets*. Vol. 10, Springer.
- Fernández-Navarro, F., Hervás-Martínez, C., and Gutiérrez, P. A. (2011). A dynamic oversampling procedure based on sensitivity

- for multi-class problems. *Pattern Recognition*, 44(8), 1821-1833.
- Krawczyk, B., Koziarski, M., and Woźniak, M. (2019). Radial-based oversampling for multiclass imbalanced data classification. *IEEE transactions on neural networks and learning systems*, 31(8), 2818-2831.
- Liang, X. W., Jiang, A. P., Li, T., Xue, Y. Y., and Wang, G. T. (2020). LR-SMOTE—An improved unbalanced data set oversampling based on K-means and SVM. *Knowledge-Based Systems*, 196, 105845.
- Liu, X.Y., Wu, J., and Zhou, Z.H. (2008). Exploratory undersampling for class-imbalance learning. *IEEE Transactions on Systems, Man, Cybernetics, Part B*, 39, 539-550.
- Pir, M. Ş. (2022). Dengesiz veri setlerinde sınıflandırma problemlerinin çözümünde melez yöntem uygulaması (Master's thesis, Bursa Uludag University (Turkey)).
- Piyadasa, T. D., and Gunawardana, K. (2023). A Review on Oversampling Techniques for Solving the Data Imbalance Problem in Classification. *The International Journal on Advances in ICT for Emerging Regions*, 16(1).
- Rao, R. R., and Makkithaya, K. (2017). Learning from a Class Imbalanced Public Health Dataset: a Cost-based Comparison of Classifier Performance. *International Journal of Electrical & Computer Engineering* (2088-8708), 7(4).
- Turhan, S., Özkan, Y., Yürekli, B. S., Suner, A., and Doğu, E. (2020). Sınıf dengesizliği varlığında hastalık tanısı için kolektif öğrenme yöntemlerinin karşılaştırılması: Diyabet tanısı örneği. *Turkiye Klinikleri Journal of Biostatistics*, 12(1), 16-26.
- Wang, S., Dai, Y., Shen, J., and Xuan, J. (2021). Research on expansion and classification of imbalanced data based on SMOTE algorithm. *Scientific reports*, 11(1), 24039.
- Wongvorachan, T., He, S., and Bulut, O. (2023). A comparison of undersampling, oversampling, and SMOTE methods for dealing with imbalanced classification in educational data mining. *Information*, 14(1), 54.

- Wu, G., Chang, E.Y. (2003). Class-boundary alignment for imbalanced dataset learning. In ICML 2003 workshop on learning from imbalanced data sets II, Washington, DC, 49-56, 2003.
- Yu, H., Ni, J., and Zhao, J. (2013). ACOSampling: An ant colony optimization-based undersampling method for classifying imbalanced DNA microarray data. *Neurocomputing*, 101, 309-318.
- Zheng, Z., Cai, Y., and Li, Y. (2015). Oversampling method for imbalanced classification. *Computing and Informatics*, 34.
- Zhou, Q., and Sun, B. (2024). Adaptive K-means clustering based under-sampling methods to solve the class imbalance problem. *Data and Information Management*, 8(3), 100064.

CHAPTER 14

IMPACTS OF ROADS ON WILDLIFE

Ph.D. Şirin Bahar KARAHASAN¹

DOI: <https://dx.doi.org/10.5281/zenodo.14259337>

¹ Gazi University, Graduate School of Natural and Applied Sciences, Biology Department, Ankara, Türkiye. sirinbahark@gmail.com, Orcid ID: 0000-0001-5787-5228

INTRODUCTION

Roads are man-made corridors that facilitate the movement of people and materials through the environment (Figure 1). Road networks are extensive in both length and the area they occupy, covering most terrestrial landscapes and habitats (Bennett, 1991). Roads play a crucial role in economic and social development, providing access to markets, workplaces, businesses, healthcare, family services, recreational activities, and education (van der Ree et al., 2015).



Figure 1. A view of the Anadolu Highway from Ankara, the capital of Türkiye (source: Şirin Bahar Karahasan)

For thousands of years, roads have been used by humans, animals, and vehicles for transportation. In the 20th century, the sharp rise in motor vehicle numbers and the increase in movement led to a vast expansion of the road network. Roads and motorised transportation have become an integral to life in many parts of the world, contributing greatly to the high levels of communication and mobility that define today's technological society (Bennett, 1991). The growth in global

mobility will impact more than just energy and emissions. Analysis by the International Energy Agency (IEA) shows that, as global passenger and freight travel grows over the next 40 years, infrastructure for transport (roads and railways) will need significant expansion by 2050. In the 4°C increase scenario within the 2012 ETP (Energy Technology Perspectives) analysis, it is projected that by 2050, there will be approximately 25 million kilometers of paved roads, and 335,000 kilometers of railway tracks worldwide, a 60% increase from 2010 (Dulac, 2013). As of 2023, Türkiye alone has a total road network of 68,726 km under the Ministry of Transport and Infrastructure. Of these, 30,852 km are highways, 34,152 km are state roads, and 3,722 km are provincial roads. The total railway length in Türkiye is 13,919 km (Republic of Türkiye Ministry of Transport and Infrastructure, 2023). According to the CIA, the global road network comprises about 52 million kilometres. Of this, approximately 6.5 million kilometers are in the United States, 6.2 million in India, and 5 million in China (CIA, 2024).

Road ecology as a term was first introduced in scientific literature 22 years ago (Forman, 1998; Forman and Alexander, 1998). The goal of this field is to examine the relationships between roads, traffic, and the environment (Forman, 1998; Forman et al., 2003). Research in road ecology covers a wide range of topics, including collisions between wildlife and vehicles, avoidance of roads by animals, landscape connectivity, habitat fragmentation, barrier effects, pathways for biological invasions, pollution, and behavioral changes in wildlife (Forman and Alexander, 1998; Trombulak and Frissell, 2000). Additionally, road ecology investigates the efficiency and potential advantages of mitigation strategies, such as the construction of wildlife crossings (D'Amico et al., 2018).

Global economic and technological developments have led to a rapid increase in existing roads, new road construction, and traffic. These developments can have significant impacts on wildlife populations and landscapes. The effects start during road construction and persist as long as the road is in use, with most being detrimental. If

the impacts are large enough, they can reduce wildlife populations and increase the risk of local extinction (van der Ree et al., 2015).

Roads affect nature both directly and indirectly. They create new habitat edges, alter hydrological systems, and disrupt natural processes. Road maintenance and traffic introduce chemical pollutants and noise into the environment. Additionally, traffic restricts the movement of many terrestrial animals and causes the death of millions of animals each year. Biotic and abiotic factors work together, leading to habitat loss, isolation, and the fragmentation of landscapes (Seiler, 2001).

General Effects of Roads

Roads and traffic affect wildlife in various ways, increasing mortality in some animal populations, restricting movement, and reducing the quantity and quality of habitat. This, in turn, limits the availability of essential resources like food, shelter, and space necessary for species survival. These impacts have become a key focus of research in emerging fields such as landscape and road ecology (Grilo et al., 2010; Can and Hasbenli, 2021).

The primary ecological impacts of roads on wildlife can be categorized into five main groups (Zande and Vos, 1984; Bennett, 1991; Seiler, 2001; van der Ree et al., 2015):

1. **Habitat loss:** The construction of roads and railways leads to a net loss of natural habitats and degradation of roadside habitats. This contributes to habitat fragmentation and reduces the available space for wildlife.
2. **Disturbance:** Roads and traffic cause physical, chemical, and biological disruptions to the environment, affecting habitat suitability across broader areas beyond the road itself.
3. **Corridor:** In some cases, roads can provide new habitats or movement corridors for wildlife, but this requires careful management and design by planners.
4. **Mortality rate:** Traffic causes the deaths of many animals that attempt to cross roads or live near them. These roadkill

incidents pose a significant threat to some species and also raise concerns about traffic safety.

5. **Barrier:** Roads act as barriers for most flightless terrestrial animals, restricting movement, limiting access to habitats, and leading to population isolation. This barrier effect is a key factor in the overall fragmentation caused by roads.

In addition to the five main impacts, one factor that increases the barrier effect is that some wildlife avoid areas near roads due to the disturbance caused by roads and traffic. Furthermore, roads and roadsides can attract certain animals by providing resources. For example, road surfaces offer suitable basking areas for reptiles, herbivores may forage in the enhanced vegetation along roadsides, and scavengers are drawn to roadkill. Additionally, many animals use roads for easier movement (van der Ree et al., 2015). This attraction effect can also lead to an increase in roadkill incidents.

Paved roads generally have much larger environmental impacts than unpaved roads. In wetter regions, paved roads provide year-round access to natural resources such as timber, minerals, or agricultural land, while unpaved roads may become impassable during certain seasons. Paved roads are also typically wider and have faster and more frequent traffic, posing a greater danger and movement barrier for wildlife (Laurance et al., 2002; Kirby et al., 2006; Barber et al., 2014; van der Ree et al., 2015).

The most noticeable impact of roads and traffic on wildlife is vehicle collisions (A). Some species are attracted to roads due to resources like carrion, spilled grain, or heat for shelter (B), which can lead to death depending on their ability to avoid traffic (C). The barrier effect restricts animal movement (D), and some individuals die while attempting to cross (E). While some animals cross roads (F), others actively avoid both the road and the degraded habitat nearby (G, H) (Figure 2) (van der Ree et al., 2015).

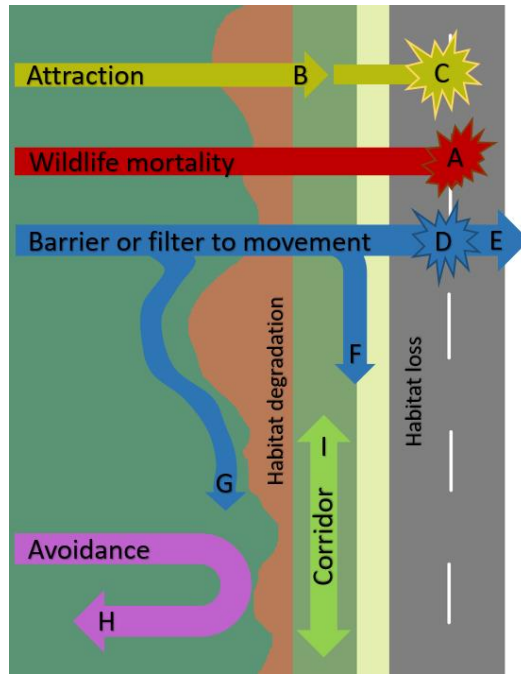


Figure 2. The impacts of roads on wildlife, populations and ecosystems are shown (Modified from van der Ree et al., 2015).

The effects of roads and traffic extend beyond the road itself and its surrounding habitats; disturbances such as habitat modification, noise, light, and chemical pollution reach into adjacent habitats (Forman and Deblinger, 2000). This "road-effect zone" varies depending on road characteristics, traffic volume, and the features of the surrounding landscape (Reijnen et al., 1995; Forman and Deblinger, 2000; Boarman and Sazaki, 2006; Eigenbrod et al., 2009; Benítez-López et al., 2010; Shanley and Pyare, 2011; van der Ree et al., 2015). Road effects are generally strongest near the road and gradually decrease with distance (Eigenbrod et al., 2009). The road-effect zone is useful for assessing and mitigating the environmental impacts of roads (Forman, 2000; van der Ree et al., 2015).

The size of the road-effect zone is influenced by several factors, including vegetation type, wind and water flow directions, topography, and road and traffic characteristics. However, the relative size of the road-effect zone for each parameter is purely descriptive and cannot serve as a precise indicator (van der Ree et al., 2015).

Artificial light

Light serves as a natural stimulus that affects the physiology, behavior, and movement of all organisms. Artificial lighting disrupts the natural photoperiod (daily exposure to light), which inevitably influences the sensory ecology of various species. Furthermore, the presence of multiple light sources in a given area can lead to cumulative effects on ecosystems. When lighting is required for roadways, it is essential to consider not only human sensitivity to different wavelengths for the safety of drivers and pedestrians but also the biological significance of lighting for local organisms (van der Ree et al., 2015). The response to artificial light varies among species according to their visual systems. Natural light plays a significant role in determining the timing of seasonal events and mate selection in birds, whereas artificial light can disrupt these processes (Dawson et al., 2001; de Molenaar et al., 2006; van der Ree et al., 2015). Furthermore, artificial lighting can interfere with birds' magnetic compass, which is essential for navigation during nocturnal migration (Poot et al., 2008). It can further affect the quality of breeding habitats, prey availability, singing patterns, and foraging, drawing birds to illuminated areas and increasing their exposure to predators (Negro et al., 2000; Miller, 2006; Santos et al., 2010; van der Ree et al., 2015). For bats, artificial light may present an opportunity by attracting insects (Eisenbeis, 2006), but non-insectivorous species may experience negative effects from light avoidance (Rydell, 2006; Zurcher et al., 2010; Stone et al., 2012; van der Ree et al., 2015). Bats attracted to artificial lighting may also be at risk of vehicle collisions (Zurcher et al., 2010). In other terrestrial mammals, artificial light disrupts photoperiods, interferes with migration, and increases predation risks associated with lighting (Patricelli and Blickley, 2006; van der Ree et al., 2015).

Noise

Road noise includes both the noise generated during road construction and the noise caused by vehicle traffic; these types of noise differ from natural sounds in many ways. Although construction

noise is temporary, traffic noise is continuous and can extend beyond 2 km depending on traffic volume, speed, topography, and weather conditions (van der Ree et al., 2015). Easily disturbed by noise, animals may temporarily or permanently avoid areas affected by road noise, which reduces the habitat available to them (van der Ree et al., 2015). Animals unable or unwilling to leave noisy areas may suffer from chronic physiological stress, which can lead to secondary effects such as weakened immune function and lower reproductive success (McEwen and Wingfield, 2003; Wikelski and Cooke, 2006; Kight and Swaddle, 2011; Blickley et al., 2012).

Various animal groups, including insects, fish, amphibians, birds, and mammals, rely on sound for communication. For example, birds use songs to attract mates, defend territories, and maintain contact with their young. Hearing is also crucial for detecting predators or locating prey. Acoustic interference happens when background noise reduces the range at which sounds can be perceived. Although animals have developed strategies to cope with natural noise (e.g., Brumm and Slabbekoorn, 2005), road noise adds an extra layer of difficulty. It can disrupt social interactions and reduce reproductive success, potentially leading to changes in ecological communities (Patricelli and Blickley, 2006; Kight et al., 2012; Proppe et al., 2013).

Certain animals have been observed modifying their songs or calls to ensure they can be heard over road traffic noise. For example, they might sing louder or vocalize during quieter periods of the day to evade the noisiest traffic times (Barber et al., 2010). Nevertheless, these adaptations typically do not fully recover the lost communication distance (Parris et al., 2009; Parris and McCarthy, 2013). Acoustic interference from road noise can heighten animals' vulnerability to predators or diminish the hunting success of those that rely on sound to locate prey. Increased background noise levels also lead to greater vigilance among animals; since they cannot hear approaching predators, they tend to spend more time monitoring their surroundings and less time foraging (Barber et al., 2010). Evidence suggests that animals, such as bats, avoid foraging near noisy highways where it becomes more difficult to detect their prey (Schaub et al., 2008). A

recent behavioral experiment using simulated highway noise revealed that the foraging efficiency of the greater mouse-eared bat significantly decreased as it approached the simulated road. These noise effects may have broader implications for predator-prey interactions and food webs within ecological communities (Seiler, 2001; Siemers and Schaub, 2011). Noise from road construction or traffic can result in temporary or permanent hearing loss in animals. An animal's hearing threshold is defined as the point at which a sound becomes audible; a higher threshold indicates that the sound must be louder to be detected. Elevated noise levels can damage the cochlea, leading to a temporary or permanent increase in hearing thresholds (Kight and Swaddle, 2011).

Pollution

Most pollutants accumulate near the road, but long-distance transport (downwind or downhill for several hundred meters) is not uncommon (e.g., Hamilton and Harrison, 1991). Traffic generates dust from the road surface, which then settles along the edges and on adjacent vegetation. Epiphytic lichens and mosses in wetlands and Arctic ecosystems are particularly susceptible to this form of pollution (Auerbach et al., 1997). Moreover, de-icing road salts (NaCl, CaCl₂, KCl, MgCl₂) create a substantial environmental concern in boreal and alpine regions (Blomqvist, 1998). Road salt can inflict considerable harm on vegetation, especially coniferous forests, contaminate drinking water sources, and decrease soil pH, thereby enhancing the mobility of heavy metals (Bauske and Goetz, 1993; Reck and Kaule, 1993). Heavy metals and trace elements, including Pb, Zn, Cu, Cr, Cd, and Al, are dispersed through de-icing salts or aerosols, leading to their accumulation in plant and animal tissues, which can negatively impact reproduction and survival (Scanlon, 1987)..

Traffic exhaust releases polycyclic aromatic hydrocarbons, dioxins, ozone, and various fertilizer chemicals, which can cause physiological distress in plants and animals at high concentrations (Scanlon, 1991; Reck and Kaule, 1993). Alterations in plant growth and species diversity related to traffic exhaust have been observed in lakes

and heathlands located more than 200 meters away from roads (Gjessing et al., 1984; Angold, 1997).

Vehicle Collisions

Roadkill is likely the most well-known impact of traffic on wildlife, as the sight of dead animals on open roads is common (Figure 3-7). For many years, biologists have been concerned about animals killed on roads (e.g., Stoner, 1925; Trombulak and Frissell, 2000). As traffic increases and infrastructure expands, the number of casualties continues to rise (Seiler, 2001).

Roads with vehicle traffic have likely become the main human cause of vertebrate deaths, outpacing hunting (Forman and Alexander, 1998). The sheer number of roadkill alone tells a tragic story (Seiler, 2001). Hodson (1966) estimated that approximately 4 million birds were killed on roads annually in England in 1960. In the Netherlands, Van den Tempel (1993) reported a roadkill rate of at least 2 million birds per year. Comprehensive field inventories in Belgium indicated that road traffic results in the loss of around 4 million large vertebrates each year (Rodts et al., 1998). Hansen (1982) estimated that in Denmark, 1.5 million mammals, 3.7 million birds, and over 3.1 million amphibians are killed on roads each year. Göransson et al. (1978) reported that in Sweden during the mid-1970s, 1 million birds and 0.5 million medium-sized mammals were lost annually. More recent estimates based on different sampling methods suggest that as many as 8.5 million birds die on Swedish roads (Svensson, 1998). In the U.S., evaluations from the 1960s indicated that at least 1 million animals were killed on roads each day (Lalo, 1987). The number of animals killed on roads is indeed alarming. Collisions between vehicles and wildlife (Figures 3-7) present an escalating issue not only for species conservation and game management but also for traffic safety and the economy (e.g., Harris and Gallagher, 1989; Hartwig, 1993; Romin and Bissonette, 1996; Putman, 1997). In many countries, traffic safety is the primary motivation behind mitigation efforts aimed at reducing wildlife casualties. Although human fatalities from wildlife-vehicle collisions are relatively infrequent, the number of injuries is substantial, and the

total economic costs, including vehicle damage, can be considerable. Police records from Europe (excluding Russia) indicate that there are over half a million ungulate-vehicle collisions each year, resulting in at least 300 human deaths, 30,000 injuries, and more than 1 billion USD in property damage (GrootBruinderink and Hazebroek, 1996).



Figure 3. Bird carcass found on the roadside (source: Şirin Bahar Karahasan)



Figure 4. Bird carcass found on the roadside (source: Merve Seyfe)



Figure 5. Hedhehog carcass found on the roadside (source: Tolga Kankılıç)



Figure 6. Stone marten carcass found on the roadside (source: Tolga Kankılıç)



Figure 7. Red fox carcass found on the roadside (source: Tolga Kankılıç)

From a humane perspective, road accidents are also concerning: many animals struck by vehicles do not die immediately but later succumb to injuries or shock. Fehlberg (1994) noted that drivers trying to avoid causing unnecessary suffering to animals they hit are acting in violation of German animal welfare laws. In northern Sweden, train drivers have reported distressing encounters when colliding with groups of reindeer and deer (Åhren and Larsson, 1999).

The presence of large mammal carcasses along roadsides or on road surfaces is increasingly becoming a source of discomfort for the public. Ongoing research initiatives, photography exhibitions, and guides on 'flattened fauna' (e.g., Knutson, 1987; Rodts et al., 1998)

further enhance public awareness of this issue. Therefore, even if roadkill does not pose a direct threat to a species' survival, the economic and ethical implications require the establishment of mitigation measures. To determine when and where roadkill reduction is needed, the issue must be examined from both ecological and human perspectives (Seiler, 2001).

Assessing the ecological importance of roadkill for a species necessitates taking into account the population size and recruitment rate. A high number of deaths within a species does not automatically jeopardize its survival; rather, it may reflect that the species is abundant and widely distributed. For numerous common wildlife species, such as rodents, rabbits, foxes, sparrows, and blackbirds, mortality caused by traffic is usually deemed minimal, constituting less than 5% of overall deaths (e.g., Haugen, 1944; Bergmann, 1974; Schmidley and Wilkins, 1977; Bennett, 1991; Rodts, 1998). For species such as red deer (*Cervus elaphus*), roe deer, and wild boar (*Sus scrofa*), traffic-related mortality typically represents less than 5% of the annual spring populations in Europe (e.g., GrootBruinderink and Hazebroek, 1996). "Data from Swedish police records from the early 1990s reveal that collisions between vehicles and deer represented about 6% of the yearly national harvest of roe deer and red deer (Lavsund and Sandegren, 1991). Traffic mortality differs from natural predation in that it is not compensative; the rate of deaths does not depend on population density and instead tends to vary linearly with the size of the population. This indicates those roads can considerably affect rare species. Species found in small, isolated populations, those that require large habitats, or those that undertake long migrations are particularly vulnerable to road deaths. As the habitat size increases, the more often individuals come across roads, and in smaller populations, each individual holds greater significance. In fact, for numerous endangered mammal species across the globe, traffic is regarded as one of the primary causes of mortality (e.g., Harris and Gallagher, 1989).

For the threatened Florida panther (*Felis concolor*), road fatalities constitute more than 50% of all recorded deaths, establishing it as the primary cause of mortality (Harris and Gallagher, 1989; Harris and

Scheck, 1991). For the Iberian lynx, road traffic accounts for 6-10% of deaths, making it the second most significant cause of mortality (Rodriguez and Delibes, 1992). In Italy, traffic was accountable for 7-25% of the recorded annual death rate in wolves and up to 100% of the documented death rate in bears from 1974 to 1984 (Boscali, 1987). In the Netherlands, approximately 20% of the yearly badger population is lost to road accidents, with vehicle traffic recognized as a significant threat to the species (e.g., Van der Zee et al., 1992; Broekhuisen and Derckx, 1996). In Barn owl (*Tyto alba*), a yearly traffic death rate of 7-10% during the breeding season could substantially decrease population growth in the Netherlands (Van den Tempel, 1993). The hedgehog is among the small mammals found in Europe that appears to be greatly impacted by road traffic and may need targeted conservation efforts to avoid local extinction (Göransson et al., 1978; Reicholf and Esser, 1981; Huijser et al., 1998; Rodts et al., 1998). Amphibians have garnered considerable attention, as infrastructure is identified as a major contributor to their worldwide decline (Vestjens, 1973; Blaustein and Wake, 1990; Reh and Seitz, 1990; Fahrig et al., 1995). Due to their migrations of the season to breeding ponds, which often require crossing roads, amphibians are particularly vulnerable to road mortality. For instance, Van Gelder (1973) discovered that roads with just 10 vehicles per hour could result in a 30% mortality rate among female *Bufo bufo*. Roads with over 60 vehicles per hour created nearly an impenetrable barrier. Vos and Chardon (1998) found that breeding ponds located near highways were considerably less likely to support frog populations compared to undisturbed ponds situated further away. Sjögren-Gulve (1994) discovered that roads in the suburbs of Stockholm effectively separated amphibian populations. As road density and traffic volume increased, the risk of local extinction rose significantly (Seiler, 2001).

The risk of animal-vehicle collisions is affected by several factors. Typically, the rate of these collisions escalates with higher traffic density, increased animal activity, and greater population density. Temporal fluctuations in roadkill numbers correspond to biological cycles that affect species behavior, including feeding and

resting habits, mating and breeding periods, juvenile dispersal, and seasonal migrations (e.g., Van Gelder, 1973; Bergmann, 1974; Göransson et al., 1978; Aaris-Sorensen, 1995; GrootBruinderink and Hazebroek, 1996). Variations in temperature, precipitation, or snow cover can also impact the frequency and timing of wildlife-vehicle collisions (e.g., Jaren et al., 1991; Belant, 1995c; Gundersen and Andreassen, 1998). While wildlife-vehicle collisions generally occur in areas where roads or railways disrupt a species' habitat, local environmental factors can greatly influence this relationship. While roadkill appears to rise with increasing traffic volume, excessively high levels of traffic may deter animals from crossing roads, thereby mitigating further mortality increases (e.g., Oxley et al., 1974; Berthoud, 1987; Van der Zee et al., 1992; Clarke et al., 1998). Mitigation measures like fences or wildlife crossings can clearly impact the risk of for instance, clearing vegetation along roadsides and railways has been demonstrated to reduce deer collisions by about 20% and 50% in Scandinavia, respectively (Lavsund and Sandegren, 1991; Jaren et al., 1991). Conversely, when roadsides offer appealing resources for wildlife, the likelihood of vehicle-wildlife collisions may rise and should be balanced against the benefits of habitat enhancement (e.g., Feldhamer et al., 1986; Steiof, 1996; GrootBruinderink and Hazebroek, 1996).

Railways

Railways and trains influence wildlife in ways comparable to roads and vehicles, although the extent of their impact varies. Similar to roads, railways can adversely affect wildlife through collisions, as well as noise, light and chemical pollution (Figure 8). Four primary types of impacts have been identified (Dorsey, 2011), the most apparent being direct wildlife-train collisions (WTC). The other effects include habitat alteration, fragmentation, and barriers to movement (van der Grift, 1999).



Figure 8. Highway, normal and high-speed train lines that increase the barrier effect by coming side by side (Location: Kirikkale, Balıışeyh, Türkiye) (source: Şirin Bahar Karahasan).

In certain instances, railway impacts on wildlife may surpass those associated with roads and are often more challenging to observe. Wildlife fatalities along railways can result from direct train collisions, electrocution, rail entrapment, and collisions with overhead wires. Sometimes, animals may find themselves trapped between the rails, resulting in deadly overheating due to extended exposure to sunlight (Kornilev et al., 2006; van der Ree et al., 2015).

Impacts on some animal populations

To safeguard a species, it is crucial to comprehend how roads impact the viability of populations as a whole, rather than focusing solely on individual animals. The central issue is whether roads and traffic can decrease or eradicate a population, and if so, in what manner. Wildlife populations are affected by roads and traffic in three primary ways: they increase mortality rates, decrease habitat quantity and quality, and divide populations into smaller subpopulations that are more susceptible to local extinction (van der Ree et al., 2015).

A species' susceptibility to roads and traffic is shaped by its ecological traits and behavioral adaptations. Key ecological traits include reproductive rate (higher rates help populations recover from

roadkill) and mobility (more mobile species are more likely to encounter roads frequently). Four behavioral responses influence the impact of roads and traffic on populations: evading the road surface, steering clear of disturbances caused by traffic (such as noise, lights, and chemical emissions), avoiding vehicles themselves, and, in some cases, being drawn to roads. Species that steer clear of road surfaces are at a lower risk of being killed, but they may face challenges in reaching vital habitats or resources. Similarly, species that avoid traffic disturbances may be less prone to roadkill but can be fragmented into smaller, more vulnerable populations. Avoidance of traffic also reduces available habitat near roads (road impact zone) (van der Ree et al., 2015).

Mammals

Most population-level studies on mammals have focused on three groups: rodents (27 species), hoofed mammals (specifically ungulates) (16 species), and carnivores (24 species). Overall, rodent and ungulate populations typically rise in response to the presence of roads, whereas carnivore populations experience a decline. Among the rodent species studied, only a small number were adversely impacted by roads, while a greater proportion exhibited positive or neutral reactions (van der Ree et al., 2015).

Rodents that show positive or neutral responses to roads are generally smaller species. Among ungulates, the number of species that demonstrate positive population-level effects due to roads is nearly double that of those negatively affected. Species that suffer negative impacts include North American elk, wild boar, European roe deer, woodland caribou, and mule deer. Conversely, species that benefit from roads consist of white-tailed deer, moose, Peter's duiker, and yellow-backed duiker. The positive effects of roads on large herbivores, including white-tailed deer and smaller mammals, may arise from decreased predation pressure, as many of their main predators tend to decline in areas with high road density (Munro et al., 2012; van der Ree et al., 2015). Overall, carnivores are the most negatively affected mammalian group by roads. Examples include the bear family (such as the sloth bear, grizzly bear, and black bear), the mustelid family

(including the Eurasian badger, fisher, and wolverine), and the felid family (which features the leopard, Iberian lynx, and Eurasian lynx). Among the species examined, the only carnivore that exhibits a positive response to roads is the Siberian weasel, likely because of its higher reproductive rate and smaller litter size compared to larger carnivores (van der Ree et al., 2015).

Larger, more mobile mammals that have lower reproductive rates tend to be more vulnerable to the adverse impacts of roads on their populations than smaller, less mobile species. Species that have lower reproductive rates are less able to rebound from population declines resulting from road mortality. Species that cover greater distances or maintain larger territories are probably more impacted by roadkill as they come into contact with roads more often. Overall, larger species experience a greater impact than smaller ones due to their typically lower reproductive rates and higher mobility. Nonetheless, there are exceptions, as species that are abundant in local areas yet possess restricted geographic ranges or limited dispersal capabilities may still be susceptible to the impacts of roads, even if they have high reproductive rates or lower mobility (van der Ree et al., 2015).

Birds

A review of 16 studies conducted across 8 countries, encompassing 194 bird species, yielded 270 records concerning the effects of roads and traffic. The majority of research regarding the influence of roads on avian populations centered on perching birds, particularly songbirds (comprising 153 of the 194 species). Although some species exhibited negative population impacts, the overall effect was not strongly pronounced. Species identified as negatively impacted include chats and oldworld flycatchers (such as the northern wheatear and European robin), sandpipers (like the common redshank), wrens (including the winter wren and sedge wren), and Australian treecreepers (the brown treecreeper and white-throated treecreeper). Conversely, species demonstrating neutral or positive responses encompass buntings, American sparrows (such as the song sparrow and rock bunting), and new world warblers (including the black-throated blue warbler and Nashville warbler) (van der Ree et al., 2015).

Generally, more mobile bird species—those with larger territories—are at a greater risk from road impacts compared to less mobile ones (van der Ree et al., 2015). Ground-dwelling birds are believed to face a heightened danger of wildlife-vehicle collisions (WVC) because they spend more time on the road surface or tend to fly at lower altitudes (Jacobson, 2005). Furthermore, birds that are heavier in relation to their wing size (such as female owls) or those with a low takeoff trajectory are also considered more vulnerable to WVC (Kociolek and Clevenger, 2011). Species that require movement between different habitat types—like certain forest birds and wintering waterfowl—are likely to be more sensitive to the effects of roads (van der Ree et al., 2015).

There is limited research on how birds behave in response to roads and traffic. However, road attraction behavior has been noted in two species: the common raven and the black kite. In both cases, although these species experience fatalities due to collisions, their populations appear to remain stable and unaffected by the presence of roads (Palomino and Carrascale, 2007). While there are no quantitative studies specifically measuring vehicle avoidance in these species, it is possible that if they exhibit avoidance behavior and also benefit from roadkill as a food source, the positive effects on their reproductive success could offset or neutralize the negative impacts of road fatalities. This could explain the observed neutral effects of roads on their populations (van der Ree et al., 2015).

Numerous researchers have proposed or assumed that traffic noise is the main factor contributing to the adverse impacts of roads on bird populations. Traffic noise can disrupt birds' communication via song, complicating the ability of certain species to attract mates or defend their territories (Rheindt, 2003). Noise can also divert individuals' attention, increasing their vulnerability to predation. These findings are supported by observations of reduced bird presence and heightened traffic noise in proximity to roads. However, as road mortality rates are also higher near roads, it is unclear whether noise, mortality, or both factors contribute to the detrimental impacts on bird populations. Differentiating between these factors is crucial for designing effective mitigation strategies (Summers et al., 2011). The observation that more mobile bird species are more susceptible to the

impacts of roads than their less mobile counterparts provide indirect support for the mortality hypothesis rather than the noise disturbance hypothesis. Additionally, certain research on the impacts of roads on bird populations may have conflated road distance with habitat edge effects. This implies that the observed effects related to roads could be partly or predominantly attributed to edge effects instead (Delgado García et al., 2007; Summers et al., 2011).

Amphibians and Reptiles

For amphibians, a review of 16 studies conducted across 6 countries, encompassing 23 species, revealed 42 records pertaining to road and traffic effects. Generally, roads and traffic are found to diminish populations of frogs, toads, and salamanders. In contrast, for reptiles, 9 studies from 3 countries were examined, which covered 11 species and resulted in 16 records of road impacts. Turtles, snakes, and lizards typically experience negative impacts from roads. While amphibians and reptiles face a higher risk compared to mammals or birds, there is a relative lack of studies addressing the population-level effects of roads on these groups. The existing research indicates that amphibians are predominantly adversely impacted by roads, with only one species demonstrating a positive response. (northern two-lined salamander) showing a positive effect. Amphibian species that experience negative effects include the spring peeper, European tree frog, and tiger salamander. In reptiles, snake species exhibit both negative and neutral responses, while only one species, the eastern diamondback rattlesnake, demonstrates a slight positive effect (van der Ree et al., 2015).

The impact of roads on turtle populations differs among species: three species, namely the desert tortoise, wood turtle, and spotted turtle, exhibit negative effects; two species, the common snapping turtle and musk turtle, show neutral effects; while one species, the painted turtle, demonstrates positive effects (van der Ree et al., 2015). Generally, amphibians that have lower reproductive rates tend to be more susceptible to the impacts of roads. Many reptiles, on the other hand, are long-lived and exhibit high annual survival rates for adults, frequently traveling considerable distances on land to locate mates or nesting sites. These characteristics, along with their slow movement on

roadways, render them especially susceptible to road-related mortality. Estimating reptile population sizes is difficult, which may lead to underestimating the true impact of roads. Moreover, for species that nest near roads, such as painted turtles, a decrease in nest predation might mitigate the negative impacts of road mortality (Langen, 2009). Species that require movement between different habitats are particularly at risk of roadkill and habitat fragmentation. For example, many frogs and salamanders need to travel between aquatic breeding sites, upland feeding areas, and specific overwintering locations. If these habitats are not close together, they may have to cover significant distances. In regions with high road density, it is unlikely that all these habitats will be situated in a road-free area, and in some instances, animals may have to navigate across roads, leading to elevated mortality rates (van der Ree et al., 2015).

Road deaths have an indirect impact on amphibian and reptile populations by lowering reproductive rates. As these species mature, their reproductive output tends to rise, with larger individuals producing more eggs and continuing to grow throughout their lifespan. However, roadkill skews the population dynamics towards younger, smaller individuals, which ultimately results in a decrease in the overall reproductive rate (Karraker and Gibbs, 2011).

Invertebrates

Invertebrate species are estimated to account for nearly 99% of all animal species on Earth, with many yet to be discovered or documented. About 75% of these invertebrates are insects, such as beetles, bees, butterflies, and crickets. The remainder includes mollusks (7%), crustaceans (4%), spiders (8%), and worms (5%). Given the incredible diversity and differences among invertebrates, providing a brief overview of them is almost impossible (van der Ree et al., 2015).

Current statistics indicate that invertebrate mortality rates significantly surpass those of vertebrates. Many butterfly species typically avoid crossing roads; however, those that attempt to do so often face high mortality rates, with studies showing that up to one in three individuals may die while trying to cross in certain situations. Population-level studies on invertebrates near roads are scarce, but

many species, especially moths, exhibit significantly lower population densities in high-traffic areas. A major challenge in studying invertebrate road mortality is the difficulty in detecting dead individuals, and in many cases, the impact on vehicles is minimal. Additionally, insect deaths can be attributed to traffic lights; in some locations, the accumulation of dead insects beneath streetlights can reach depths of several centimeters. Invertebrates are highly sensitive to environmental pollution. Pollutants from vehicles, such as exhaust fumes and tire wear, as well as those from roads, like dust from unpaved surfaces or de-icing chemicals, can accumulate in the soil and vegetation near roadways, adversely affecting invertebrate communities. For instance, a study conducted near Moscow, Russia, revealed that the population density of earthworms located 30 meters from a road with 3,000 vehicles passing daily was 50% lower than in comparable habitats situated 200 meters away (Bykov and Lysikov, 1991). Pollutants can indirectly change the composition of plant species along roadsides, affecting the suitability of habitats for various organisms. Nonetheless, the impacts of traffic pollution on invertebrates are not well understood and are infrequently considered in environmental impact assessments (van der Ree et al., 2015).

Several transnational regulations and agreements address wildlife deaths on roads and the barrier effects of roads. The EU Habitats Directive, Birds Directive, Environmental Liability Directive, EIA Directive, as well as the Bonn and Bern Conventions, explicitly focus on species protection. These legal frameworks set out conservation objectives, responsibilities, acceptable levels of impact, priority species, mitigation principles, and research and monitoring requirements. Road fatalities are prohibited under these laws and can be considered deliberate killings (van der Grift et al., 2017).

The Habitats Directive, Birds Directive, and Bern Convention prohibit the deliberate killing of listed species. The distinction between deliberate and non-deliberate killing remains debated, but current road guidelines indicate that road fatalities are not automatically classified as non-deliberate. Road projects must ensure that impacts on species remain within acceptable levels. The Habitats Directive, Environmental

Liability Directive, and Bonn Convention define an acceptable level of impact on widespread species as "favorable conservation status." This status requires population dynamics data to demonstrate that species are maintaining themselves in the long term and that their distribution is not declining (van der Grift et al., 2017).

The "Transportation and Service Corridors" threat category in the IUCN Red List addresses DD transportation corridors outside of urban areas. These corridors contribute to biodiversity loss through habitat fragmentation and pose additional threats such as agriculture, poaching, and invasive species (Figure 9) (IUCN, 2024).

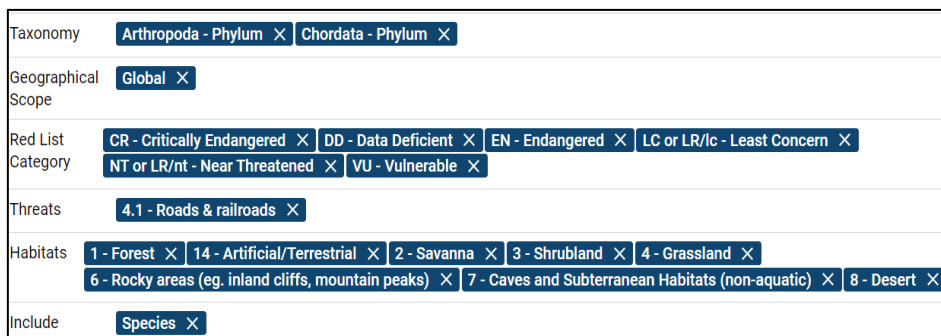


Figure 9. Selected categories in the IUCN red list to understand the impacts of roads on vertebrates and arthropods (IUCN, 2024).

According to an analysis on the IUCN Red List, about 50% of the species affected by roads as a threat factor are classified in critical danger categories (CR, EN, VU) (Figure 10). Forests are the most impacted terrestrial ecosystem by roads (Figure 11) (IUCN, 2024).

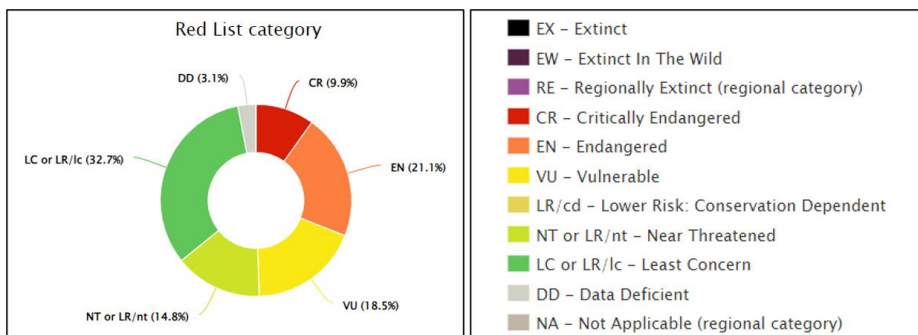


Figure 10. Distribution of animal species threatened by roads and railways according to IUCN threat categories (IUCN, 2024)

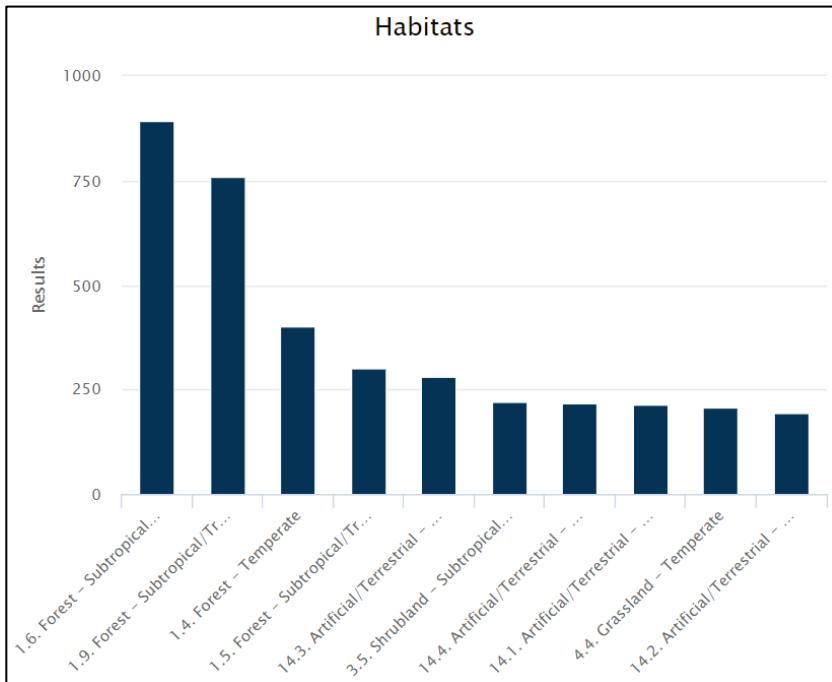


Figure 11. Distribution of animal species numbers in the top ten terrestrial habitat types affected by roads and railways according to IUCN (IUCN, 2024)

The effects of roads and traffic on ecosystems, wildlife populations, and overall biodiversity have grown increasingly complex due to urbanization and industrialization. This complexity arises from the interplay of various factors, including habitat fragmentation, increased mortality rates, and altered animal behaviors, all of which contribute to the decline of many species and disrupt ecological balance. As human activities expand, understanding and addressing these impacts becomes essential for effective conservation and sustainable development. Roads disrupt the natural cycles and habitats of wildlife through both direct and indirect means, not only leading to population declines but also causing genetic isolation between species. The primary factors affecting the biotic and abiotic components of ecosystems surrounding roads include habitat fragmentation, barrier effects, wildlife-vehicle collisions (WVCs), traffic noise, light pollution, and chemical pollutants. While the known and predicted

negative effects of roads are significant, solution-oriented approaches remain limited, and this issue has not received the attention it deserves.

The reduction of habitats for predator species due to roads can trigger cascading changes in prey-population dynamics, potentially destabilizing ecosystem processes. Roads also reduce genetic diversity for insects and other small species, threatening the overall health of populations. This situation could lead to biodiversity loss on both regional and worldwide scales. Moreover, the barrier effect of roads restricts animal movements, significantly disrupting their feeding, breeding, and migration behaviors. This disruption can lead to decreased access to essential habitats, increased mortality rates, and ultimately contribute to population declines. As animals are forced to navigate around these barriers, their ability to find food, mates, and suitable nesting sites is compromised, which can further exacerbate the challenges they face in an increasingly fragmented landscape. In particular, smaller species, such as insects, are especially vulnerable to the loss of genetic diversity, which undermines population health. For larger mammals, habitat fragmentation and the barrier effect of roads can significantly disrupt migration and reproductive behaviors, leading to population declines and ecosystem imbalance.

The IUCN Red List highlights that a significant portion of species affected by roads fall into critical danger categories (CR, EN, VU). Terrestrial ecosystems, particularly forests, are among the most impacted by road development, with many endemic and sensitive species at risk due to habitat loss. The physical barrier created by roads disrupts not only animal movements but also ecosystem interactions, potentially leading to significant declines in biodiversity. Although roads are increasingly recognized as a major threat to species, their impact on biodiversity is often overlooked in environmental assessments.

While this review does not specifically focus on mitigation, it is clear that addressing the impact of roads requires comprehensive environmental policy and infrastructure planning. Every new road project (e.g., wind farms, mining operations) should include a thorough evaluation of its ecological impacts within its Environmental Impact

Assessment (EIA). As human populations expand, the demand for infrastructure and transportation networks intensifies, further amplifying the adverse impacts of roads on wildlife and biodiversity. The future of many species is at stake if effective mitigation measures are not put in place. It is essential to adapt conservation strategies, enhance public awareness, and incorporate the effects of roads on ecosystems into every new infrastructure project. This proactive approach can help minimize habitat fragmentation, reduce wildlife mortality, and ultimately support the preservation of biodiversity in the face of ongoing urbanization and development pressures.

As a result, more effective conservation strategies are needed to reduce the impacts of roads on wildlife and ecosystems. Applied scientific research must develop solutions that demonstrate species' long-term sustainability and the preservation of population dynamics. Addressing these impacts at both local and international levels is a critical step in protecting biodiversity. Mitigation measures should be aligned with these impacts, and public awareness of the issue must be increased.

REFERENCES

- Aaris-Sorensen, J. (1995). Road-kills of badgers (*Meles meles*) in Denmark. *Annales Zoologici Fennici*, 32, 31-36.
- Åhrén, T. and Larsson, P.O. (1999). Train collisions with reindeer (Renspåkörningar) – In Swedish. 46 pages. Report from Swedish National Rail authorities, Banverket Norra Regionen, Luleå, Sweden.
- Angold, P.G. (1997). The impact of a road upon adjacent heathland vegetation: Effects on plant species composition. *Journal of Applied Ecology*, 34, 409-417.
- Auerbach, N.A., Walker, M.D., Walker, D.A. (1997). Effects of roadside disturbance on substrate and vegetation properties in arctic tundra. *Ecological Applications*, 7(1), 218-235.
- Barber, C.P., Cochrane, M.A. Souza Jr, C.M., Laurance, W.F. (2014). Roads, deforestation, and the mitigating effect of protected areas in the Amazon. *Biological Conservation*, 177, 203–209.
- Barber, J.R., Crooks, K.R., Frstrup, K.M. (2010). The costs of chronic noise exposure for terrestrial organisms. *Trends in Ecology & Evolution*, 25, 180–189.
- Bauske, B. and Goetz, D. (1993). Effects on de-icing salts on heavy metal mobility. *Acta Hydrochimica Et Hydrobiologica*, 21, 38-42.
- Belant, J.L. (1995). Moose collisions with vehicles and trains in northeastern Minnesota. *Alces*, 31, 45-52.
- Benítez-López, A., Alkemade, R., Verweij, P.A. (2010). The impacts of roads and other infrastructure on mammal and bird populations: A meta-analysis. *Biological Conservation*, 143(6), 1307–1316.
- Bennett, A.F. (1991). Roads, roadsides and wildlife conservation: a review. In: Saunders, D.A. and Hobbs, R.J., (Eds.) *Nature conservation 2: The role of corridors*, pp. 99-118.
- Bergmann, H.H. (1974). Zur Phänologie und Ökologie des Strassentods der Vögel. *Vogelwelt*, 95, 1-21.
- Berthoud, G. (1987). Impact d'une route sur une population de chevreuils. In: Bernard, J.-M., Lansiaart, M., Kempf, C. and Tille, M., (Eds.) *Actes du colloques "Route et fauna sauvage"*. Strasbourg, 1985, pp. 167-170. Colmar, France.: Ministère de

- l'Équipement, du Longement, de l'Aménagement du Territoire et des Transports.
- Blaustein, A.R. and Wake, D.B. (1990). Declining amphibian populations: a global phenomenon? *TREE* 5, 203-204.
- Blickley, J.L., Word, K., Krakauer, A.H., Phillips, J.L., Sells, S., Taff, C.C., Wingfield, J.C., Patricelli, G.L. (2012). The effect of experimental exposure to chronic noise on fecal corticosteroid metabolites in lekking male greater sagegrouse (*Centrocercus urophasianus*). *PLoS One*, 7, e50462.
- Blomqvist, G. (1998). Impact of de-icing salt on roadside vegetation- a literature review. VTI rapport 427A, pp.1-36.
- Boscali, G. (1987). Wolves, bears and highways in Italy. In: Bernard, J.M., Lansiaart, M., Kempf, C., Tille, M., (Eds.) Actes du colloques "Route et fauna sauvage". Strasbourg, 1985, pp. 237-239. Colmar, France.: Ministère de l'Équipement, du Longement, de l'Aménagement du Territoire et des Transports.
- Broekhuisen, S. and Derckx, H. (1996). Passages for badgers and their efficacy. *Zeitschrift für Jagdwissenschaft*, 42, 134- 142.
- Brumm, H. and Slabbekoorn, H. (2005). Acoustic communication in noise. *Advances in the Study of Behavior*, 35, 151-209.
- Bykov, A.V. and Lysikov, A.B. (1991). Mole burrows and pollution of forest soils adjacent to highways. *Pochvovedenie*, 8, 31-39.
- Can, Ş. B. and Hasbenli, A. (2021). Camera trap method as an alternative method for bat monitoring in highway drainage structures. *Biodicon*, 14(2), 249-257.
- Central Intelligence Agency (CIA). (2024). The World Factbook: Country Comparison- Roadways. <https://www.cia.gov/the-world-factbook/about/archives/2024/field/roadways/country-comparison> (Accessed: 21.10.2024).
- Clarke, G. B., White, P.C.L. and Harris, S. (1998). Effects of roads on badger *Meles meles* populations in south-west England. *Biological Conservation*, 86, 117-124.
- Dawson, A., King, V.M., Bentley, G.E., Ball, G.F. (2001). Photoperiodic control of seasonality in birds. *Journal of Biological Rhythms*, 16, 365-380.
- D'Amico, M., Ascensão, F., Fabrizio, M., Barrientos, R., Gortázar, C. (2018). Twenty years of Road Ecology: A Topical Collection

- looking forward for new perspectives. *European Journal of Wildlife Research*, 64(3), 26.
- Delgado García, J.D., Arévalo, J. R., Fernández-Palacios, J. M. (2007). Road edge effect on the abundance of the lizard *Gallotia galloti* (Sauria: Lacertidae) in two Canary Islands forests. *Biodiversity and Conservation*, 16, 2949–2963.
- de Molenaar, J.G., Sanders, M. E., Jonkers, D.A. (2006). Road lighting and grasslands birds: local influence of road lighting on a black-tailed godwit population. Pages 114–136 in C. Rich and T. Longcore, editors. *Ecological consequences of artificial night lighting*. Island Press, Washington, DC.
- Dorsey, B. (2011). Factors affecting bear and ungulate mortalities along the Canadian Pacific Railroad through Banff and Yoho National Parks. Master's thesis, Montana State University. Available from <https://scholarworks.montana.edu/server/api/core/bitstreams/6c7939e7-a1c2-4905-9013-5cd558cdef8d/content> (Accessed 21 October 2024).
- Dulac, J. (2013). Global land transport infrastructure requirements: estimating road and railway infrastructure capacity and costs to 2050. International Energy Agency, Paris.
- Eisenbeis, G. (2006). Artificial night lighting and insects: attraction of insects to streetlamps in a rural setting in Germany. Pages 281–304 in C. Rich and T. Longcore, editors. *Ecological consequences of artificial night lighting*. Island Press, Washington, DC.
- Fahrig, L., Pedlar, J.H., Pope, S.E., Taylor, P.D., Wegener, J.F. (1995). Effect of road traffic on amphibian density. *Biological Conservation*, 73, 177-182.
- Fehlberg, U. (1994). Ökologische Barrierewirkung von Straßen auf wildlebende Säugetiere- ein Tierschutzproblem? *Die Berliner und Münchener Tierärztliche Wochenschrift*, 101, 81-132.
- Feldhamer, G.A., Gates, J.E., Harman, D.M., Loranger, A.J. and Dixon, K.R. (1986). Effects of interstate highway fencing on white-tailed deer activity. *Journal of Wildlife Management*, 50, 497-503.

- Forman, R.T.T. and Alexander, L.E. (1998). Roads and Their Major Ecological Effects. *Annual Review of Ecology and Systematics*, 29, 207-231.
- Forman, R.T.T. and Deblinger, R.D. (2000). The ecological road-effect zone of a Massachusetts (U.S.A.) suburban highway. *Conservation Biology*, 14, 36–46.
- Forman, R.T.T. (1998). Road ecology: A solution for the giant embracing us. *Landscape Ecology*, 13, iii-v.
- Gjessing, E., Lygren, E., Berglind, L., Gullbranden, T., Skanne, R. (1984). Effect of highway runoff on lake water quality. *Science of the Total Environment*, 33, 247-257.
- Göransson, G., Karlsson, J., Lindgren, A. (1978). Influence of roads on the surrounding nature: II. Fauna. Swedish Environmental Protection Agency, SNV PM 1069.
- Grilo, C., Bissonette, J.A., Cramer, P.C. (2010). Mitigation Measures to Reduce Impacts on Biodiversity. In S. R. Jones (Ed.), *Highways: Construction, Management, and Maintenance* (pp. 73–114). Hauppauge, NY: Nova Science Publishers.
- GrootBruinderink, G.W.T.A. and Hazebroek, E. (1996). Ungulate traffic collisions in Europe. *Conservation Biology*, 10(4), 1059-1067.
- Gundersen, H. and Andreassen, H.P. (1998). The risk of moose *Alces alces* collision: A predictive logistic model for moose-train accidents. *Wildlife Biology*, 110.
- Hansen, L. (1982). Road kills in Denmark (in danish with english abstract). - *Dansk Ornitologisk Forenings Tidsskrift*, 76, 97-110.
- Hamilton, R.S. and Harrison, R.M. (1991). *Highway pollution: Studies in environmental sciences*. Amsterdam: Elsevier.
- Harris, L.D. and Gallagher, P.B. (1989). New initiatives for wildlife conservation: The need for movement corridors. In *In defense of wildlife: Preserving communities and corridors* (pp. 11-34). Island Press.
- Harris, L.D. and Scheck, J. (1991). From implications to applications: the dispersal corridor principle applied to the conservation of biological diversity. In: Saunders, D.A. and Hobbs, R.J., (Eds.) *Nature conservation 2: The role of corridors*, pp. 189-220. Chipping Norton: Surrey Beatty & Sons.

- Hartwig, D. (1993). Auswertung der durch Wild verursachten Verkehrsunfälle nach der Statistik für Nordrhein-Westfalen. *Zeitschrift für Jagdwissenschaft*, 39, 22-33.
- Haugen, A.O. (1944). Highway mortality in southern Michigan. *Journal of Mammalogy*, 25: 177-184.
- Hodson, N.L. (1966). A survey of road mortality in mammals (and including data for the grass snake and common frog). *Journal of Zoology*, 148(4), 576-579.
- Huijser, M.P., Bergers, P.J.M., De Vries, J.G. (1998). Hedgehog traffic victims: how to quantify effects on the population level and the prospects for mitigation. In: Evink, G.L., Garrett, P., Zeigler, D. and Berry, J., (Eds.) *Proceedings of the International Conference on Wildlife Ecology and Transportation.*, pp. 171-180. Tallahassee, Florida: Florida Department of Transportation, FL-ER-69-98.
- Jacobson, S.J. (2005). Mitigation measures for highway-caused impacts to birds. General technical report PSW-GTR-191. USDA Forest Service, Washington, DC.
- Jaren, V., Andersen, R., Ulleberg, M., Pedersen, P.-H., Wiseth, B. (1991) Moose-train collisions: the effects of vegetation removal with a cost-benefit analysis. *Alces*, 27, 93-99.
- Karraker, N.E. and Gibbs, J.P. (2011). Contrasting road effect signals in reproduction of long- versus short-lived amphibians. *Hydrobiologia*, 66, 213–218.
- Kight, C.R. and Swaddle, J.P. (2011). How and why environmental noise impacts animals: an integrative, mechanistic review. *Ecology Letters*, 14, 1052–1061.
- Kight, C.R., Saha, M.S., Swaddle, J.P. (2012). Anthropogenic noise is associated with reductions in the productivity of breeding Eastern Bluebirds (*Sialia sialis*). *Ecological Applications*, 22, 1989–1996.
- Kirby, K.R., Laurance, W.F., Albernaz, A.K., Schroth, G., Fearnside, P.M., Bergen, S., Venticinque, E. M., da Costa, C. (2006). The future of deforestation in the Brazilian Amazon. *Futures*, 38, 432–453.
- Knutson, R. (1987). A field guide to common animals of roads, streets, and highways. Berkely, USA: Ten Speed Press.

- Kociolek, A.V. and Clevenger, A.P. (2011). Effects of paved roads on birds: a literature review and recommendations for the Yellowstone to Yukon ecoregion. Technical report #8. Yellowstone to Yukon Conservation Initiative, Canmore, Alberta.
- Kornilev, Y., Price, S., Dorcas, M. (2006). Between a rock and a hard place: responses of eastern box turtles (*Terrapene carolina*) when trapped between railroad tracks. *Herpetological Review*, 37, 145–148.
- Lalo, J. (1987). The problem of road kill. *Amer.Forests*, 72, 50-52.
- Lassen, D. (1990) Unzerschnittene verkehrsarme Räume über 100km²-eine Resource für die ruhige Erholung. *Natur und Landschaft*, 65, 326-327.
- Langen, T. A. (2009). Design and testing of prototype barriers and tunnels to reduce the impact of roads on turtle survival and reproductive success. Final report MOU AM05405. New York State Department of Environmental Conservation US Fish & Wildlife Service, Albany, NY.
- Laurance, W.F., Albernaz, A.K.M., Schroth, G., Fearnside, P.M., Venticinque, E., Da Costa, C. (2002). Predictors of deforestation in the Brazilian Amazon. *Journal of Biogeography*, 29, 737–748.
- Lavsund, S. and Sandegren, F. (1991). Moose-vehicle relations in Sweden. *Alces*, 27, 118-126.
- McEwen, B.S. and Wingfield, J.C. (2003). The concept of allostasis in biology and biomedicine. *Hormones and Behavior*, 43, 2–15.
- Miller, M.W. (2006). Apparent effects of light pollution on singing behavior of American robins. *Condor* 108:130–139.
- Munro, K.G., Bowman, J., Fahrig, L. (2012). Effect of paved road density on abundance of white-tailed deer. *Wildlife Research*, 39, 478–487.
- Negro, J.J., Bustamante, J., Melguizo, C., Ruiz, J.L., Grande, J.M. (2000). Nocturnal activity of lesser kestrels under artificial lighting conditions in Seville, Spain. *Journal of Raptor Research*, 34, 327–329.
- Oxley, D.J., Fenton, M.B., Carmody, G.R. (1974). The effects of roads on populations of small mammals. *Journal of Applied Ecology*, 11, 51-59.

- Palomino, D. and Carrascale, L.M. (2007). Threshold distances to nearby cities and roads influence the bird community of a mosaic landscape. *Biological Conservation*, 140, 100–109.
- Parris, K.M. and Schneider, A. (2009). Impacts of traffic noise and traffic volume on birds of roadside habitats. *Ecology and Society*, 14, 29.
- Parris, K.M. and McCarthy, M.A. (2013). Predicting the effect of urban noise on the active space of avian vocal signals. *The American Naturalist*, 182, 452–464.
- Patricelli, G.L. and Blickley, J.L. (2006). Avian communication in urban noise: causes and consequences of vocal adjustment. *The Auk*, 123, 639–649.
- Rheindt, F.E. (2003). The impact of roads on birds: does song frequency play a role in determining susceptibility to noise pollution? *Journal für Ornithologie*, 144, 295–306.
- Rodríguez, A. and Delibes, M. (1992). Current range and status of the Iberian lynx *Felis pardina* Temminck, 1824 in Spain. *Biological Conservation*, 61, 189–196.
- Pfister, H.P., Keller, V., Reck, H., Georgii, B. (1997). Bio- ökologische Wirksamkeit von Grünbrücken über Verkehrswege [Bio-ecological effectiveness of green bridges across transport infrastructure]. *Forschung Strassenbau und Strassenverkehrstechnik*, 756. German Federal Ministry of Transport.
- Poot, H., Ens, B.J., de Vries, H., Donners, M.A.H., Wernand, M.R., Marquenie, J.M. (2008). Green light for nocturnally migrating birds. *Ecology and Society*, 13, 47.
- Proppe, D.S., Sturdy, C.B., Cassady St Clair, C. (2013). Anthropogenic noise decreases urban songbird diversity and may contribute to homogenization. *Global Change Biology*, 19, 1075–1084.
- Putman, R.J. (1997). Deer and road traffic accidents: Options for management. *Journal Of Environmental Management*, 51, 43–57.
- Reck, H. and Kaule, G. (1993). *Strassen und Lebensräume: Ermittlung und Beurteilung strassenbedingter Auswirkungen auf Pflanzen, Tiere und ihre Lebensräume*. Bonn-Bad Godesberg, Germany.: Bundesministerium für Verkehr, Abteilung Strassenbau.

- Reh, W. and Seitz, A. (1990). The influence of land use on the genetic structure of populations of the common frog (*Rana temporaria*). *Biological Conservation*, 54, 239-249.
- Reicholf, J.v. and Esser, J. (1981). Daten zur Mortalität des Igels (*Erıcaneus europaeus*) verursacht durch den Strassenverkehr. *Zeitschrift für Säugetierkunde*, 46, 216-222.
- Reijnen, R., Foppen, R., ter Braak, C., Thissen, J. (1995). The effects of car traffic on breeding bird populations in woodland. III. Reduction of density in relation to the proximity of main roads. *Journal of Applied Ecology*, 32, 187–202.
- Republic of Türkiye Ministry of Transport and Infrastructure. (2023). Reaching and Accessible Turkey 2002-2023. <https://www.uab.gov.tr/uploads/pages/bakanlik-yayinlari/ulasan-erisen-turkiye-2002-2023-20240710.pdf> (Accessed: 21.10.2024).x
- Rodriguez, A. and Delibes, M. (1992). Current range and status of the Iberian lynx (*Felis pardina*) in Spain. *Biological Conservation*, 61(3), 189-196.
- Rodts, J., Holsbeek, L., Muylldermons, S. (1998). Dieren onder onze wielen. - Koninklijk Belgisch Verbond voor de Bescherming van de Vogels.
- Romin, L.A. and Bissonette, J.A. (1996). Deer-vehicle collisions: Status of state monitoring activities and mitigation efforts. *Wildlife Society Bulletin*, 24, 276-283.
- Rydell, J. (2006). Bats and their insect prey at streetlights. Pages 43–60 in C. Rich and T. Longcore, editors. *Ecological consequences of artificial night lighting*. Island Press, Washington, DC.
- Santos, C.D., Miranda, A.C., Granadeiro, J.P., Lourenco, P.M., Saraiva, S., Palmeirim, J.M. (2010). Effects of artificial illumination on the nocturnal foraging of waders. *Acta Oecologica*, 36, 166–172.
- Scanlon, P.F. (1987). Heavy metals in small mammals in roadside environments- implications for food chains. *Science of the Total Environment* 59, 317-323.
- Scanlon, P.F. (1991). Effects of highway pollutants upon terrestrial ecosystems. In: Hamilton, R.S. and Harrison, R.M., (Eds.) *Highway pollution*. Studies in environmental sciences, pp. 281-338.

- Schaub, A., Ostwald, J., Siemers, B.M. (2008). Foraging bats avoid noise. *Journal of Experimental Biology*, 211, 3174–3180.
- Schmidley, D.J. and Wilkins, K.T. (1977). Composition of small mammal populations on highway right-of-way in east Texas. Texas State Department of Highways and Public Transportation, Research Report 197-1F.
- Seiler, A. (2001). Ecological Effects of Roads—A review. Introductory Research Essay Department of Conservation Biology, 9, 40
- Shanley, C.S. and Pyare, S. (2011). Evaluating the road-effect zone on wildlife distribution in a rural landscape. *Ecosphere*, 2(2), 1–16.
- Siemers, B.M. and Schaub, A. (2011). Hunting at the highway: traffic noise reduces foraging efficiency in acoustic predators. *Proceedings of the Royal Society B*, 278, 1646–1652.
- Sjögren-Gulve, P. (1994). Distribution and extinction patterns within a northern metapopulation of the pool frog, *Rana lessonae*. *Ecology*, 75, 1357-1367.
- Stief, K. (1996). Roadside vegetation- a death-trap for birds. (Verkehrsbegleitendes Grün als Todesfalle für Vögel). *Natur und Landschaft*, 71, 527-532.
- Stone, E.L., Jones, G., Harris, S. (2012). Conserving energy at a cost to biodiversity? Impacts of LED lighting on bats. *Global Change Biology*, 18, 2458–2465.
- Stoner, D. (1925). The toll of the automobile. – *Science*, 61, 56-58.
- Svensson, S. (1998). Birds kills on roads: is this mortality factor seriously underestimated? - *Ornis Svecica*, 8, 183-187.
- Summers, P.D., Cunnington, G.M., Fahrig, L. (2011). Are negative effects of roads on breeding birds caused by traffic noise? *Journal of Applied Ecology*, 48, 1527–1534.
- Svensson, S. (1998). Birds kills on roads: is this mortality factor seriously underestimated? - *Ornis Svecica*, 8, 183-187.
- Trombulak, S.C. and Frissell, C.A. (2000). Review of ecological effects of roads on terrestrial and aquatic communities. *Conservation Biology*, 14, 18-30.
- Van der Grift, E.A. (1999). Mammals and railroads: Impacts and management implications. *Lutra*, 42, 77-98.

- van der Grift, E.A., Seiler, A., Rosell, C., Simeonova, V. (2017). Safe Roads for Wildlife and People. CEDR Transnational Road Research Programme Call 2013: Roads and Wildlife, 56.
- van der Ree, R., Smith, D.J., Grilo, C. (2015). Handbook of Road Ecology. John Wiley & Sons, Ltd., 552.
- Van der Zee, F.F., Wiertz, J., Terbraak, C.J., Van Apeldoorn, R.C. (1992). Landscape change as a possible cause of the badger *Meles meles* L. decline in the Netherlands. Biological Conservation, 61, 17-22.
- Van den Tempel, R. (1993). Vogelslachtoffers in het wegverkeer (in Dutch with English summary). - Vogelbescherming Nederland, Ministerie van Verkeer en Waterstaat, Directoraat-Generaal Rijkswaterstaat.
- Van Gelder, J.J. (1973). A quantitative approach to the mortality resulting from traffic in a population of *Bufo bufo*. Oecologia, 13, 93-95.
- Vestjens, W.J.M. (1973). Wildlife mortality on a road in New South Wales. Emu, 73, 107-112.
- Vos, C.C. and Chardon, J.P. (1998). Effects of habitat fragmentation and road density on the distribution pattern of the moor frog *Rana arvalis*. Journal of Applied Ecology, 35, 44-56.
- Wikelski, M. and Cooke, S.J. (2006). Conservation physiology. Trends in Ecology and Evolution, 21, 38-46.
- Zande, A.N. van der and Vos, P. (1984). Impact of a Semi-experimental increase in recreation intensity on the densities of birds in groves and hedges on a lake shore in The Netherlands. Biological Conservation, 30(3), 237-259.
- Zurcher, A.A., Sparks, D.W., Bennett, V.J. (2010). Why the bat did not cross the road? Acta Chiropterologica, 12, 337-340.

CHAPTER 15

DATA VISUALIZATION TOOLS AND TECHNIQUES: DIABETE DATASET EXAMPLE

Assoc. Prof. Dr. Haydar KOÇ¹ and Assoc. Prof. Dr. Tuba KOÇ¹

DOI: <https://dx.doi.org/10.5281/zenodo.14259391>

¹ Çankırı Karatekin University, Faculty of Science, Department of Statistics, Çankırı, Türkiye.haydarkoc@karatekin.edu.tr, Orcid ID: 0000-0002-8568-4717, tubakoc@karatekin.edu.tr, Orcid ID: 0000-0001-5204-0846

INTRODUCTION

Various techniques are used to transfer information and the most effective one among them is data visualization. Data visualization is a method that makes data more understandable and accessible. By facilitating the analysis of large and complex data sets, it visually presents patterns, trends and relationships within the data (Gürler et al., 2018). This process is usually carried out using visual tools such as graphs, tables, maps, diagrams and infographics. Data visualization allows us to understand patterns, trends and relationships of data more quickly and effectively so that users can make decisions based on accurate information. In addition, data visualization enables information to be perceived and shared faster (Bilgin and Çamurcu, 2008). It plays a critical role in many areas such as big data analysis, financial reporting, health data, scientific research and business strategy. Data visualization serves two main purposes. The first is to better understand ideas, rules and concepts. Since this is all information, this type of visualization is called knowledge visualization. The other purpose is to use graphics and pictures to generate new ideas, establish new relationships, test the accuracy of a hypothesis, discover new structures or organize these structures (Güzelci, 2017). In summary, these processes are about using the human visual perception system to solve logical problems (Bilgin and Çamurcu, 2008).

A strength of data visualization is that it simplifies complex data, making it easier to understand and track. Data visualization helps to present complex data in an understandable and effective way in many fields. It is used in many sectors such as business, finance, health, education, scientific research and public administration. For example, businesses make strategic decisions by visualizing sales and performance analysis, while the financial sector uses visual tools to analyze stock prices and economic indicators. In healthcare, data such as disease prevalence, treatment outcomes and healthcare efficiency are visualized to help healthcare professionals make decisions. In education, data such as student achievement and the impact of teaching materials are visualized. In government, data such as population

density, environmental changes and infrastructure needs are effectively used with visualization techniques in policy development processes. Data visualization is an essential tool for rapid data analysis, communication and decision support.

THE ROLE OF ARTIFICIAL INTELLIGENCE TECHNIQUES IN DATA VISUALIZATION PROCESSES

Advances in technology have positioned artificial intelligence as a key component in data visualization processes, addressing the complexity and time-consuming nature of analyzing and visualizing large datasets. Artificial Intelligence (AI) techniques enhance efficiency, allowing data analysts and decision-makers to gain faster and more accurate insights (Alkan and Oduncu, 2024). The role of AI in data visualization can be examined from multiple perspectives:

Data Preprocessing: By automating the process of cleaning and organizing data, AI can detect missing data, identify anomalies and convert data into the appropriate format. This facilitates data preparation before starting the visualization process.

Data Analysis: AI can identify the most important data to visualize by quickly discovering meaningful patterns, trends and relationships from large data sets. Machine learning algorithms discover hidden relationships in data, highlighting the right data for visualization.

Automatic Visualization Selection: AI can suggest the most appropriate type of visualization based on the nature of the data. For example, a machine learning model may suggest line graphs for continuous data, bar charts for categorical data, or scatter plots to see relationships. This makes it easier for users to choose the right visualization.

Data Visualization Improvement: AI can make automatic improvements to visualization. By optimizing visual elements such as color, size and labels in charts, it enables data to be presented in a more understandable and effective way. In addition, AI-powered algorithms

allow the visual representation of data to be more user-friendly and interactive.

Data Interpretation: Artificial intelligence can use natural language processing techniques to make sense of the data presented through visualizations. In this way, descriptions and comments about the visualized data are automatically generated, making it easier to interpret the data.

Dynamic and Real-Time Visualizations: AI can perform real-time data analysis and visualization. For example, visualization of instant changes in financial markets or social media data can be presented through dynamic and constantly updated graphics with AI algorithms.

DATA VISUALIZATION TECHNIQUES

Data visualization uses different types of graphs and charts to make data easier to understand. Line graphs show time series data, showing the change in variables over time. Bar charts are ideal for comparing categorical data, as they visually represent the values of each category. Pie charts represent parts of a whole, showing the proportions of categories within the whole. Scatter plots are used to visualize the relationship between two continuous variables. Heat maps use color to represent the density of the data and provide a visual representation of the density in the data set. Box plots show the distribution of the data and the extreme values, providing information about the median, quartiles and outliers. Histograms are used to examine the distribution of continuous data, while network charts visualize linked data and relationships. Complex diagrams are used to show processes or workflows and are particularly effective for visualizing data flows. Geographical maps are used to visualize location-based data, especially traffic and population density. Tree maps visualize the hierarchy in large data sets. These types make it easier to understand data and quickly find the information needed for different analyses and decisions. Some of the most popular data

visualization techniques and some of the popular programs and packages that can use these techniques are listed below.

Line Charts

Line charts are used to show numerical changes over time or on a continuing basis. When grouped, line charts show trends and relationships among data (Çubukçu, 2021).

Microsoft Excel: You can create line charts in a simple and effective way. When you enter your data set, you can select your data and choose Line Charts from the Insert menu.

Tableau: A powerful platform for data visualization, Tableau helps you create more complex and interactive line charts (Cebeci, 2018). You can easily design charts by importing data.

Power BI: Power BI, Microsoft's business intelligence tool, is very powerful in visualizing large data sets. It provides many visual tools, including line graphs (Power, 2021).

R program: The ggplot2 library in R allows you to create advanced and aesthetically pleasing line graphs. It is a very common tool for data analysis and visualization (Wickham et al, 2016).

Python: The library commonly used for data visualization with Python is the Matplotlib library. Seaborn is a library that provides a high-level interface to the Matplotlib library and is widely used for creating line graphs in Python (Sial et al. 2021).

Scatter Plots

A scatter plot is a type of graph used to visualize the relationship between two variables. The graph shows one variable on the vertical axis and the other on the horizontal axis; each data point is represented as a point at the intersection of these two variables. Scatter plots are particularly useful in determining the correlation or a possible trend between two continuous variables. Scatter plots can also be used in multidimensional analyses, and additional variables can be visualized with a variety of colors or icons (Cleveland, 1993).

Tableau: Scatter plots can be made to show the relationship between continuous data.

Power BI: Used to visualize the relationship between two variables.

R program: Scatter plots can be created with the `geom_point()` function in the `ggplot2` library.

Python: Matplotlib is very effective for visualizing the relationship between two variables.

Bar Charts

The classic bar chart uses horizontal or vertical columns to distinguish between categories and show numerical comparisons. One axis of the graph shows the categories being compared and the other axis shows a scale of values. Bar charts differ from histograms in that they do not show continuous and uninterrupted trends over a period (Archambault et al. 2015).

Tableau: Categorical data are compared with bar charts.

Power BI: Interactive bar charts can be created for categorical data.

R program: A bar chart can be created using the `geom_bar()` function in the `ggplot2` library.

Python: Matplotlib and Seaborn are widely used to visualize categorical data.

Histogram

A histogram is a type of graph used to visualize the distribution of a data set by dividing the data into intervals and showing the frequency within those intervals with vertical bars. The main difference between a histogram and a bar graph is that a histogram usually works with continuous data and the bars are adjacent to each other, emphasizing the continuity between intervals. The bar graph is usually

used for categorical data and there is a gap between the bars (Freedman et al. 2007).

Tableau: Histograms are used to show the distribution of continuous data.

Power BI: Histograms can be created to analyze the distribution of data.

R program: Histograms can be plotted using the `geom_histogram()` function in the `ggplot2` library.

Python: Matplotlib is very efficient for plotting histograms.

Pie Charts

A pie chart is a type of chart that displays data as slices within a circle. Each slice represents a portion of the total, and its size is proportional to the proportion of the category it represents. This type of chart is particularly useful for presenting ratios or percentages. Pie charts are an effective tool for showing the distribution of data within a total in a quick and easy to understand way. However, if there are too many categories or the proportions are close together, they can become visually cluttered and difficult to interpret. Therefore, they are generally recommended for data sets that are simple and contain few categories (Evergreen. 2016).

Tableau: Pie charts are created to show the proportions of categories.

Power BI: Used to visualize the relationships between categories.

R (ggplot2): Pie charts can be generated using the `coord_polar()` function in the `ggplot2` library.

Python: Matplotlib is used to create pie charts in a quick and easy way.

Box Plots

Box plot is a type of graph used to visualize central tendency and dispersion characteristics in a data set. It is often used to show the quartiles (lower quartile, median and upper quartile), minimum and maximum values (excluding outliers other than the interquartile range) and outliers of a variable. The box plot provides an at-a-glance understanding of the summary statistics (median, minimum, maximum and interquartile range) of the data set. Especially when comparing multiple groups, box plots provide a quick and effective comparison (McGill et al., 1978).

Tableau: Box plots can be created to provide information about data distribution and outliers.

Power BI: Box plots are used for statistical analysis and to view data distribution.

R program: In the ggplot2 library, boxplots can be easily created using the `geom_boxplot()` function.

Python: Boxplots can be created using Matplotlib and Seaborn.

Heatmaps

Heatmaps are a type of graph that visualizes data using color gradients and are often used to show values such as density, frequency or magnitude. This type of graph is a highly effective tool for identifying patterns or anomalies in large data sets, allowing you to quickly see the magnitude of values in a matrix. For example, a heat map of a website can be used to highlight the areas where users click the most. In academic or commercial applications, heat maps are often used in fields such as biology, finance, geography and social sciences. They are also a powerful way to understand how data points change over time and space, or to perform comparative analysis (Tufte, 2001).

Tableau: Use the heat map to visualize data density with colors.

Power BI: Create interactive heat maps showing data density with color.

R program: Heatmap and ggplot2 packages can be used for the heat map.

Python: Heatmap can be created using Seaborn and Matplotlib.

Word Clouds

It is a type of graphic used to visualize the most frequently used words in a text. In these graphics, words are usually sized according to their frequency of occurrence in the text, with frequent words being larger and more prominent, and infrequent words being smaller and less conspicuous. The purpose of visualization is to quickly understand the main themes of a text or document. It is used to summarize large amounts of textual data and detect trends, especially in areas such as text mining, social media analyses, feedback evaluations, academic studies and marketing strategies. In addition, word clouds provide an aesthetic appearance, allowing results to be presented in a more attractive way (Heimerl, 2014).

Tableau: Word clouds can be created to analyze and visualize text data.

Power BI: It is possible to visualize text data with word clouds.

R program: The word cloud package is widely used to create word clouds from text data.

Python: Word clouds can be created with the WordCloud library in Python.

Network Diagrams

Network diagrams are a visual representation of the components of a system or process and the relationships between them. These diagrams are constructed using nodes and edges. The nodes represent the main elements in the system and the edges represent the relationships between these elements or the process flow (Morris, 2013).

Tableau: Create network maps to analyze social networks and visualize relationships.

Power BI: Network diagrams can be used to visualize connections and relationships.

R program: Network diagrams can be created using the `igraph` and `networkD3` packages.

Python: Network diagrams can be created and visualized using `NetworkX` and `Plotly`.

Area Charts

An area chart is a type of chart used to visually show the change and magnitude of a data set over time. This chart overlays an area over the data, like a line chart, and thus provides a clearer view of trends over time. The area chart is often used to show time series data because it clearly shows both the trends of the data and the ratios between categories. The horizontal axis is usually time, and the vertical axis is the measured value. This type of chart is used to visually emphasize relationships between data and comparisons between categories. The area chart is particularly useful when comparing the change of multiple categories or data sets over time. It is also used to understand how totals change and the share of subcategories in these totals (Knafllic, 2015).

Tableau: To draw an area chart, click on the Show Me tab and select the area chart type. This will display the data as an area chart.

Power BI: The area chart can be drawn in the visualizations panel for visualization of time series data.

R program: Area charts can be created with the `geom_area()` function in the `ggplot2` package.

Python: Area charts can be visualized with `Matplotlib` and `Plotly` libraries.

These visualization techniques can make your data more understandable and interactive, allowing users to quickly analyze the data. Each technique can be performed using different programs and packages, depending on your purpose and the nature of your data.

APPLICATION

Data Set

The Pima Indians Diabetes dataset contains data on the risk of diabetes among women from Pima Indians (Smith and Hothorn, 2007). This dataset consists of the explanatory variables Pregnancies, Glucose, BloodPressure, SkinThickness, Insulin, Body Mass Index, DiabetesPedigreeFunction, Age and the dependent variable Outcome diabetes status. There are a total of 768 observation values in the dataset.

The following is a detailed description of the visualization steps on the Pima Indians Diabetes dataset using the R package.

Data pre-processing was carried out first. Missing values in the diabetes dataset are shown as 0. These values were filled in with the mean as a simple method. The R codes for these operations are shown in Figure 1 below.

```
library(dplyr)
library(ggplot2)
library(readr)
url <- "https://raw.githubusercontent.com/jbrownlee/Datasets/master/pima-indians-diabetes.data.csv"
column_names <- c("Pregnancies", "Glucose", "BloodPressure", "SkinThickness", "Insulin",
                  "BMI", "DiabetesPedigreeFunction", "Age", "Outcome")
data <- read_csv(url, header = FALSE, col.names = column_names)
head(data)
data[data == 0] <- NA
summary(data)
data$Glucose[is.na(data$Glucose)] <- mean(data$Glucose, na.rm = TRUE)
data$BloodPressure[is.na(data$BloodPressure)] <- mean(data$BloodPressure, na.rm = TRUE)
data$SkinThickness[is.na(data$SkinThickness)] <- mean(data$SkinThickness, na.rm = TRUE)
data$Insulin[is.na(data$Insulin)] <- mean(data$Insulin, na.rm = TRUE)
data$BMI[is.na(data$BMI)] <- mean(data$BMI, na.rm = TRUE)
data$DiabetesPedigreeFunction[is.na(data$DiabetesPedigreeFunction)] <- mean(data$DiabetesPedigreeFunction, na.rm = TRUE)
data$Age[is.na(data$Age)] <- mean(data$Age, na.rm = TRUE)
```

Figure 1. The R program codes for data preprocessing operations

We have created a line chart for the data on diabetes dataset. The codes of the R program for the line chart are given in Figure 2.

```
# We create a Line Chart visualising the relationship between glucose and insulin
ggplot(data, aes(x = Glucose, y = Insulin)) +
  geom_line(color = "blue") +
  labs(
    x = "Glucose Level",
    y = "Insulin Level") +
  theme_minimal()
```

Figure 2. The R program codes for line chart graph drawing of diabetes dataset

The line chart selected as an example from the diabetes data, showing the relationship between insulin levels and glucose levels, is as follows.

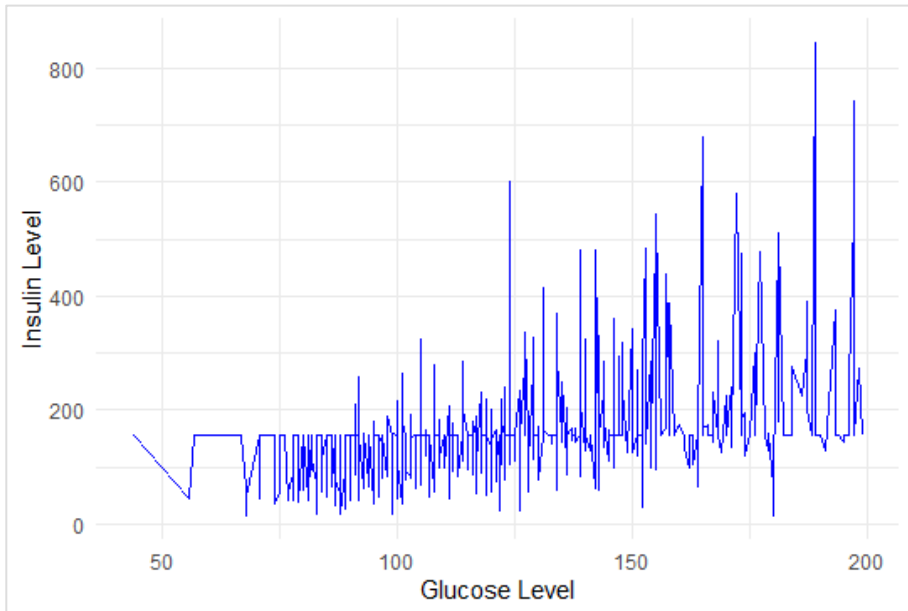


Figure 3. The Line chart showing the relationship between insulin and glucose levels

We have created a scatter plot for the data on diabetes dataset. The codes of the R program for the scatter plot chart are given in Figure 4.

```
# We create a Scatter plot visualising the relationship glucose and age
ggplot(data, aes(x = Glucose, y = Age, color = factor(outcome))) +
  geom_point(alpha = 0.6) +
  labs(x = "Glucose Level", y = "Age", color = "Diabetes Status") +
  theme_minimal()
```

Figure 4: The R program codes for scatter plot graph drawing of diabetes dataset

The scatter plot shows the relationship between the risk of diabetes and glucose levels and age factors is as follows.

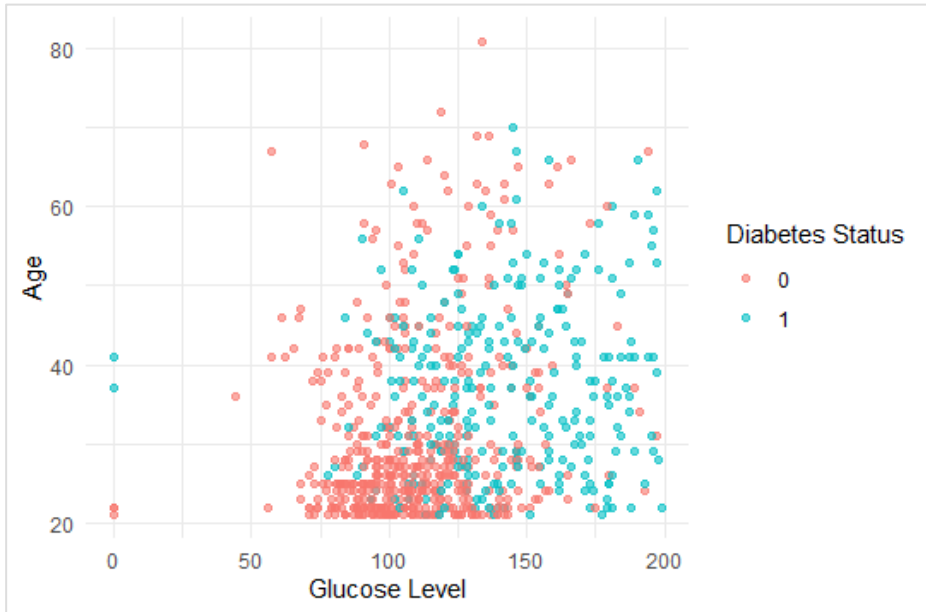


Figure 5. The Scatter plot showing the relationship between age and glucose levels according to diabetes status

We have created a bar chart for the data on diabetes dataset. The codes of the R program for the bar chart are given in Figure 6.

```
# we create a Bar Chart visualising the relationship between diabetes status and age mean
ggplot(data, aes(x = factor(outcome), y = Age, fill = factor(outcome))) +
  geom_bar(stat = "summary", fun = "mean", width = 0.5) +
  labs(x = "Diabetes Status", y = "Age Mean", fill = "Diabetes Status") +
  theme_minimal()
```

Figure 6. The R program codes for bar chart graph drawing of diabetes dataset

We compared the mean of the age factor according to diabetes status with a bar chart.

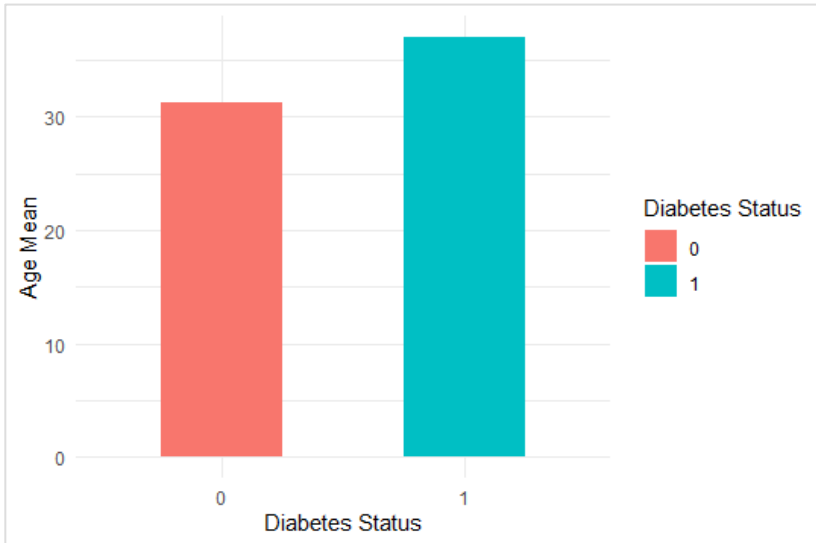


Figure 7. The Bar chart showing the relationship between diabetes status and age mean

We have created a histogram for the data on diabetes dataset. The codes of the R program for the bar chart are given in Figure 8.

```
# We create a Histogram that visualizes the distribution of BMI values by diabetes status
ggplot(data, aes(x = BMI, fill = factor(outcome))) +
  geom_histogram(binwidth = 1, alpha = 0.6, position = "identity", color = "black") +
  labs(x = "Body Mass Index (BMI)", y = "Frekans", fill = "Diabetes Status") +
  theme_minimal()
```

Figure 8. The R program codes for histogram drawing of diabetes dataset

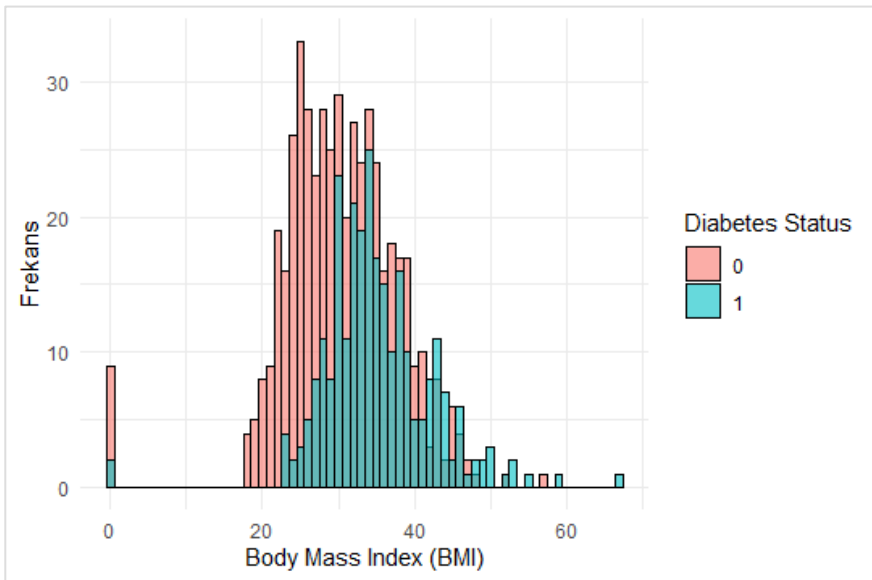


Figure 9. The Histogram chart of BMI values according to diabetes status variable

We have created a pie chart for the data on diabetes dataset. The codes of the R program for the bar chart are given in Figure 10.

```
# We create a Pie chart that shows the distribution of individuals according to diabetes status variable.
outcome_counts <- data %>%
  count(outcome) %>%
  mutate(percentage = n / sum(n) * 100)
ggplot(outcome_counts, aes(x = "", y = n, fill = factor(outcome))) +
  geom_bar(stat = "identity", width = 1, color = "black") +
  coord_polar(theta = "y") +
  labs(fill = "diabetes Status") +
  theme_minimal() +
  theme(axis.text.x = element_blank())
```

Figure 10. The R program codes for pie chart drawing of diabetes dataset

A pie chart showing the distribution of individuals by diabetes status is given below.

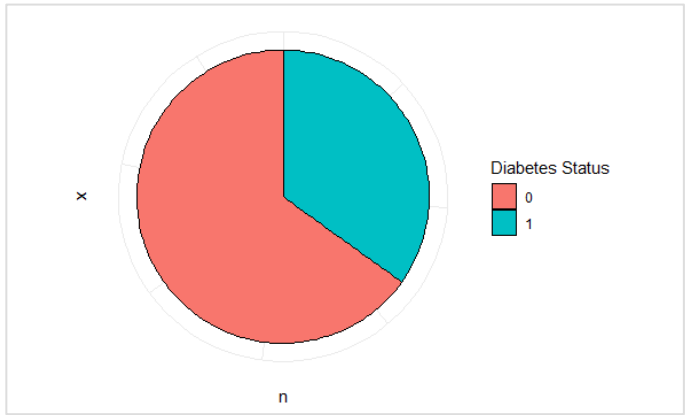


Figure 11. The Pie chart for diabetes status variable

We have created a box plot for the data on diabetes dataset. The codes of the R program for the box plot are given in Figure 12.

```
# we create a Box plot comparing diabetes status by BMI
ggplot(data, aes(x = factor(outcome), y = BMI, fill = factor(outcome))) +
  geom_boxplot() +
  labs(x = "Diabetes Status", y = "BMI", fill = "Diabetes Status") +
  theme_minimal()
```

Figure 12. The R program codes for box plot drawing of diabetes dataset

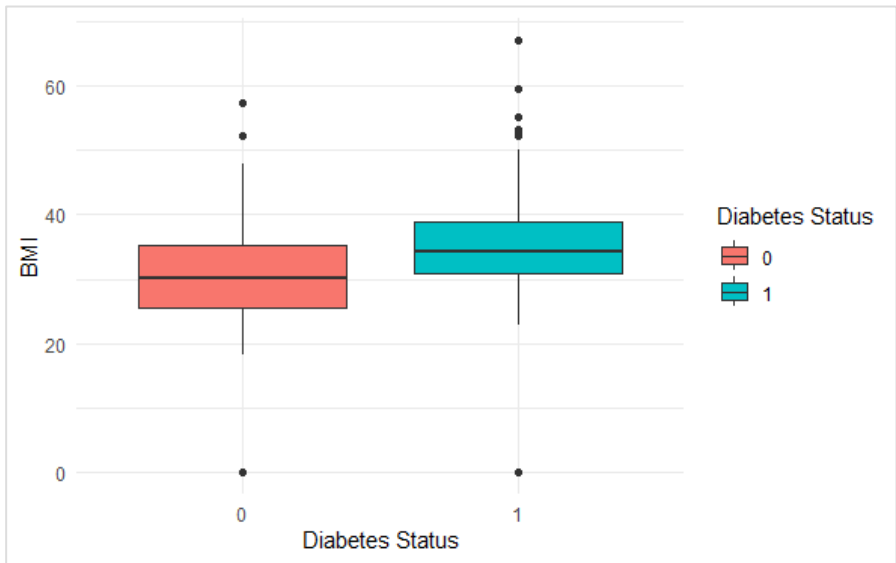


Figure 13. The Box plot for diabetes status by BMI

We have created a heatmap for the data on diabetes dataset. The codes of the R program for the box plot are given in Figure 14.

```
# # Let's visualise with a heatmap
library(reshape2)
library(ggplot2)

cor_matrix <- cor(data[, 1:8], use = "complete.obs")
cor_matrix_melted <- melt(cor_matrix)
ggplot(cor_matrix_melted, aes(var1, var2, fill = value)) +
  geom_tile() +
  scale_fill_gradient2(low = "blue", high = "red", mid = "white", midpoint = 0) +
  labs(x = "explanatory variables", y = "explanatory variables") +
  theme_minimal() +
  theme(axis.text.x = element_text(angle = 45, hjust = 1))
```

Figure 14. The R program codes for heatmap drawing of diabetes dataset

A heatmap allows us to visualize the correlation between multiple variables in the data. Below is the heatmap showing the relationships of the correlations between all the explanatory variables.

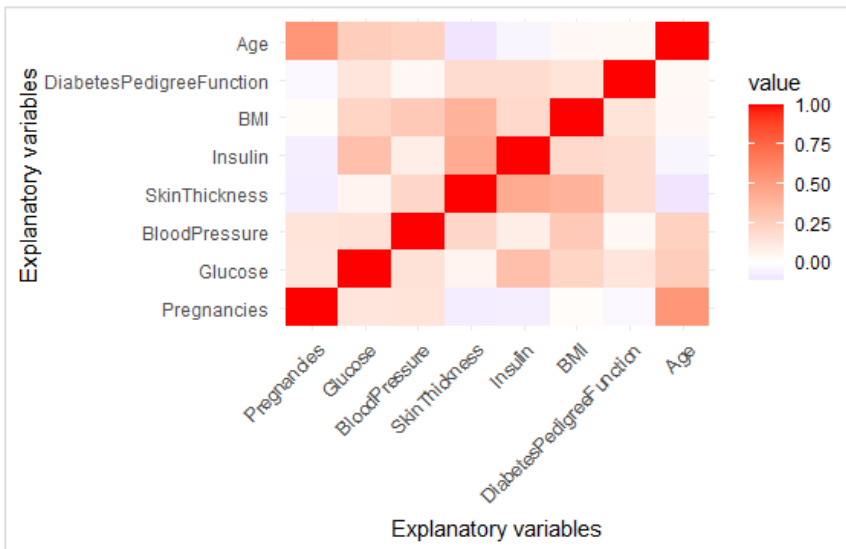


Figure 15. The heatmap showing the correlations between all variables.

We created word clouds for the data in the diabetes dataset. The R program codes for the word clouds are shown in Figure 16.

```
library(wordcloud)
library(RColorBrewer)

#Let's create a sample text data to create a word cloud in the diabetes dataset
text_data <- c("Glucose", "BloodPressure", "Insulin", "BMI", "Age",
              "DiabetesPedigreeFunction", "Pregnancies", "Outcome",
              "Diabetes", "Insulin", "Glucose", "Hypertension", "Obesity")

# Let's create the word cloud
wordcloud(words = text_data,
          freq = rep(1, length(text_data)),
          min.freq = 1,
          scale = c(3, 0.5),
          colors = brewer.pal(8, "Dark2"))
```

Figure 16. The R program codes for word clouds drawing of diabetes dataset

Word clouds are a technique often used to visualize text-based data within data. However, this type of visualization requires text in the data. Since there is no text in the diabetes dataset, we can use summary explanations of how each variable affects it instead of word clouds. For example, we can create a word cloud using keywords that describe factors related to diabetes.

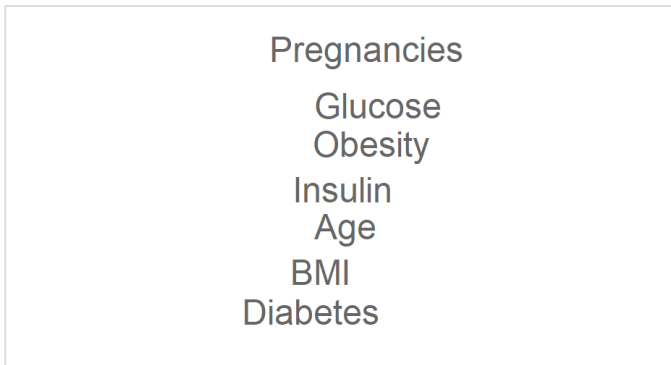


Figure 17. The Word cloud for diabetes dataset

We created a network diagram for the data in the diabetes dataset. The R program codes for the network diagram are shown in Figure 18.

```

library(igraph)
library(ggplot2)
library(corr)
cor_matrix <- data %>%
  select(-Outcome) %>% # Outcome değişkenini hariç tutuyoruz
  cor(use = "pairwise.complete.obs")

cor_data <- as.data.frame(as.table(cor_matrix))
colnames(cor_data) <- c("Var1", "Var2", "Correlation")

network_graph <- graph_from_data_frame(cor_data, directed = FALSE)

E(network_graph)$color <- ifelse(E(network_graph)$correlation > 0, "blue", "red")
E(network_graph)$width <- abs(E(network_graph)$correlation) * 5 # kenar kalınlıkları
# Plot the network graph
plot(network_graph,
      vertex.size = 40, # Düğümlerin boyutu
      vertex.label.cex = 0.8, # Etiket boyutu
      vertex.label.color = "black",
      edge.color = E(network_graph)$color, # Kenar renkleri
      edge.width = E(network_graph)$width, # Kenar kalınlıkları
      main = "Pima Indians Diabetes Ağ Diyagramı")

```

Figure 18. The R program codes for network diagram drawing of diabetes dataset

We created a network diagram to visualize the correlations between diabetes status (outcome) and other variables. Figure 19 shows the density of the connections and the strength of the relationship between the variables.

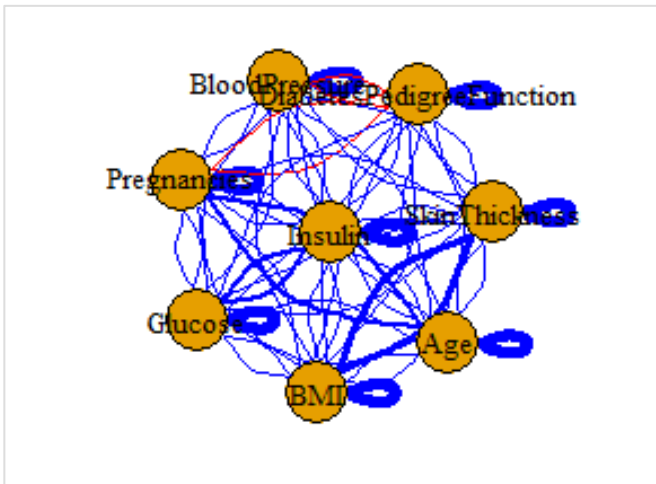


Figure 19. The Network diagram for diabetes dataset

We created an area chart for the data in the diabetes dataset. The R program codes for the area chart are shown in Figure 20.

```
#Let's prepare a dataset containing glucose level and BMI variables in the diabetes dataset
data_comparison <- data %>%
  select(Glucose, BMI)
# Let's visualize the area graph of glucose and BMI variables
ggplot(data_comparison, aes(x = Glucose, y = BMI)) +
  geom_area(fill = "red", alpha = 0.5) +
  labs(x = "Glucose Level", y = "BMI") +
  theme_minimal() # Temayı minimal yapıyoruz
```

Figure 20. The R program codes for area chart drawing of diabetes dataset

The area chart of the relationship between BMI value and glucose level is given in Figure 21.

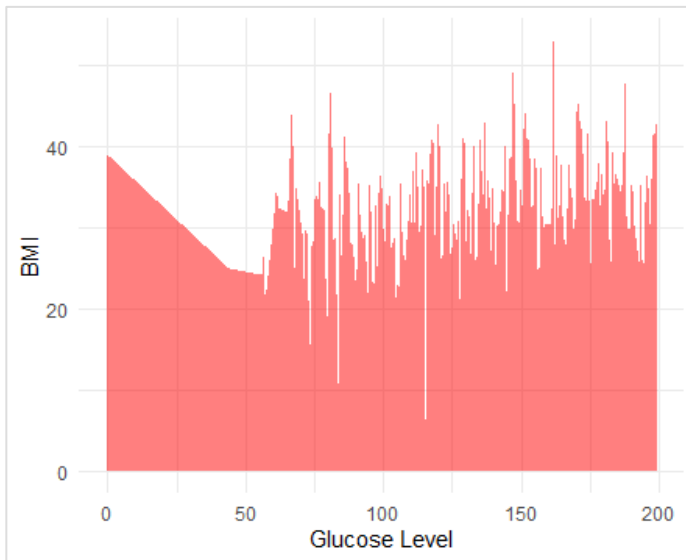


Figure 21. The Area chart of the relationship between glucose levels and BMI variables

CONCLUSION AND DISCUSSION

Nowadays, data visualization techniques play a crucial role in making large and complex data sets more understandable. This study provides a brief overview of popular data visualization techniques, and the software tools used to implement them. Using the Pima Indian Diabetes Database, the distribution and relationships of biometric variables associated with diabetes were visually explored using various data visualization methods. All visualizations were created using R

programming packages, taking advantage of R's powerful visualization tools and flexibility to present the data more effectively. These visualizations enhanced the comprehensibility of the dataset by providing a compelling visual narrative for analysts.

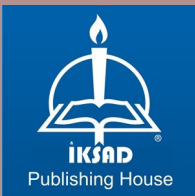
Data visualization techniques simplify the process of examining differences in magnitude and patterns of change in data. For example, area plots effectively illustrate changes over time or the relationships between two variables. Similarly, techniques such as word clouds and network diagrams are essential tools for visualizing textual data or analyzing complex relationships. These methods facilitate the rapid identification of trends and relationships, regardless of the size or complexity of the dataset. In addition, advances in technologies such as artificial intelligence and machine learning are further enriching the data visualization process, enabling deeper and more insightful analysis.

In conclusion, this study underscores the importance of data visualization in the data analysis process and highlights its potential as a valuable resource for future research.

REFERENCES

- Alkan, İ., and Oduncu, S. (2024). Yapay Zekâ'da Güncel Yaklaşımlar: Bir Tasarım Aracı Olarak Veri Görselleştirme Teknikleri. *Sanatta Dijitalizm [Özel Sayı]*, 171-182.
- Archambault, S. G., Helouvyry, J., Strohl, B., and Williams, G. (2015). Data visualization as a communication tool. *Library Hi Tech News*, 32(2), 1-9.
- Bilgin, T. T., and Çamurcu, A. Y. (2008). Çok Boyutlu Veri Görselleştirme Teknikleri. *Akademik Bilişim*, 107-112.
- Cebeci, H. I. (2018) Veri Görselleştirme ve Görsel Analitik Tableau ile Örnek Bir Uygulama.
- Cleveland, W. S. (1993). *Visualizing data*. Hobart Press.
- Çubukçu, F. (2021). *Excel 365 ile Veri Analizi ve İş Uygulamaları*. Ukrayna: Kodlab Yayıncılık.
- Evergreen, S. D. H. (2016). *Effective data visualization: The right chart for the right data*. SAGE Publications.
- Freedman, D., Pisani, R., and Purves, R. (2007). *Statistics*. W. W. Norton & Company.
- Gürler, A., Yılmaz, A. S., and Tekerek, M. (2018). Veri Görselleştirme ve İnfografikler. *KSÜ Mühendislik Bilimleri Dergisi*, s. 131-148.
- Güzelci, H. (2017). *Sanat Sergileri İçin Diyagram Tabanlı ve Kullanıcı Etkileşimli Görselleştirme Arayüzü Tasarımı*. İstanbul: T.C. İstanbul Kültür Üniversitesi Fen Bilimleri Enstitüsü.
- Heimerl, F., Lohmann, S., Lange, S., & Ertl, T. (2014). Word cloud explorer: Text analytics based on word clouds. *Proceedings of the 47th Hawaii International Conference on System Sciences*, 1833–1842.
- Knaflic, C. (2015). *Storytelling with Data: A Data Visualization Guide for Business Professionals*. Wiley.
- McGill, R., Tukey, J. W., and Larsen, W. A. (1978). Variations of box plots. *The American Statistician*.
- Morris, P. W. G. (2013). *Project Management: A Strategic Planning Approach*. Wiley.

- Power, B. I., Excel, U., Desktop, P. B., and Tiles, P. (2021). Microsoft power bi. Available here: <https://powerbi.microsoft.com/en-us>, 130.
- Sial, A. H., Rashdi, S. Y. S., and Khan, A. H. (2021). Comparative analysis of data visualization libraries Matplotlib and Seaborn in Python. *International Journal*, 10(1), 277-281.
- Smith, J., and Hothorn, T. (2007). Pima Indians Diabetes Database. UCI Machine Learning Repository.
- Wickham, H., Chang, W., and Wickham, M. H. (2016). Package 'ggplot2'. Create elegant data visualisations using the grammar of graphics. Version, 2(1), 1-189.
- Tufte, E. R. (2001). *The visual display of quantitative information*. Graphics Press.



ISBN: 978-625-367-967-5